RM A53C20

RESEARCH MEMORANDUM

SUBSONIC STATIC LONGITUDINAL STABILITY AND CONTROL CHARACTERISTICS OF A WING-BODY COMBINATION HAVING A POINTED WING OF ASPECT RATIO 2 WITH CONSTANT-PERCENT-CHORD TRAILING-EDGE ELEVONS

By Donald W. Smith and Verlin D. Reed

Ames Aeronautical Laboratory
Moffett Field, Calif.

NATIONAL ADVISORY COMMITTEE
FOR AERONAUTICS

WASHINGTON
May 22, 1953

NATIONAL ADVISORY COMMITTEE FOR AERONAUTICS

RESEARCH MEMORANDUM

SUBSONIC STATIC LONGITUDINAL STABILITY AND CONTROL CHARACTERISTICS OF A WING-BODY COMBINATION HAVING A POINTED WING OF ASPECT RATIO 2 WITH CONSTANT-PERCENT-CHORD TRAILING-EDGE ELEVONS

By Donald W. Smith and Verlin D. Reed

SUMMARY

An investigation has been made to determine the static longitudinal stability and control characteristics of a tailless wing-body combination having a pointed wing with an aspect ratio of 2 and trailing-edge elevons. The effectiveness of inset tabs in reducing the elevon hinge moment was also determined.

Data presented include the lift, drag, pitching moment, elevon hinge moment, tab hinge moment, elevon load, and center of pressure of elevon load. Data are presented for a range of angles of attack, elevon deflection, and tab deflection at Mach numbers up to 0.95. Most of the data were obtained at a Reynolds number of 3.0 million, but at a Mach number of 0.24 data were also obtained at Reynolds numbers up to 15.0 million.

The effects of compressibility on the longitudinal characteristics were similar to those on other wing-body combinations having low-aspect-ratio triangular wings.

The effectiveness of the elevons in producing both lift and pitching moment increased with increasing Mach number. The elevon hinge moment due to elevon deflection increased rapidly as the Mach number was increased above 0.80. The elevon hinge moment due to angle of attack changed from negative to positive as the Mach number increased above 0.83. The effectiveness of the tabs in reducing elevon hinge moment increased with increasing Mach number.

The data were used to estimate the longitudinal stability and control characteristics of an assumed airplane, geometrically similar to the model. Two different types of longitudinal control systems were

[redacted]

considered for the analysis: a direct elevon control and a servotab control.

With the center of gravity at a location which would provide a minimum elevon-fixed static margin of 5 percent, both the direct elevon control and the servotab control provided about the same maximum trimmed lift coefficient throughout the speed range. At the higher Mach numbers, the stick force required for the elevons with the servotab system was much smaller than that required for direct elevon control.

INTRODUCTION

Research is in progress at the various NACA facilities to determine the aerodynamic characteristics of flap-type, trailing-edge elevons on low-aspect-ratio wings at both subsonic and supersonic speeds. The effects of elevon plan form and trailing-edge profile on the aerodynamic characteristics of elevons on a thin triangular wing of aspect ratio 2 have been determined at high subsonic and low supersonic speeds and have been reported in reference 1.

As a part of this research, there are reported herein results of tests conducted in the Ames 12-foot pressure wind tunnel at Mach numbers up to 0.95 to determine the aerodynamic characteristics of constant-percent-chord, flap-type, trailing-edge elevons on a pointed wing having an aspect ratio of 2. The effectiveness of inset tabs in reducing the elevon hinge moment is also presented. The wing leading edge was swept back 56.3° and the trailing edge was swept forward 26.6°.

NOTATION

a	normal acceleration, ft/sec^2
b	wing span, ft
c	local wing chord, ft
$\bar{c}$	wing mean aerodynamic chord, $\dfrac{\int_0^{b/2} c^2 dy}{\int_0^{b/2} c\, dy}$, ft
c_e	elevon chord, ft
c_a	elevon chord through elevon centroid of area, ft

c_r	elevon reference chord, $c_a \times \cos \delta_e$, ft
c_t	tab chord, ft
g	acceleration due to gravity, ft/sec^2
l	length of body including portion removed to accommodate sting, ft
$(L/D)_{max}$	maximum lift–drag ratio
M	Mach number
M_{A_e}	first moment of area of exposed elevon behind hinge line, ft^3
M_{A_t}	first moment of area of exposed tab behind hinge line, ft^3
n	normal acceleration factor, a/g
q	free–stream dynamic pressure, lb/sq ft
R	Reynolds number based on wing mean aerodynamic chord
r	radius of body, ft
r_o	maximum body radius, ft
S	total wing area including the area formed by extending the leading and trailing edges to the plane of symmetry, sq ft
S_e	exposed area of elevon behind hinge line, sq ft
W	weight of assumed airplane, lb
V_g	gliding speed, mph
V_v	sinking speed, ft/sec
x	longitudinal distance from elevon hinge line measured in the chord plane of the wing (negative to rear of hinge line), ft
x'	longitudinal distance from nose of body, ft
y	lateral distance normal to plane of symmetry, ft
α	angle of attack of the body axis, deg

[redacted]

δ_e elevon deflection, with respect to wing-chord plane, measured in planes perpendicular to the elevon hinge line (positive downward), deg

δ_t tab deflection, with respect to elevon-chord plane, measured in planes perpendicular to the tab hinge line (positive downward), deg

$\Delta\delta_e$ elevon deflection correction due to applied load (additive), deg

$\Delta\delta_t$ tab deflection correction due to applied load (additive), deg

C_D drag coefficient, $\frac{\text{drag}}{qS}$

C_F elevon load coefficient based on elevon load normal to wing-chord plane, $\frac{\text{elevon load}}{qS_e}$

C_{h_e} elevon hinge-moment coefficient, $\frac{\text{hinge moment}}{2qM_{A_e}}$

C_{h_t} tab hinge-moment coefficient, $\frac{\text{hinge moment}}{2qM_{A_t}}$

C_L lift coefficient, $\frac{\text{lift}}{qS}$

C_m pitching-moment coefficient about the 25-percent point of the wing mean aerodynamic chord, $\frac{\text{pitching moment}}{qS\bar{c}}$

C_{F_α} rate of change of elevon normal-force coefficient with a change in angle of attack for a constant elevon angle and tab angle, $\partial C_F/\partial\alpha$, measured at $\alpha = 0$, per deg

$C_{F_{\delta_e}}$ rate of change of elevon normal-force coefficient with a change in elevon angle for a constant angle of attack and tab angle, $\partial C_F/\partial\delta_e$, measured at $\delta_e = 0$, per deg

$C_{h_{e_\alpha}}$ rate of change of elevon hinge-moment coefficient with change in angle of attack for constant elevon deflection, $\partial C_{h_e}/\partial\alpha$, measured at $\alpha = 0$, per deg

$C_{h_{e_{\delta_e}}}$ rate of change of elevon hinge-moment coefficient with change in elevon deflection for constant angle of attack and tab angle, $\partial C_{h_e}/\partial\delta_e$, measured at $\delta_e = 0$, per deg

[redacted]

$C_{h_{e\delta_t}}$ rate of change of elevon hinge-moment coefficient with change in tab deflection for constant angle of attack and elevon angle, $\partial C_{h_e}/\partial\delta_t$, measured at $\delta_t = 0$, per deg

$C_{h_{t\delta_t}}$ rate of change of tab hinge-moment coefficient with change in tab deflection for constant angle of attack and elevon angle, $\partial C_{h_t}/\partial\delta_t$, measured at $\delta_t = 0$, per deg

$C_{L_{\delta_e}}$ lift effectiveness parameter, $\partial C_L/\partial\delta_e$, measured at $\delta_e = 0$, per deg

$C_{m_{\delta_e}}$ pitching-moment effectiveness parameter, $\partial C_m/\partial\delta_e$, measured at $\delta_e = 0$, per deg

$dC_L/d\alpha$ slope of the lift curve at zero lift, per deg

dC_m/dC_L slope of the pitching-moment curve at zero lift

MODEL

The model used in this investigation was a wing-body combination having a pointed wing with an aspect ratio of 2 and full-span, trailing-edge elevons with inset tabs. Figure 1 is a photograph of the model mounted in the wind tunnel. Figure 2 is a drawing of the plan and front views of the model showing some of the model dimensions.

Model Dimensions

Body

Fineness ratio	
Basic	12.5
Modified for installation on sting	10.0
Ratio of sting diameter to base diameter of body	0.89

Wing

Area, sq ft	4.014
Aspect ratio	2.0
Taper ratio	0
Sweep, leading edge, deg	56.31
Sweep, trailing edge, deg	26.57
Incidence, deg	0
Dihedral, deg	0
Section (streamwise)	[redacted] NACA 0005-63

[redacted]

Elevon

Sweep, hinge line, deg	0
Ratio of elevon chord to wing chord, c_e/c	0.25
Ratio of exposed elevon area to exposed wing area	0.25
Gap between wing and elevons, measured chordwise	
Starboard, in.	0.015
Port, in.	0.025
Gap between elevons and body, measured spanwise, $\delta_e = 0^\circ$, in.	0.015
First moment of area of exposed elevon behind hinge line, ft^3	0.0699

Tab

Ratio of tab chord to elevon chord, c_t/c_e	0.25
Ratio of exposed tab span to exposed elevon span	0.40
Ratio of exposed tab area to exposed wing area	0.04
Gap between elevons and tabs, in.	0.015
First moment of area of exposed tab behind hinge line, ft^3	0.00321

The body, which was constructed of aluminum, was the one used in the tests reported in references 2 and 3. The wing was constructed of a tin-bismuth alloy bonded to a steel spar. Both the wing and body were accurately contoured and polished smooth.

The elevons and tabs were constructed of steel. The airfoil section behind the elevon hinge line was modified from the NACA 0005-63 to a section having straight-line elements from the elevon hinge line to the trailing edge. This resulted in a trailing-edge angle of 6° compared with 6.6° for the basic section. The modified section had a trailing-edge thickness of approximately 0.005 inch all along the span.

Cantilever, bending-type, electrical strain gages were used to measure both the elevon and tab hinge moments on the starboard wing only. The elevon on the port wing was instrumented to provide for measurement of the elevon load normal to the wing-chord plane. These loads were determined by use of electrical strain gages mounted on the elevon hinges which were located in the wing-chord plane.

The gaps between the elevons and the wing, between the elevons and the tabs, and between the elevons and the body were not sealed during the investigation.

The model was mounted on a sting support in the wind tunnel. A 4-inch-diameter, 4-component, strain-gage balance enclosed within the model body was used to measure the model forces and moments.

TESTS

Tests of the model were made to determine the effect of Mach number on the static longitudinal stability and on the effectiveness of the constant-percent-chord, trailing-edge elevons as a longitudinal control device. Tests were also made to determine the effectiveness of constant-percent-chord, inset tabs in reducing the elevon hinge moment.

The majority of the test data were obtained throughout a range of Mach numbers from 0.24 to 0.95 at a constant Reynolds number of 3.0 million. These data were obtained for elevon deflections of 0° to -15° in combination with tab deflections of 0° to 15°. Some additional data were obtained for elevon deflections of -20°, 5°, and 20°.

Data at a Mach number of 0.24 were obtained for Reynolds numbers up to 15.0 million for several representative combinations of elevon and tab deflections.

CORRECTIONS TO DATA

The data presented herein have been corrected by the method of reference 4 for the induced effects of the tunnel walls resulting from lift on the model. The magnitudes of the corrections which were added to the measured values are

$$\Delta\alpha = 0.26\ C_L$$

$$\Delta C_D = 0.0046\ C_L^2$$

The induced effects of the tunnel wall on the pitching moment and hinge moment were calculated and found to be negligible.

Correction of the data for the effects of the constriction due to the tunnel wall was calculated by the method of reference 5. This correction was calculated for the model at 0° angle of attack and was applied to the data throughout the range of angles of attack. The correction amounted to an increase of about 2 percent in the dynamic pressure at a Mach number of 0.90.

The effect of the interference between the model and sting support on the aerodynamic characteristics is not known. It is believed that the main effect of the sting was to alter the pressure at the base of the model body. Consequently, the pressure at the base of the model was measured and the drag data were adjusted to correspond to a base pressure equal to free-stream static pressure.

The basic data have not been corrected for the change in elevon and tab angles due to the deflection under load of the hinge-moment strain gages. The summary plots have been adjusted to account for these angle changes. In order to facilitate correction of the data, there is given in figure 3 a summary of the deflection of the elevons and tabs due to load at various values of Mach number and Reynolds number.

The deflection of the port elevon normal to the wing-chord plane was measured and found to be negligible.

RESULTS

The basic data are presented graphically in figures 4 through 39 and show the variation of the angle of attack, drag coefficient, and pitching-moment coefficient with lift coefficient; the variation of elevon and tab hinge-moment coefficients with angle of attack; and the variation of elevon load coefficients and the location of the center of pressure of elevon load with angle of attack. All basic data are given for uncorrected values of elevon and tab deflection. Pitching-moment data are presented about a moment center at the 25-percent point of the wing mean aerodynamic chord.

Table I lists the figures presenting the basic data and shows the range of variables covered by the tests at each Mach number and Reynolds number.

A summary of the effects of compressibility on the aerodynamic characteristics of the model and on the elevon and tab parameters is presented in figures 40 through 45.

Results of application of the data to estimate the longitudinal stability and control characteristics of an assumed airplane geometrically similar to the model are presented in figures 46 through 49.

DISCUSSION

The results will be discussed in two sections. The first section will deal with the basic characteristics of the wing-body combination, elevons, and tabs. In the second section the data will be applied to the prediction of the longitudinal stability and control characteristics of an assumed tailless airplane geometrically similar to the wind-tunnel model. Caution must be exercised in the use and interpretation

of the slope parameters. Because of the nonlinear variation of the forces and moments with angle of attack and elevon deflection, these parameters are applicable only at angles of attack and elevon deflections near zero.

Basic Characteristics

Lift and pitching moment.- The effects of compressibility on the lift, drag, and pitching moment of the wing-body combination with the controls undeflected are summarized in figure 40. With the exception of the more forward location of the aerodynamic center, the characteristics of the wing are similar to those previously measured on a triangular wing of aspect ratio 2 and reported in reference 3.

The effectiveness of the elevons in producing lift and pitching moment is summarized in figures 41 and 42, respectively. The lift effectiveness $C_{L_{\delta_e}}$ increased with increasing Mach number up to a Mach number of about 0.93 but decreased abruptly as the Mach number was further increased to 0.95. The pitching-moment effectiveness $C_{m_{\delta_e}}$ of the elevons increased with increasing Mach number up to the highest Mach number of the test, 0.95. Increasing the tab deflection from 0° to 10° increased both the lift and pitching-moment effectiveness of the elevons but caused little change in the variation of the effectiveness with Mach number.

A comparison of the lift and pitching-moment effectiveness of the elevons with those of constant-chord and constant-percent-chord elevons on a triangular wing having an aspect ratio of 2 (ref. 1) is also presented in figures 41 and 42, respectively. The elevons were less effective in producing lift and pitching moment than the constant-chord elevons on the triangular wing. They were also less effective in producing lift than the constant-percent-chord elevons on the triangular wing but were more effective in producing pitching moment.

The lift and pitching-moment effectiveness parameters were little affected by an increase of Reynolds number from 3.0 million to 15.0 million at a Mach number of 0.24 (figs. 34 through 39).

Elevon and tab parameters.- The effects of compressibility on the elevon and tab hinge-moment parameters are presented in figures 43 and 44. The absolute magnitude of $C_{h_{e_{\delta_e}}}$ increased gradually with increasing Mach number up to a Mach number of 0.80, where a further increase of Mach number to 0.95 resulted in a very rapid increase of $C_{h_{e_{\delta_e}}}$. The elevon hinge moment due to angle of attack $C_{h_{e_\alpha}}$ changed from

negative to positive as the Mach number was increased above 0.83. In the Mach number range from 0.60 to 0.90, both the elevon hinge moment due to angle of attack and that due to elevon deflection were generally smaller than the hinge moment for the elevons on the triangular wing which were reported in reference 1 (fig. 43).

An increase of tab deflection resulted in a more negative value of $C_{h_{e_{\delta_e}}}$ above a Mach number of 0.40 and a more negative value of $C_{h_{e_\alpha}}$ above a Mach number of 0.65.

The tab effectiveness, as measured by $C_{h_{e_{\delta_t}}}$, and the hinge-moment parameter, $C_{h_{t_{\delta_t}}}$, increased with an increase in Mach number (fig. 44).

The effects of Reynolds number on the elevon and tab hinge moments at a Mach number of 0.24 are shown in figures 34 through 39. Analysis of the data shows that the absolute magnitudes of both $C_{h_{e_{\delta_e}}}$ and $C_{h_{e_{\delta_t}}}$ decreased with an increase of Reynolds number from 3.0 million to 15.0 million, while $C_{h_{e_\alpha}}$ and $C_{h_{t_{\delta_t}}}$ remained essentially unchanged.

A comparison of the variation of the elevon and tab hinge-moment parameters, $C_{h_{e_{\delta_e}}}$ and $C_{h_{t_{\delta_t}}}$, with Mach number showed that the hinge moment per unit deflection and the effect of compressibility on the hinge moment were smaller for the tab than for the elevon. The implication here is that either a smaller-chord control or a partial-span control will have hinge-moment characteristics which are less affected by compressibility than those of the full-span, 25-percent-chord elevon.

The effects of compressibility and tab deflection on the elevon load parameters are presented in figure 45.

Application of Data

In order to assess the merits of this particular wing plan form and control for use in a practical application, the data have been applied to the prediction of the static longitudinal stability and control characteristics of a hypothetical airplane geometrically similar to the model. The wing area was assumed to be 450 square feet and the center of gravity was assumed to be at the 25-percent point of the wing mean aerodynamic chord. With this center-of-gravity location the airplane had a minimum elevon-fixed static margin (at $C_L = 0$) of 5 percent of the mean aerodynamic chord.

[redacted]

In the application of the data, two types of longitudinal control have been considered. For the first of these, the elevon is directly connected to the control stick; for the second, the tab is directly connected to the control stick and movement of the stick changes the elevon deflection by changing the angle for zero hinge moment (elevon floating angle).

Characteristics of the airplane in the balanced condition.- The variations with balanced lift coefficient ($C_m = 0$) of the drag coefficient, the lift-drag ratio, the angle of attack and the elevon and tab deflection are shown in figure 46. The efficiency of the airplane as represented by the lift-drag ratio is about the same for both the plain-elevon and the servotab control at the Mach numbers above 0.80. However, at the lower Mach numbers the airplane with the plain elevons was the more efficient for lift coefficients less than about 0.50. The decrement in maximum lift-drag ratio due to balancing the assumed airplane varied from about 25 percent at low speeds to about 10 percent at the intermediate Mach numbers, becoming about 23 percent as the Mach number was further increased to 0.92.

An apparent loss in elevon pitching-moment effectiveness for both control systems was shown by the nonlinear manner in which the elevon deflection varied with balanced lift coefficient. This apparent loss appeared at all Mach numbers and increased with an increase in Mach number. There were two factors which contributed to the loss in effectiveness. The first of these factors was an actual loss in elevon effectiveness at the larger elevon deflections, while the second was a rearward shift in the aerodynamic center of the wing-body combination with an increase in lift. A study of figures 4 through 11 shows that the position of the aerodynamic center (at $C_L = 0$) did not vary greatly with an increase in Mach number up to about 0.90; with further increase in Mach number it moved rapidly rearward. However, as the lift coefficient was increased there was a point at which there was a rapid increase in stability, and this rapid increase occurred at progressively lower lift coefficients as the elevon deflection was increased negatively to balance the airplane. If this point of rapid increase in stability is arbitrarily defined as the point at which the slope of the pitching-moment curve exceeded -0.15, then the following observations may be made: At a Mach number of 0.24 there was a rapid increase in stability at an angle of attack of about 21° while at a Mach number of 0.90 this increase occurred at an angle of attack of about 10°. The angle of attack at which the stability increased was relatively unaffected by elevon deflection.

For the servotab control, the variation of the tab deflection with balance lift coefficient was of such a nature as to preclude use of a simple linked tab. Due to the high negative value of $C_{h_{e_\alpha}}$ (for $\alpha > 0°$)

at the higher lift coefficients, it was actually necessary in some instances to use a negative tab angle to produce the negative elevon floating angle necessary to balance the airplane. At the higher Mach numbers, large positive tab angles were required primarily because of the large negative value of $C_{h_{e\delta_e}}$ (for $\alpha > 0°$).

Characteristics of the airplane in gliding flight.- As shown in figure 47, both longitudinal control systems were capable of balancing the assumed airplane in power-off gliding flight. Use of the plain-elevon control resulted in a lower sinking speed at gliding apeeds greater than about 155 miles per hour, while at lower gliding speeds, the servotab control resulted in smaller sinking speeds. As would be expected, the use of the servotab control with the same control gearing $\left(\frac{\text{elevon (or tab) deflection, deg}}{\text{linear stick travel, in.}}\right)$ resulted in a smaller stick force for the same range of gliding speeds.

Control deflections and forces for a longitudinally balanced airplane in level and accelerated flight.- In level flight at an altitude of 30,000 feet, a total change of elevon deflection of less than 2° was sufficient to balance the airplane at Mach numbers from 0.60 to 0.95 for wing loadings up to 60 pounds per square foot (fig. 48). The variation of elevon angle with speed was such as to indicate stick-fixed stability up to a Mach number of 0.90, but, as the Mach number was further increased, more negative elevon angles were required to balance the airplane. This increase in negative elevon angle with increase in speed above a Mach number of 0.90 was due primarily to the rapid rearward movement of the aerodynamic center. With the servotab control, the variation of tab angle with speed was such as to indicate stick-fixed instability, more positive tab angles being required to balance the airplane as the speed increased.

The variation of stick force with speed was such as to indicate stick-free instability for either control system. With a wing loading of 40 pounds per square foot, a pull of 2000 pounds was required to balance the airplane at a Mach number of 0.95 when it was initially trimmed at a Mach number of about 0.55. Comparable figures for the servotab control, as calculated from the data of figure 48, are a pull of about 120 pounds when initially trimmed at a Mach number of 0.55.

There are also presented in figure 48 the stick forces required for level flight at 30,000 feet with a wing loading of 60 pounds per square foot for the two assumed triangular-wing airplanes of reference 1. The center of gravity of each of these airplanes was assumed to be at the 35-percent point of the wing mean aerodynamic chord giving a minimum elevon-fixed static margin of 5 percent (at $C_L = 0$). The variation of

stick force with speed for the airplane with the constant-percent-chord elevons on the triangular wing was such as to indicate stick-free instability when trimmed at a Mach number of 0.85. Although the airplane with the constant-chord elevons was not trimmed in the range of Mach numbers from 0.60 to 0.90, the variation of stick force with speed was such as to indicate stick-free instability only at Mach numbers above 0.80.

The calculated characteristics of the assumed pointed-wing airplane in constant-speed, level turns producing normal accelerations up to 4g are presented in figure 49. With the elevon control, the stick-fixed and stick-free maneuver points are behind the center of gravity at Mach numbers above about 0.85, as evidenced by the more negative elevon deflections and the increasing pull forces required to increase the normal acceleration. At Mach numbers below 0.85 the stick-fixed maneuver point is still behind the center of gravity but the stick-free maneuver point is ahead of the center of gravity, as evidenced by the increased push force required to increase the load factor. With the servotab control, the stick-fixed maneuver point is behind the center of gravity at Mach numbers above about 0.85, instability being indicated at the lower Mach numbers.

Comparison of the two control systems at a Mach number of 0.95 indicates that large reductions in stick force can be provided by the servotab. At this Mach number and a normal acceleration of 2g, the calculated pull force is 3900 pounds for the elevon and 240 pounds for the servotab, the trim Mach number in each case being about 0.70. The variation of stick force with speed was such as to indicate stick-free instability for both systems at all load factors.

CONCLUSIONS

An investigation has been made of the static longitudinal stability of a wing-body combination having a pointed wing with an aspect ratio of 2. The effectiveness of trailing-edge elevons as a longitudinal-control device was also investigated, as was the effectiveness of inset tabs in reducing the elevon hinge moment. The following conclusions are based on an analysis of the data:

1. Except for a more forward location of the aerodynamic center, the aerodynamic characteristics of the wing with elevons undeflected are similar to those of a triangular wing having an aspect ratio of 2.

2. The elevon lift and pitching-moment effectiveness parameters increased with both an increase of Mach number and an increase of tab deflection.

3. The elevon hinge moment due to elevon deflection increased rapidly as the Mach number was increased above 0.80. The elevon hinge moment due to angle of attack changed from negative to positive as the Mach number increased above about 0.83.

4. The effectiveness of the tabs in reducing the elevon hinge moment increased with an increase of Mach number.

Analysis of results of application of the data to an assumed airplane with either a plain-elevon control or an elevon with servotab control resulted in the following conclusions:

1. Both the plain elevons and the elevons with servotabs were capable of balancing the airplane to about the same lift coefficients for all Mach numbers up to 0.95.

2. At an altitude of 30,000 feet with an assumed wing loading of 40 pounds per square foot, both control systems were capable of balancing the airplane in level flight and in maneuvers with a normal acceleration factor of 3.0. The stick force required for the elevons with servotabs was much less than that required for the plain elevons.

3. With the center of gravity at a longitudinal location which will provide a minimum elevon-fixed static margin of 5 percent and for flight at an altitude of 30,000 feet with a wing loading of 40 pounds per square foot, the following static instabilities are noted:

(a) Unstable variation of elevon angle with speed at Mach numbers from 0.90 to 0.95

(b) Unstable variation of stick force with speed in level flight at Mach numbers from 0.60 to 0.95

(c) Unstable variation of stick force with normal acceleration at Mach numbers below 0.85

(d) Unstable variation of servotab angle with speed at Mach numbers from 0.60 to 0.95

(e) Unstable variation of servotab angle with normal acceleration at Mach numbers below 0.75

Ames Aeronautical Laboratory
National Advisory Committee for Aeronautics
Moffett Field, Calif.

[redacted]

REFERENCES

1. Boyd, John W.: Aerodynamic Characteristics of Two 25-Percent-Area Trailing-Edge Flaps on an Aspect Ratio 2 Triangular Wing at Subsonic and Supersonic Speeds. NACA RM A52D01c, 1952.

2. Jones, J. Lloyd, and Demele, Fred A.: Aerodynamic Study of a Wing-Fuselage Combination Employing a Wing Swept Back 63°.- Characteristics Throughout the Subsonic Speed Range with the Wing Cambered and Twisted for a Uniform Load at a Lift Coefficient of 0.25. NACA RM A9D25, 1949.

3. Smith Donald W., and Heitmeyer, John C.: Lift, Drag, and Pitching Moment of Low-Aspect-Ratio Wings at Subsonic and Supersonic Speeds - Plane Triangular Wing of Aspect Ratio 2 with NACA 0005-63 Section. NACA RM A50K21, 1951.

4. Glauert, H.: The Elements of Aerofoil and Airscrew Theory. Ch. XIV, The University Press, Cambridge, England, 1926.

5. Herriot, John G.: Blockage Corrections for Three-Dimensional-Flow Closed-Throat Wind Tunnels, with Consideration of the Effect of Compressibility. NACA Rep. 995, 1950. (Formerly NACA RM A7B28.)

[redacted]

TABLE I.- SUMMARY OF BASIC DATA

Figure number	Mach number	Reynolds number	Elevon deflection, δ_e, deg	Tab deflection, δ_t, deg
(a) Effect of Elevon Deflection				
4	0.24	3.0×10^6	20,5,0,-5, -10,-15,-20	0
5	.40		0,-10,-20	
6	.60		20,5,0,-5 -10,-15,-20	
7	.80			
8	.85			
9	.90			
10	.92			
11	.95			
12	.24		0,-5,-10,-15	5
13	.60			
14	.80			
15	.85			
16	.90			
17	.92			
18	.95			
19	.24		0,-5,-10, -15,-20	10
20	.40		0,-10,-20	
21	.60		0,-5,-10, -15,-20	
22	.80			
23	.85			
24	.90			
25	.92			
26	.95			
27	.24		0,-5,-10,-15	15
28	.60			
29	.80			
30	.85			
31	.90			
32	.92			
33	.95			
(b) Effect of Reynolds Number				
34	.24	3.0,5.0,8.0, 15.0×10^6	0	0
35			-10	0
36			-20	0
37			0	10
38			-10	10
39			-20	10

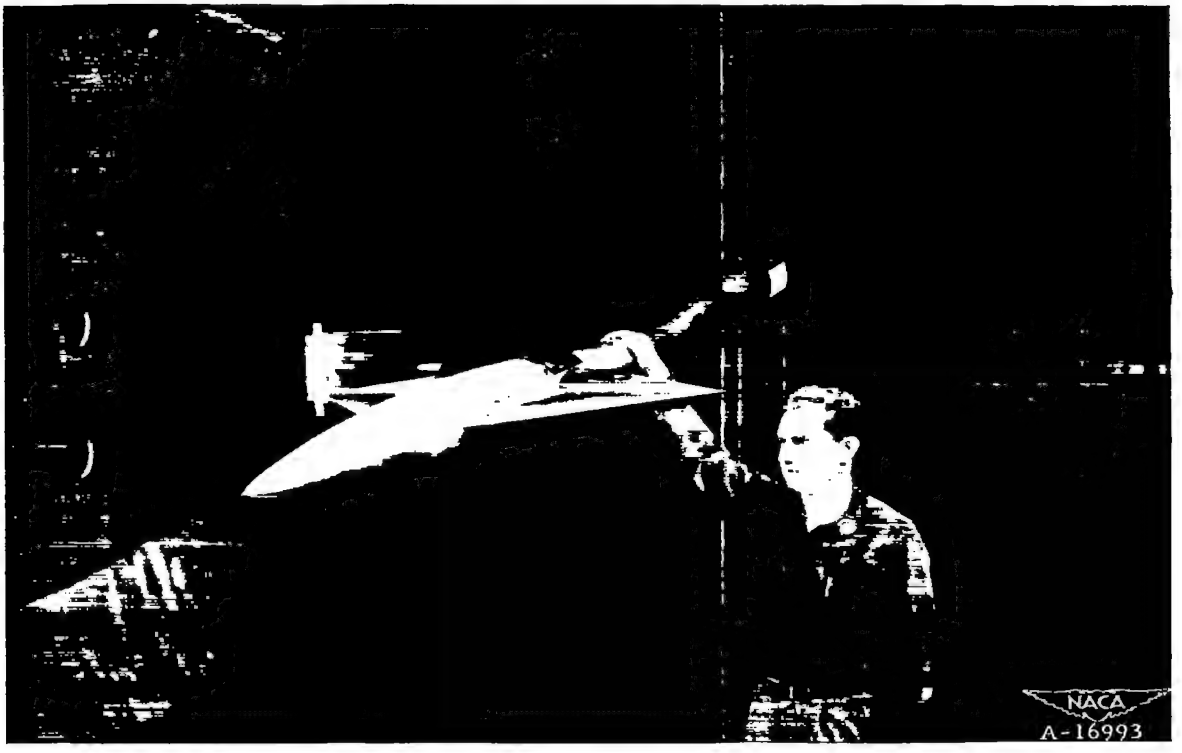

Figure 1.– A photograph of the model in the Ames 12–foot pressure wind tunnel.

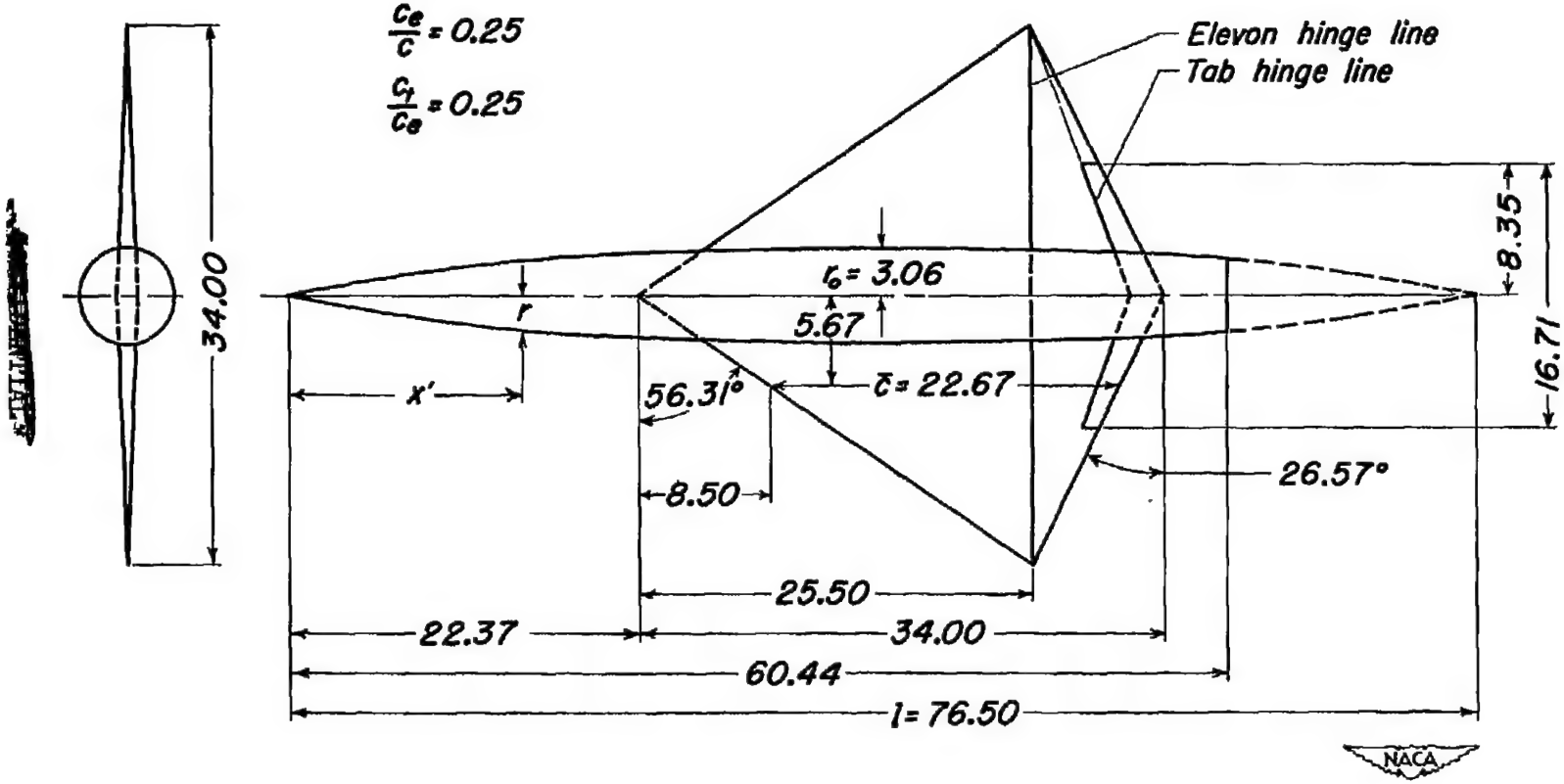

Figure 2.- Plan and front views of the model.

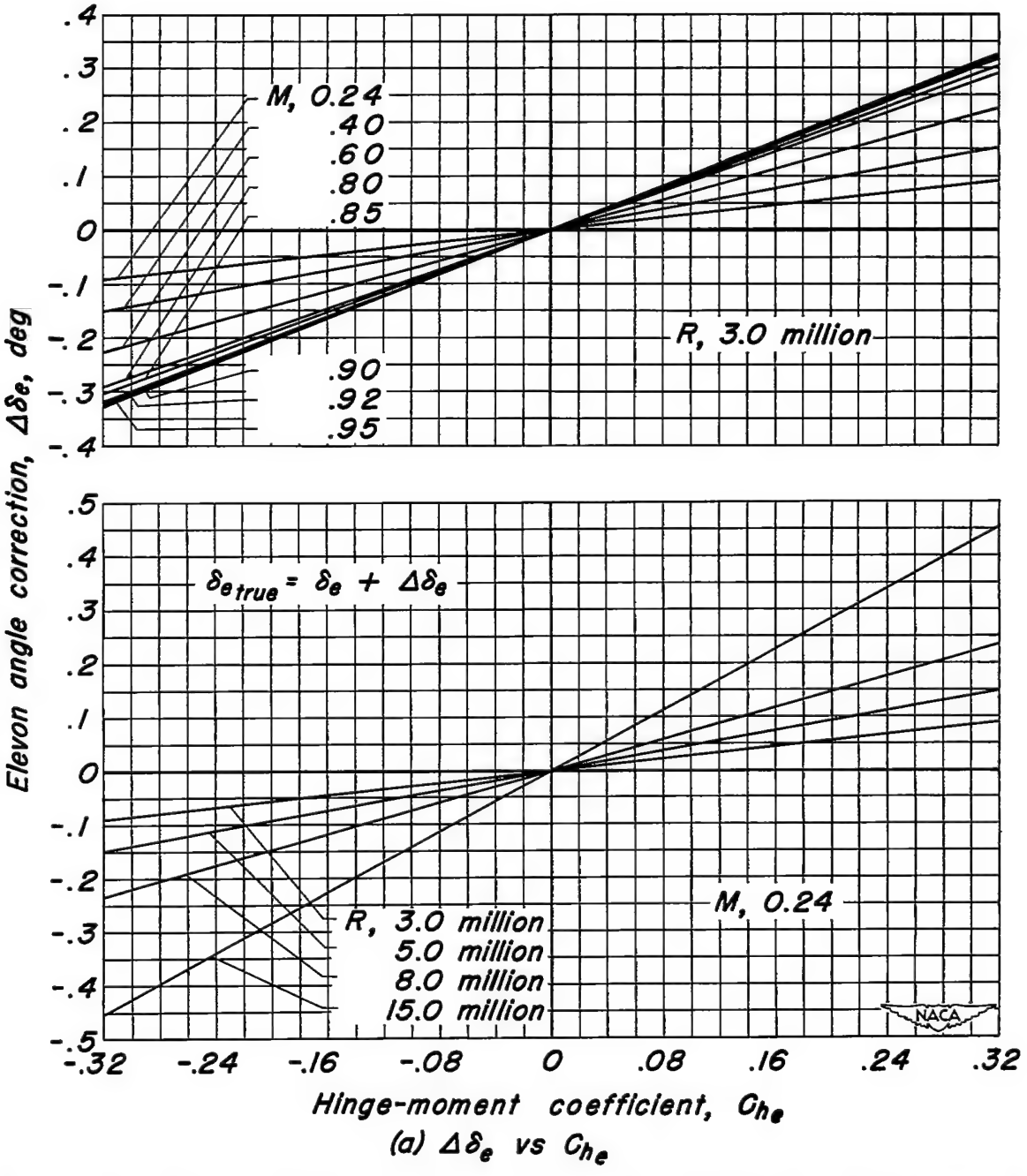

(a) $\Delta\delta_e$ vs C_{h_e}

Figure 3.- The variation with hinge-moment coefficient of the elevon and tab-angle corrections, $\Delta\delta$, at various Mach numbers and Reynolds numbers.

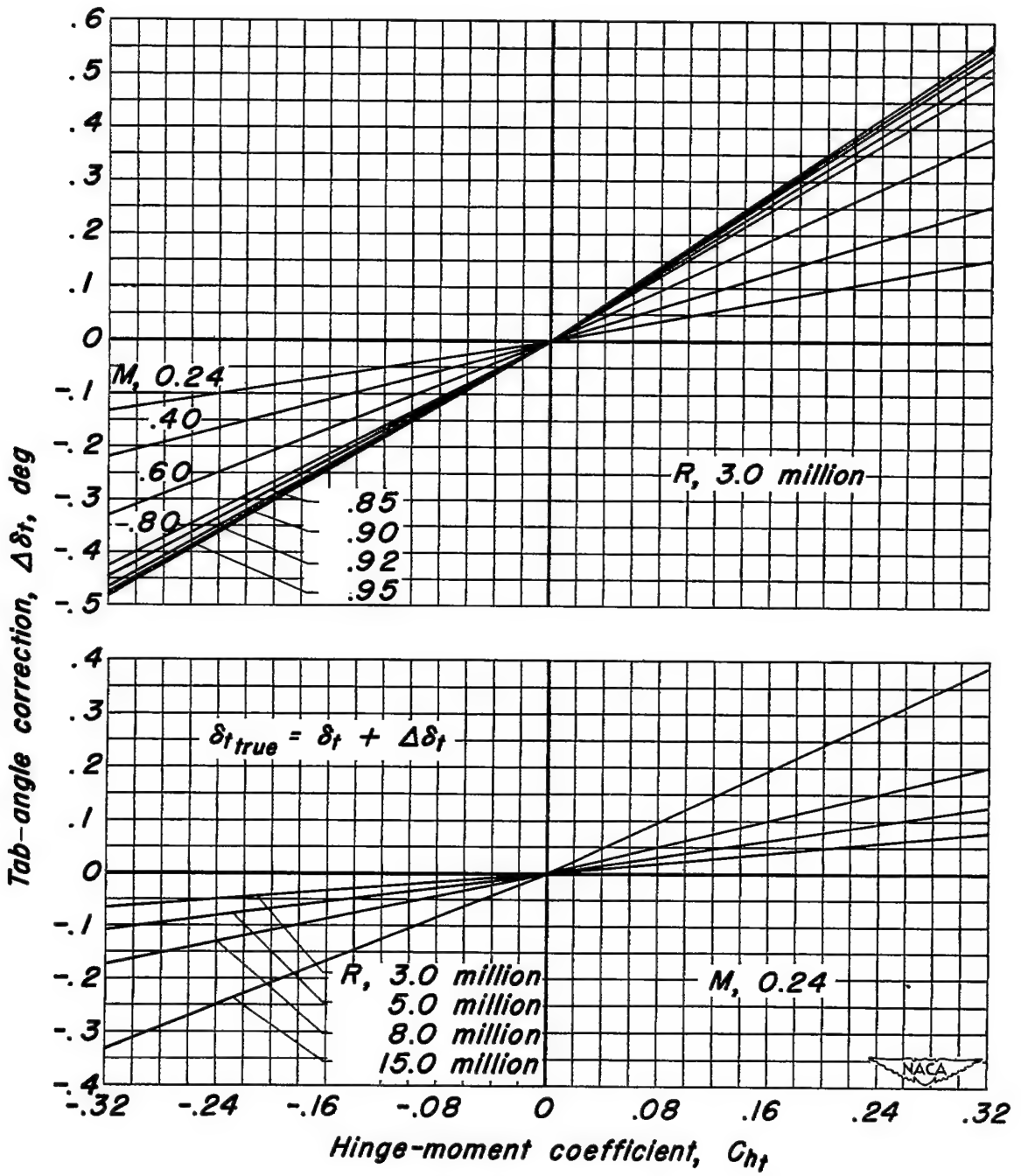

(b) $\Delta\delta_t$ vs C_{h_t}

Figure 3.- Concluded.

[redacted]

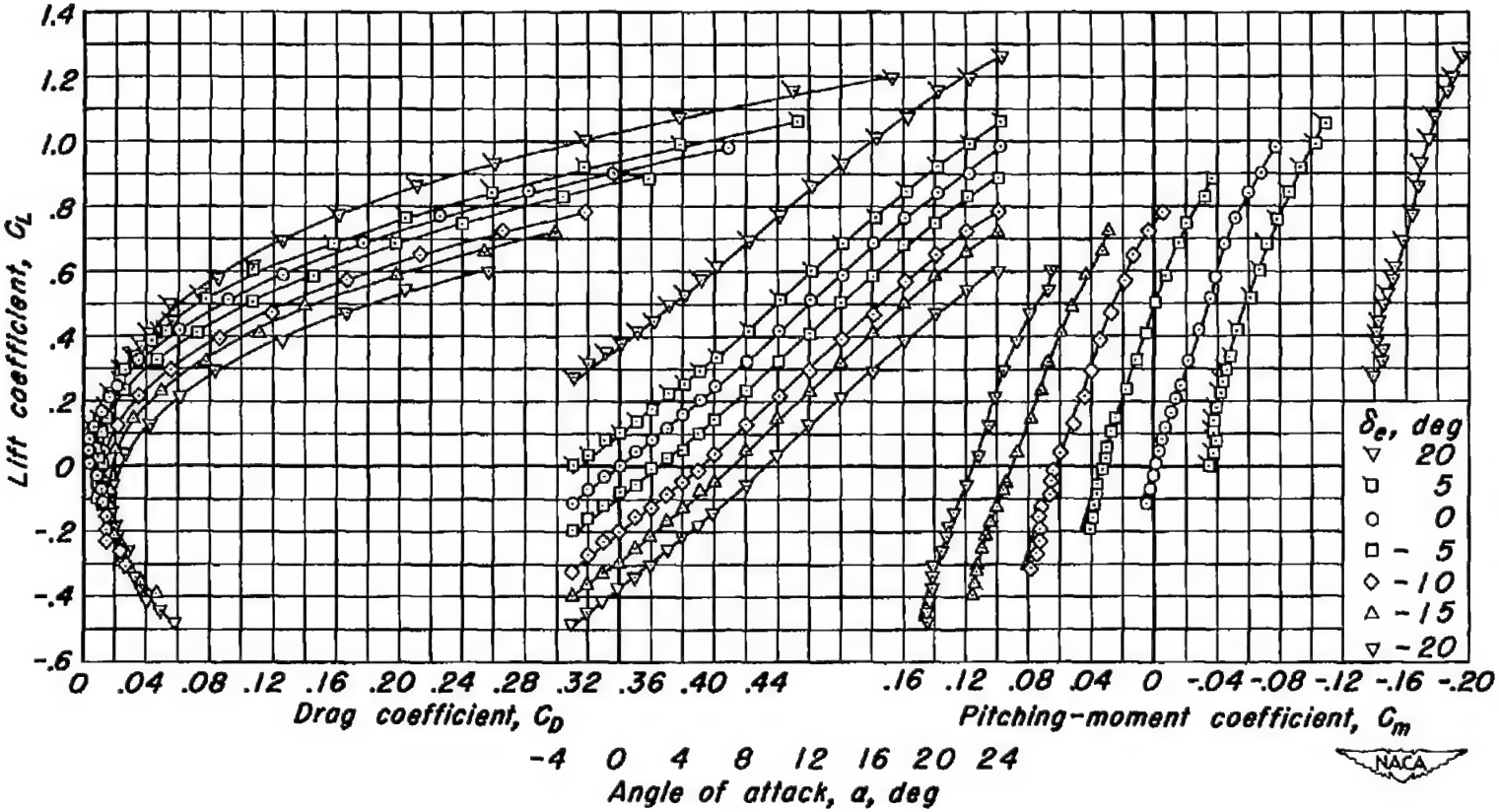

(a) C_L vs C_D, C_L vs α, C_L vs C_m

Figure 4.- The effect of elevon deflection on the aerodynamic characteristics at a Mach number of 0.24. R, 3.0 million; δ_t, 0°.

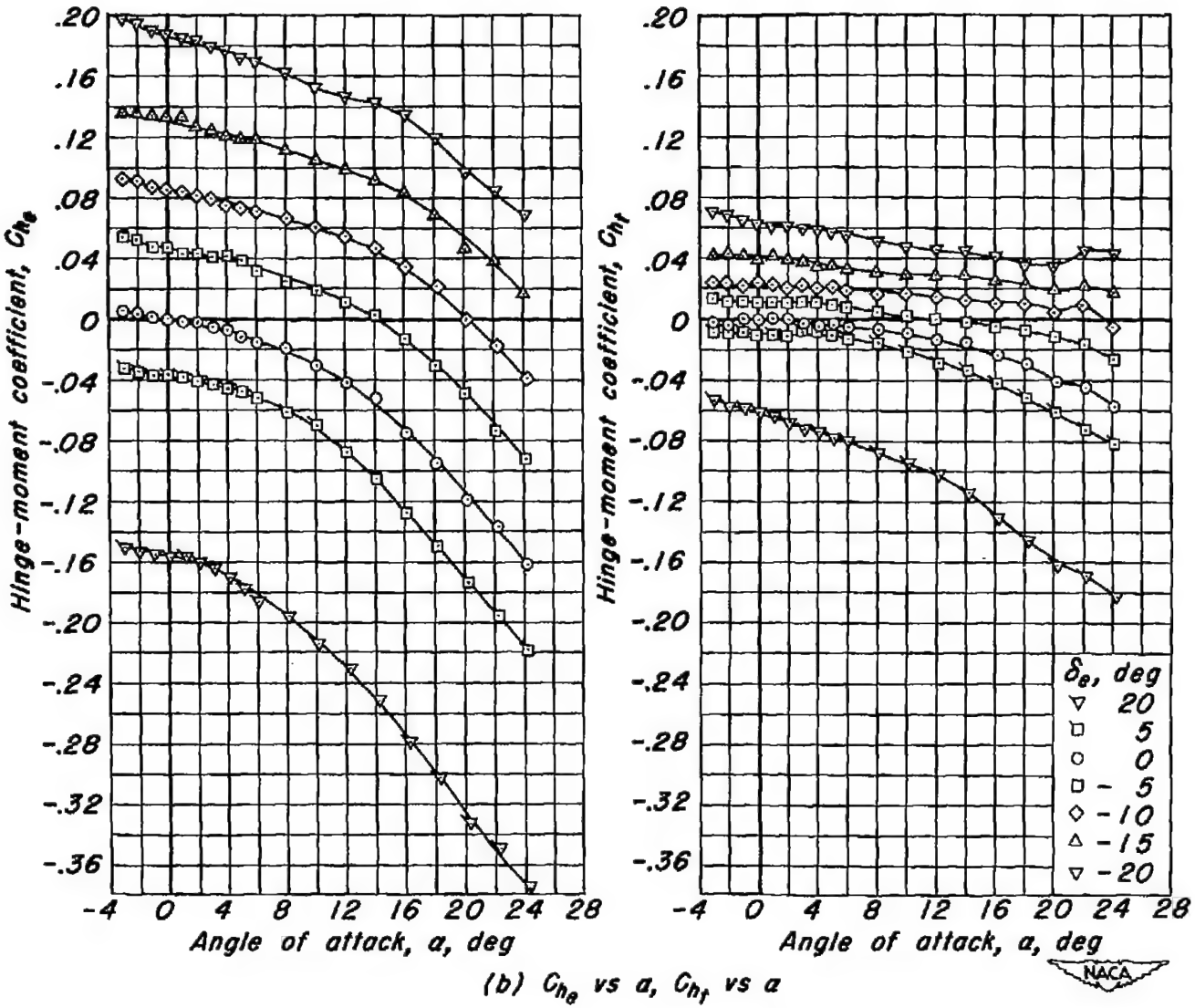

(b) C_{h_e} vs α, C_{h_f} vs α

Figure 4.- Continued.

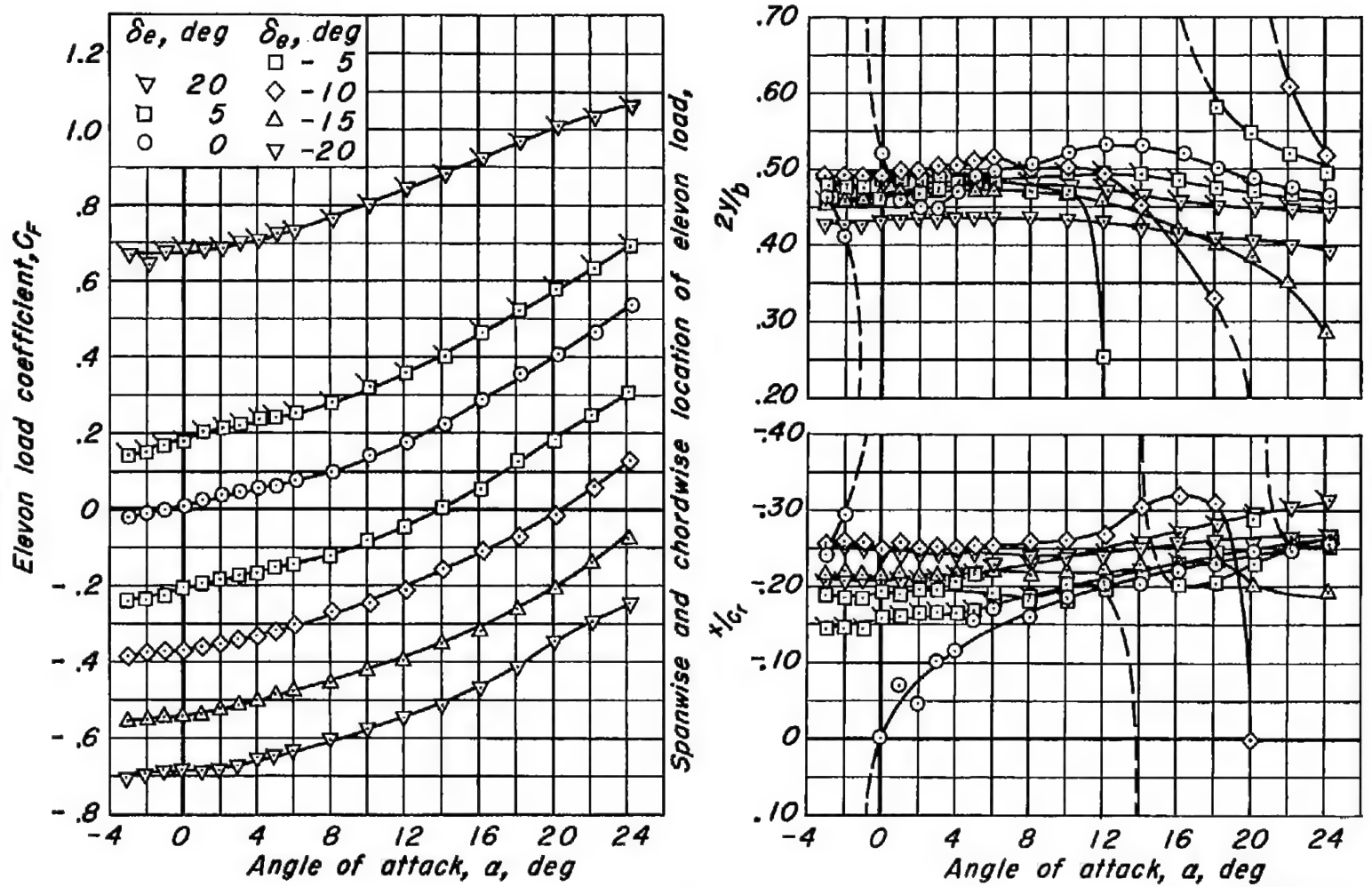

(c) C_F vs α, $2y/b$ vs α, x/c_r vs α

Figure 4.- Concluded.

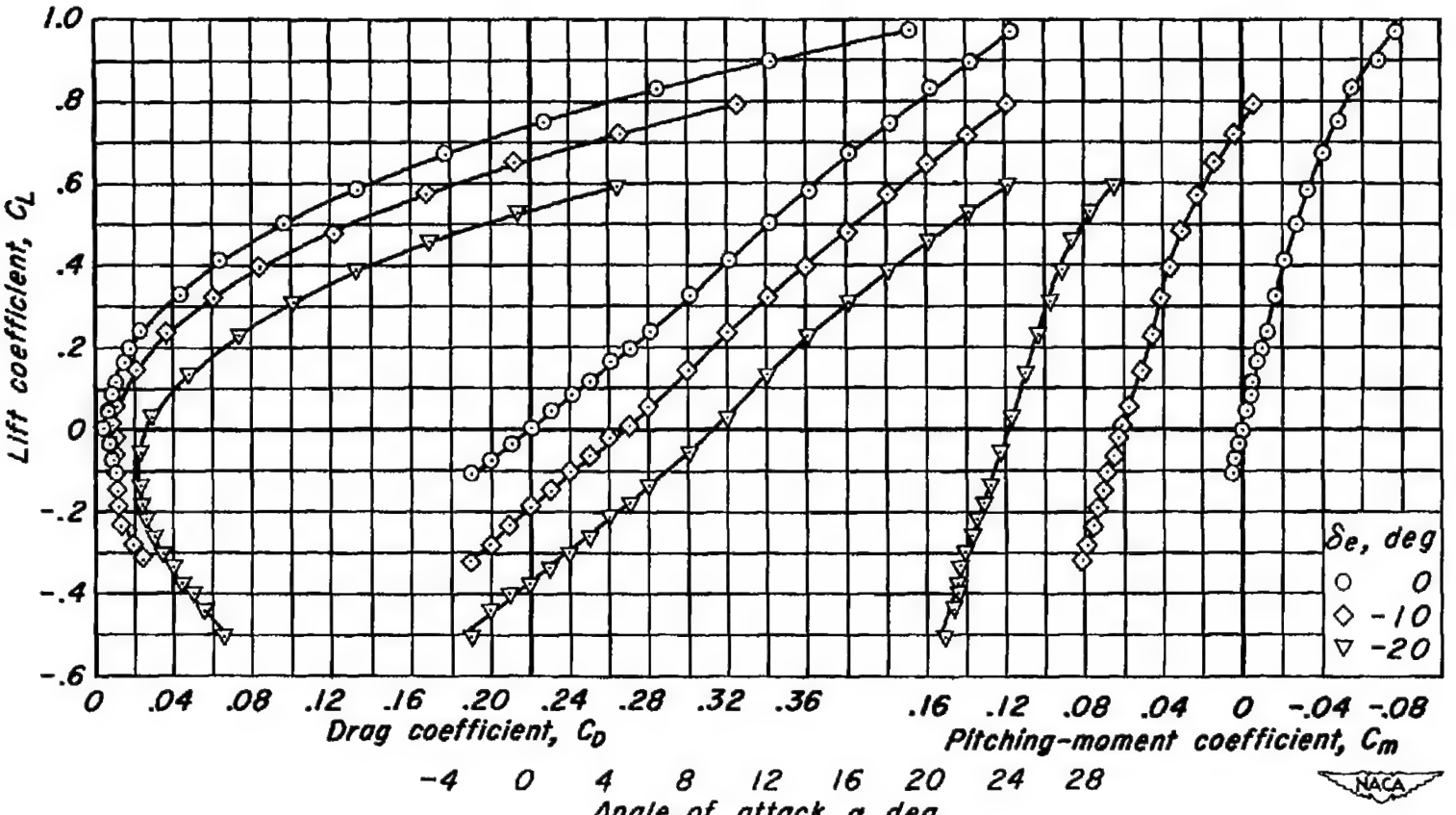

(a) C_L vs C_D, C_L vs a, C_L vs C_m

Figure 5.- The effect of elevon deflection on the aerodynamic characteristics at a Mach number of 0.40. R, 3.0 million; δ_f, 0°.

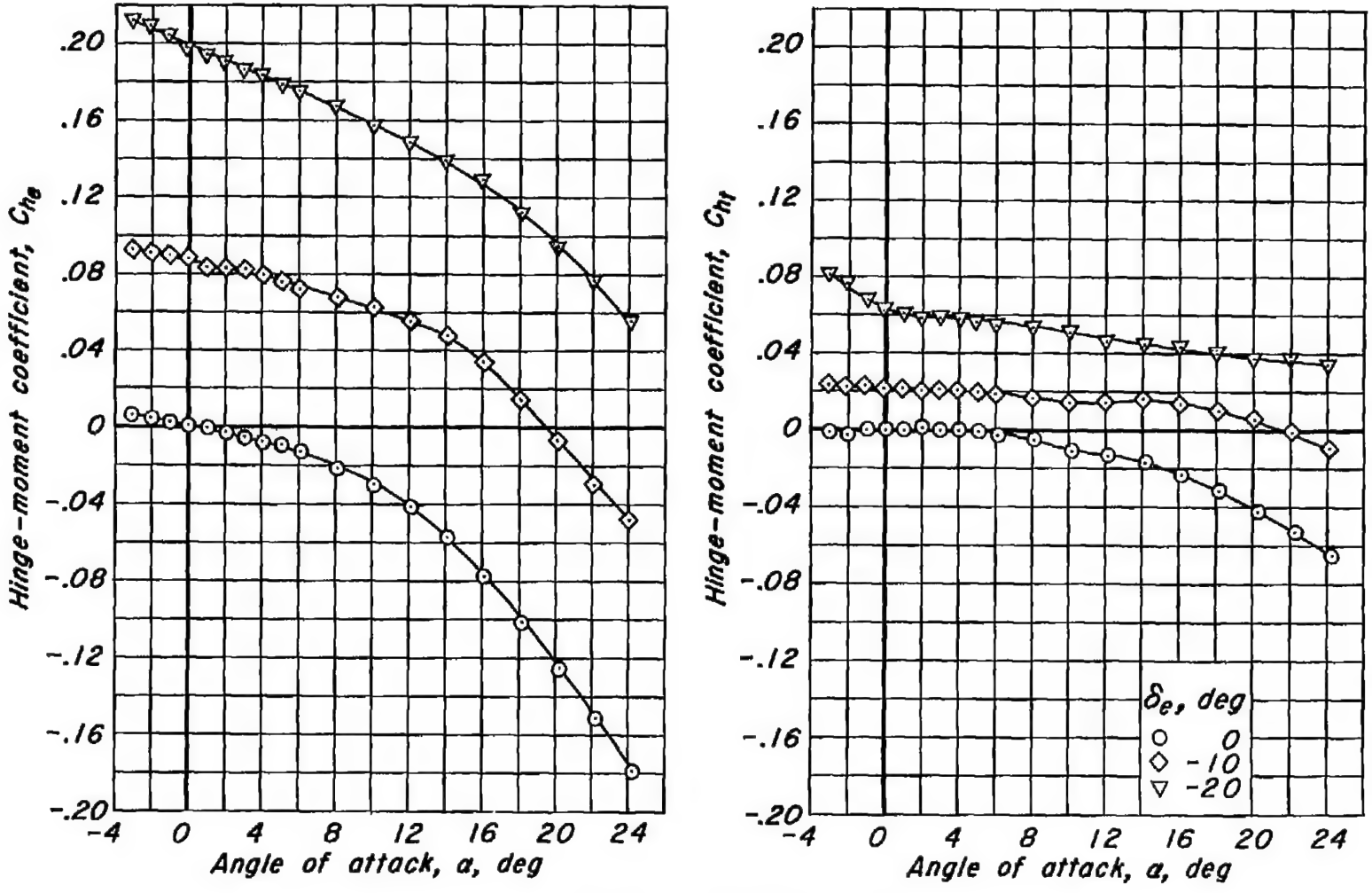

(b) C_{h_e} vs α, C_{h_f} vs α

Figure 5.- Continued.

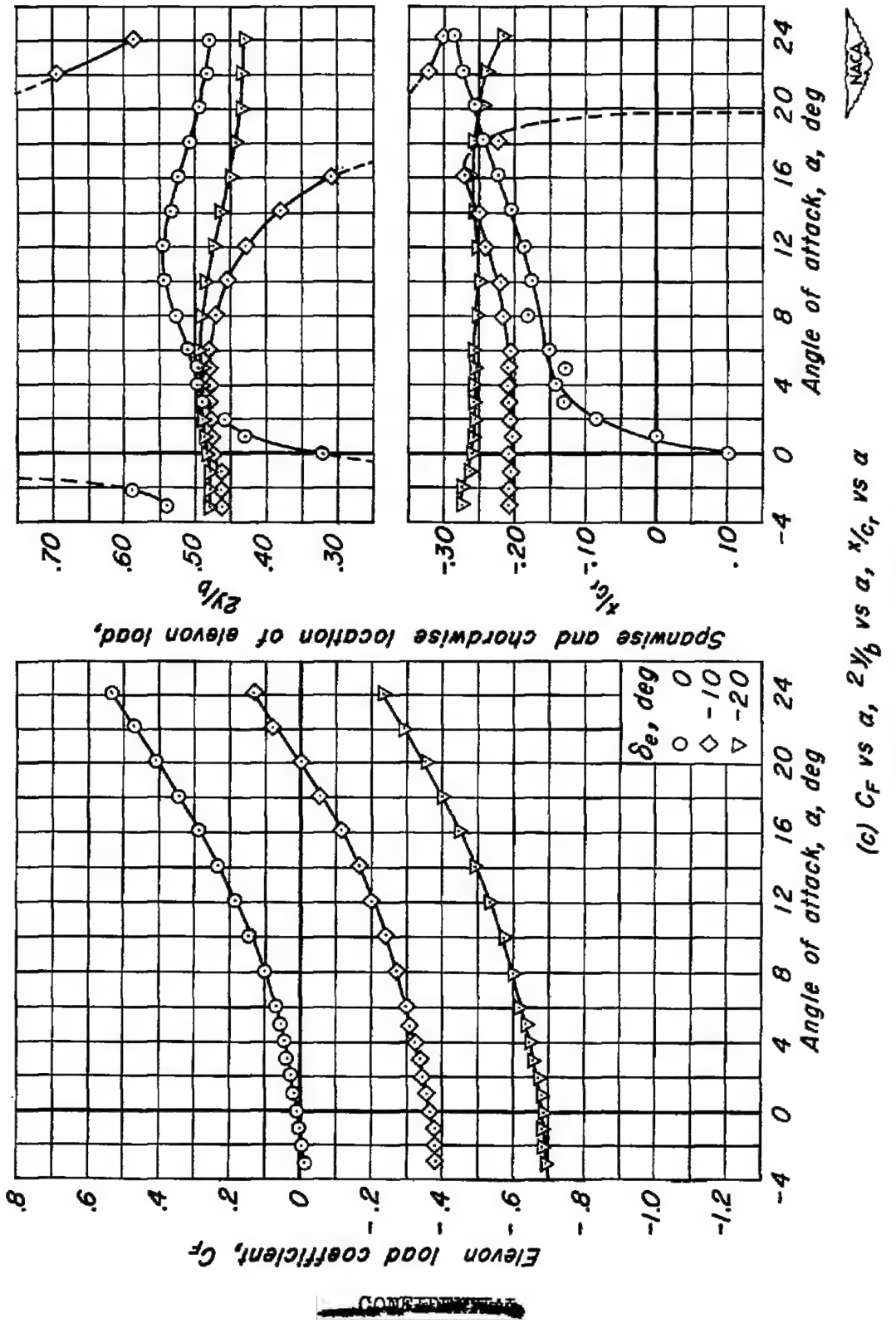

(c) C_F vs α, $2y/b$ vs α, x/c_r vs α

Figure 5.- Concluded.

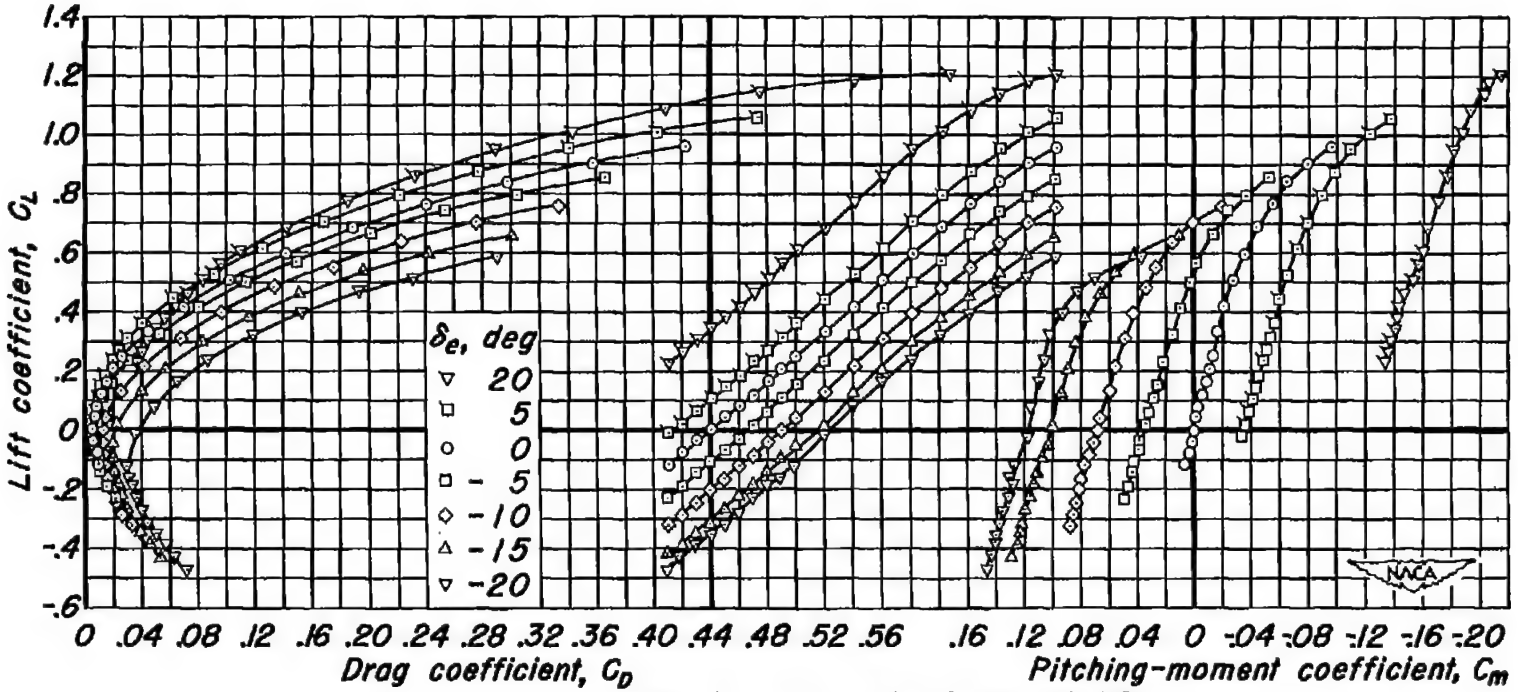

(a) C_L vs C_D, C_L vs α, C_L vs C_m

Figure 6.- The effect of elevon deflection on the aerodynamic characteristics at a Mach number of 0.60. R, 3.0 million; δ_f, 0°.

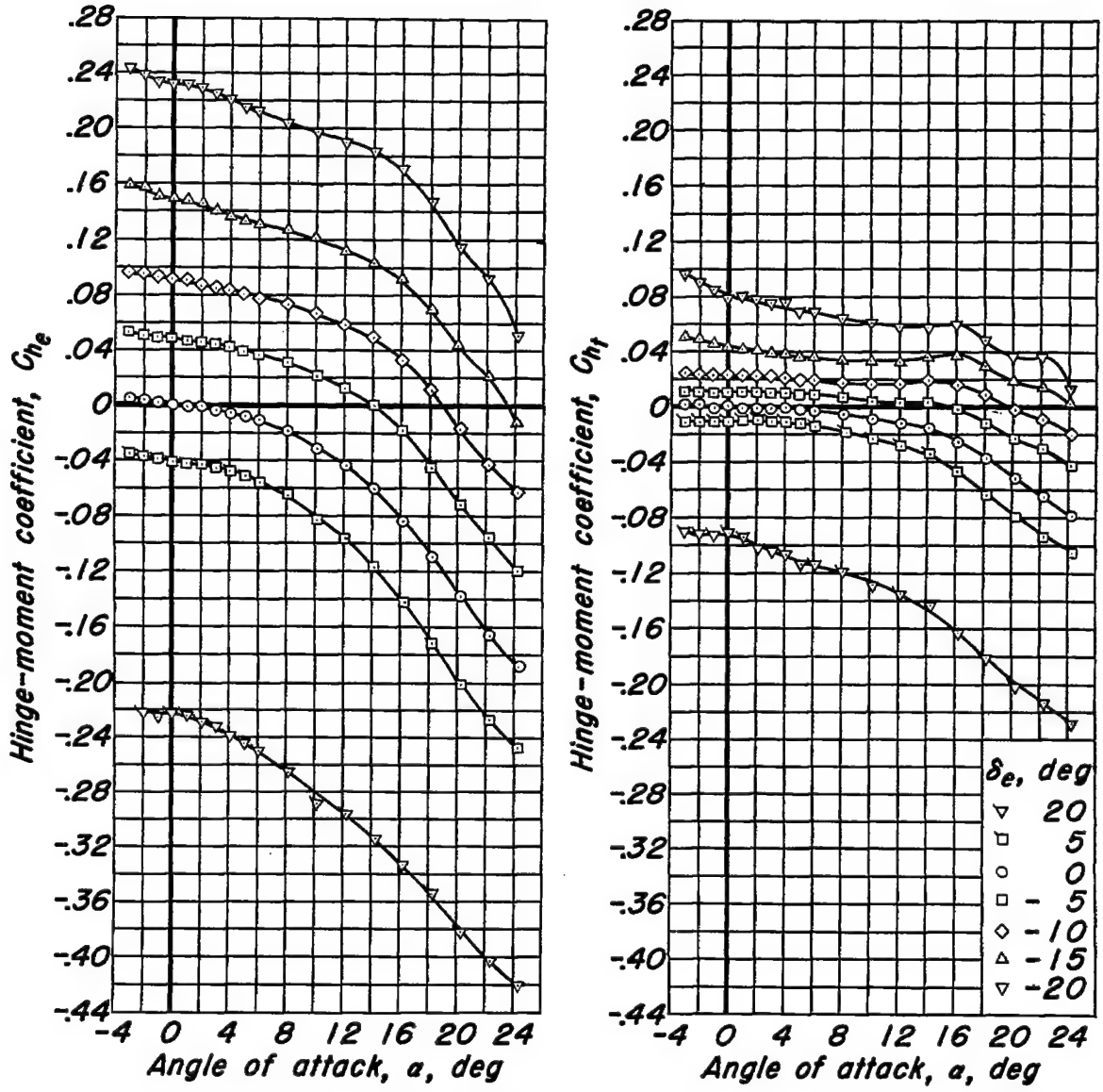

(b) C_{h_e} vs α, C_{h_t} vs α

Figure 6.- Continued.

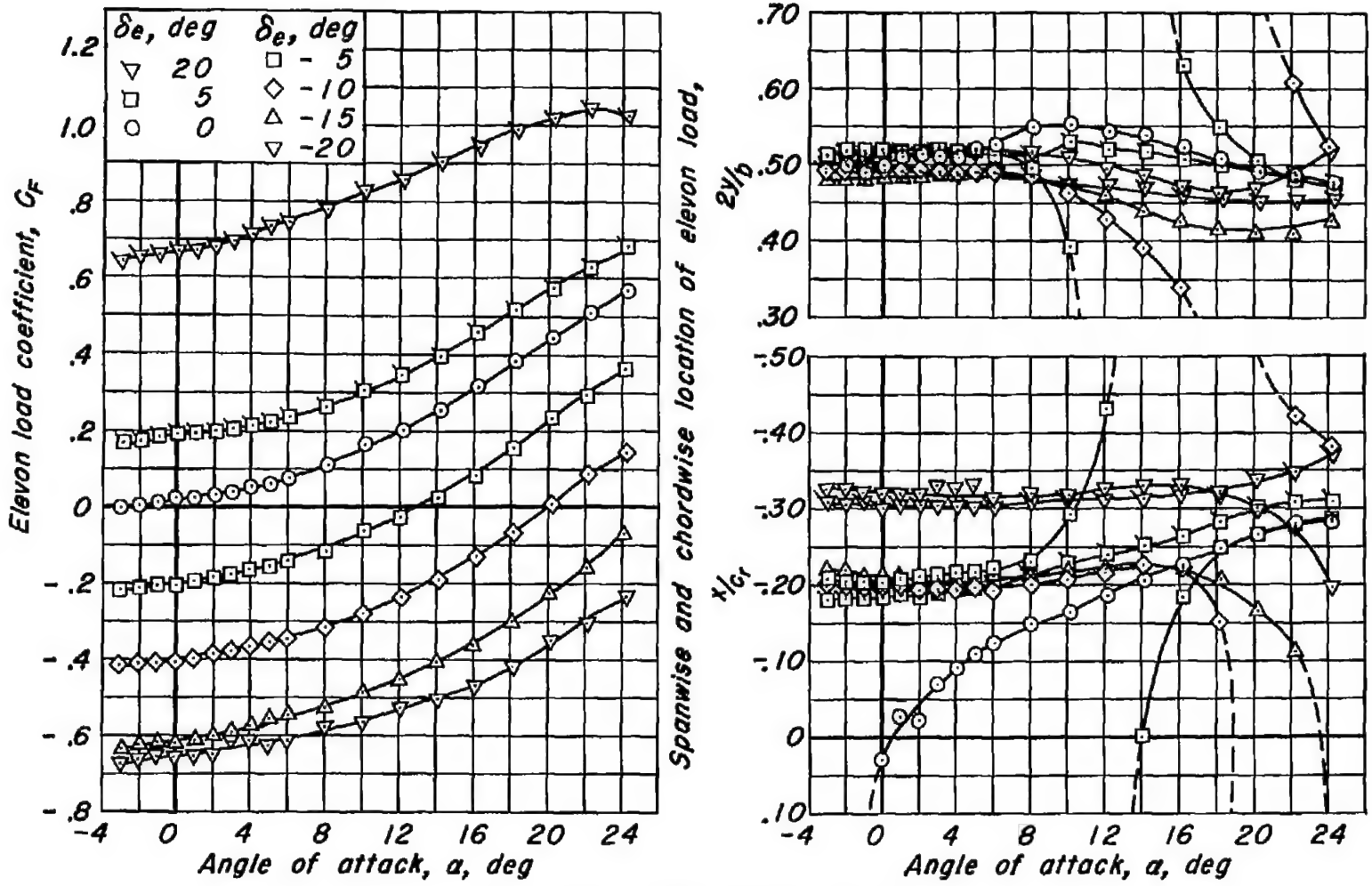

(c) C_F vs α, $2y/b$ vs α, x/c_r vs α

Figure 6.- Concluded.

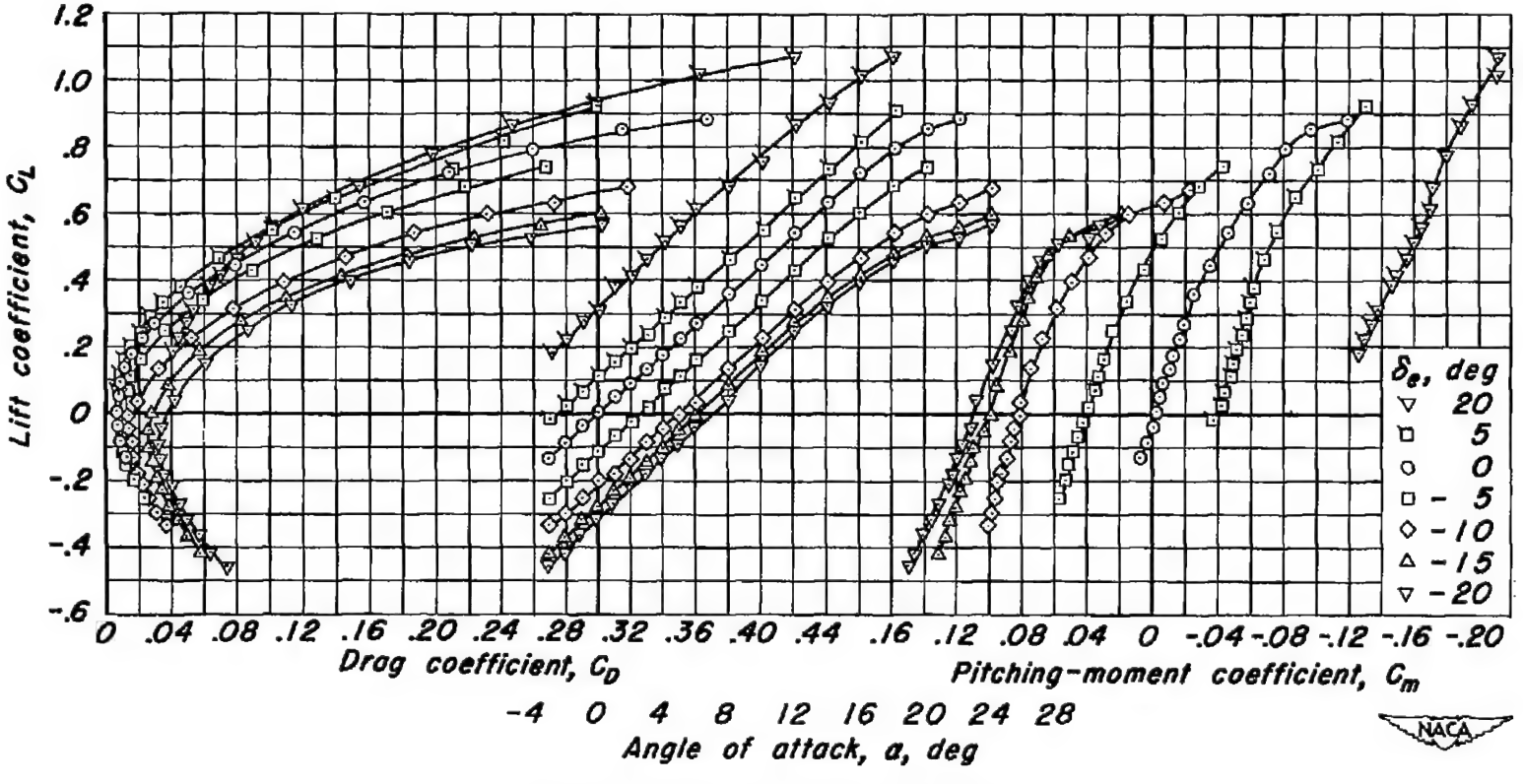

(a) C_L vs C_D, C_L vs α, C_L vs C_m

Figure 7.- The effect of elevon deflection on the aerodynamic characteristics at a Mach number of 0.80. R, 3.0 million; δ_f, 0°.

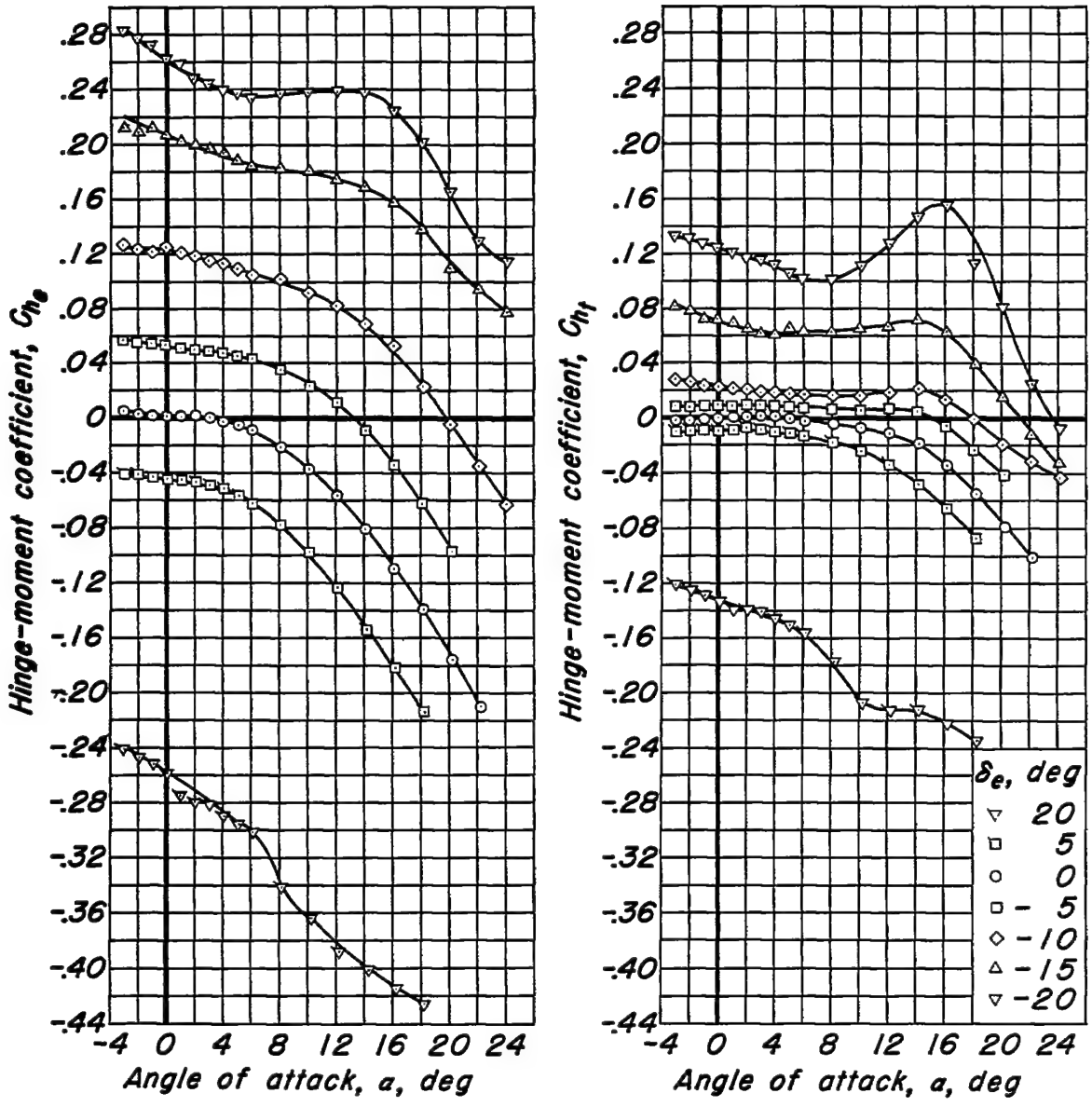

(b) C_{h_e} vs α, C_{h_f} vs α

Figure 7.- Continued.

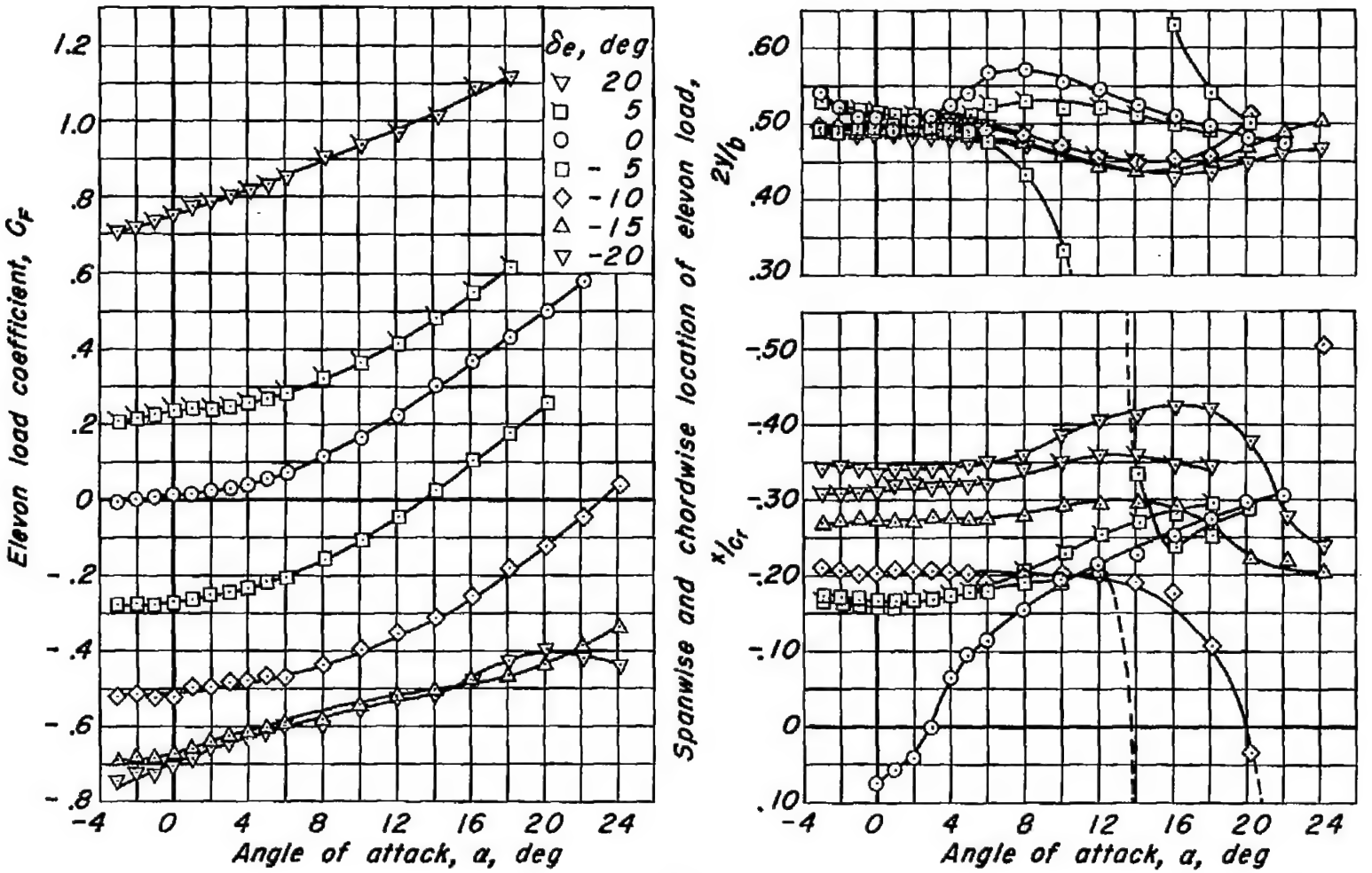

(c) C_F vs α, $2y/b$ vs α, x/c_r vs α

Figure 7.- Concluded.

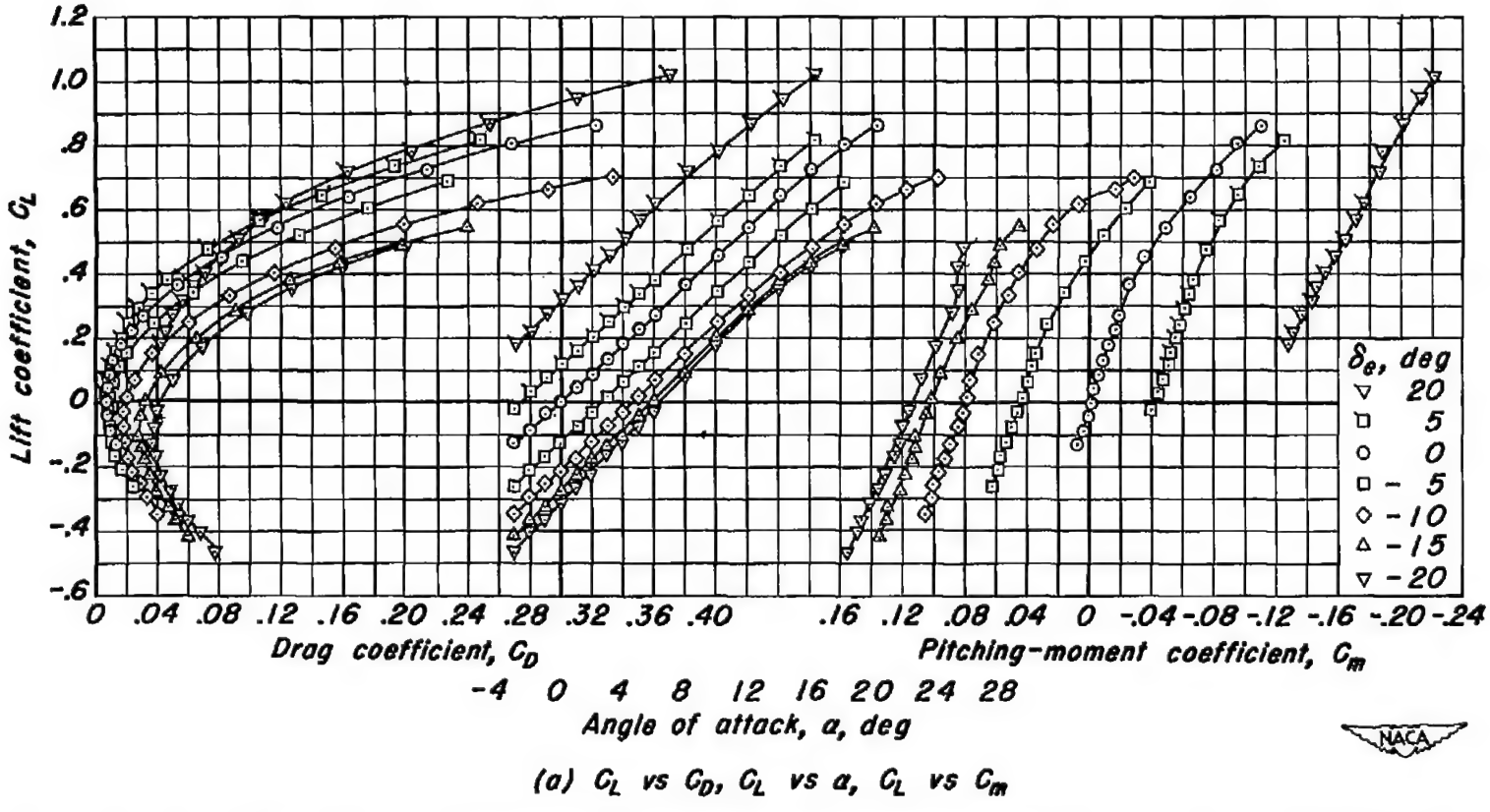

(a) C_L vs C_D, C_L vs α, C_L vs C_m

Figure 8.- The effect of elevon deflection on the aerodynamic characteristics at a Mach number of 0.85. R, 3.0 million; δ_t, 0°.

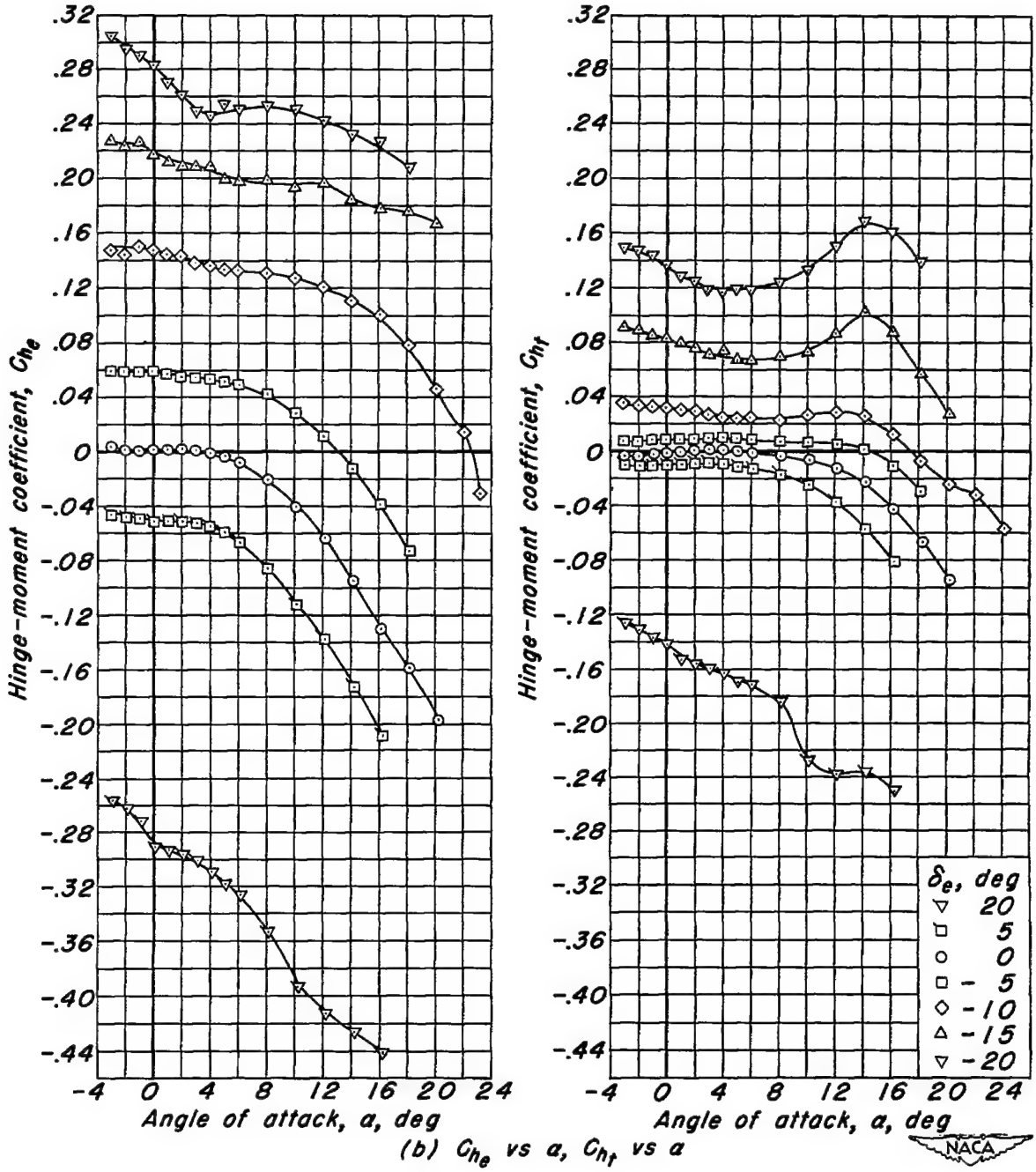

(b) C_{h_e} vs α, C_{h_f} vs α

Figure 8.- Continued.

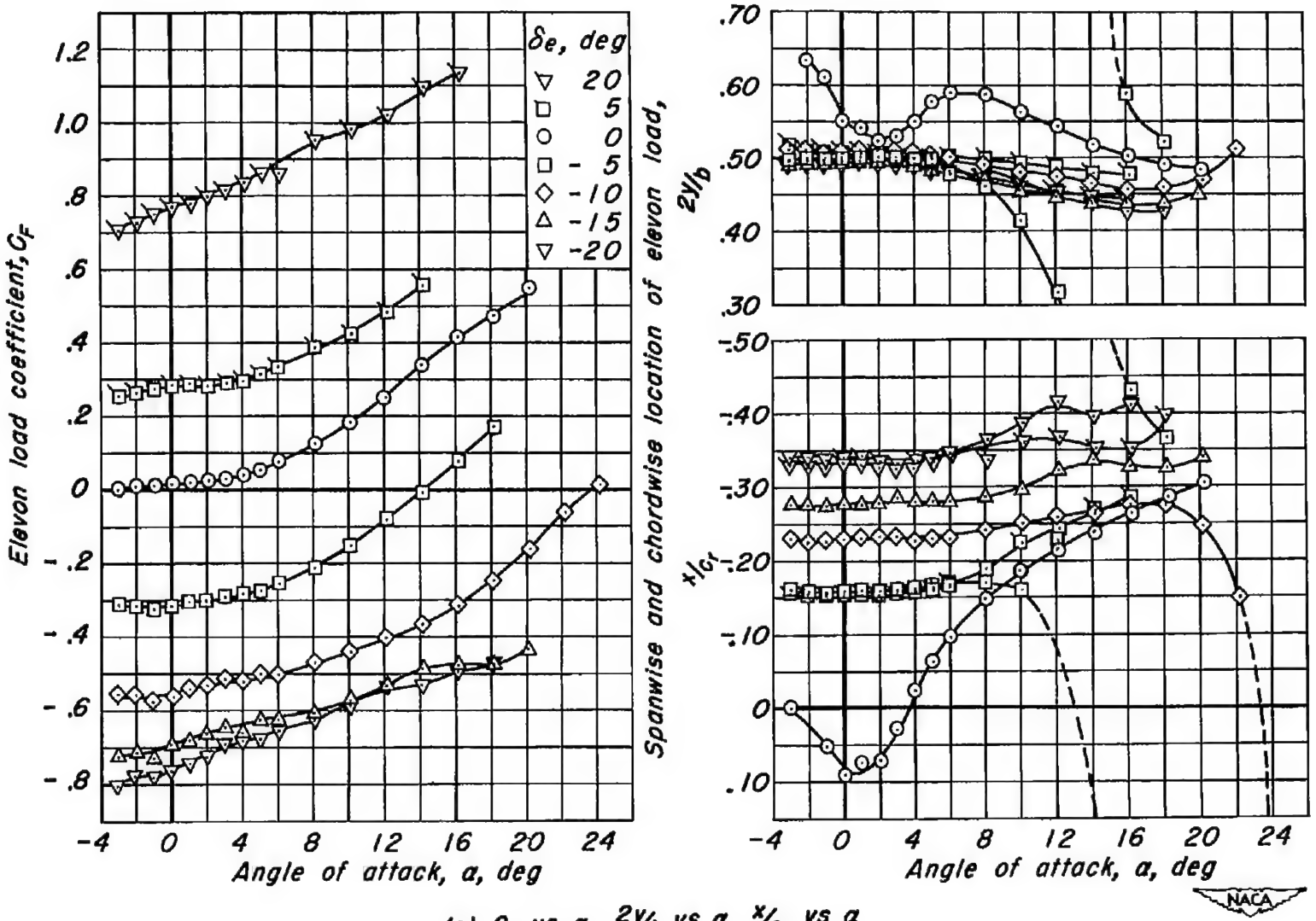

(c) C_F vs α, $2y/b$ vs α, x/c_r vs α

Figure 8.- Concluded.

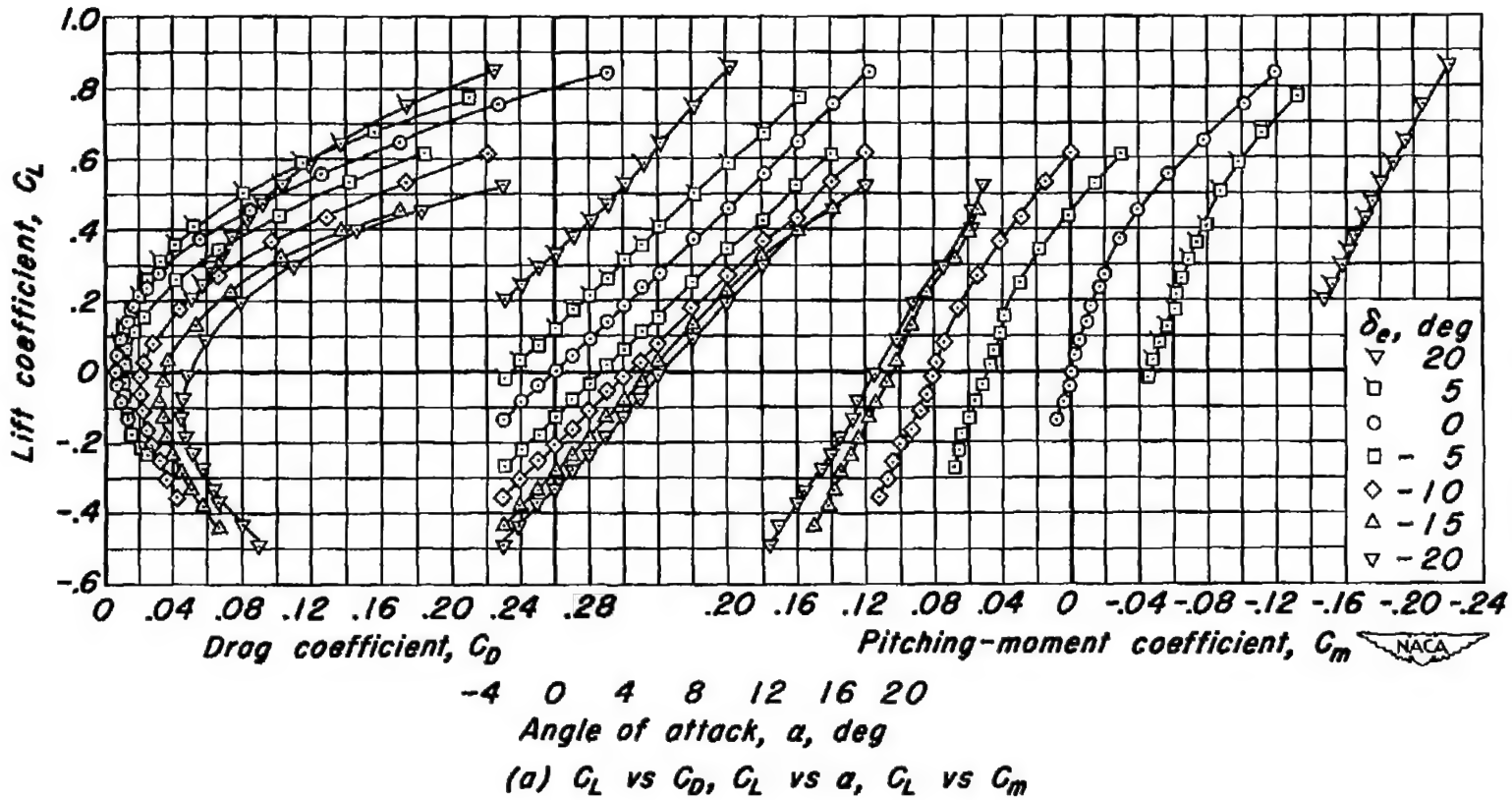

(a) C_L vs C_D, C_L vs α, C_L vs C_m

Figure 9.–The effect of elevon deflection on the aerodynamic characteristics at a Mach number of 0.90. R, 3.0 million; δ_t, 0°.

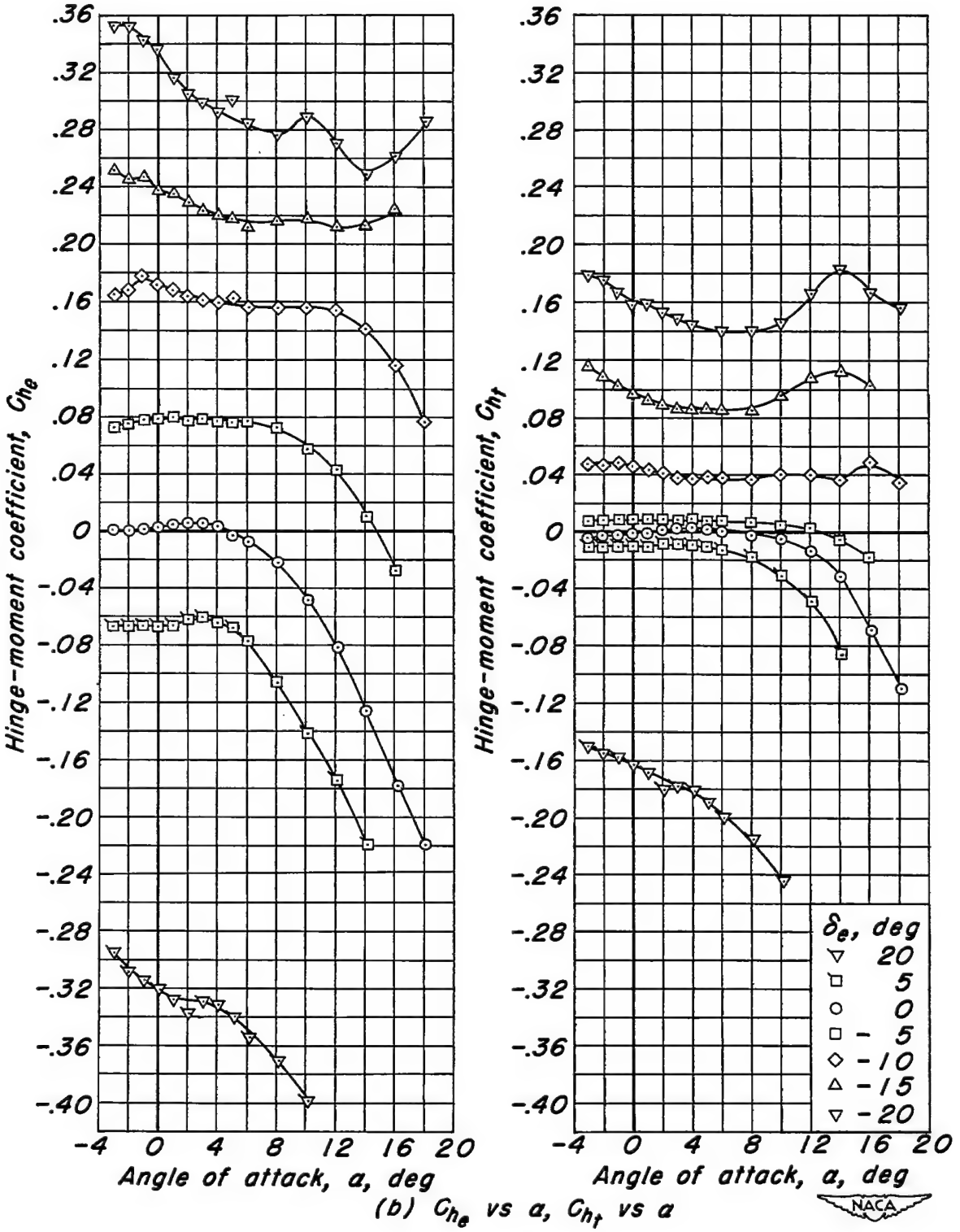

(b) C_{h_e} vs α, C_{h_t} vs α

Figure 9.- Continued.

[redacted]

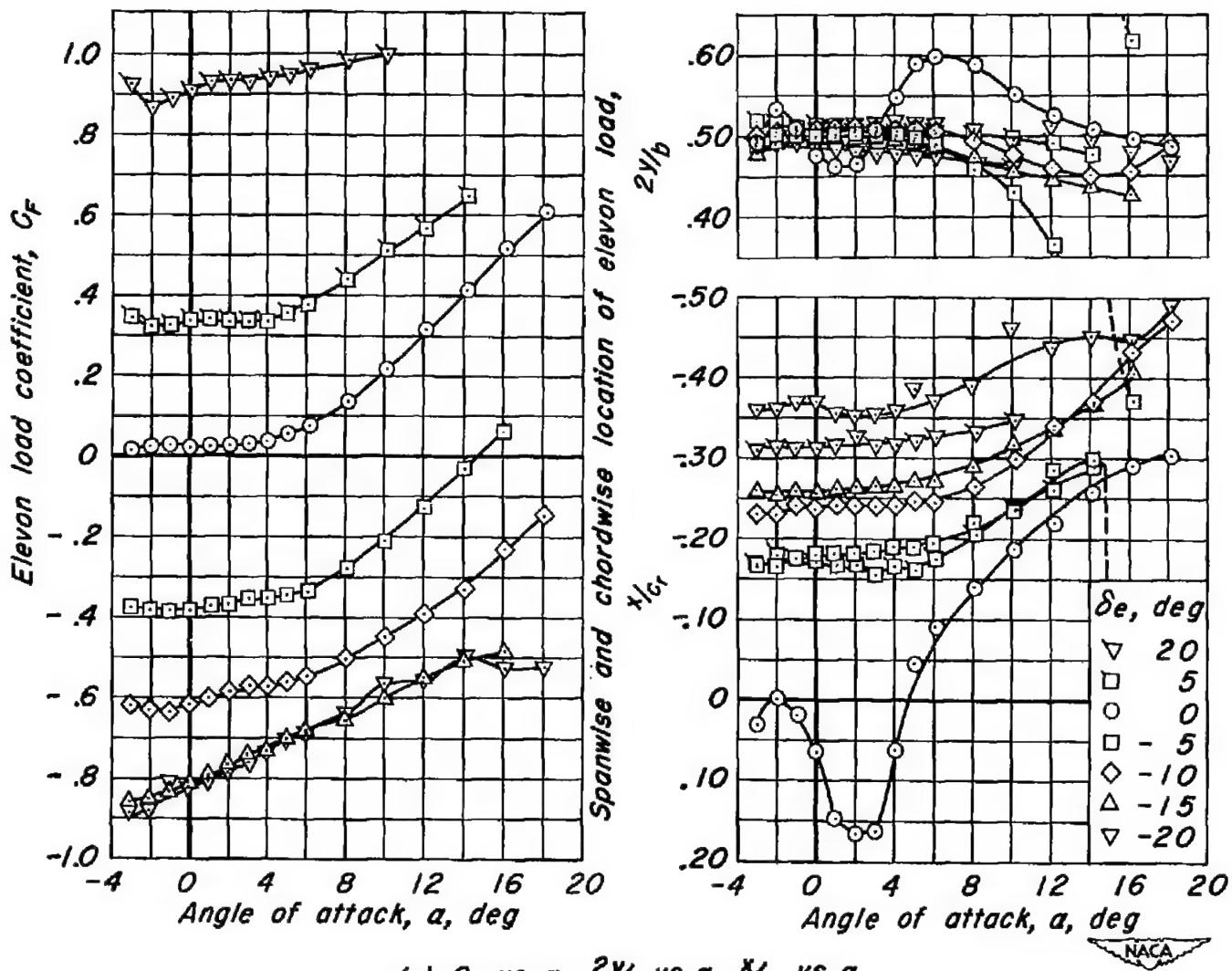

(c) C_F vs a, $2y/b$ vs a, x/c_r vs a

Figure 9.- Concluded.

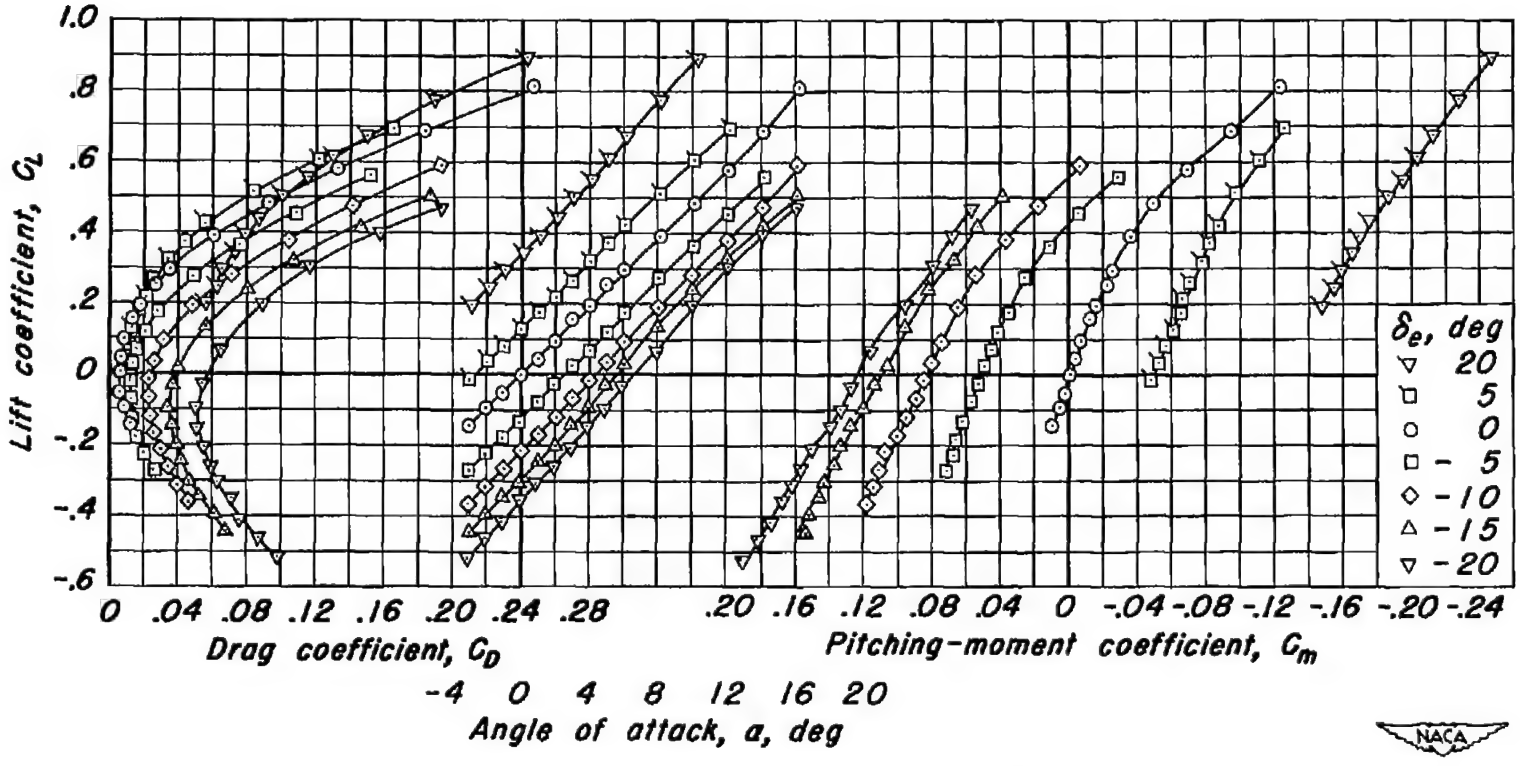

(a) C_L vs C_D, C_L vs α, C_L vs C_m

Figure 10.- The effect of elevon deflection on the aerodynamic characteristics at a Mach number of 0.92. R, 3.0 million; δ_t, 0°.

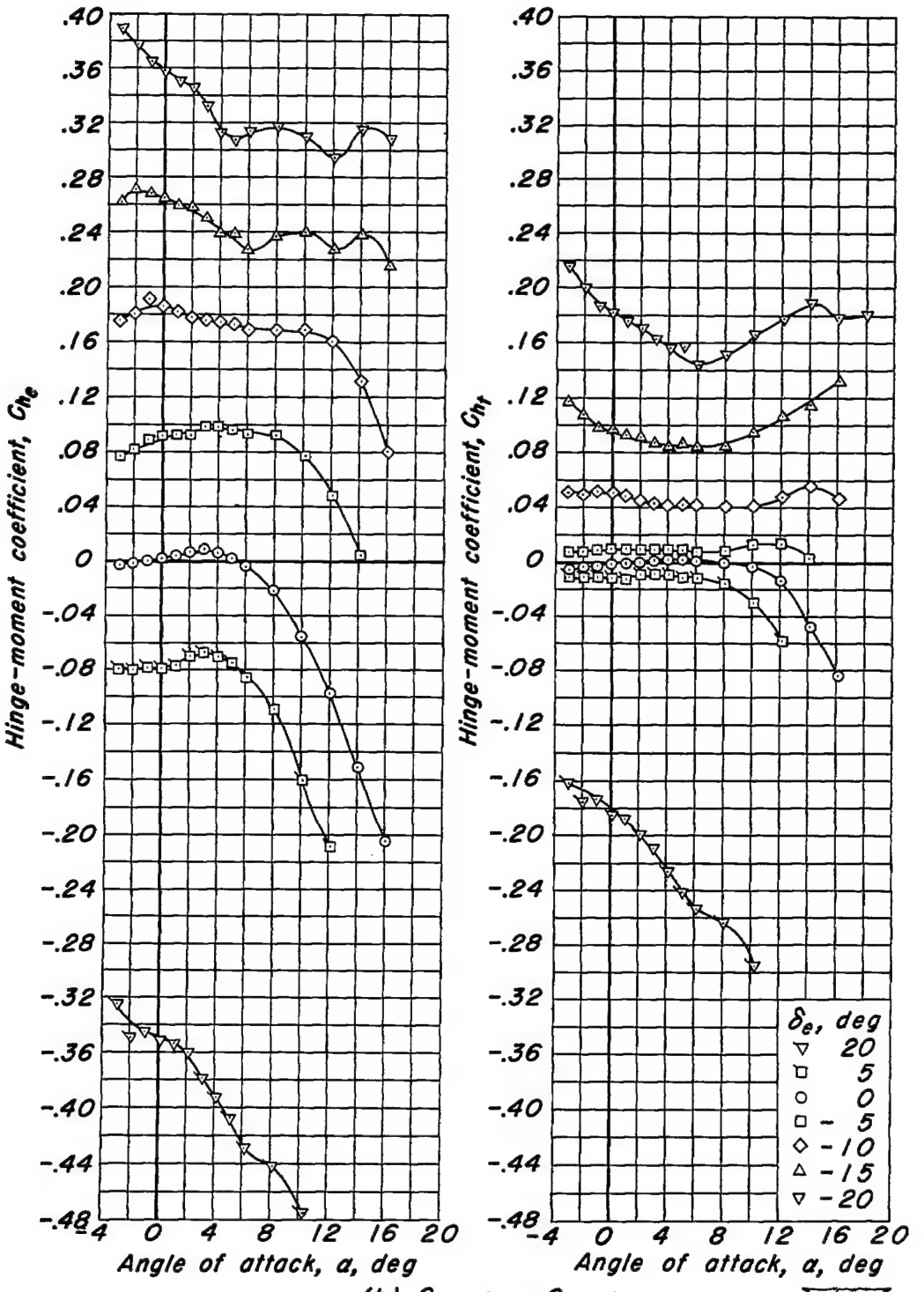

(b) C_{h_e} vs α, C_{h_f} vs α

Figure 10.- Continued.

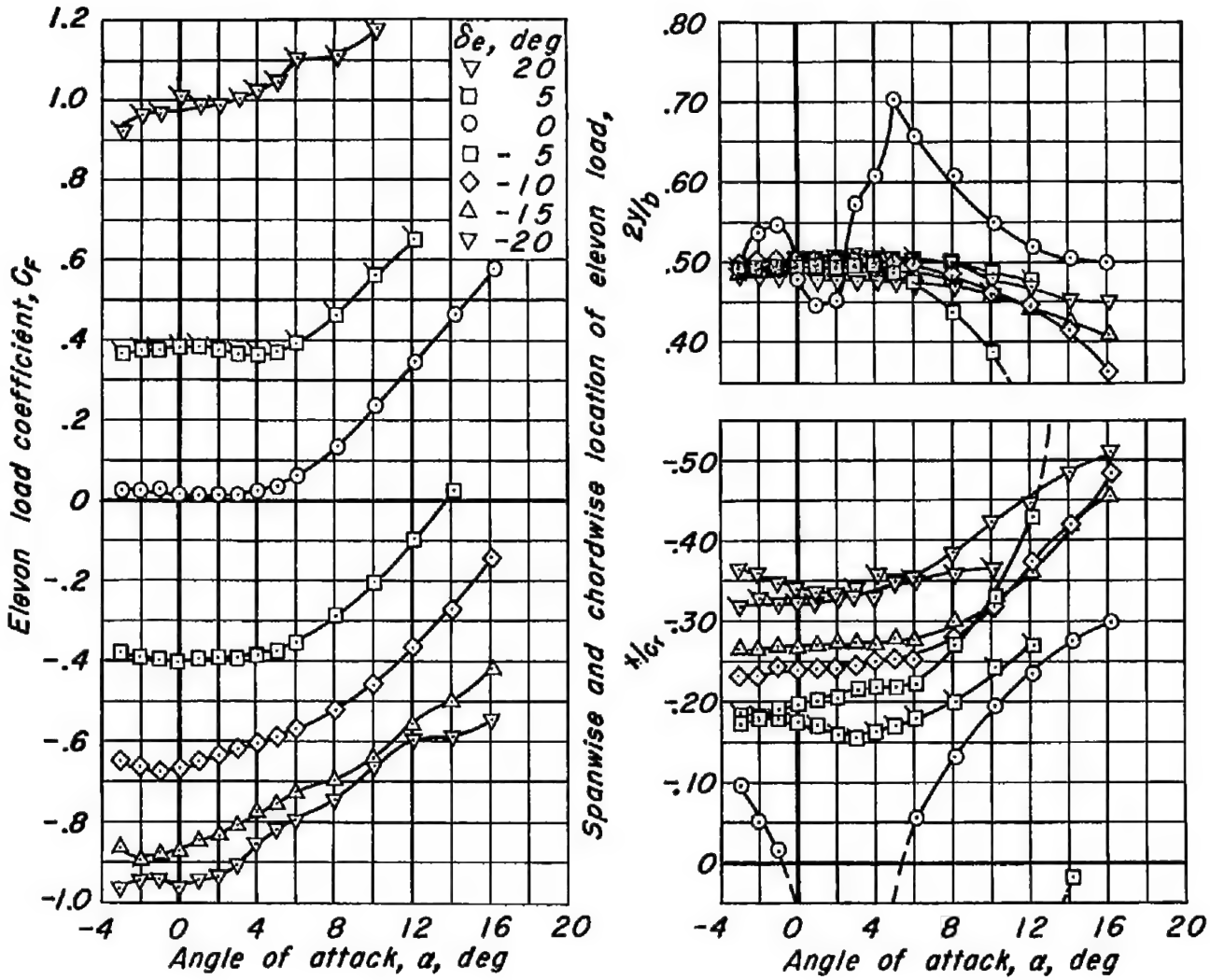

(c) C_F vs α, $2y/b$ vs α, x/c_r vs α

Figure 10.- Concluded.

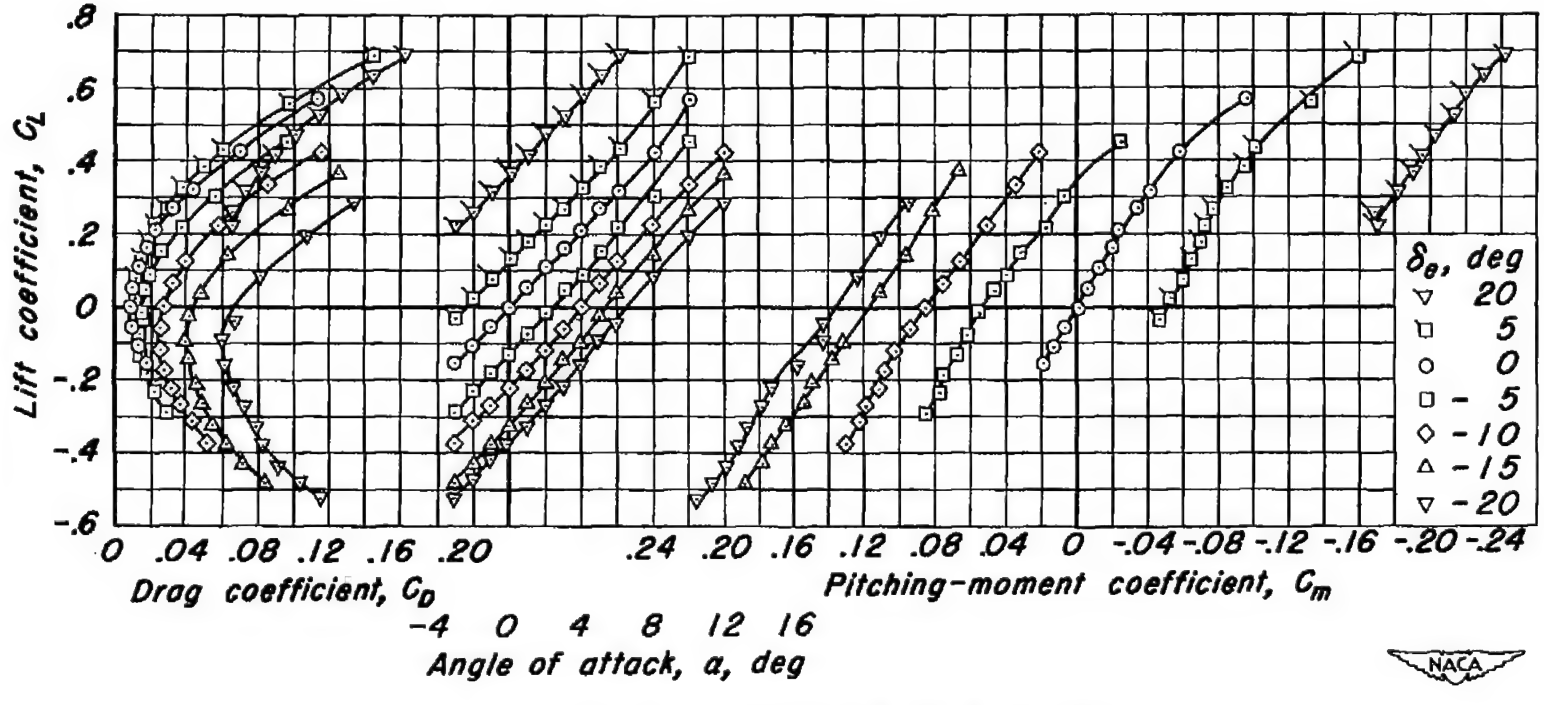

(a) C_L vs C_D, C_L vs α, C_L vs C_m

Figure 11.- The effect of elevon deflection on the aerodynamic characteristics at a Mach number of 0.95. R, 3.0 million; δ_t, 0°.

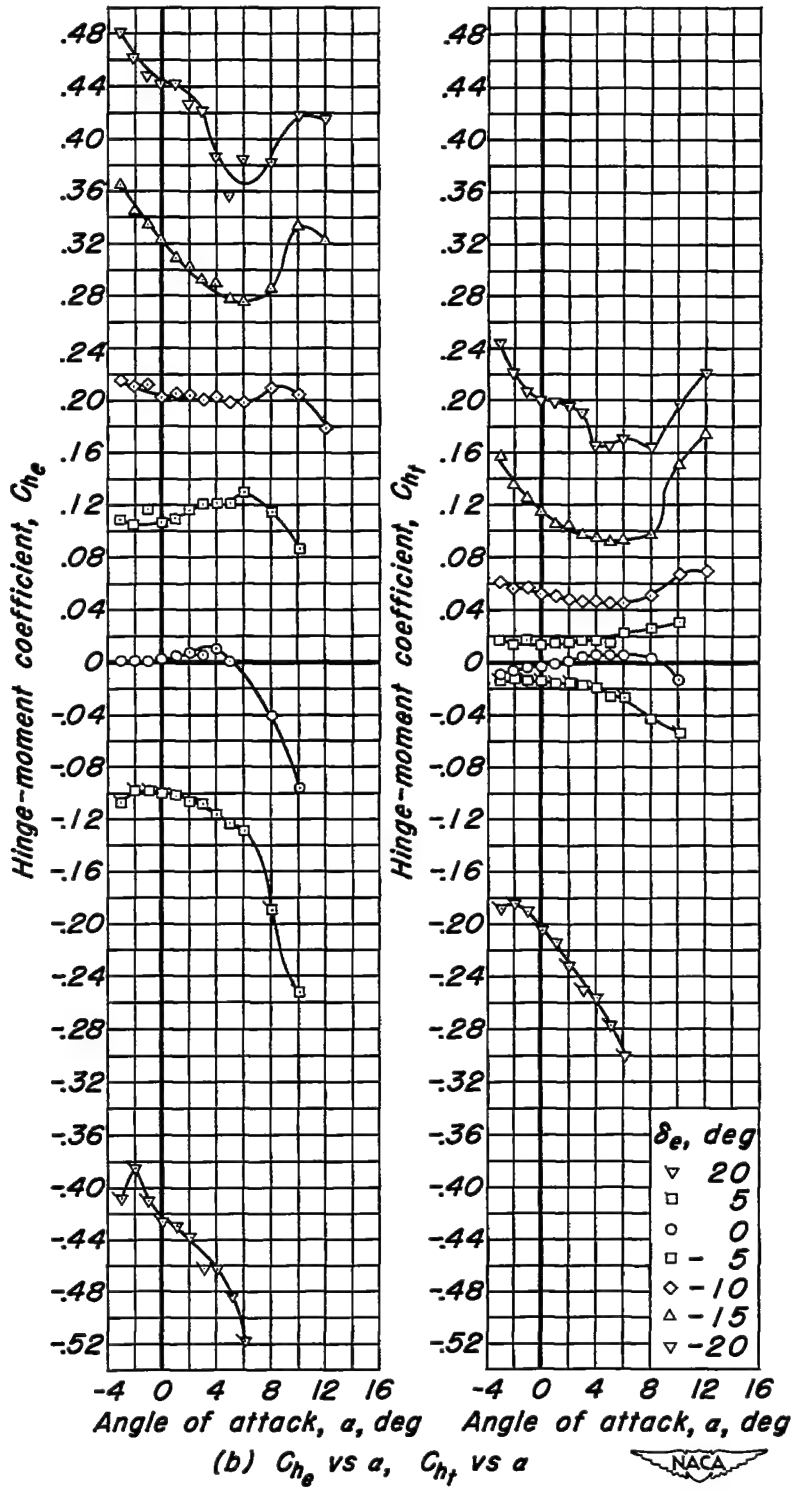

(b) C_{h_e} vs α, C_{h_t} vs α

Figure 11.- Continued.

[redacted]

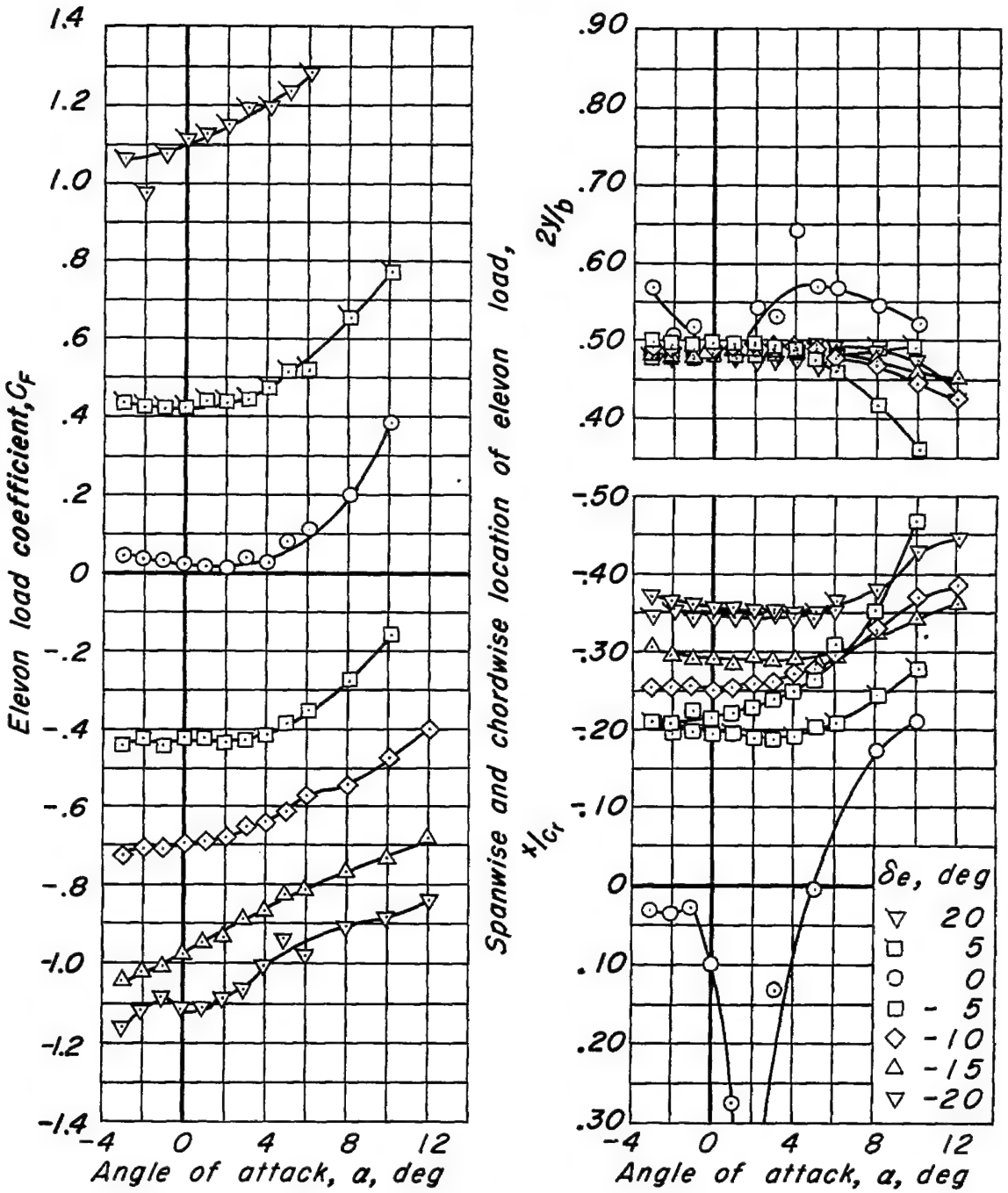

(c) C_F vs α, $2y/b$ vs α, x/c_r vs α

Figure 11.- Concluded.

[redacted]

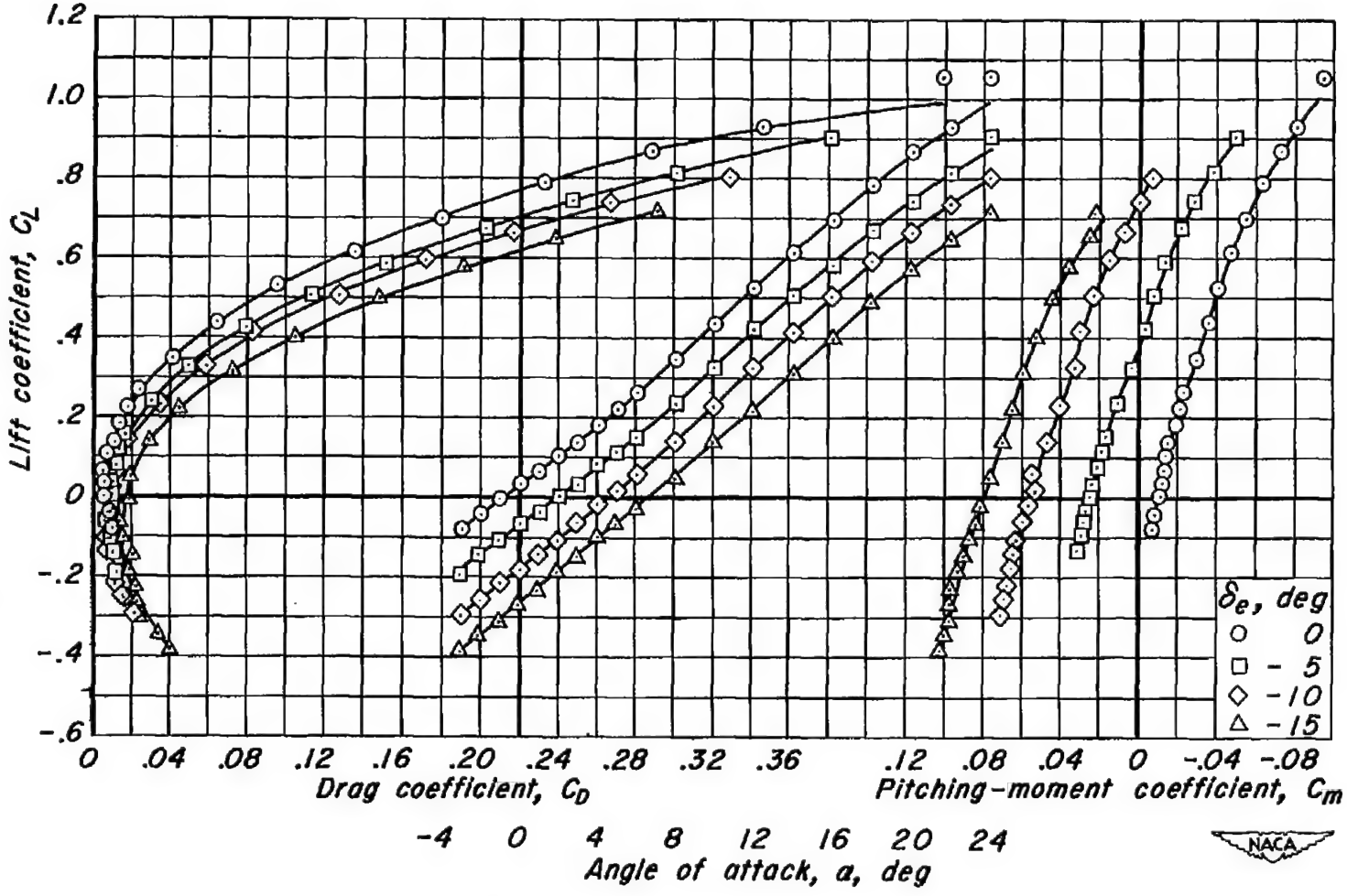

(a) C_L vs C_D, C_L vs α, C_L vs C_m

Figure 12.- The effect of elevon deflection on the aerodynamic characteristics at a Mach number of 0.24. R, 3.0 million; δ_t, 5°.

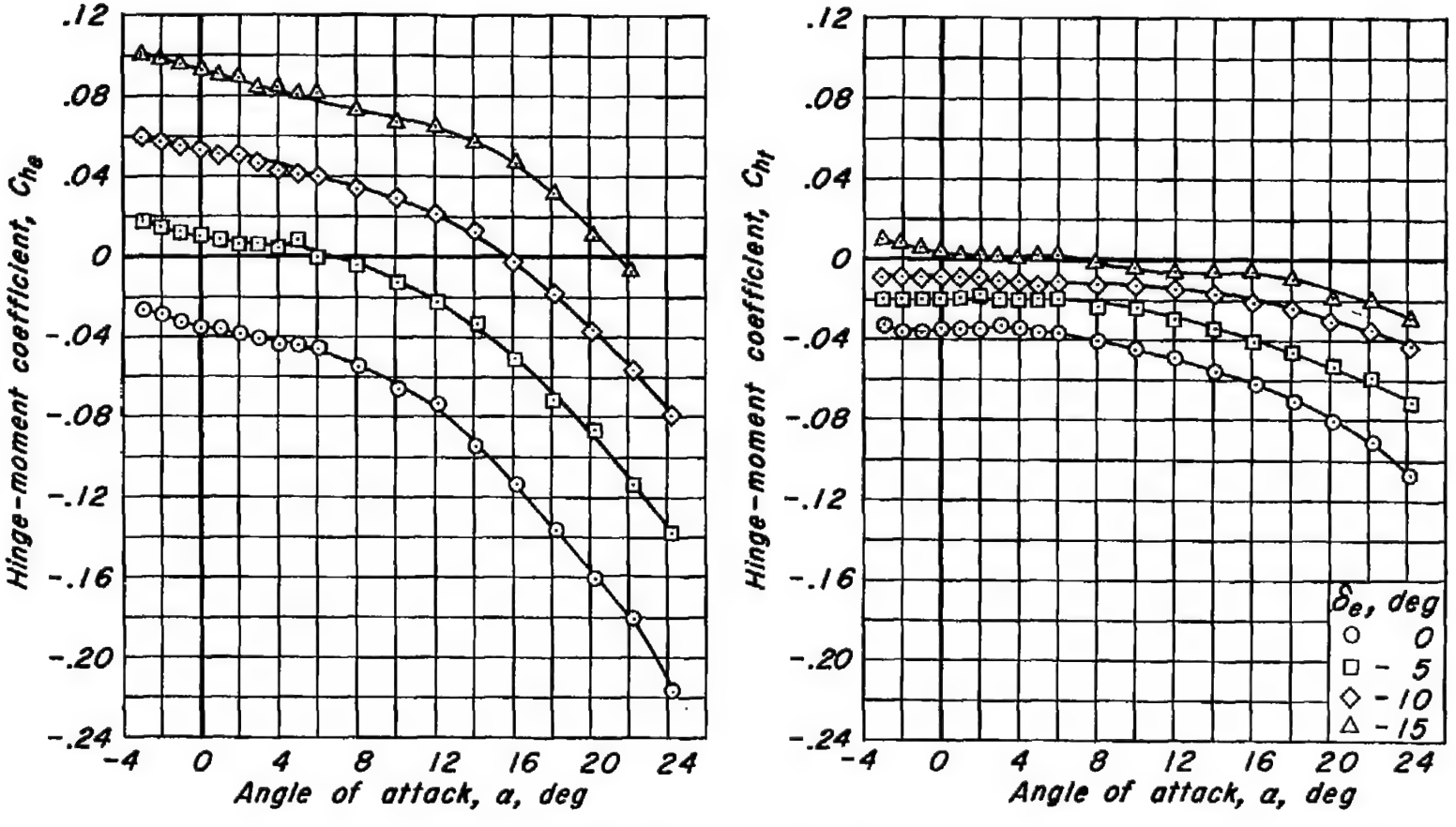

(b) C_{h_e} vs α, C_{h_t} vs α

Figure 12.- Continued.

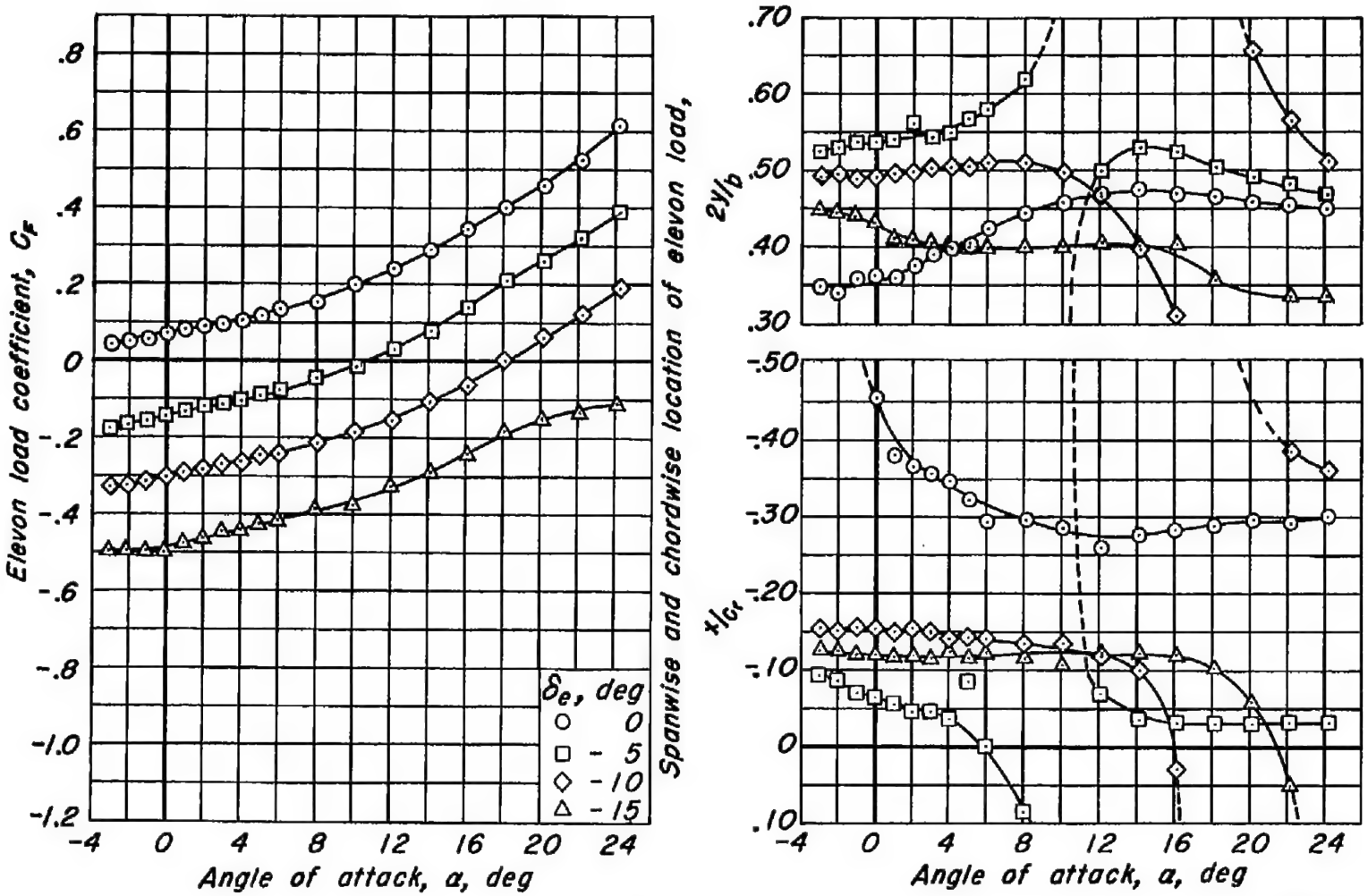

(c) C_F vs α, $2y/b$ vs α, x/c_r vs α

Figure 12.- Concluded.

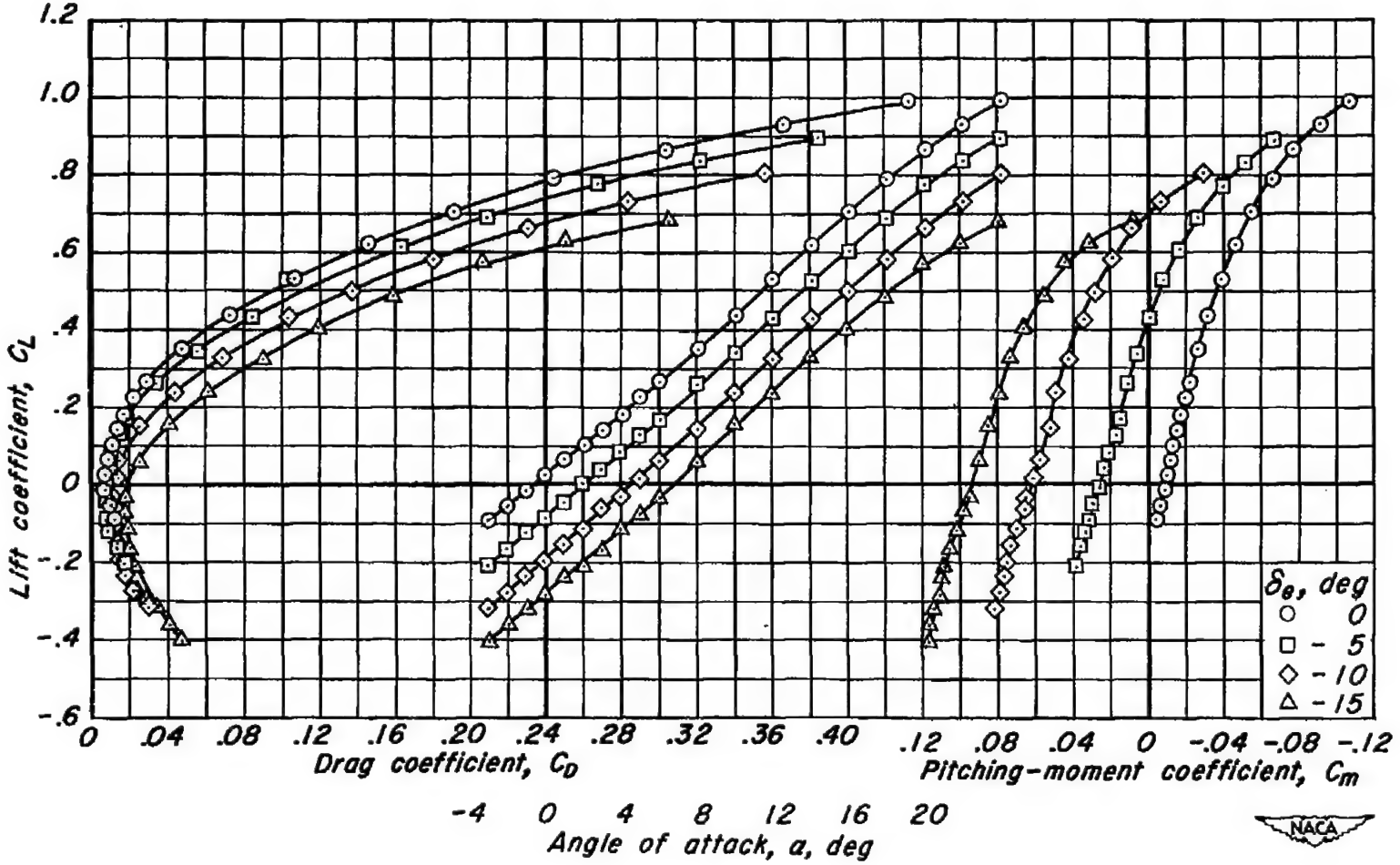

(a) C_L vs C_D, C_L vs a, C_L vs C_m

Figure 13.- The effect of elevon deflection on the aerodynamic characteristics at a Mach number of 0.60. R, 3.0 million; δ_t, 5°.

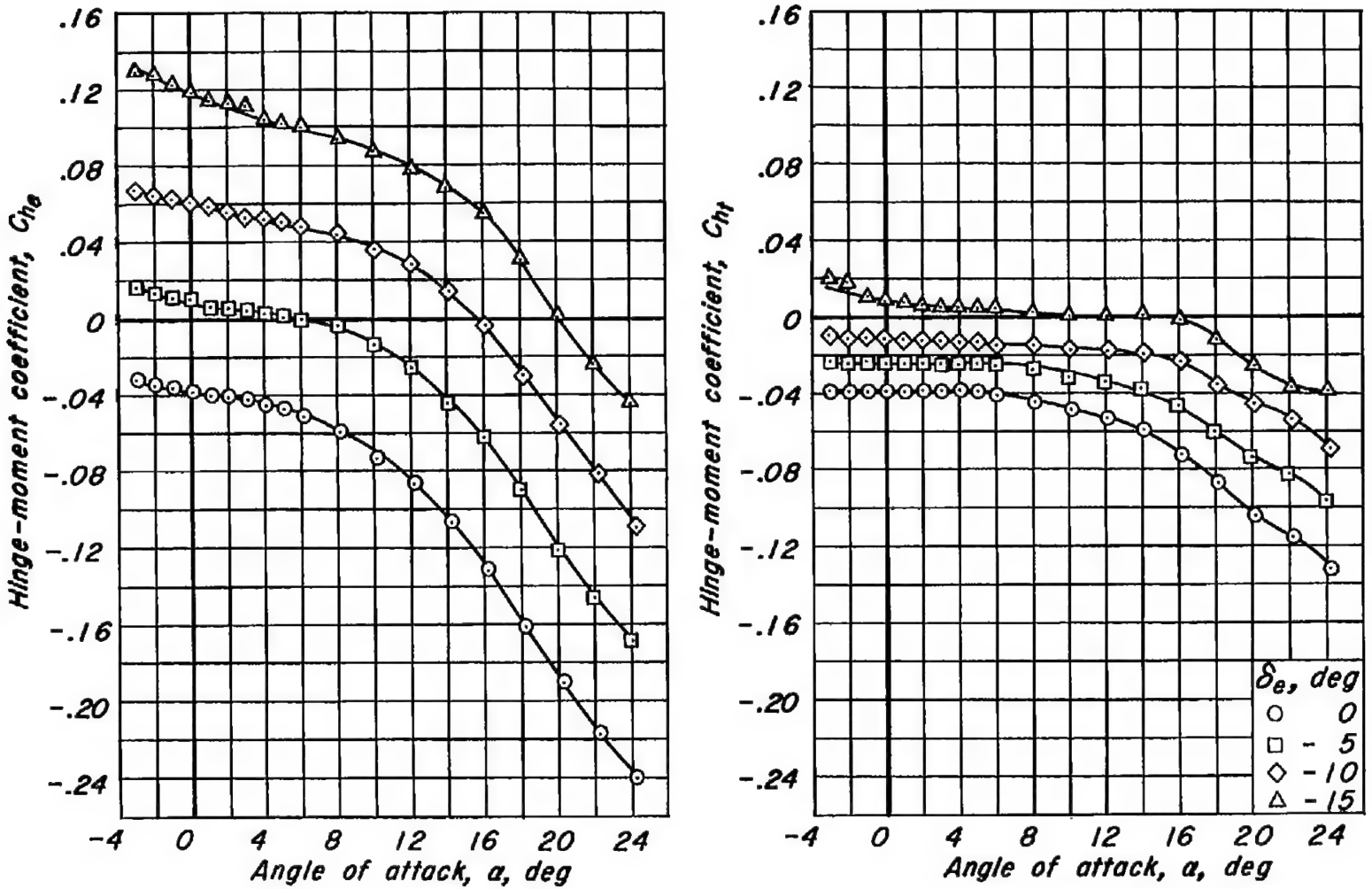

(b) C_{h_e} vs α, C_{h_t} vs α

Figure 13.- Continued.

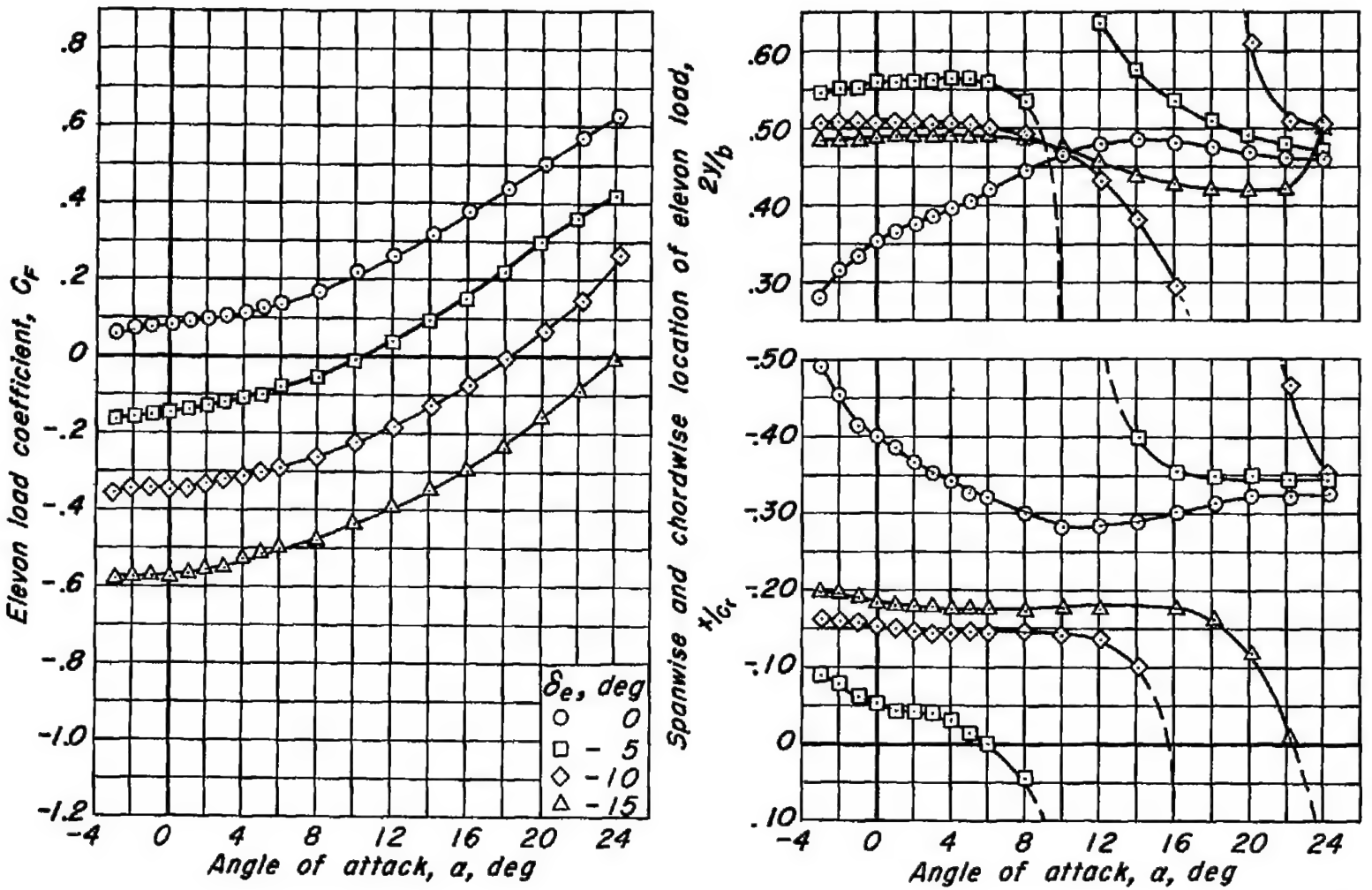

(c) C_F vs α, $2y/b$ vs α, x/c_r vs α

Figure 13.- Concluded.

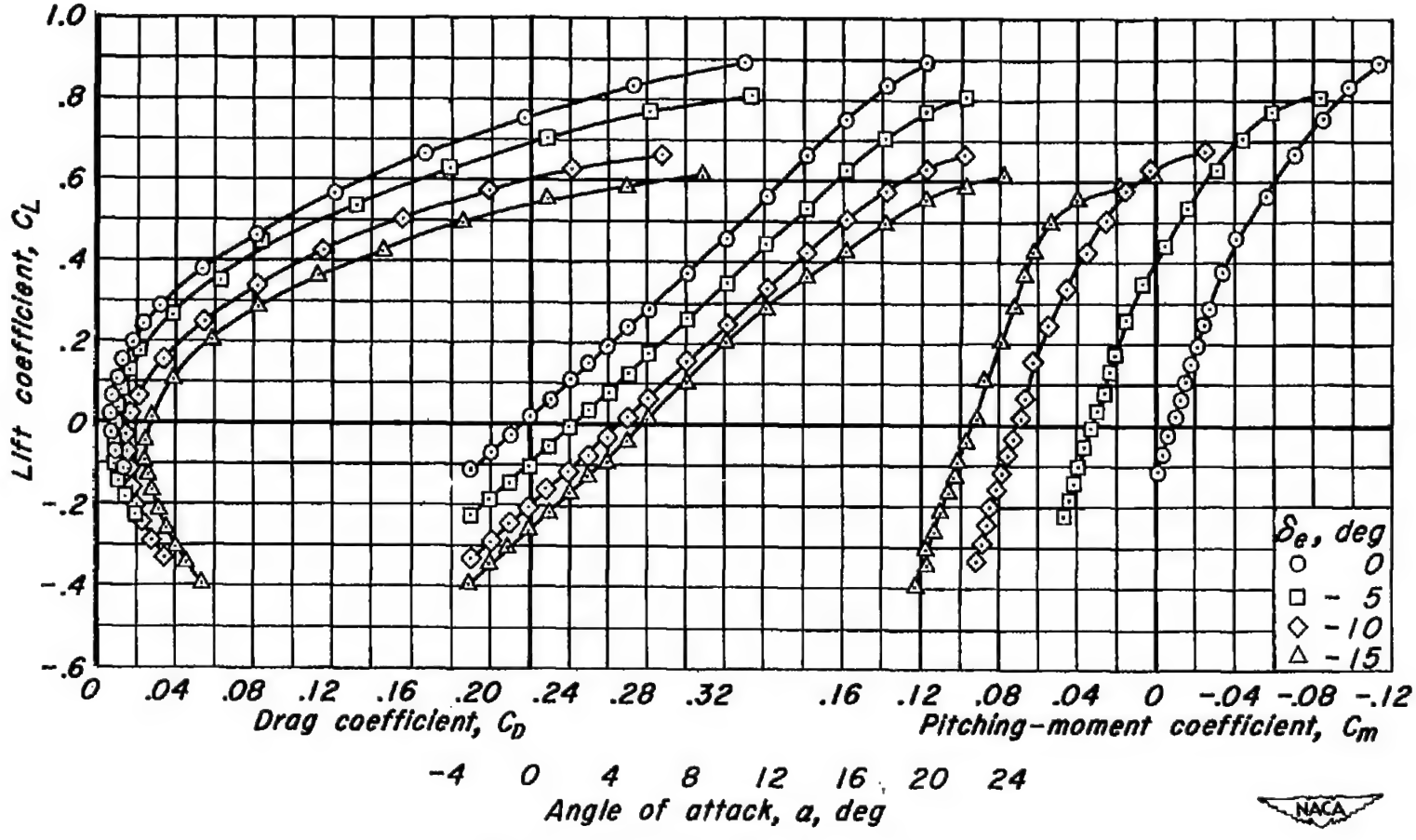

(a) C_L vs C_D, C_L vs α, C_L vs C_m

Figure 14.- The effect of elevon deflection on the aerodynamic characteristics at a Mach number of 0.80. R, 3.0 million; δ_t, 5°.

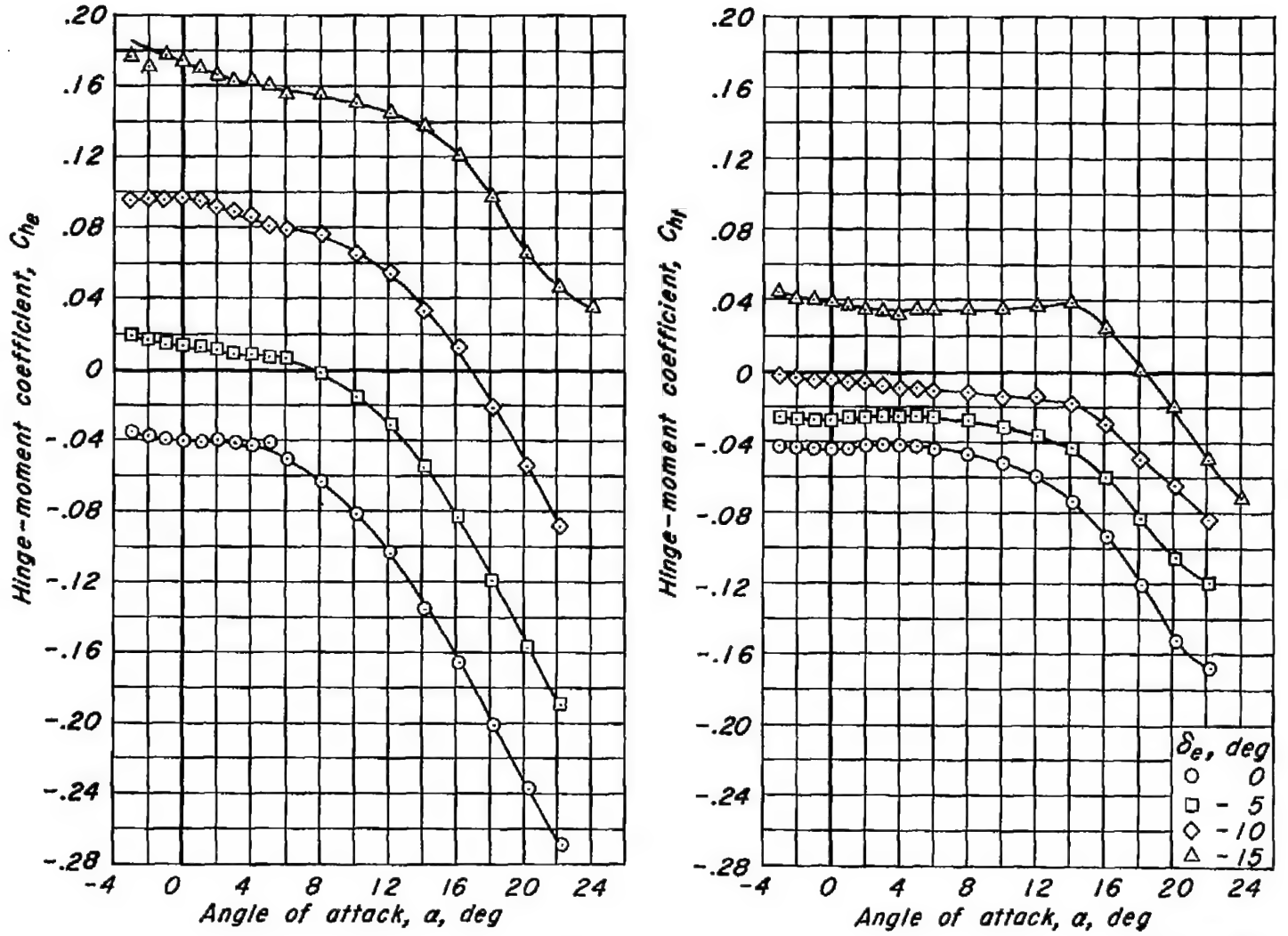

(b) C_{h_e} vs α, C_{h_f} vs α

Figure 14.- Continued.

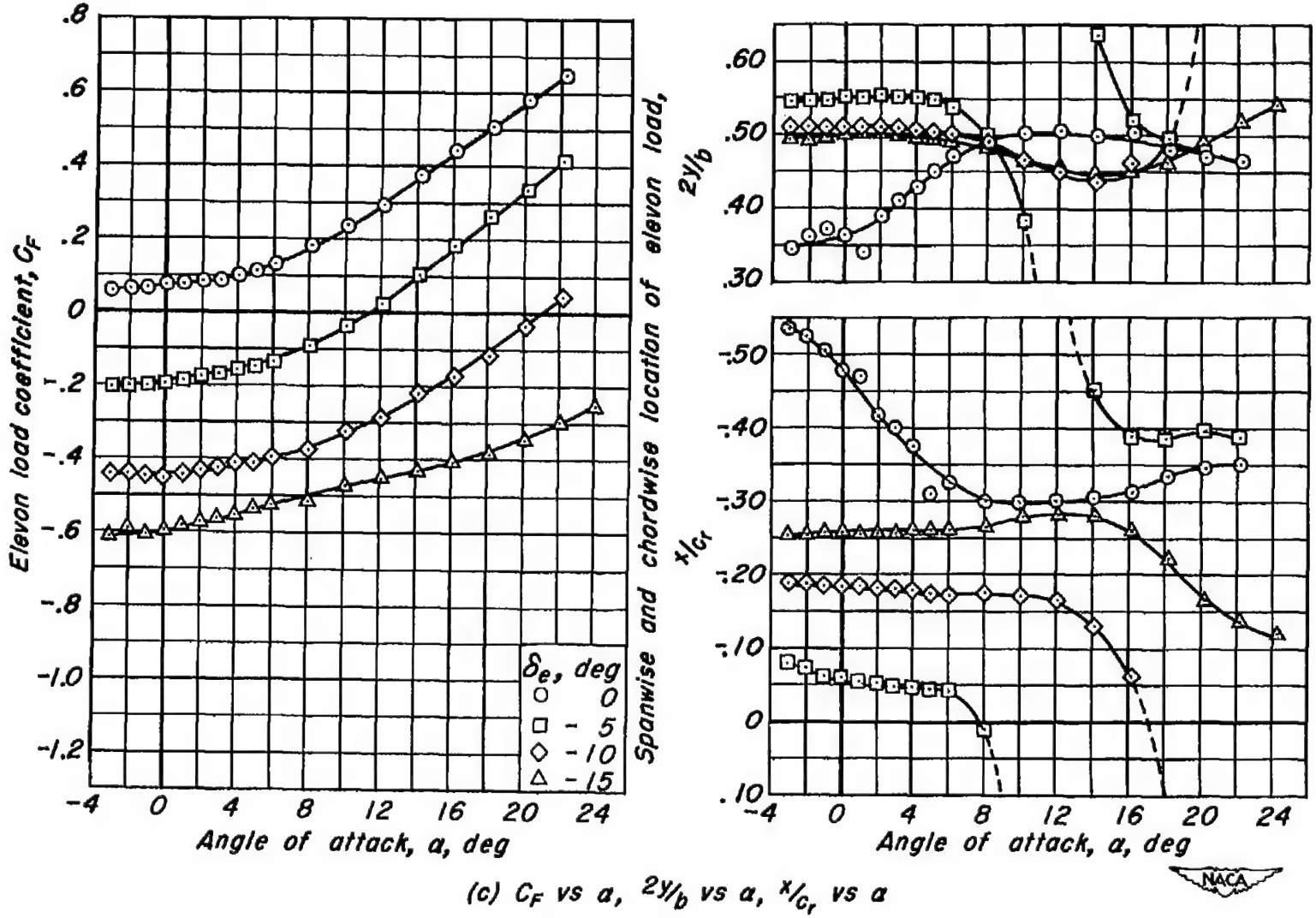

(c) C_F vs α, $2y/b$ vs α, x/c_r vs α

Figure 14.- Concluded.

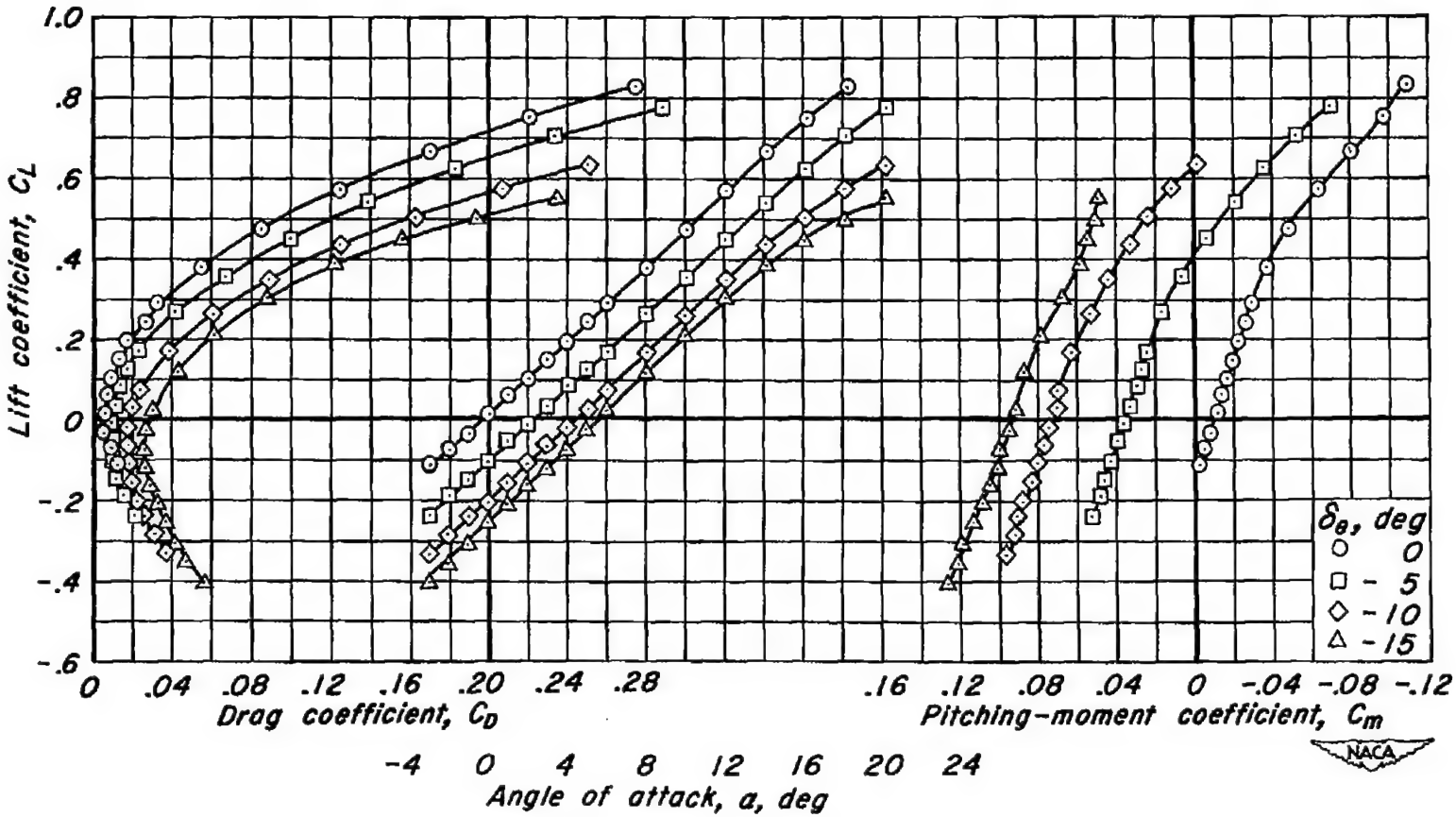

(a) C_L vs C_D, C_L vs α, C_L vs C_m

Figure 15.- The effect of elevon deflection on the aerodynamic characteristics at a Mach number of 0.85. R, 3.0 million; δ_t, 5°.

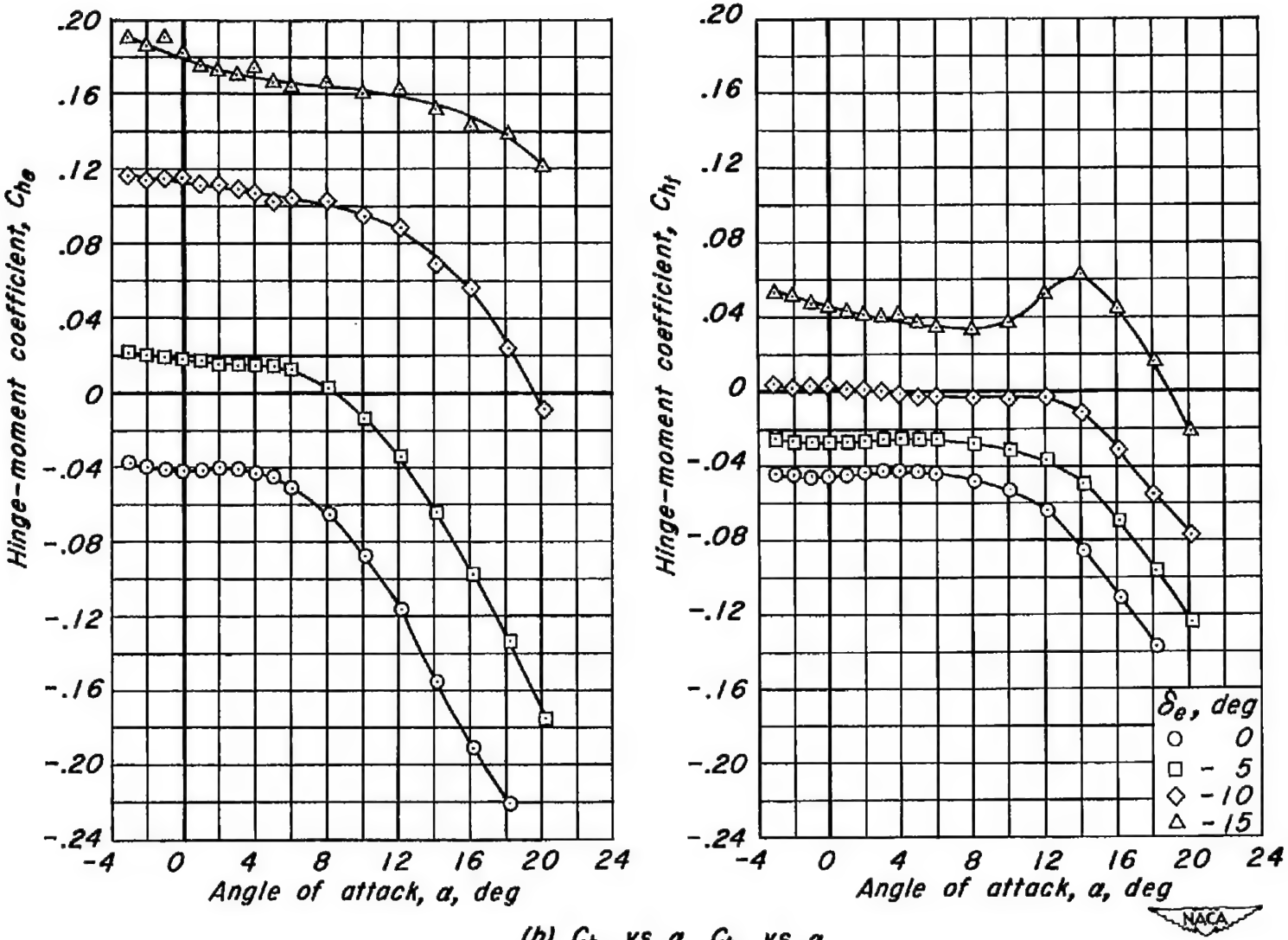

(b) C_{h_e} vs α, C_{h_f} vs α

Figure 15.- Continued.

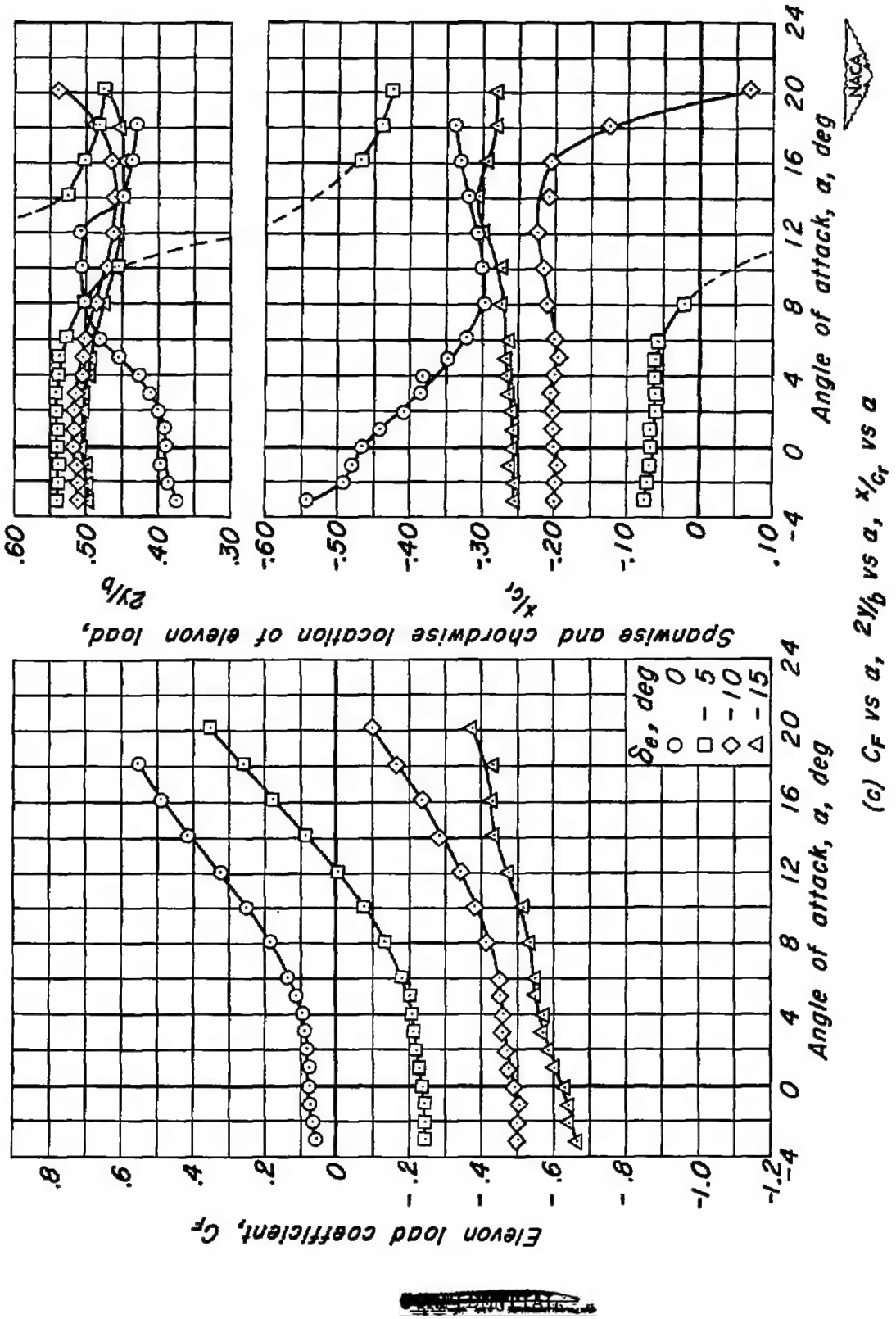

(c) C_F vs α, $2y/b$ vs α, x/c_r vs α

Figure 15.- Concluded.

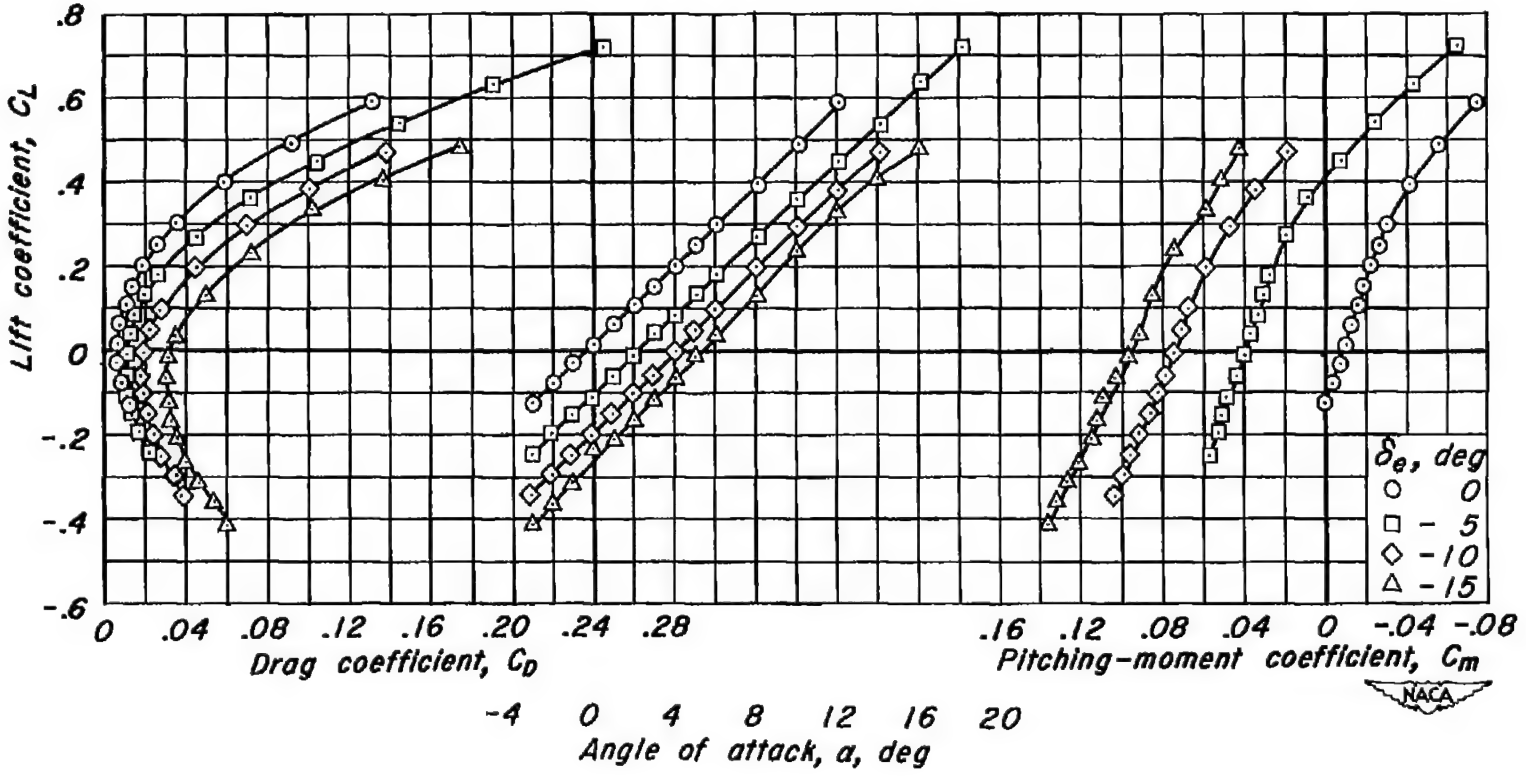

(a) C_L vs C_D, C_L vs α, C_L vs C_m

Figure 16.- The effect of elevon deflection on the aerodynamic characteristics at a Mach number of 0.90. R, 3.0 million; δ_t, 5°.

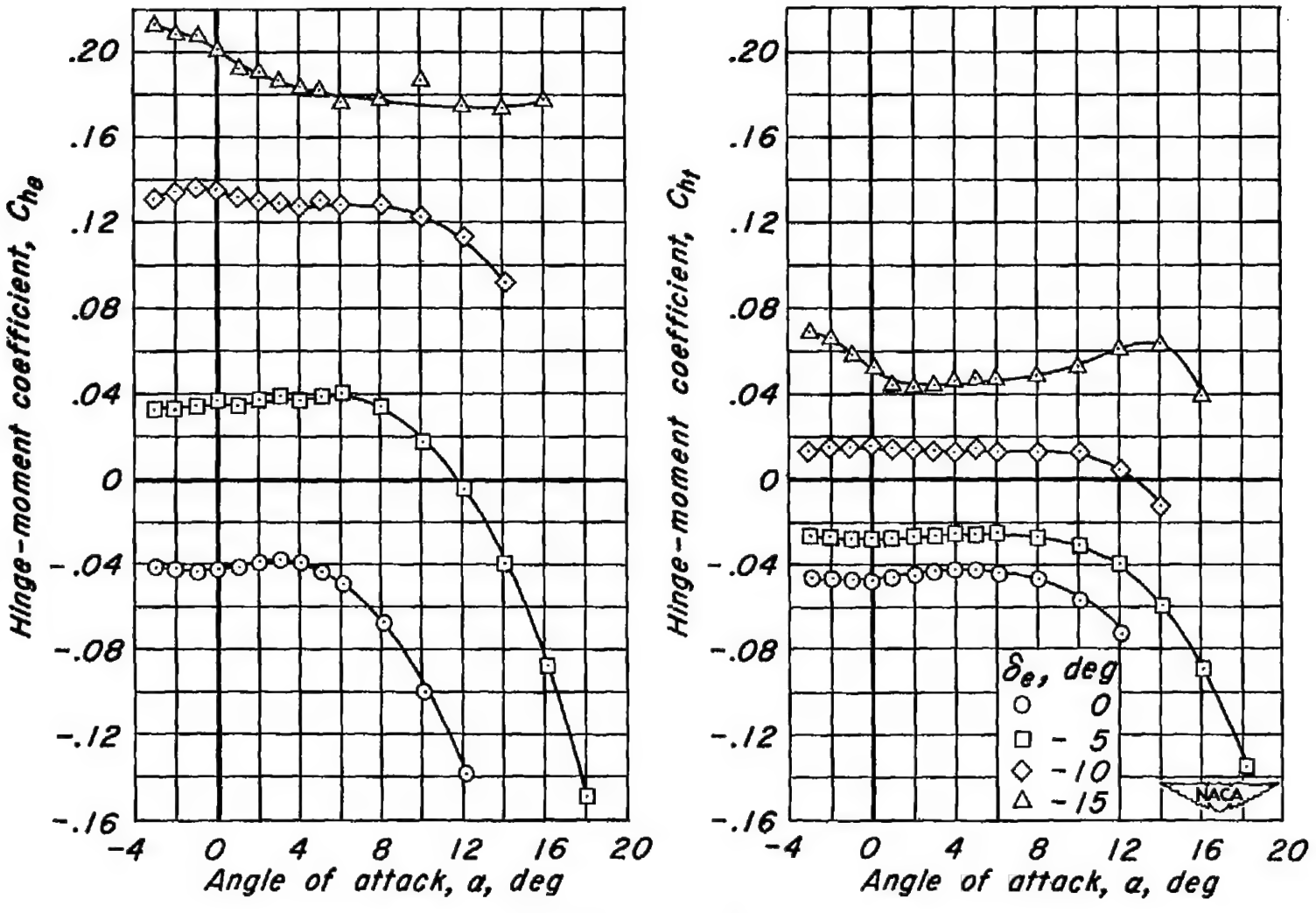

(b) C_{h_e} vs α, C_{h_t} vs α

Figure 16.- Continued.

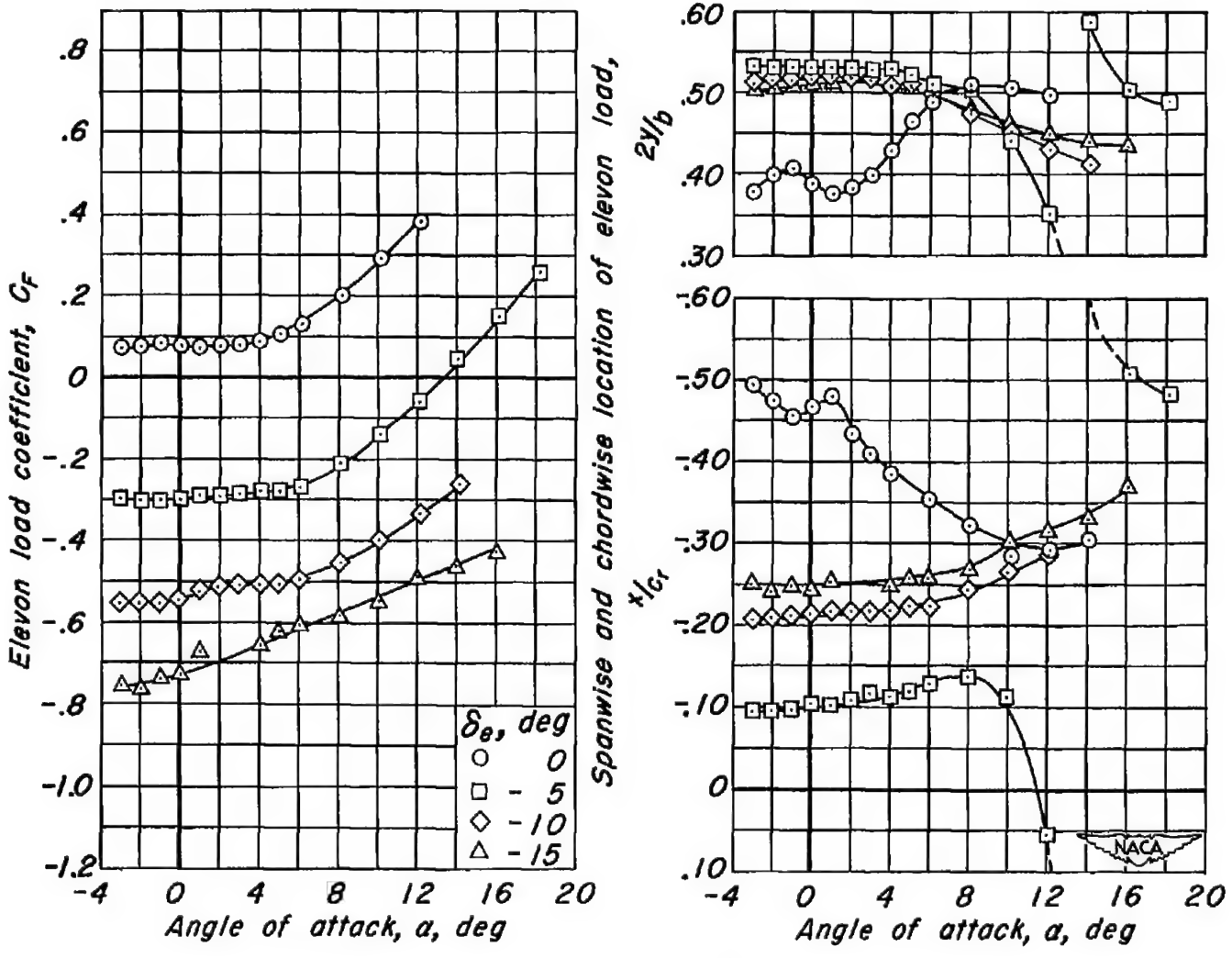

(c) C_F vs α, $2y/b$ vs α, x/c_r vs α

Figure 16.- Concluded.

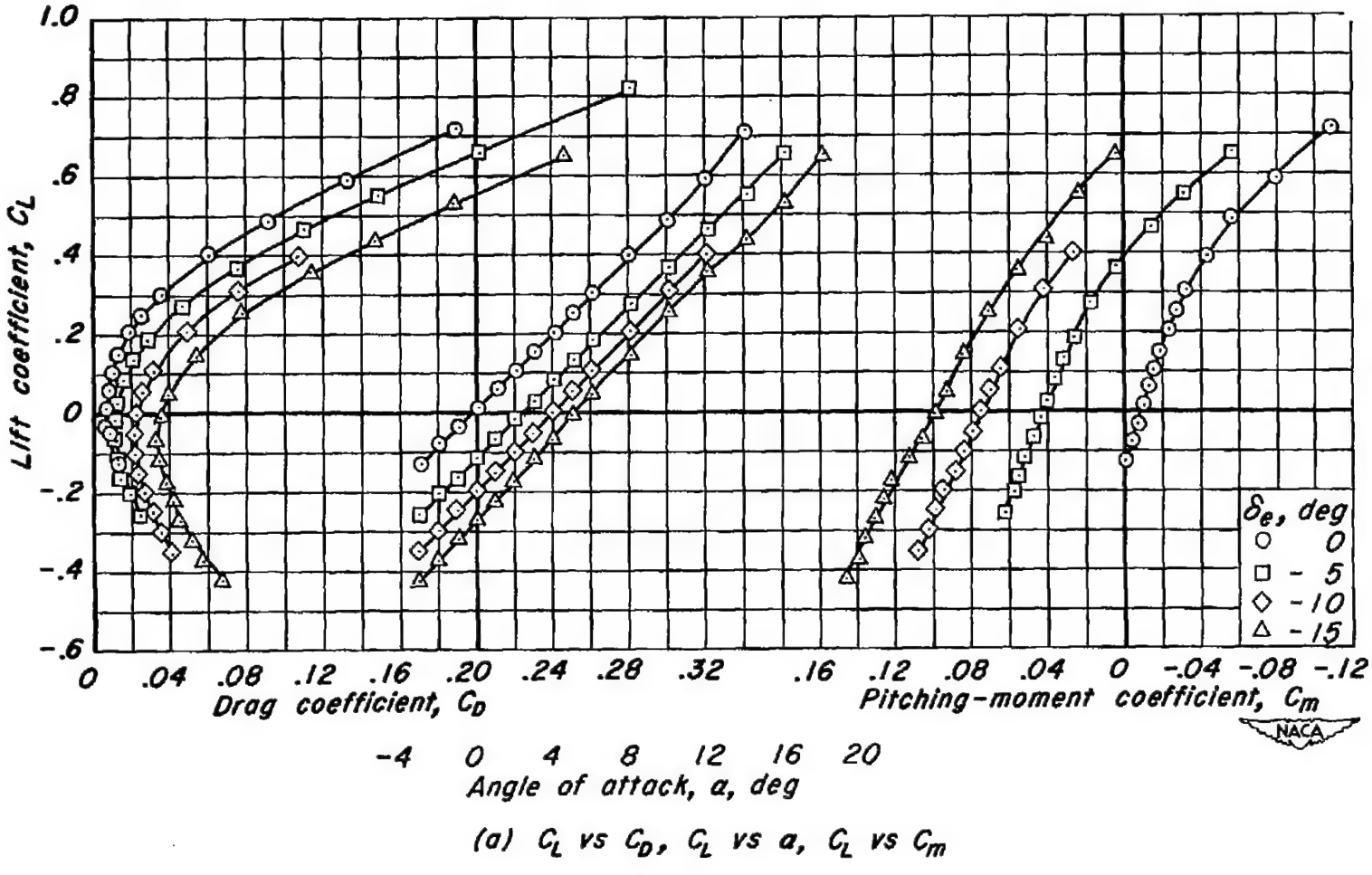

(a) C_L vs C_D, C_L vs α, C_L vs C_m

Figure 17.- The effect of elevon deflection on the aerodynamic characteristics at a Mach number of 0.92. R, 3.0 million; δ_f, 5°.

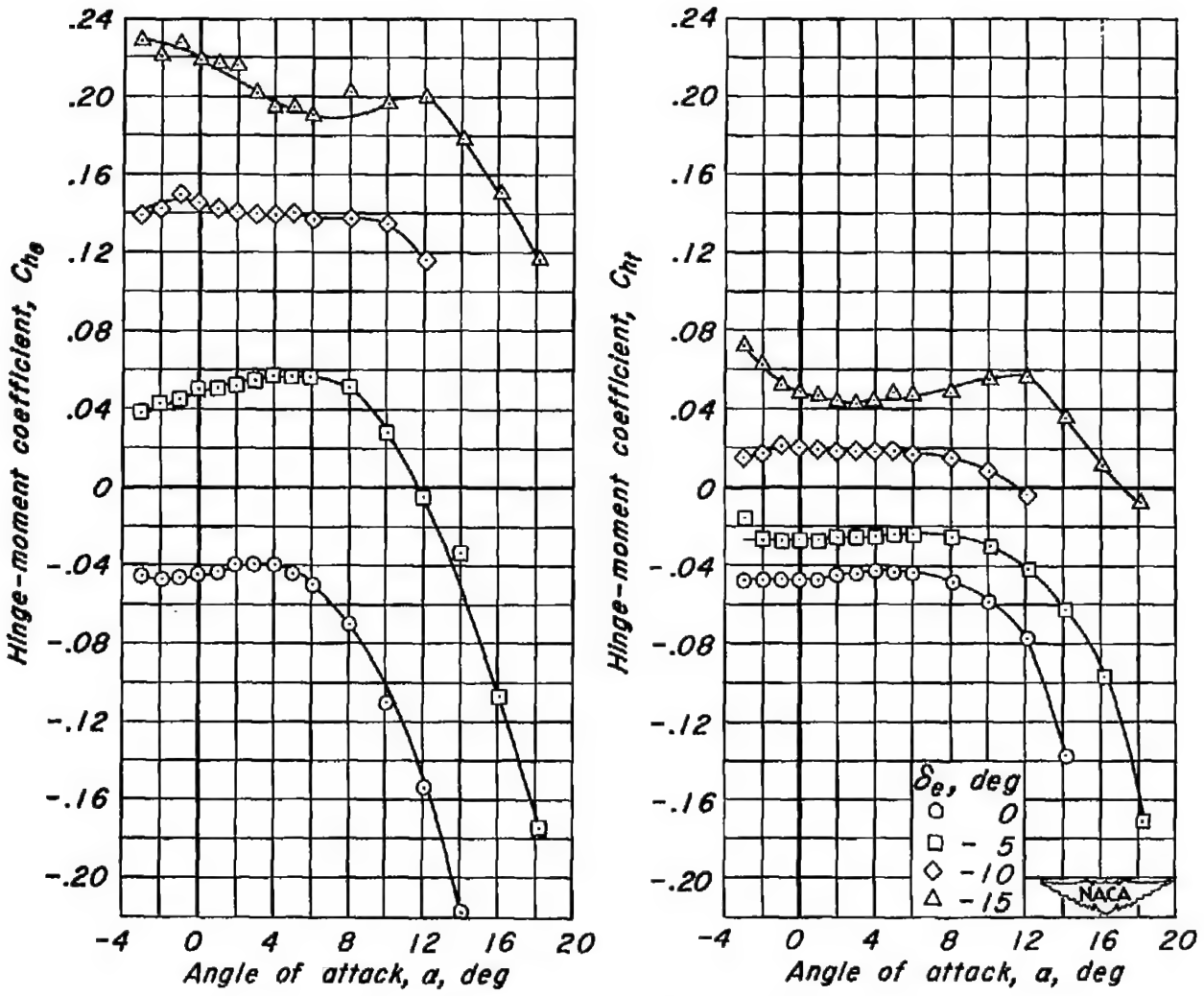

(b) C_{h_e} vs α, C_{h_t} vs α

Figure 17.- Continued.

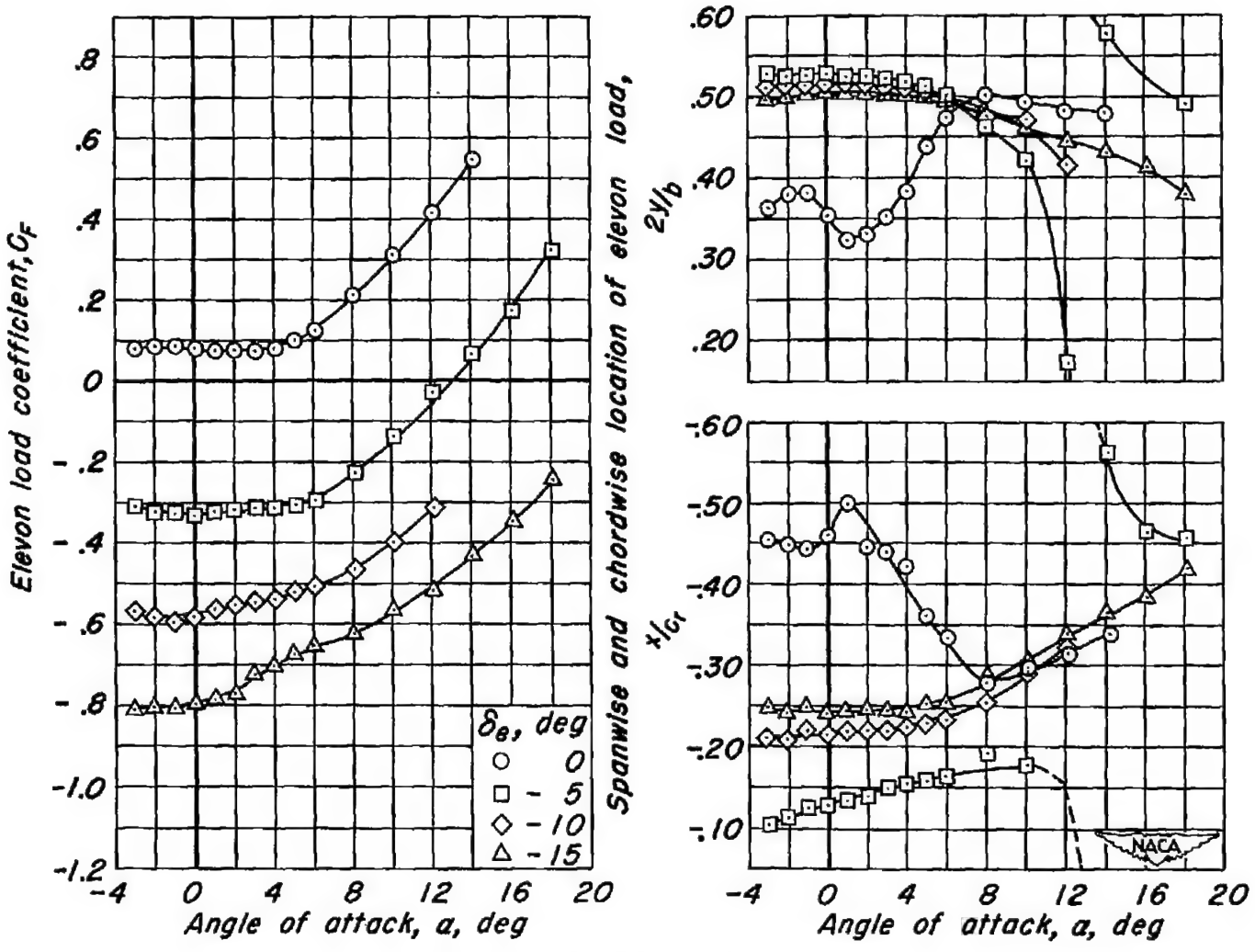

(c) C_F vs α, $2y/b$ vs α, x/c_r vs α

Figure 17.- Concluded.

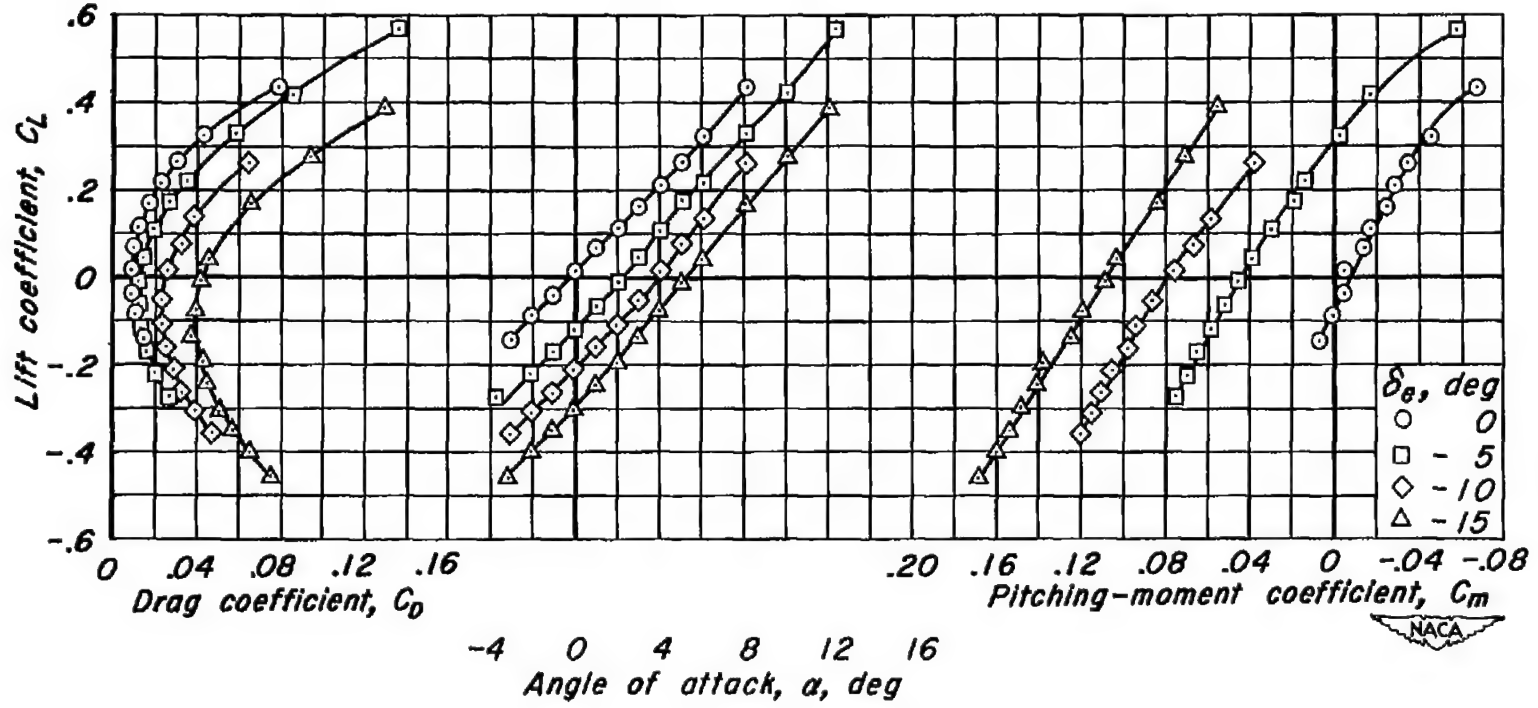

(a) C_L vs C_D, C_L vs α, C_L vs C_m

Figure 18.- The effect of elevon deflection on the aerodynamic characteristics at a Mach number of 0.95. R, 3.0 million; δ_t, 5°.

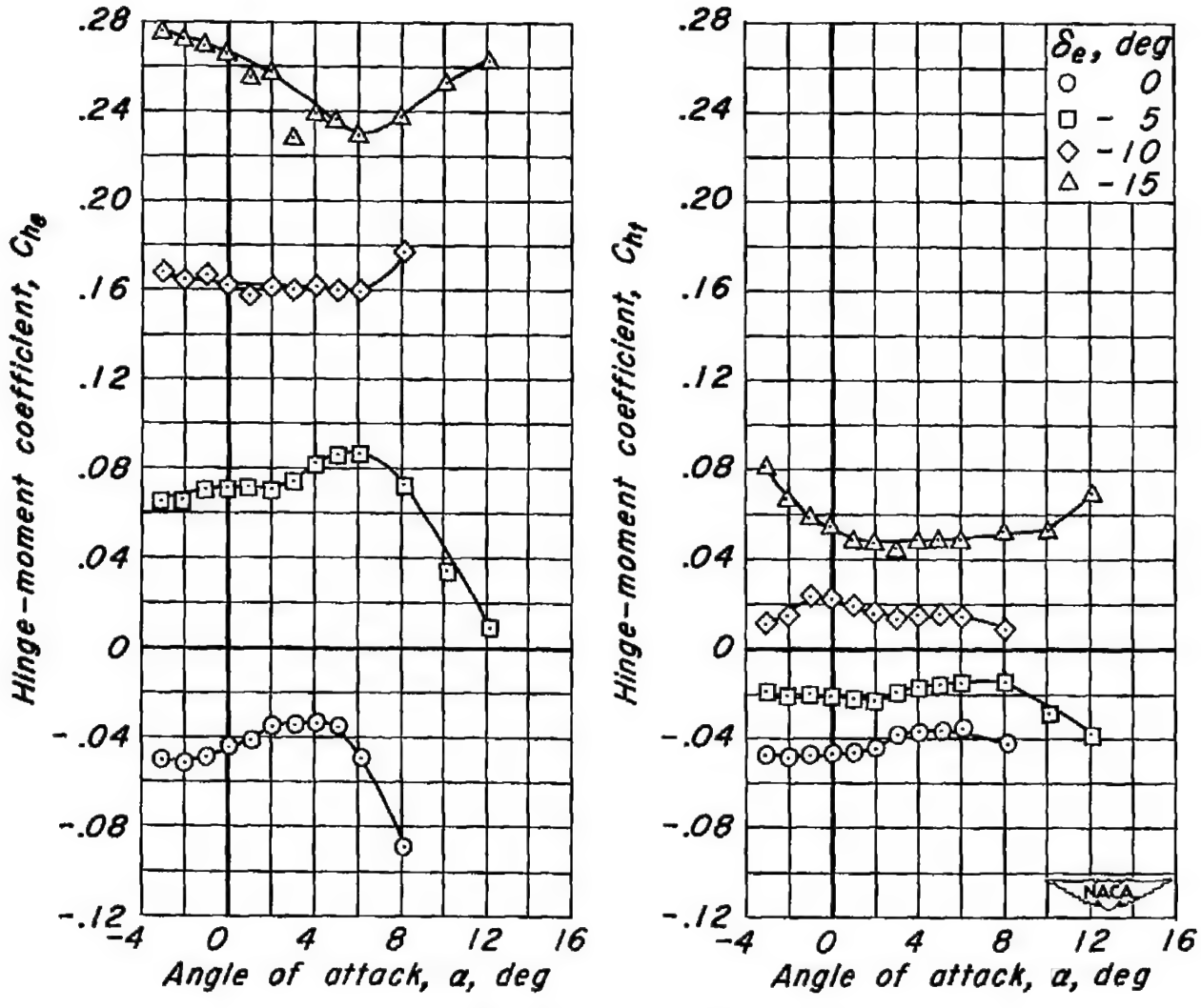

(b) C_{h_e} vs α, C_{h_f} vs α

Figure 18.- Continued.

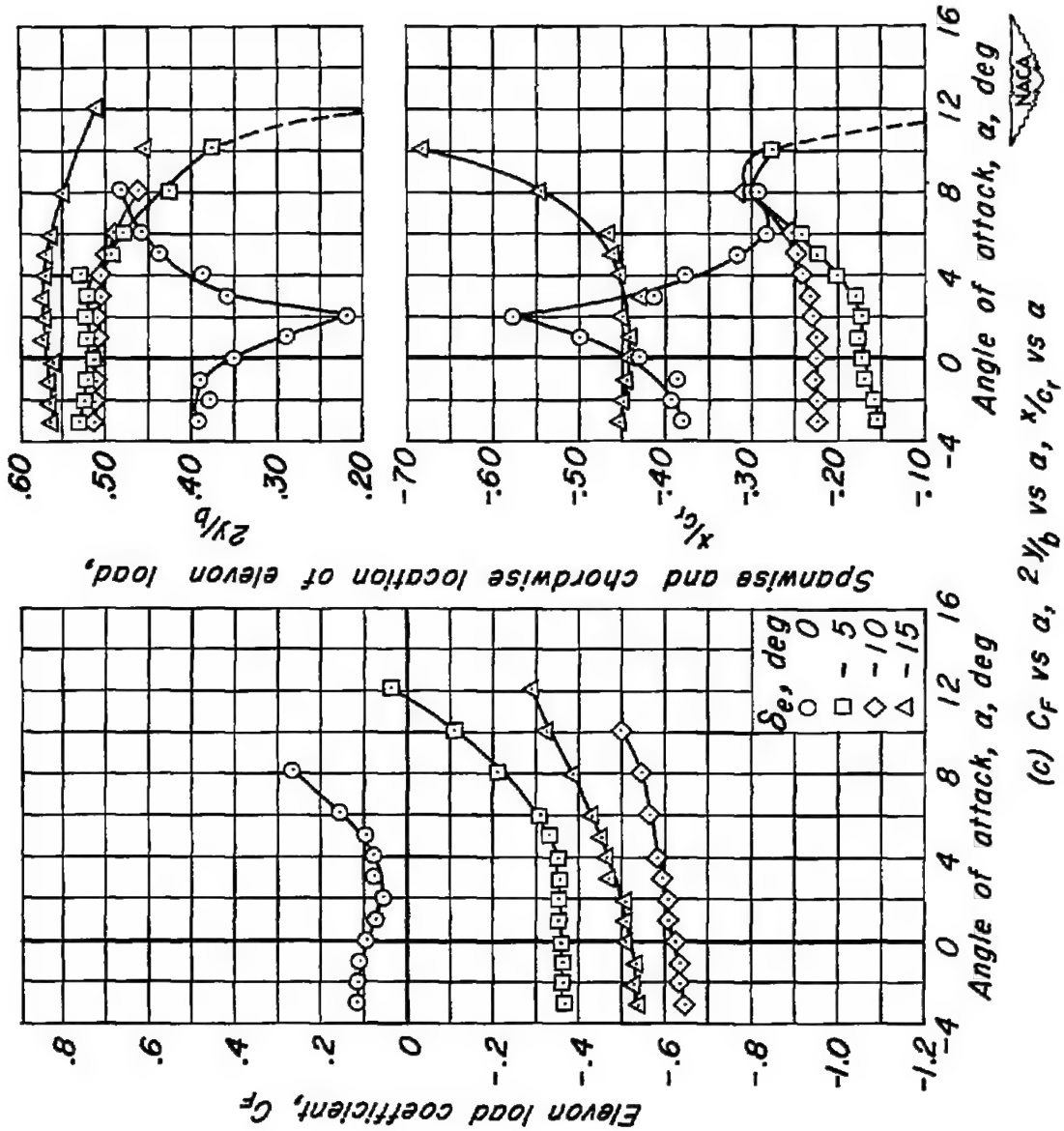

(c) C_F vs α, $2y/b$ vs α, x/c_r vs α

Figure 18.- Concluded.

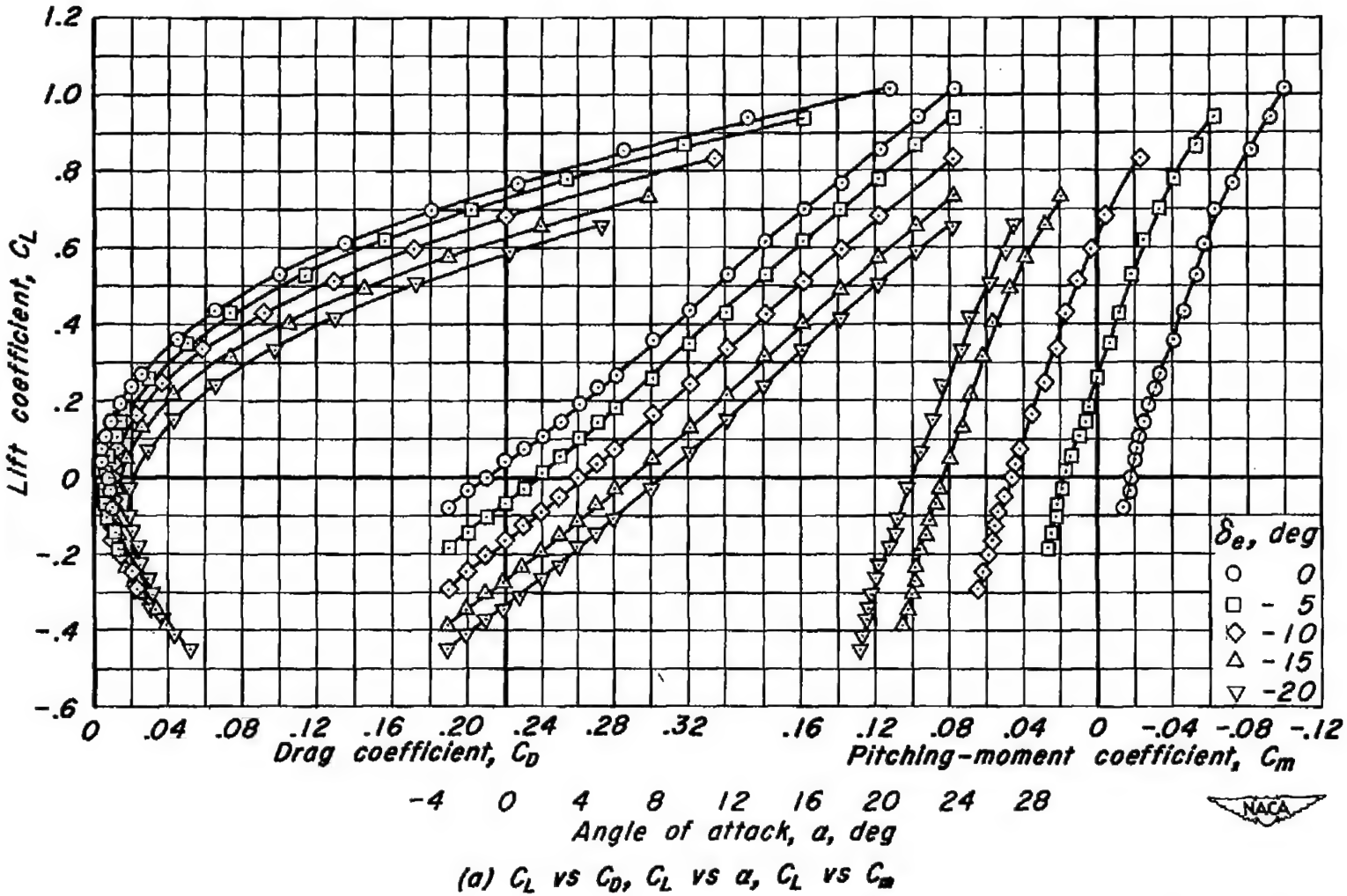

(a) C_L vs C_D, C_L vs α, C_L vs C_m

Figure 19.- The effect of elevon deflection on the aerodynamic characteristics at a Mach number of 0.24. R, 3.0 million; δ_t, 10°.

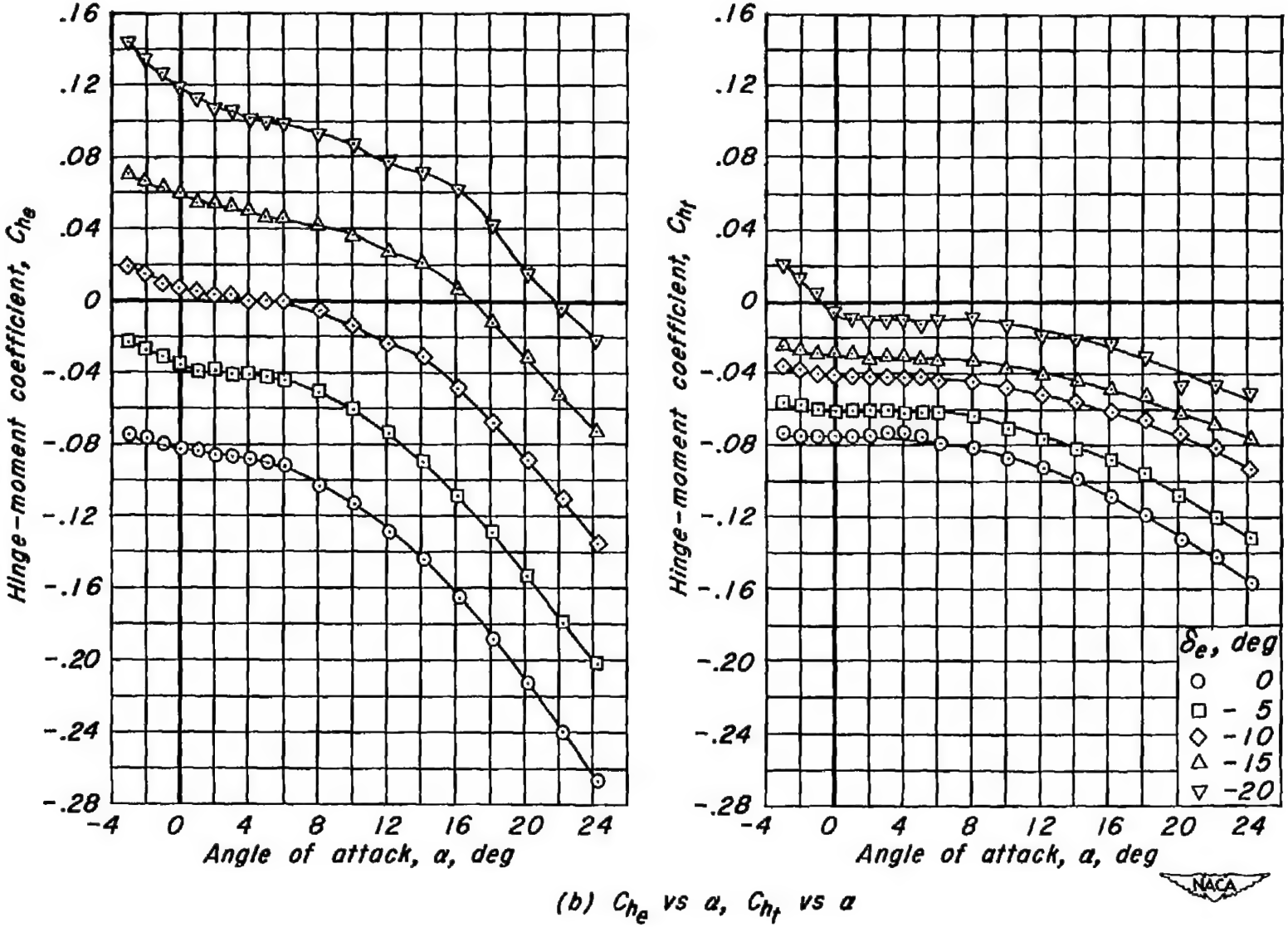

(b) C_{h_e} vs α, C_{h_t} vs α

Figure 19.- Continued.

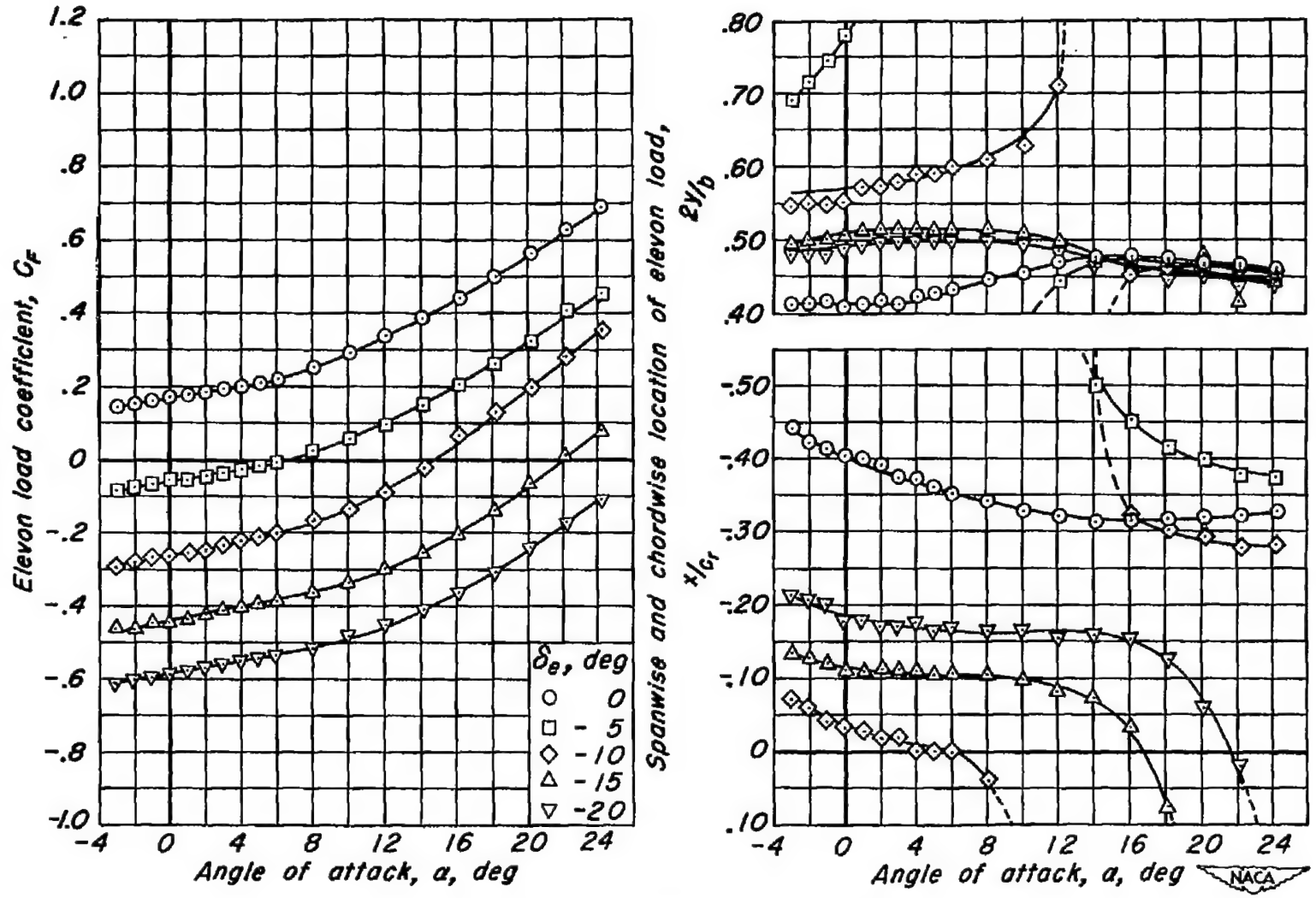

(c) C_F vs α, $2y/b$ vs α, x/c_r vs α

Figure 19.- Concluded.

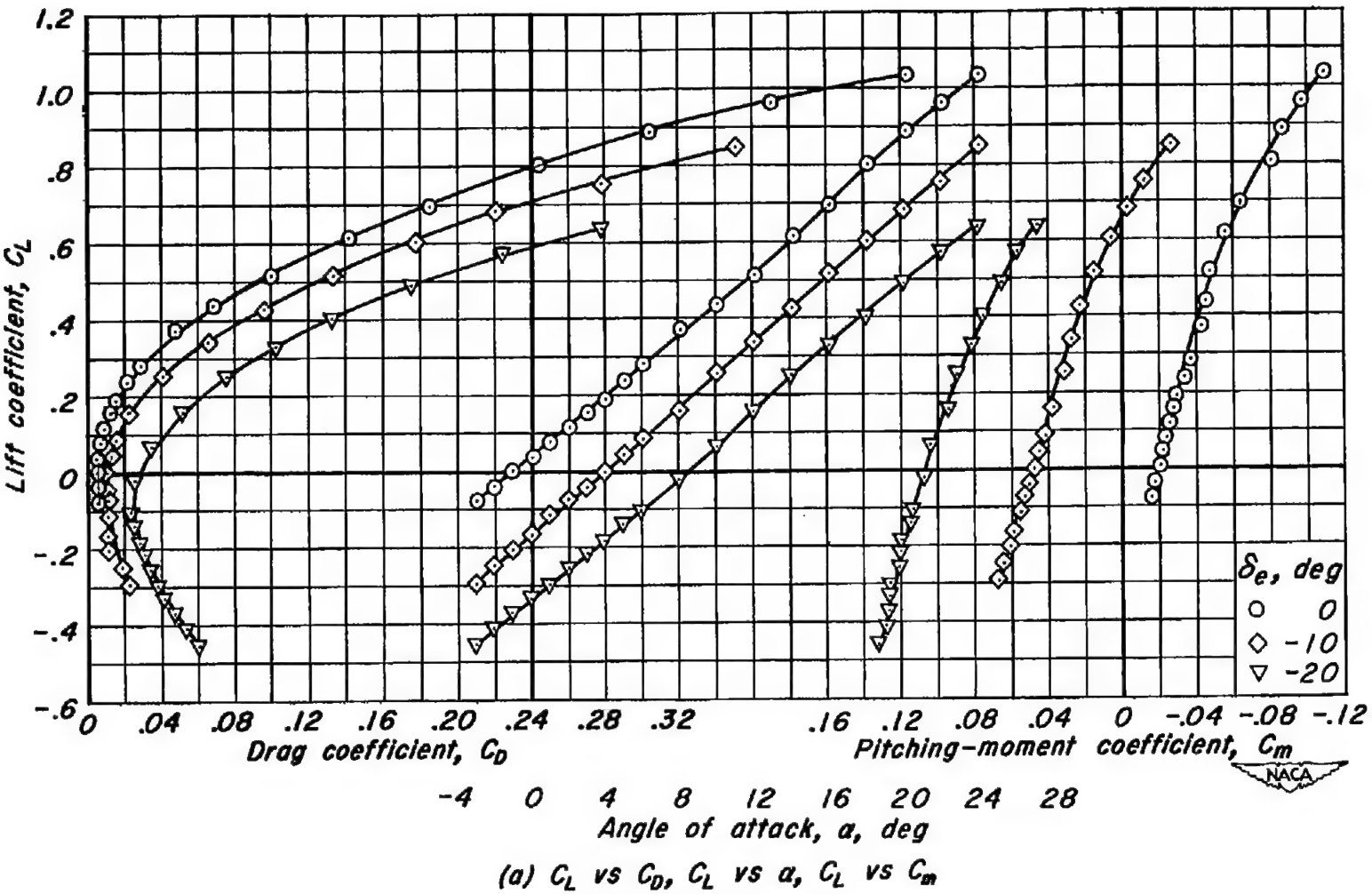

(a) C_L vs C_D, C_L vs α, C_L vs C_m

Figure 20.- The effect of elevon deflection on the aerodynamic characteristics at a Mach number of 0.40. R, 3.0 million; δ_t, 10°.

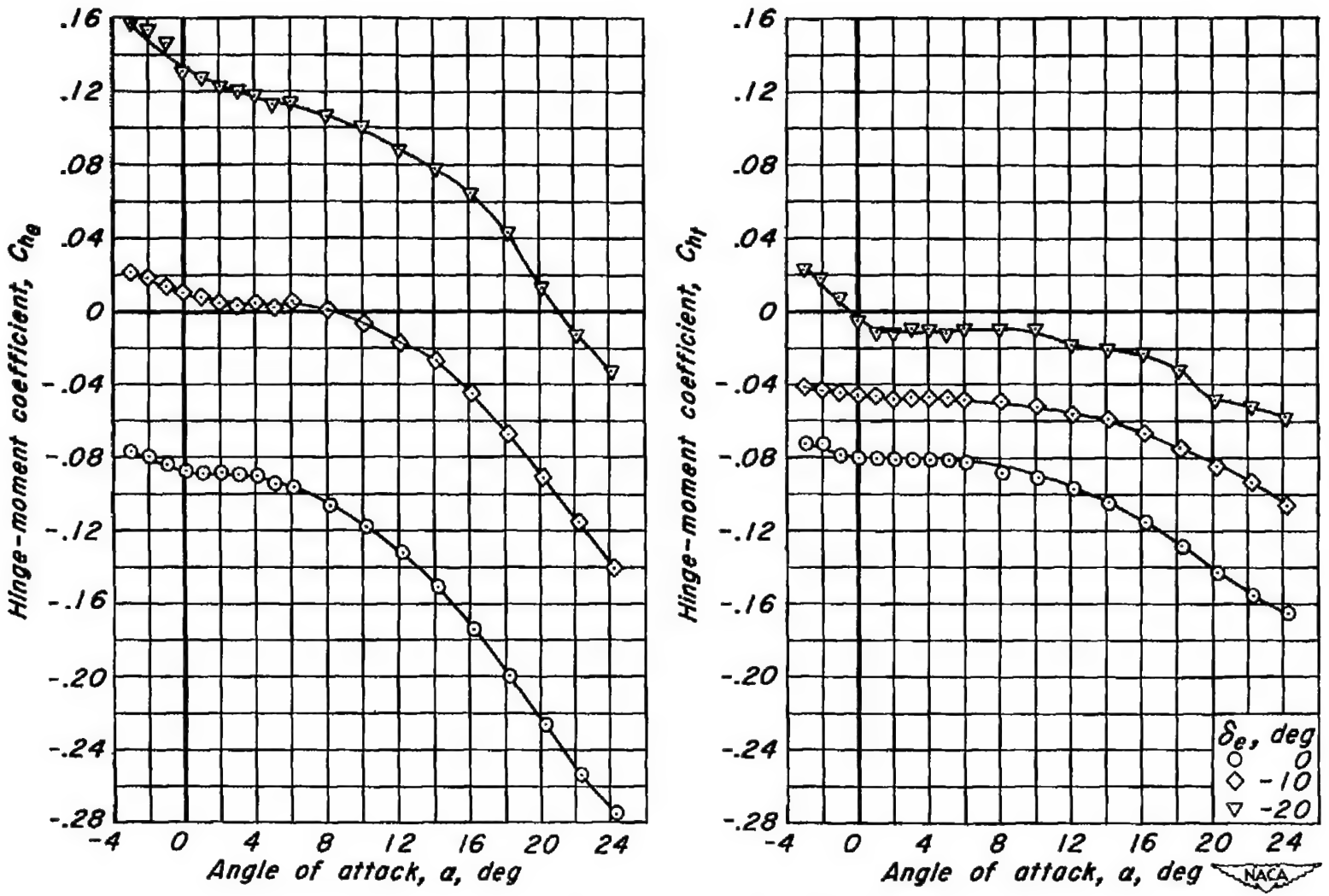

(b) C_{h_e} vs α, C_{h_t} vs α

Figure 20.- Continued.

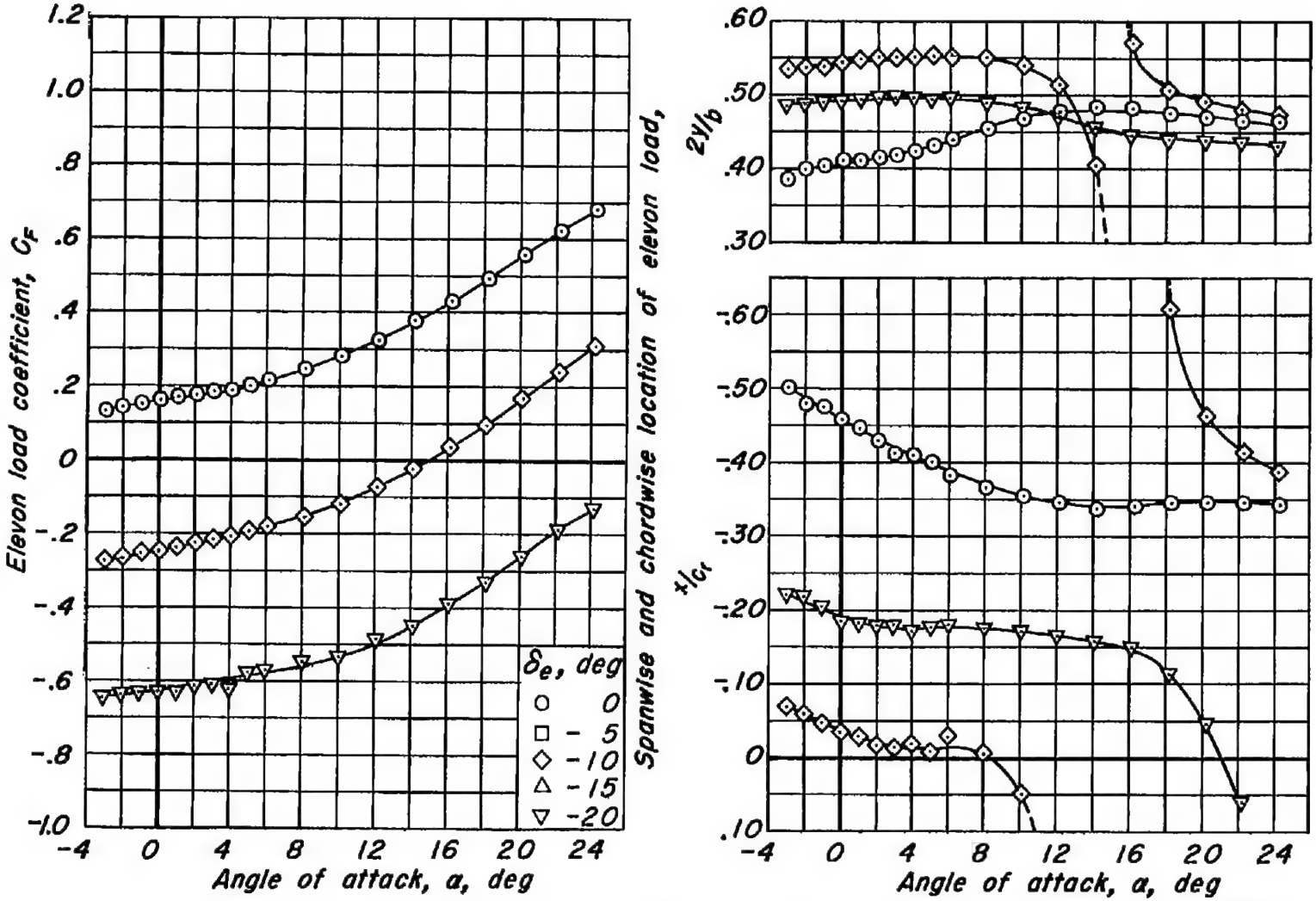

(c) C_F vs α, $2y/b$ vs α, x/c_r vs α

Figure 20.- Concluded.

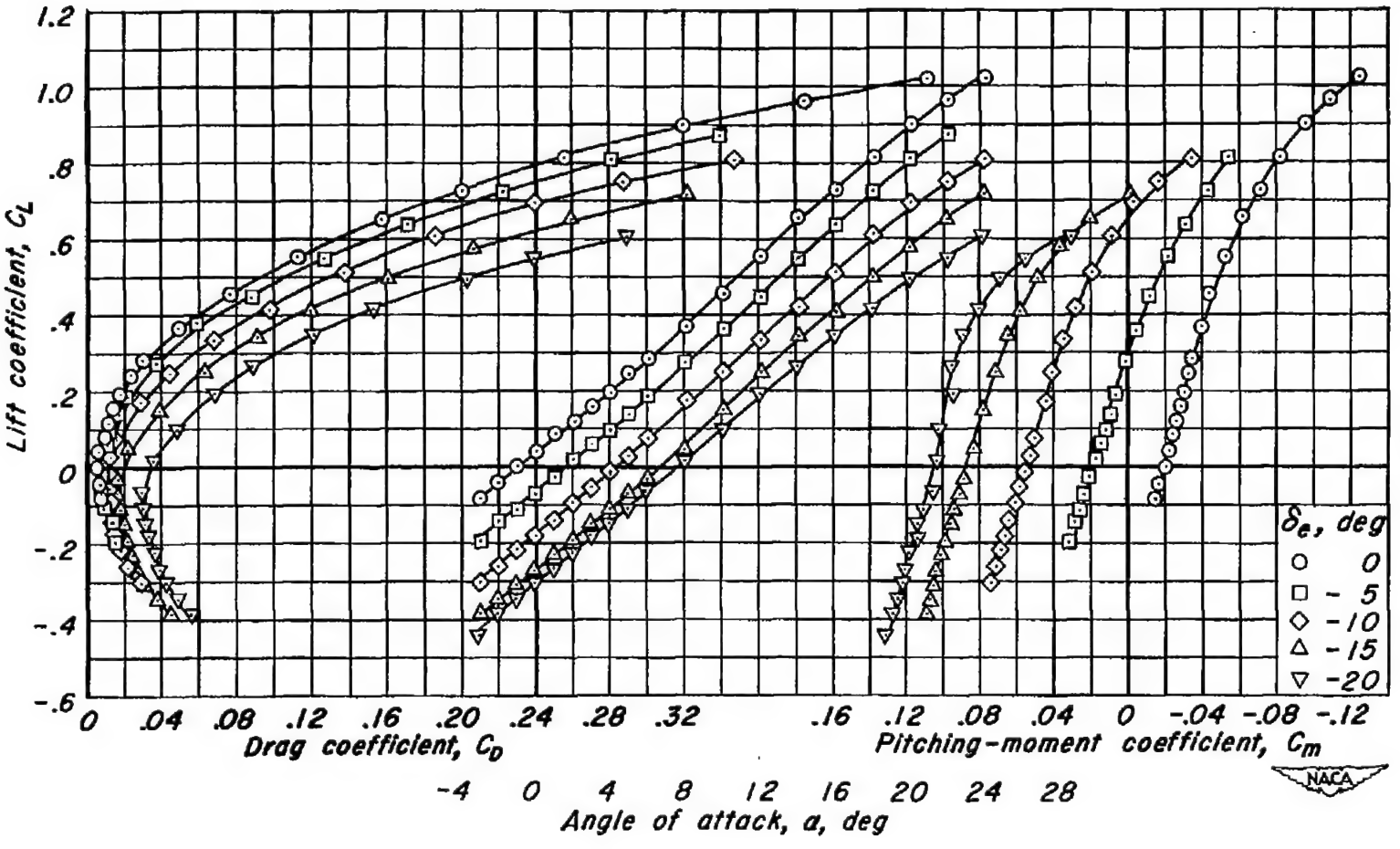

(a) C_L vs C_D, C_L vs a, C_L vs C_m

Figure 21.- The effect of elevon deflection on the aerodynamic characteristics at a Mach number of 0.60. R, 3.0 million; δ_t, 10°.

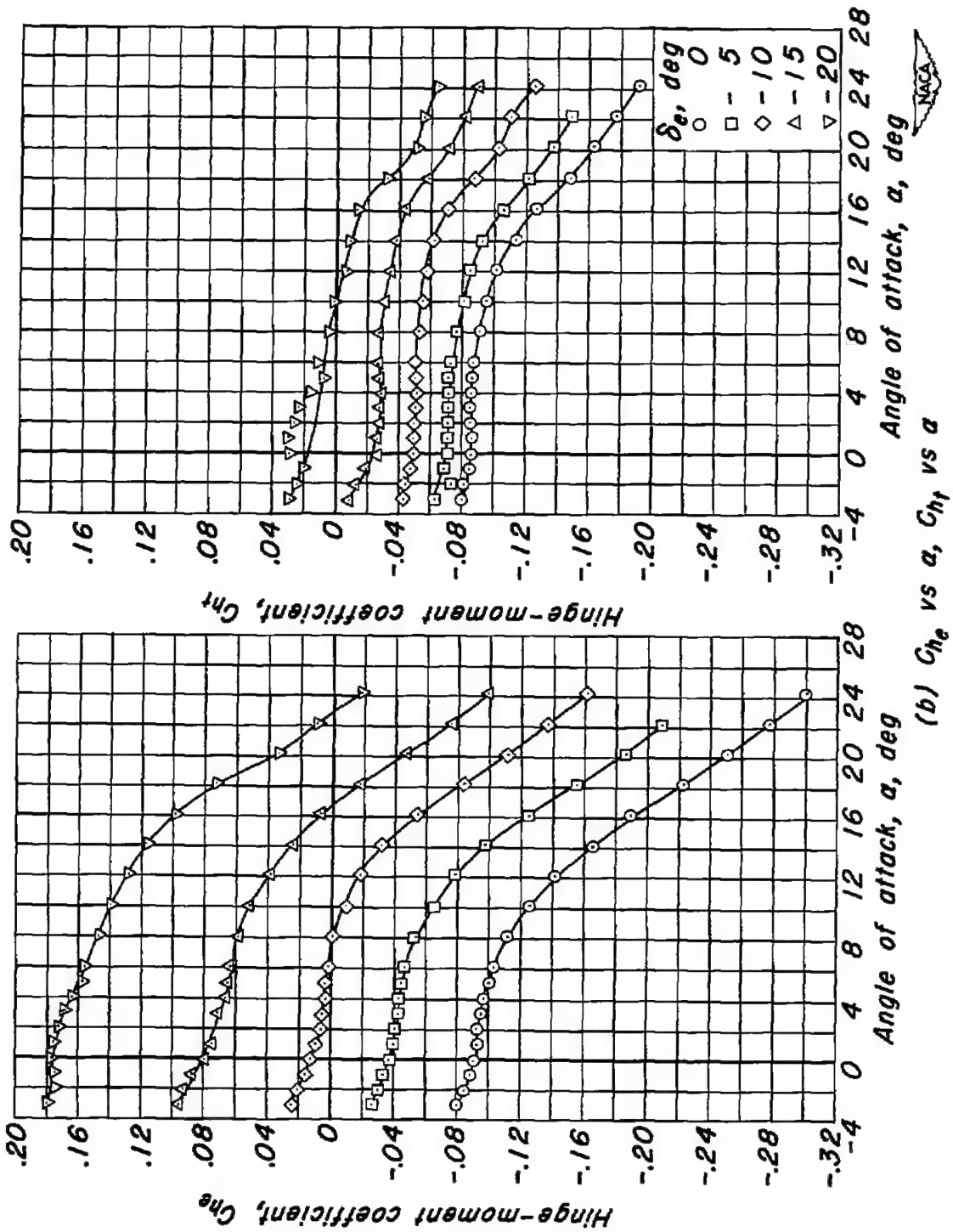

(b) C_{h_e} vs α, C_{h_t} vs α

Figure 21.- Continued.

[redacted]

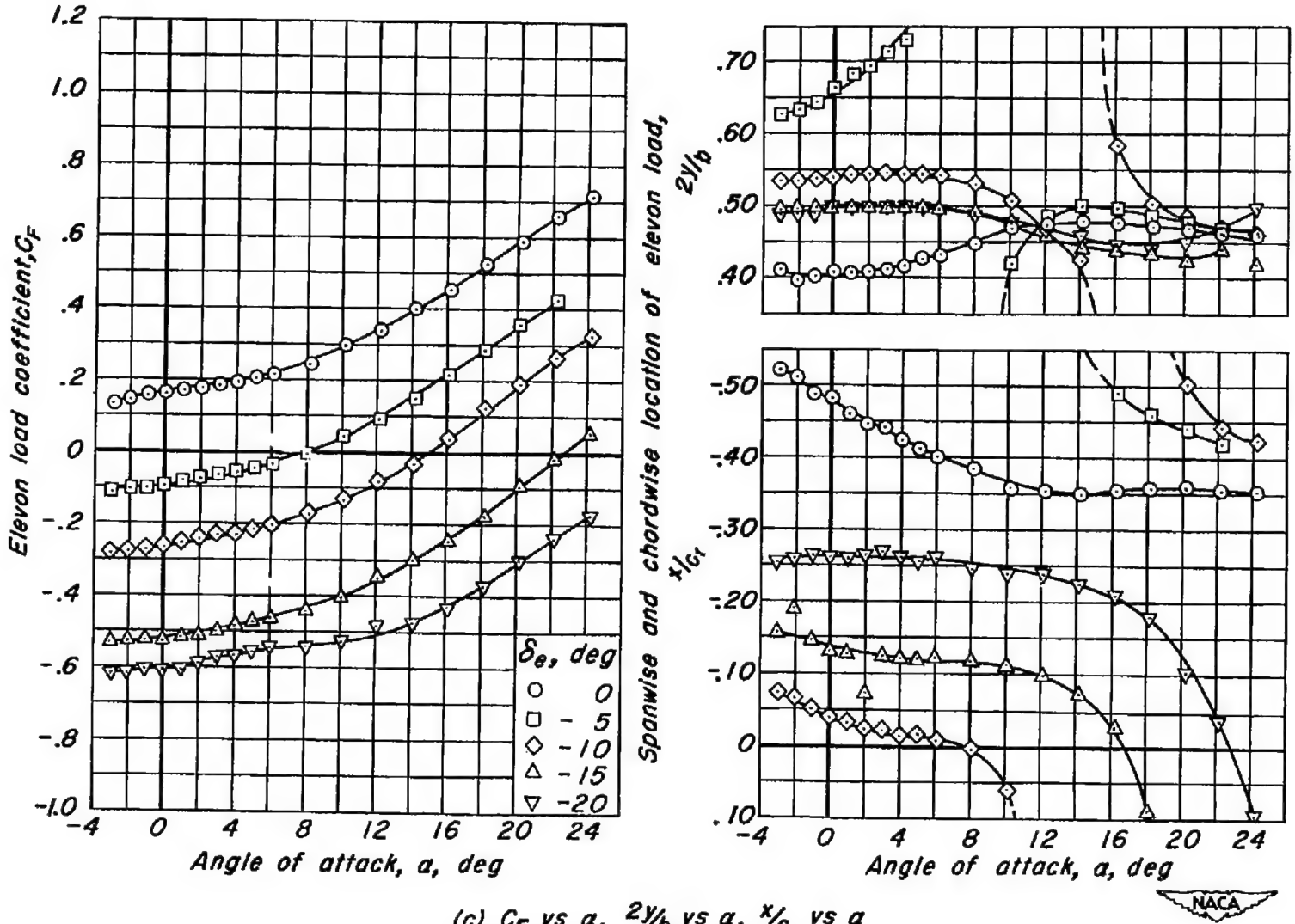

(c) C_F vs α, $2y/b$ vs α, x/c_r vs α

Figure 21.- Concluded.

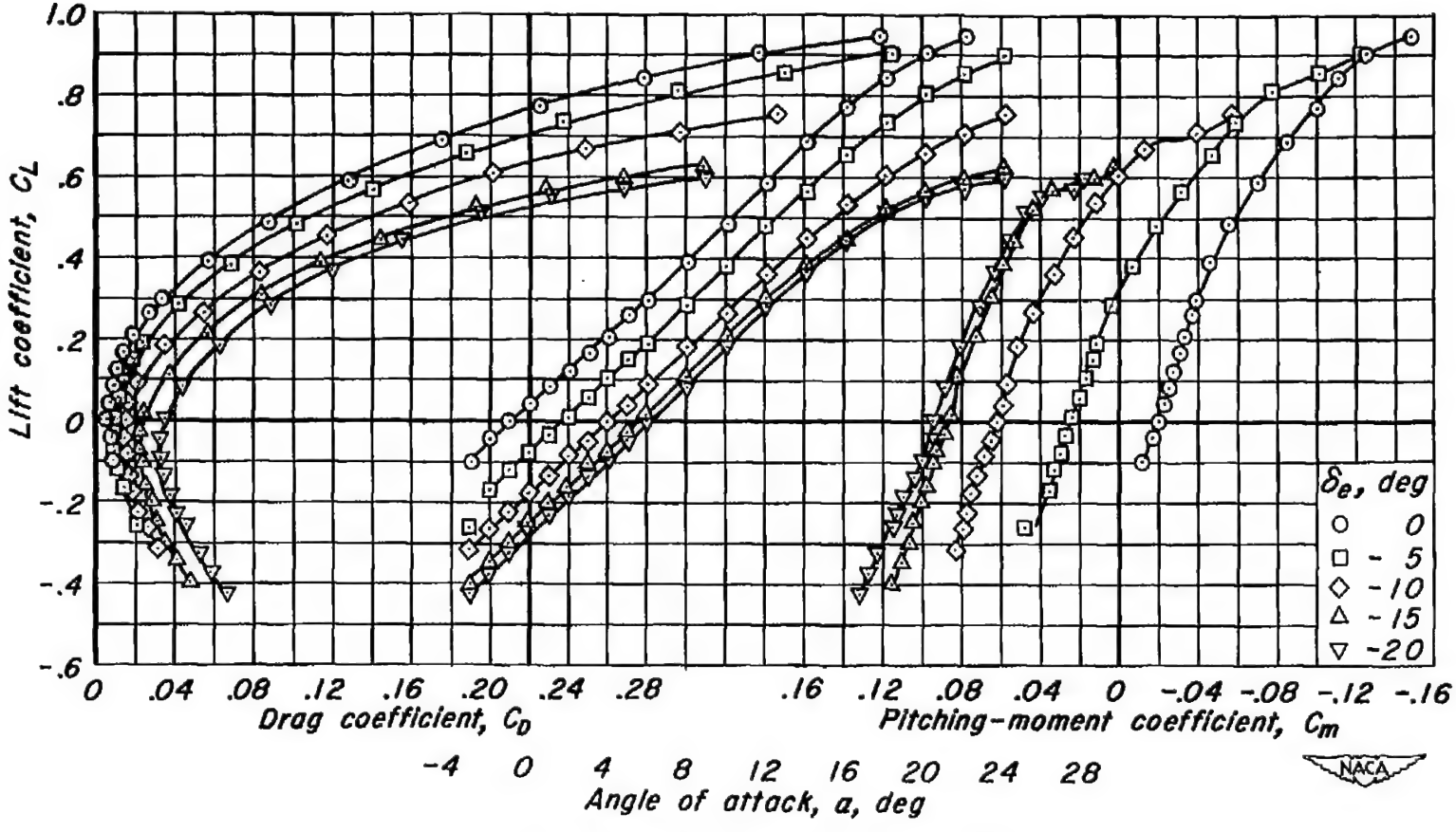

(a) C_L vs C_D, C_L vs α, C_L vs C_m

Figure 22.- The effect of elevon deflection on the aerodynamic characteristics at a Mach number of 0.80. R, 3.0 million; δ_t, 10°.

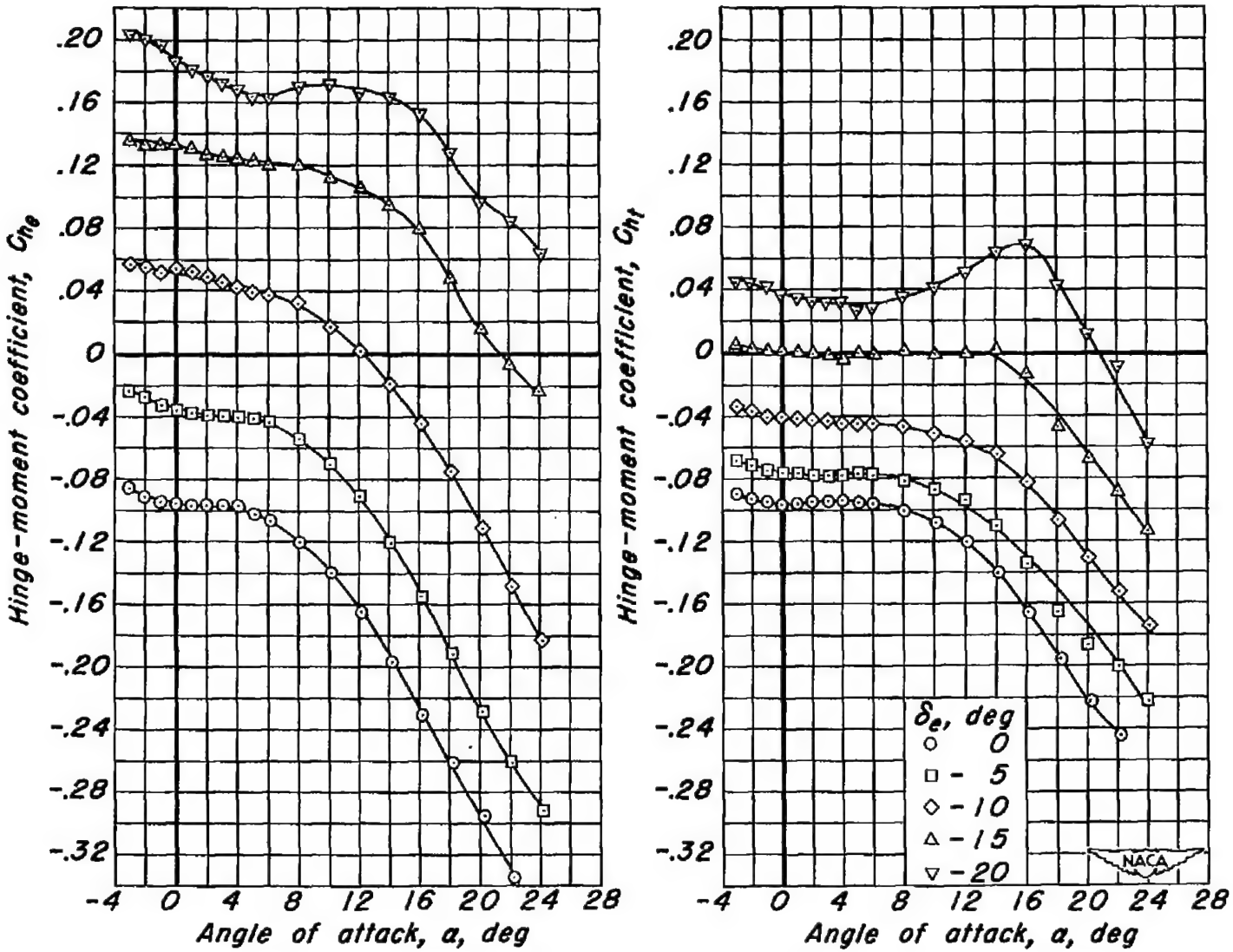

(b) C_{h_e} vs α, C_{h_t} vs α

Figure 22.- Continued.

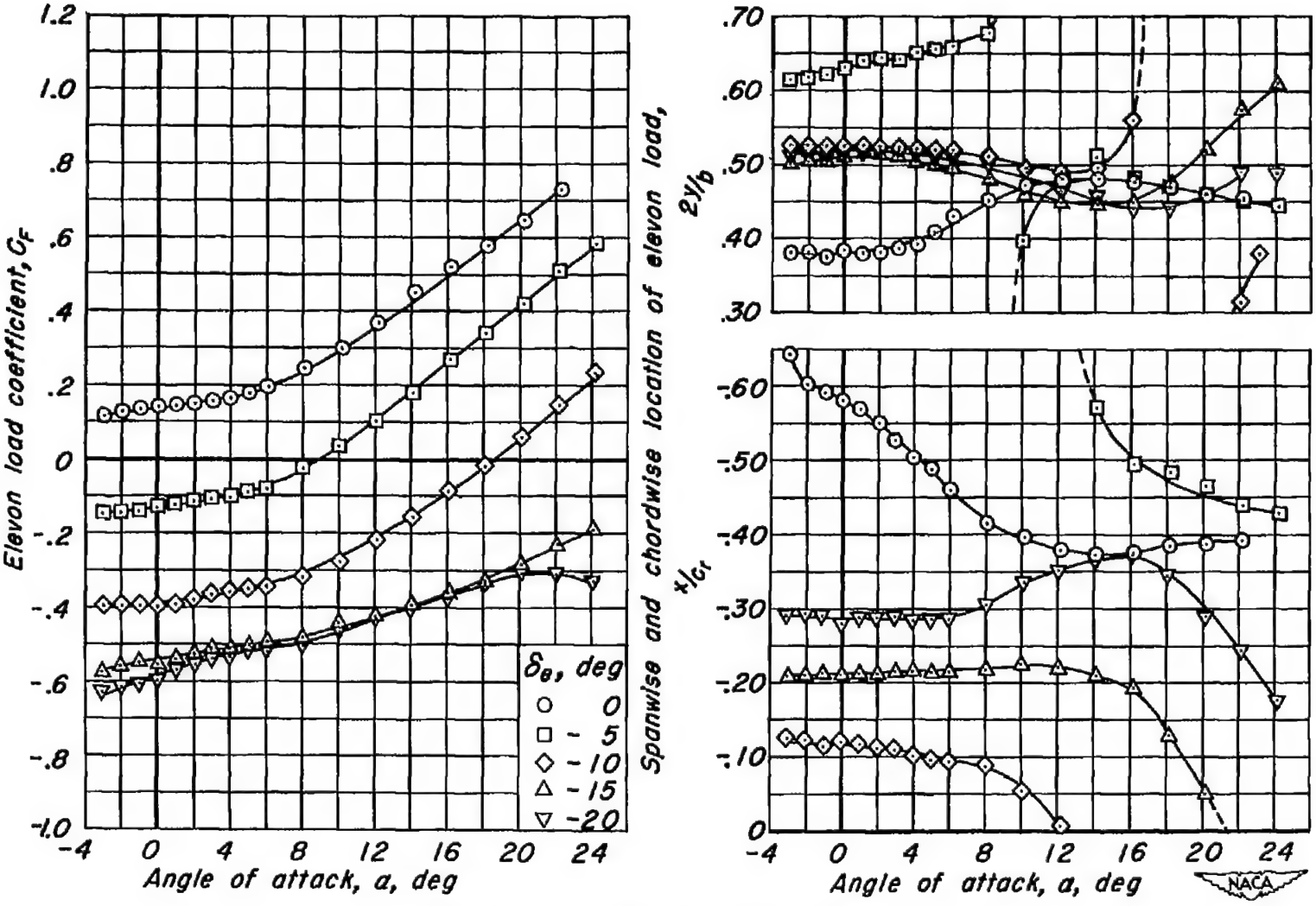

(c) C_F vs a, $2y/b$ vs a, x/c_r vs a

Figure 22.- Concluded.

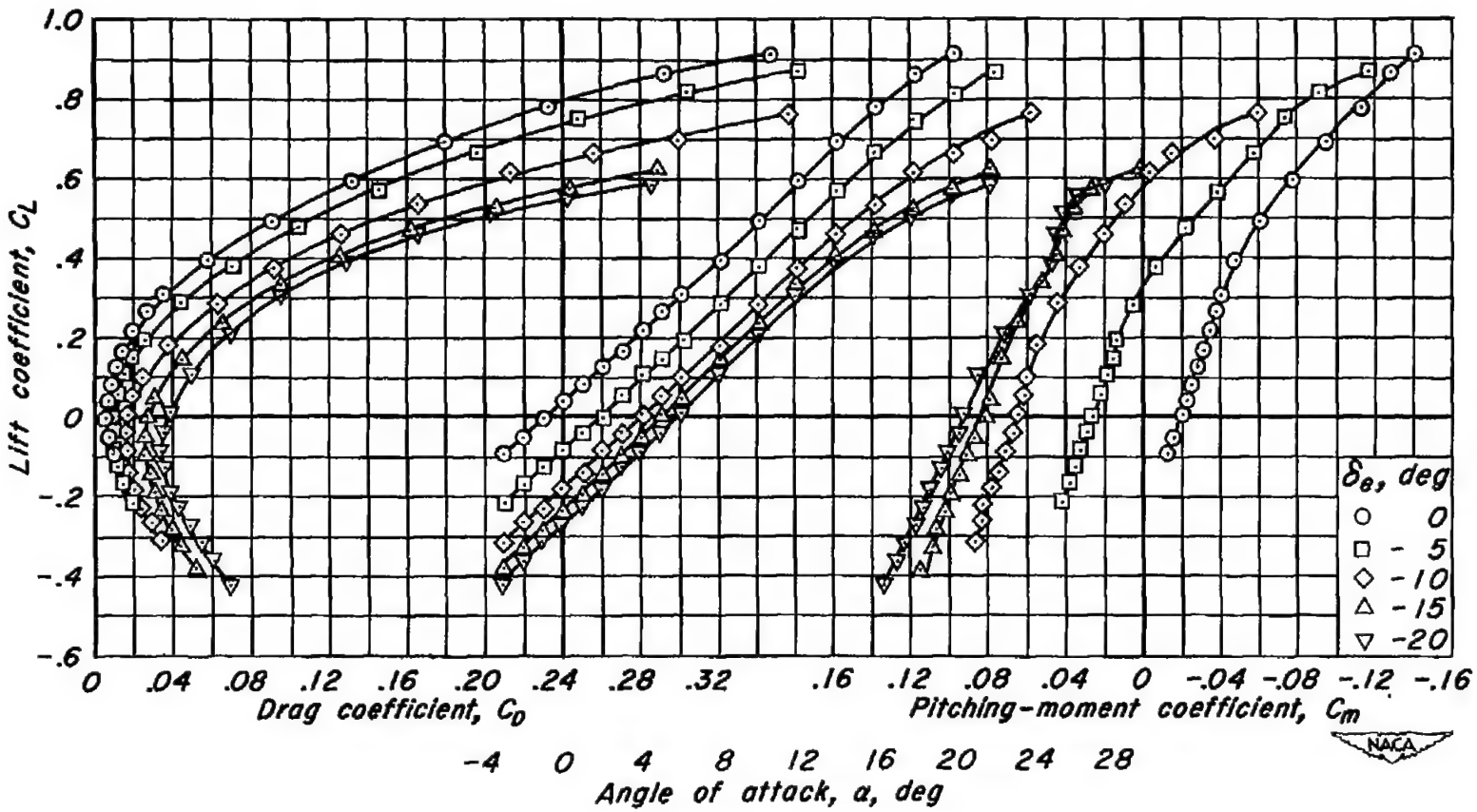

(a) C_L vs C_D, C_L vs α, C_L vs C_m

Figure 23.- The effect of elevon deflection on the aerodynamic characteristics at a Mach number of 0.85. R, 3.0 million; δ_t, 10°.

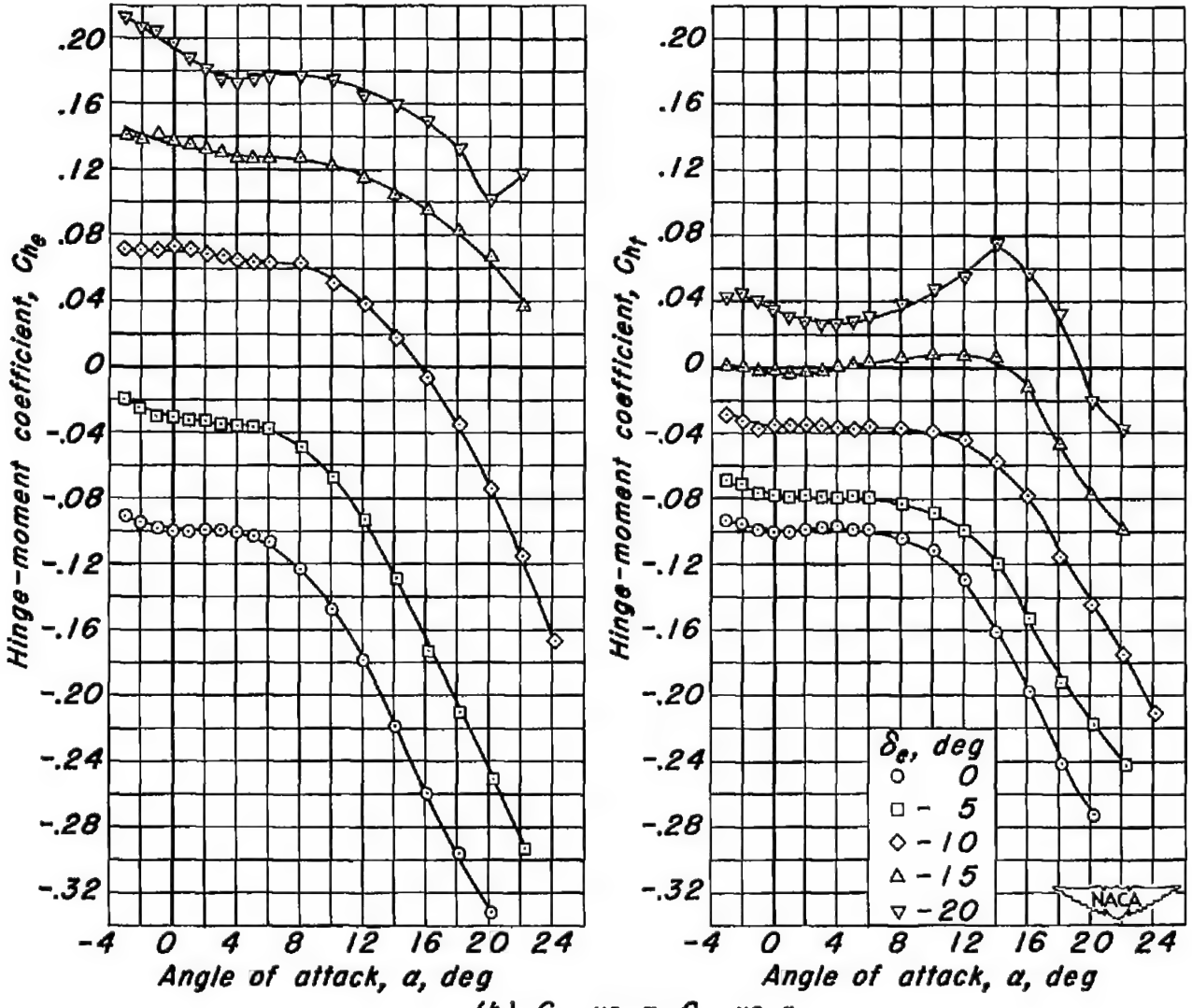

(b) C_{h_e} vs α, C_{h_t} vs α.

Figure 23.- Continued.

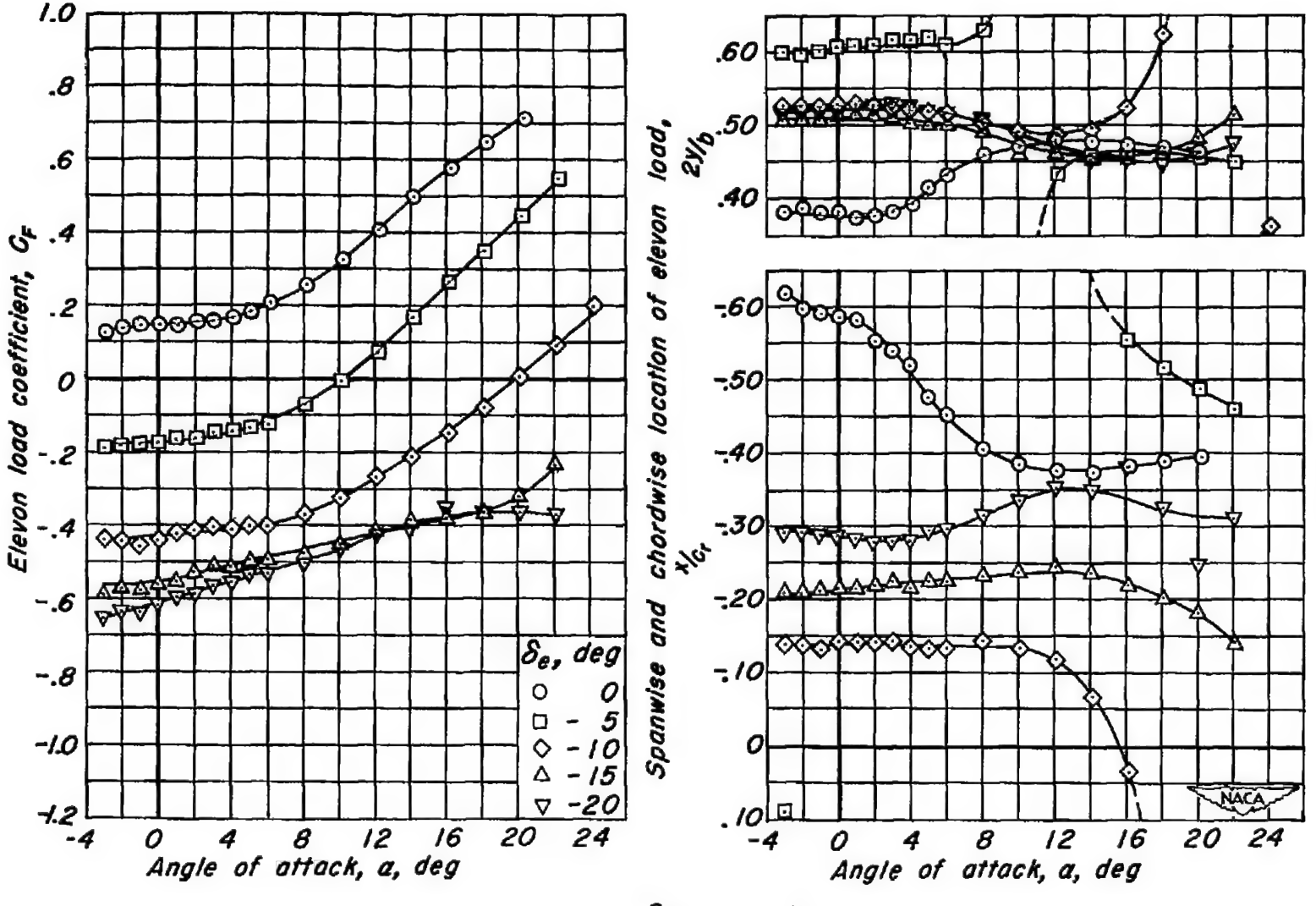

(c) C_F vs α, $2y/b$ vs α, x/c_r vs α

Figure 23.- Concluded.

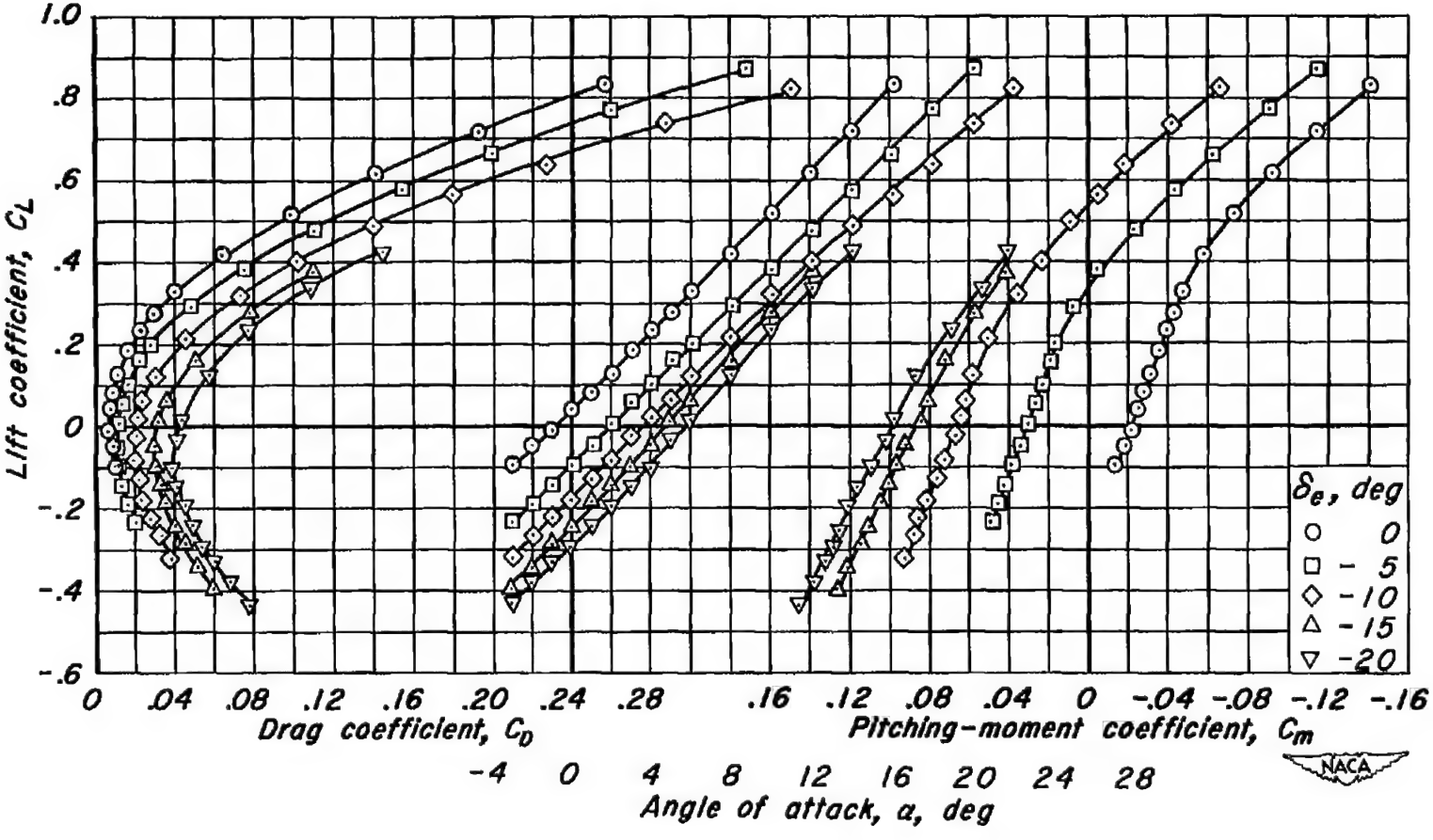

(a) C_L vs C_D, C_L vs α, C_L vs C_m

Figure 24.- The effect of elevon deflection on the aerodynamic characteristics at a Mach number of 0.90. R, 3.0 million; δ_t, 10°.

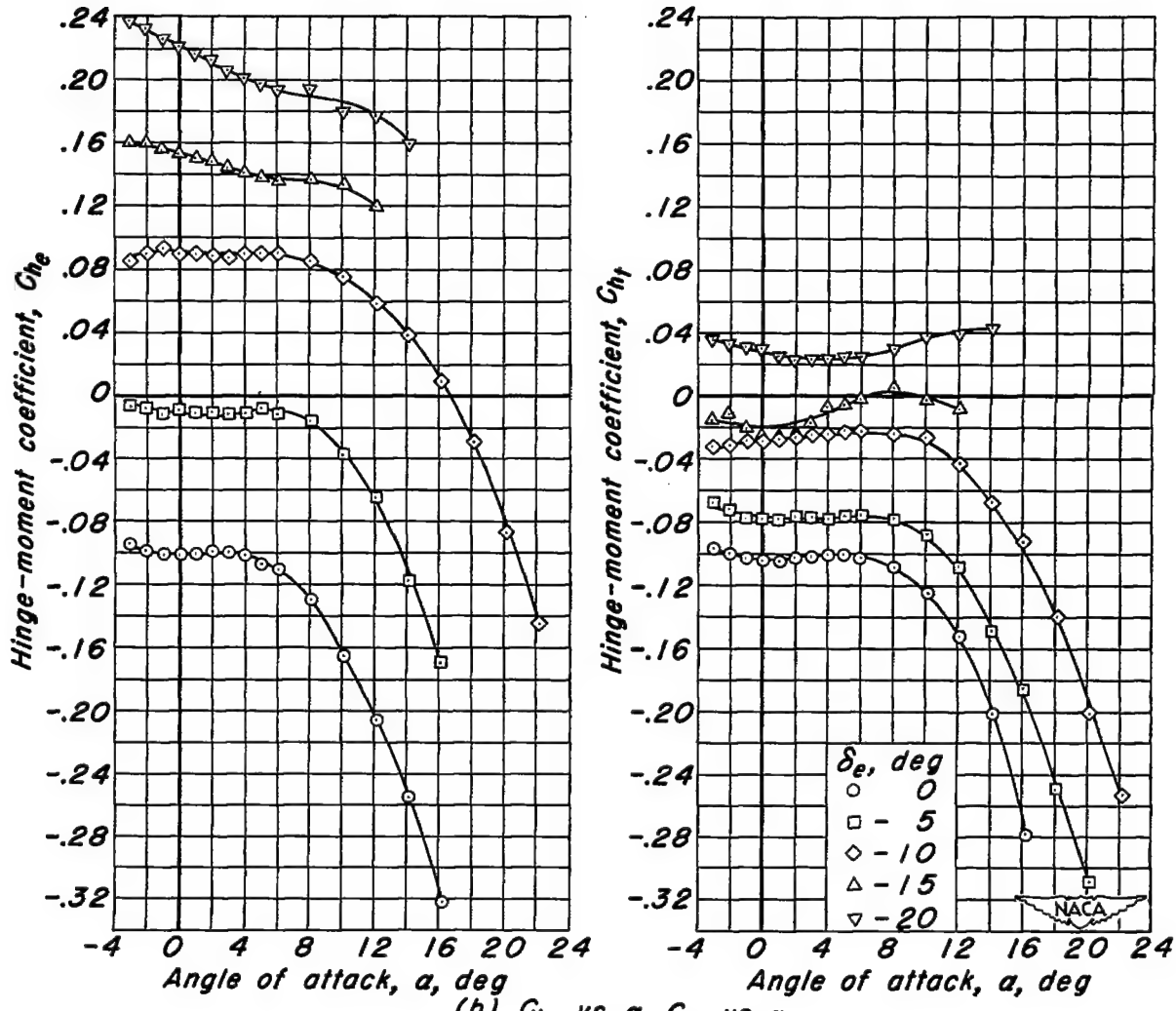

(b) C_{h_e} vs α, C_{h_t} vs α

Figure 24.- Continued.

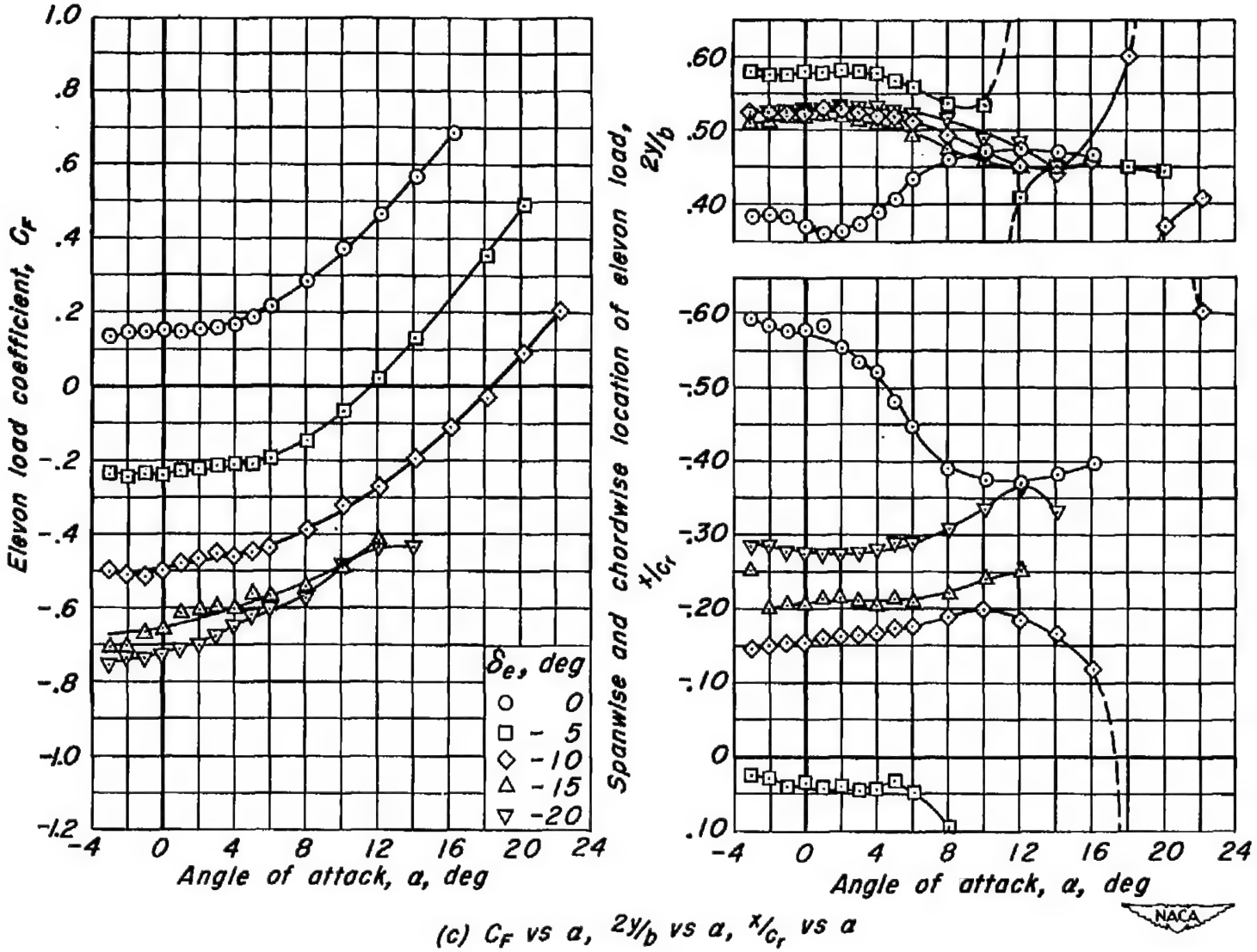

(c) C_F vs α, $2y/b$ vs α, x/c_r vs α

Figure 24.- Concluded.

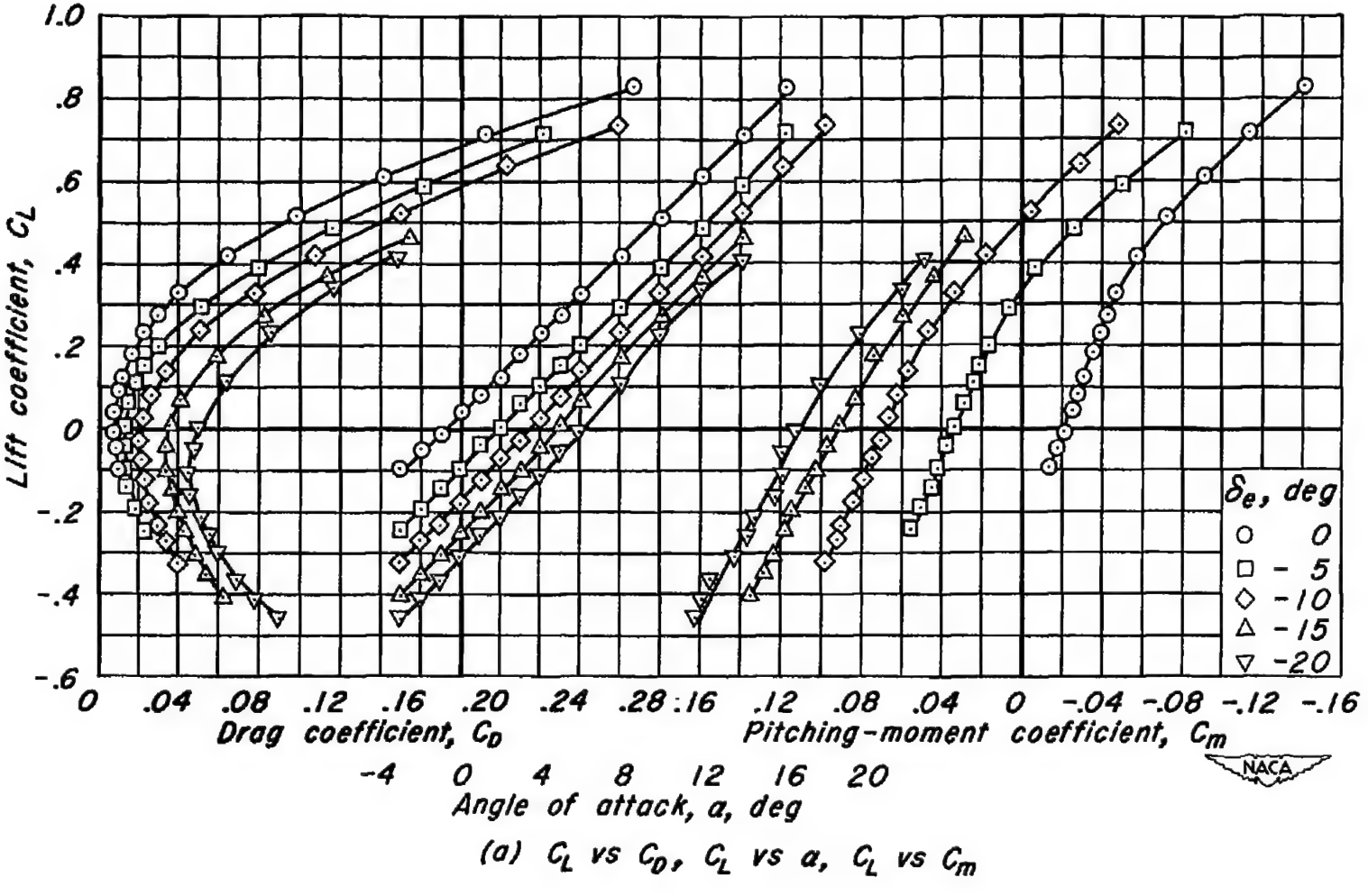

(a) C_L vs C_D, C_L vs a, C_L vs C_m

Figure 25.- The effect of elevon deflection on the aerodynamic characteristics at a Mach number of 0.92. R, 3.0 million; δ_t, 10°.

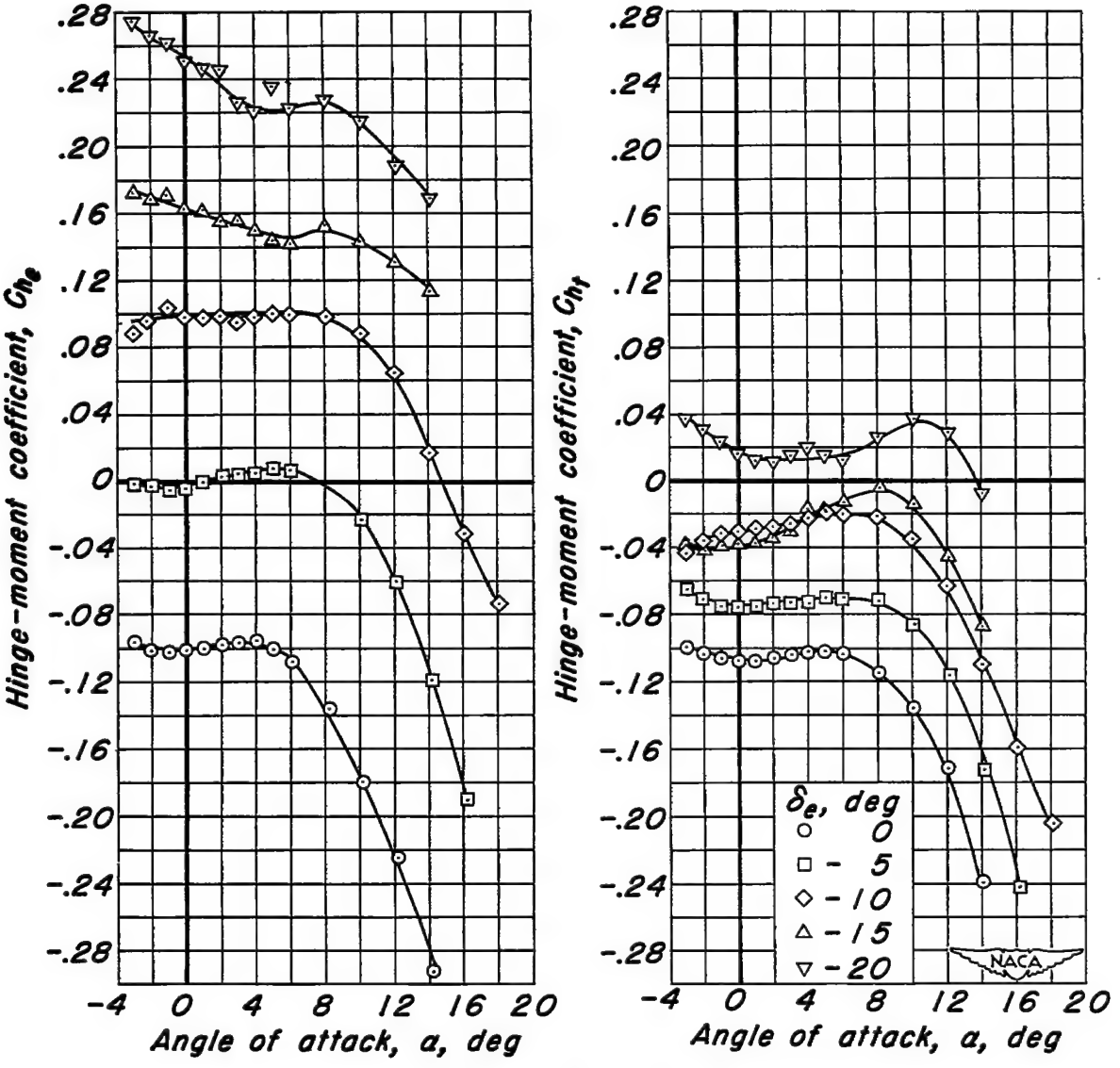

(b) C_{h_e} vs α, C_{h_t} vs α

Figure 25.- Continued.

[redacted]

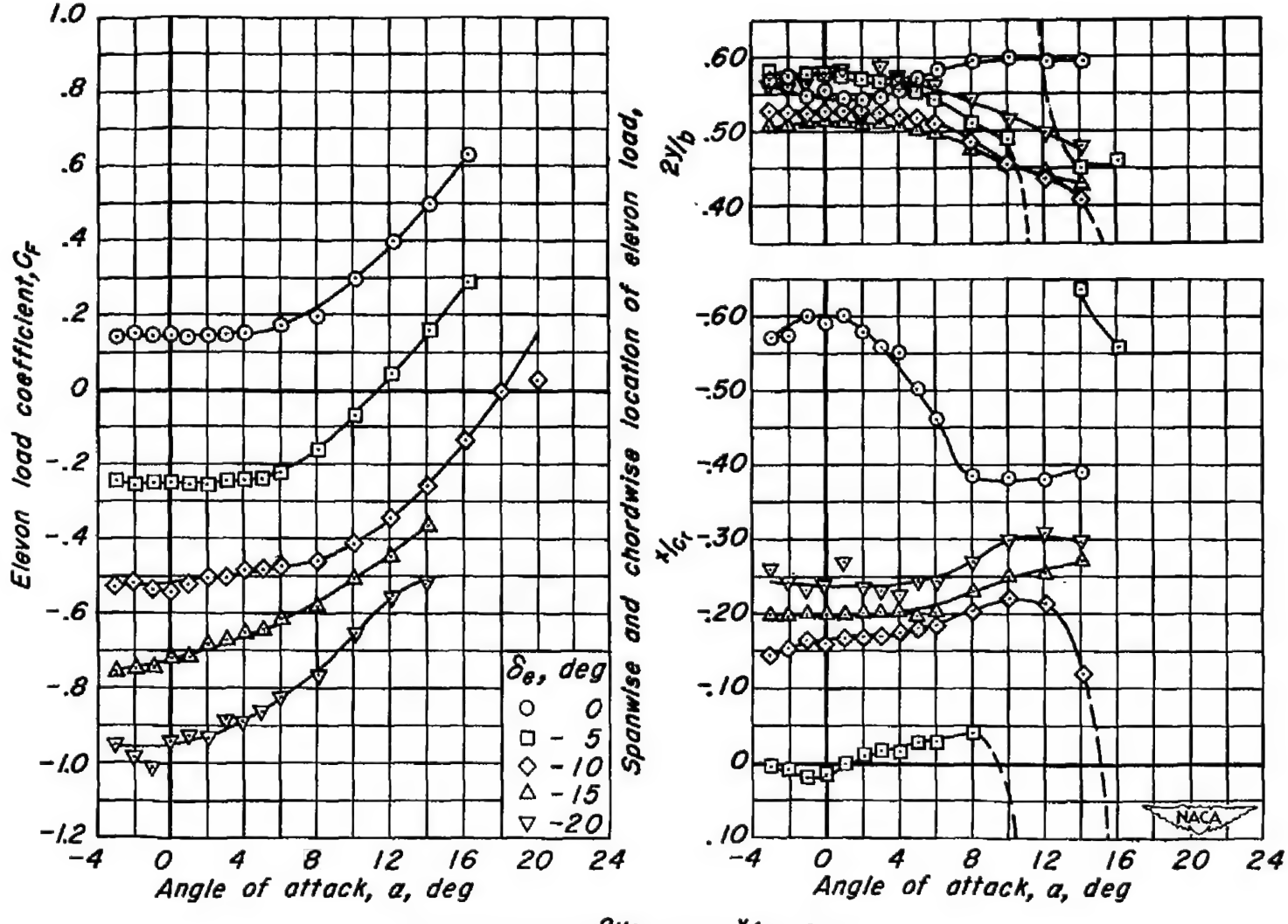

(c) C_F vs α, $2y/b$ vs α, x/c_r vs α

Figure 25.- Concluded.

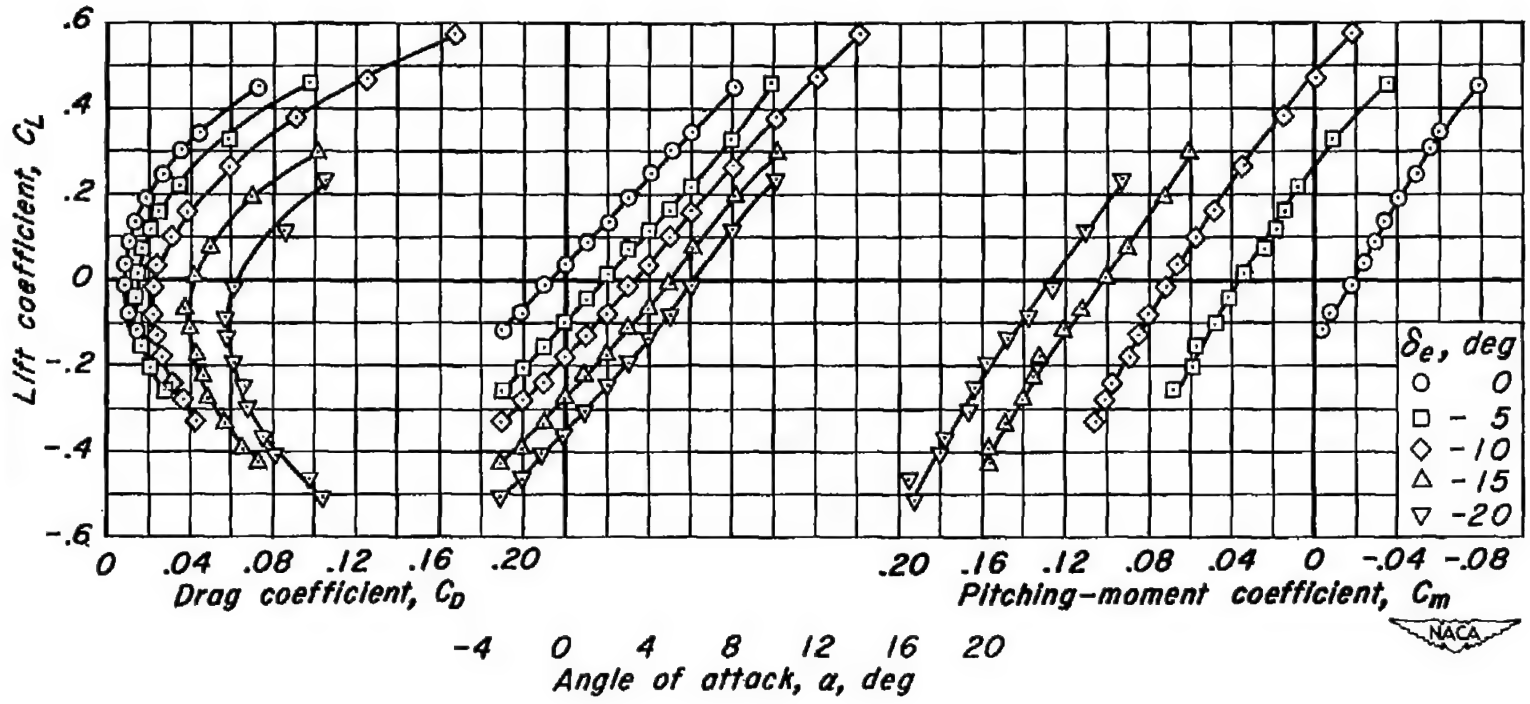

(a) C_L vs C_D, C_L vs α, C_L vs C_m

Figure 26.- The effect of elevon deflection on the aerodynamic characteristics at a Mach number of 0.95. R, 3.0 million; δ_t, 10°.

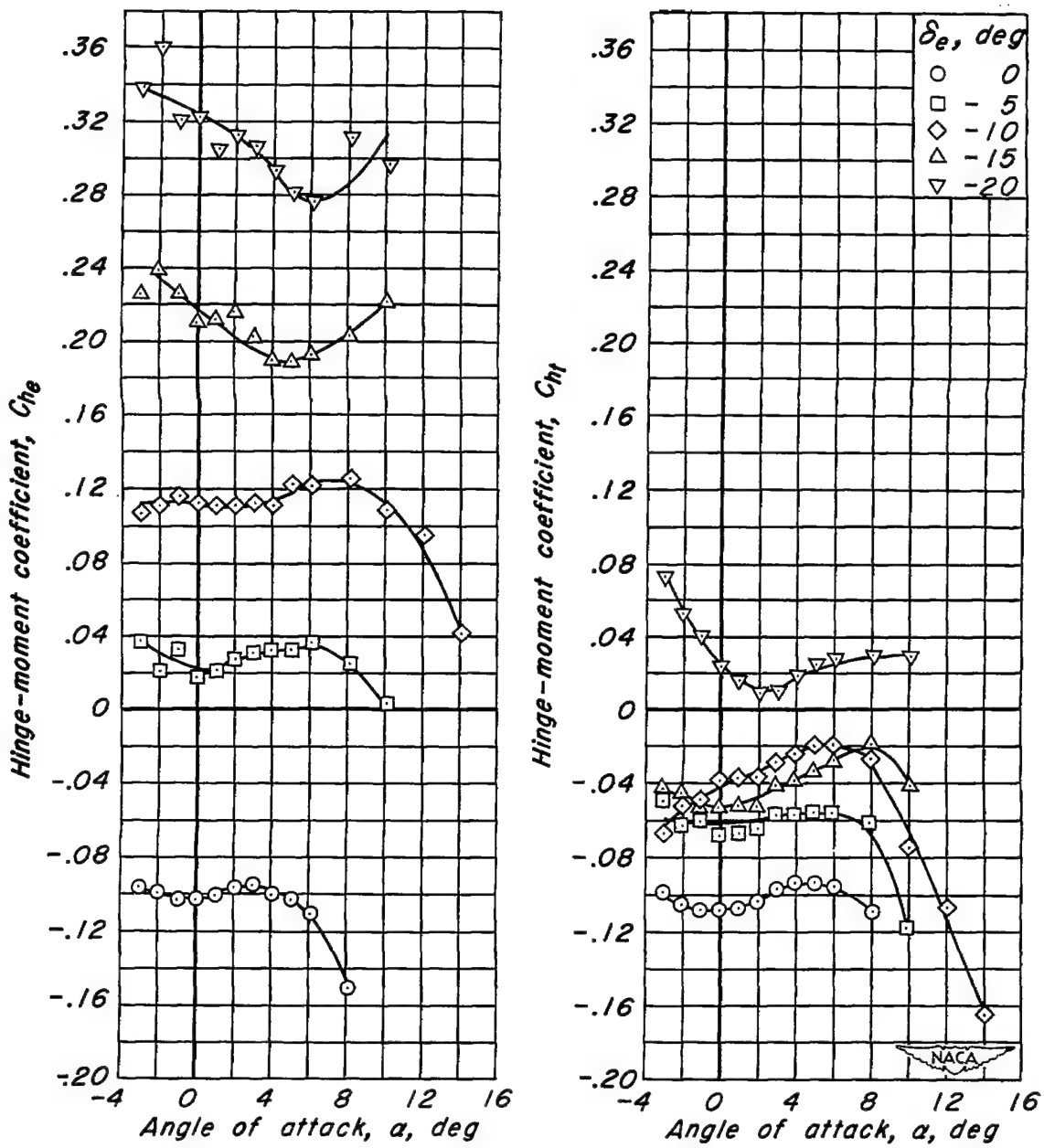

(b) C_{h_e} vs α, C_{h_t} vs α

Figure 26.-Continued.

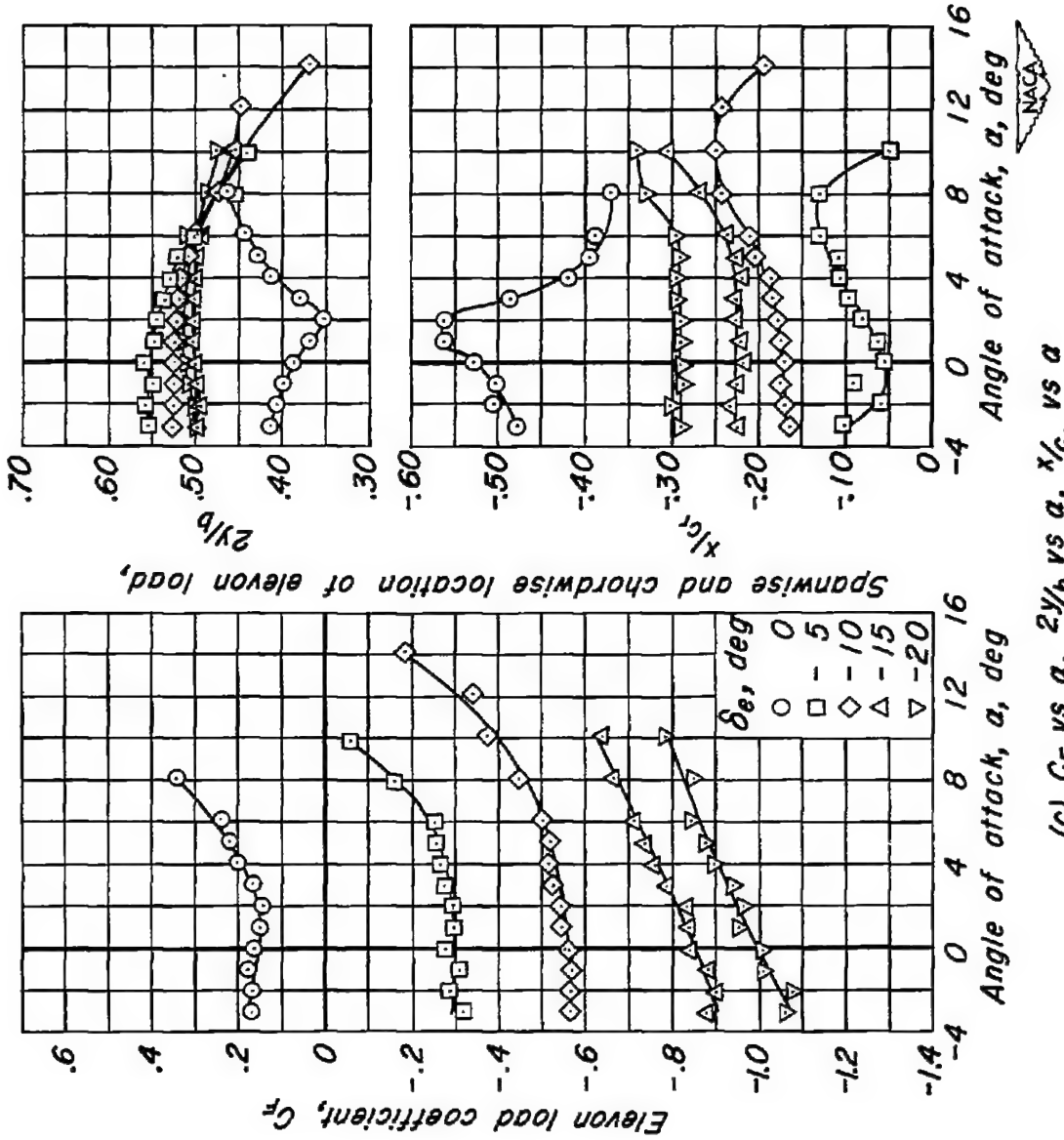

(c) C_F vs α, $2y/b$ vs α, x/c_r vs α

Figure 26.- Concluded.

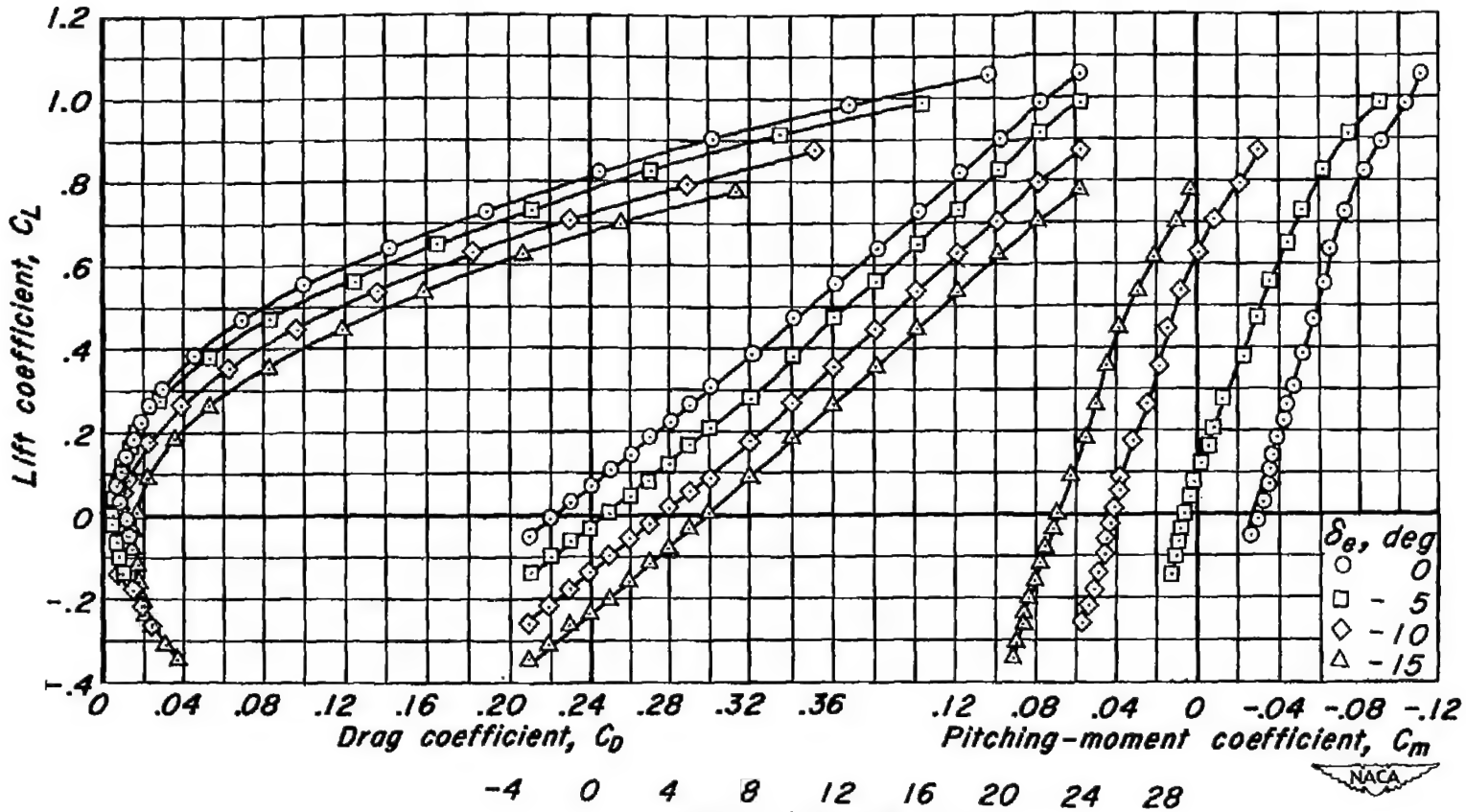

(a) C_L vs C_D, C_L vs α, C_L vs C_m

Figure 27.- The effect of elevon deflection on the aerodynamic characteristics at a Mach number of 0.24. R, 3.0 million; δ_t, 15°.

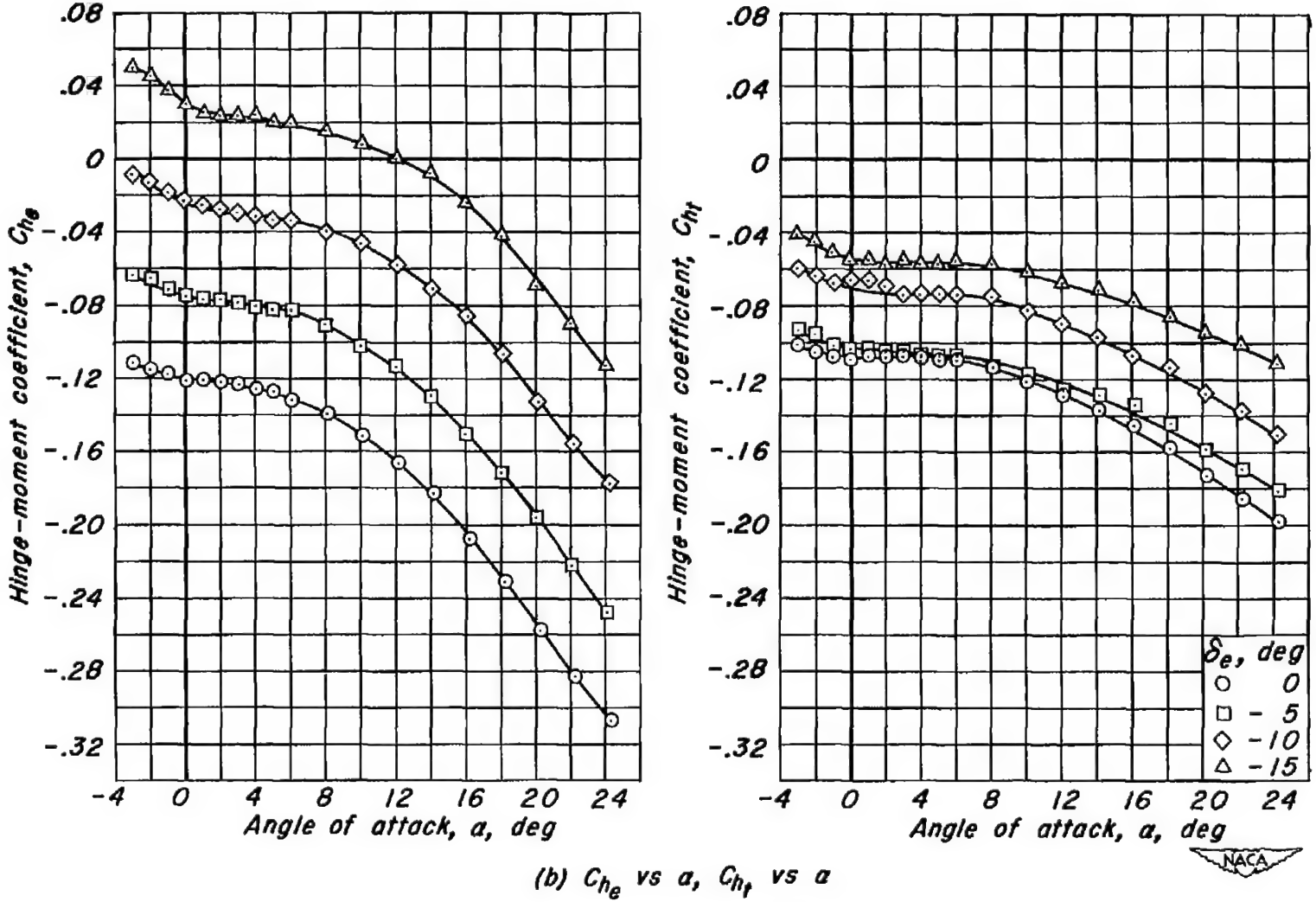

(b) C_{h_e} vs α, C_{h_t} vs α

Figure 27.- Continued.

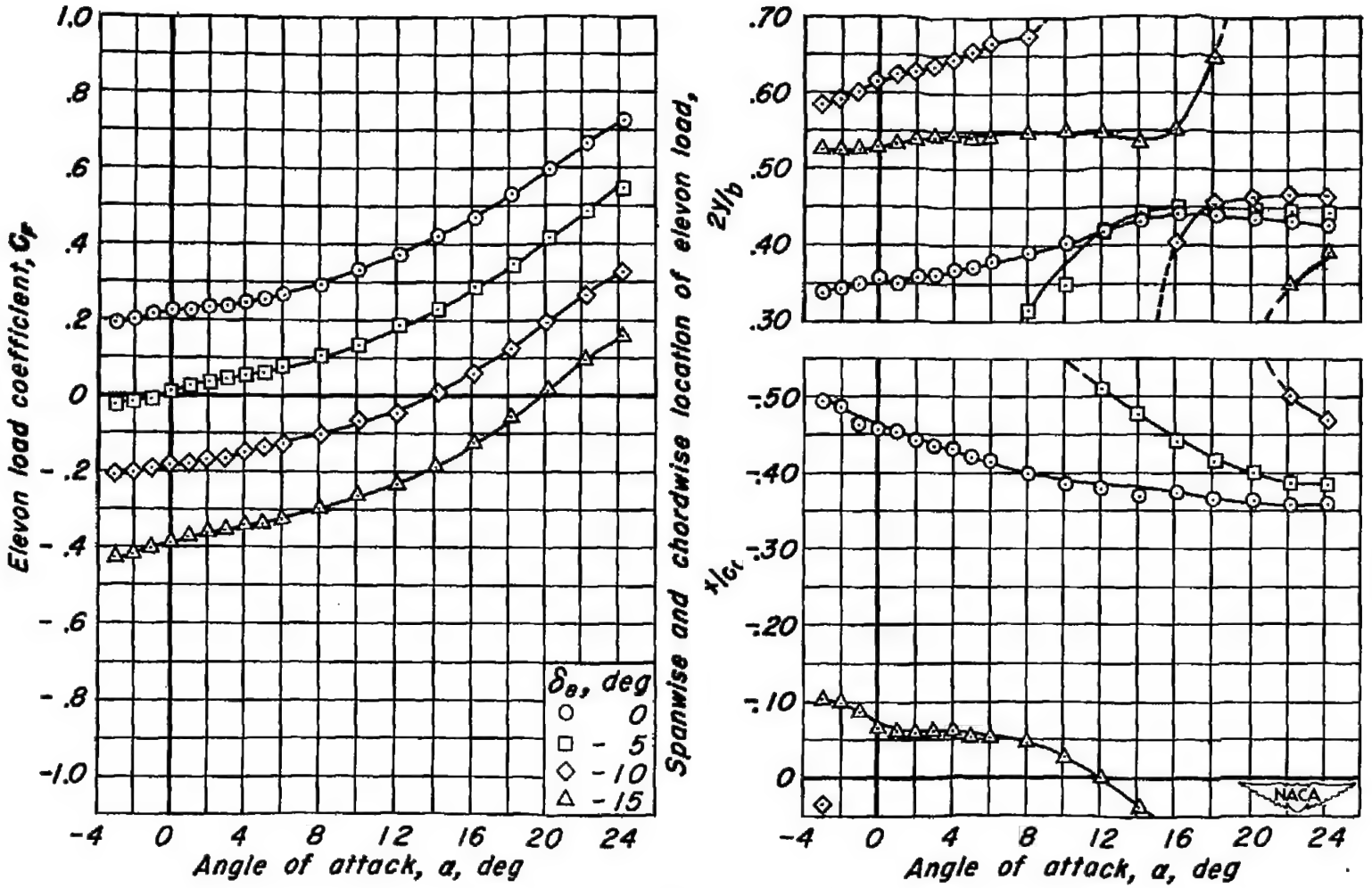

(c) C_F vs α, $2y/b$ vs α, x/c_r vs α

Figure 27.- Concluded.

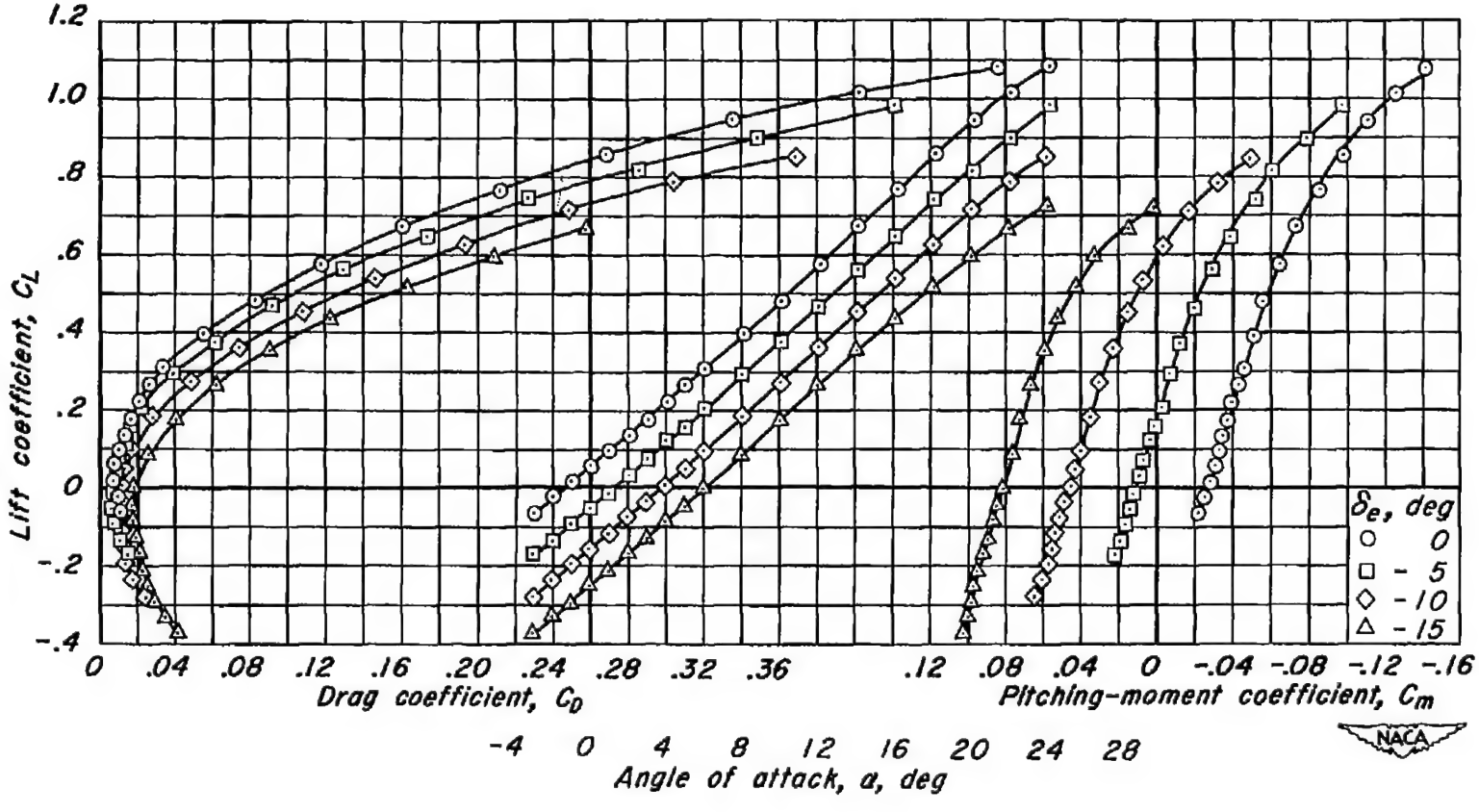

(a) C_L vs C_D, C_L vs α, C_L vs C_m

Figure 28.- The effect of elevon deflection on the aerodynamic characteristics at a Mach number of 0.60. R, 3.0 million; δ_f, 15°.

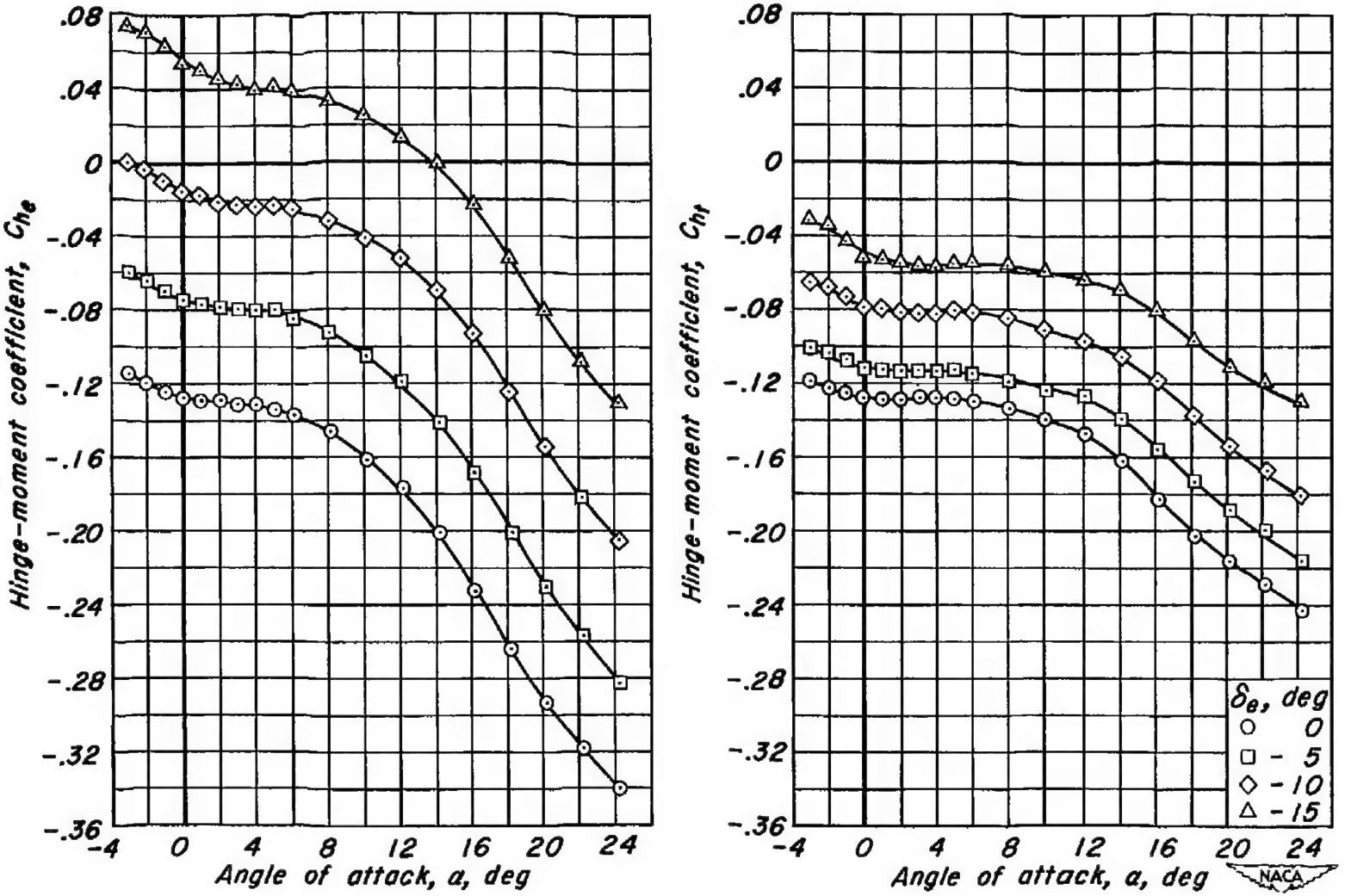

(b) C_{h_e} vs α, C_{h_f} vs α

Figure 28.-Continued.

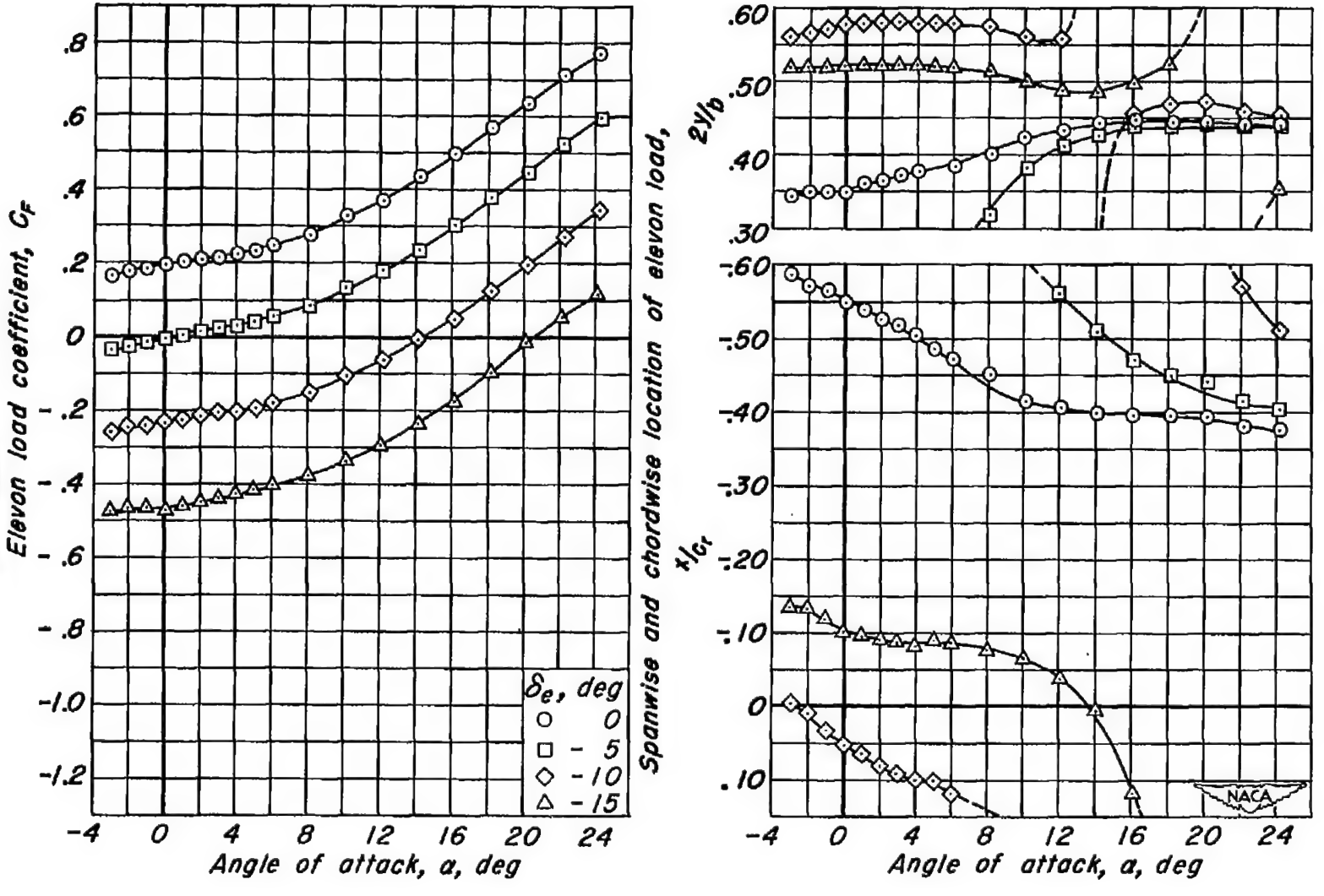

(c) C_F vs α, $2y/b$ vs α, x/c_r vs α

Figure 28.- Concluded.

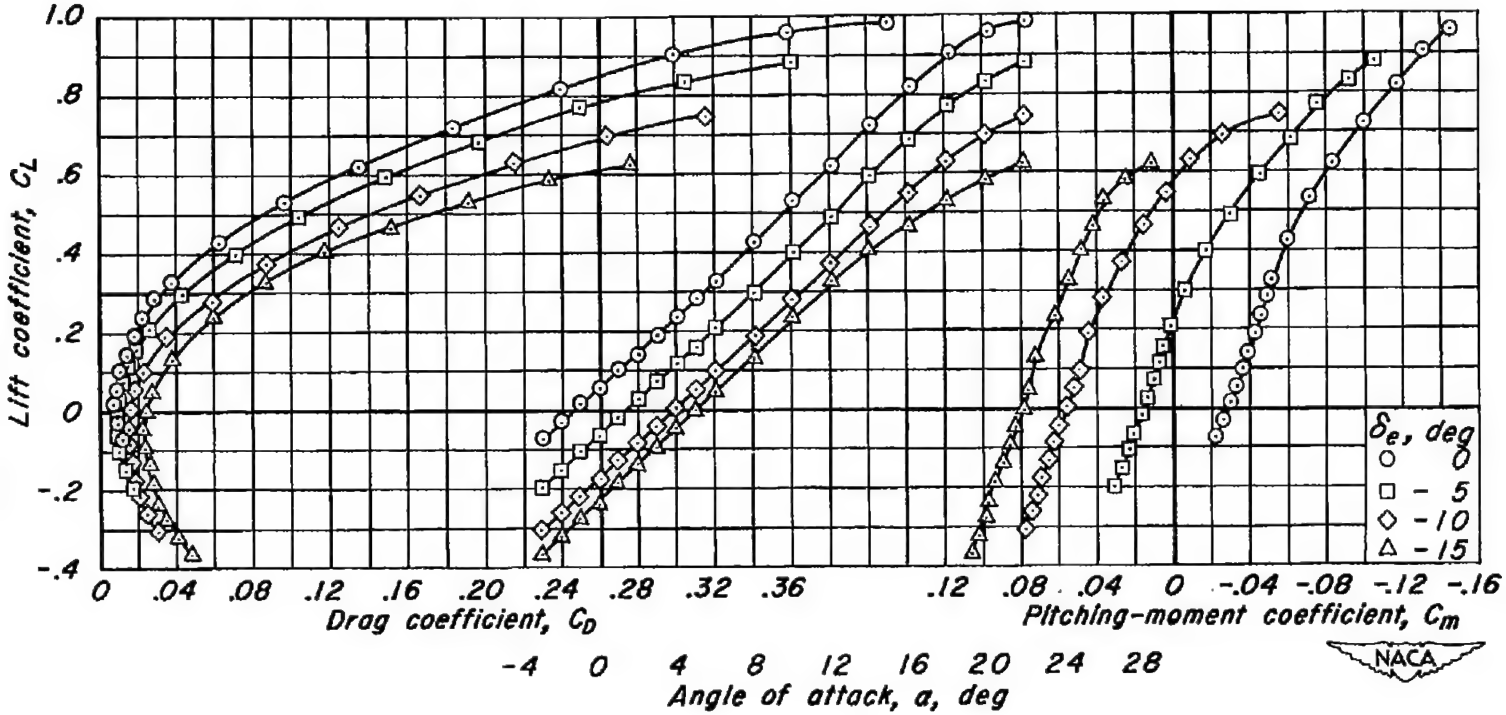

(a) C_L vs C_D, C_L vs α, C_L vs C_m

Figure 29.- The effect of elevon deflection on the aerodynamic characteristics at a Mach number of 0.80. R, 3.0 million; δ_t, 15°.

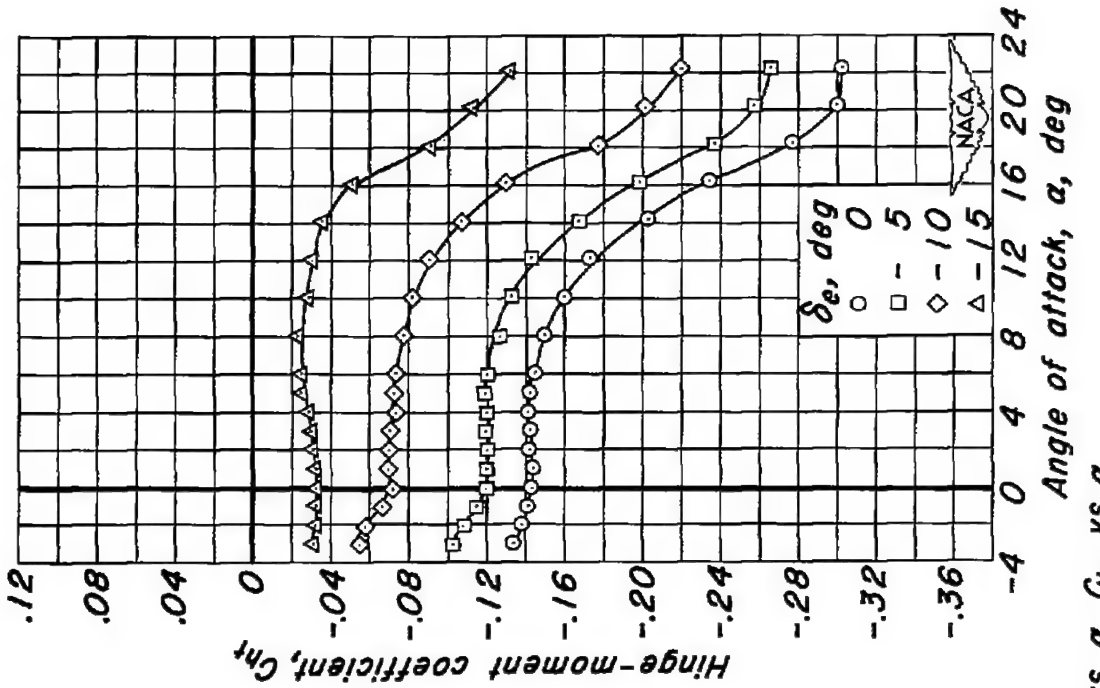

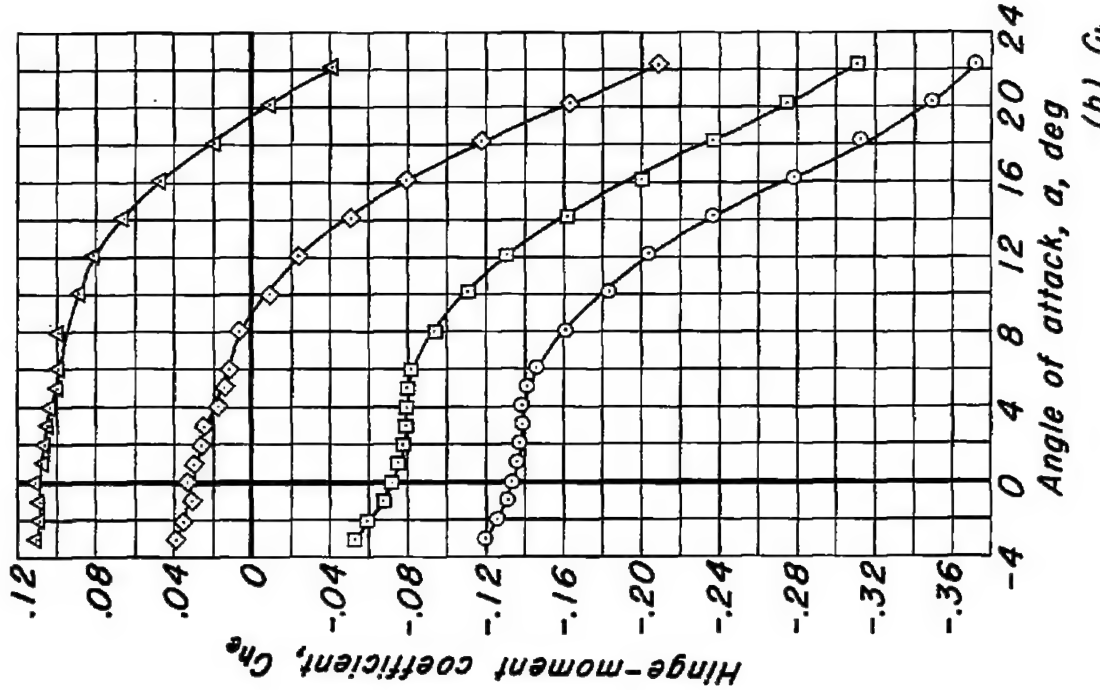

(b) C_{h_e} vs α, C_{h_t} vs α

Figure 29.- Continued.

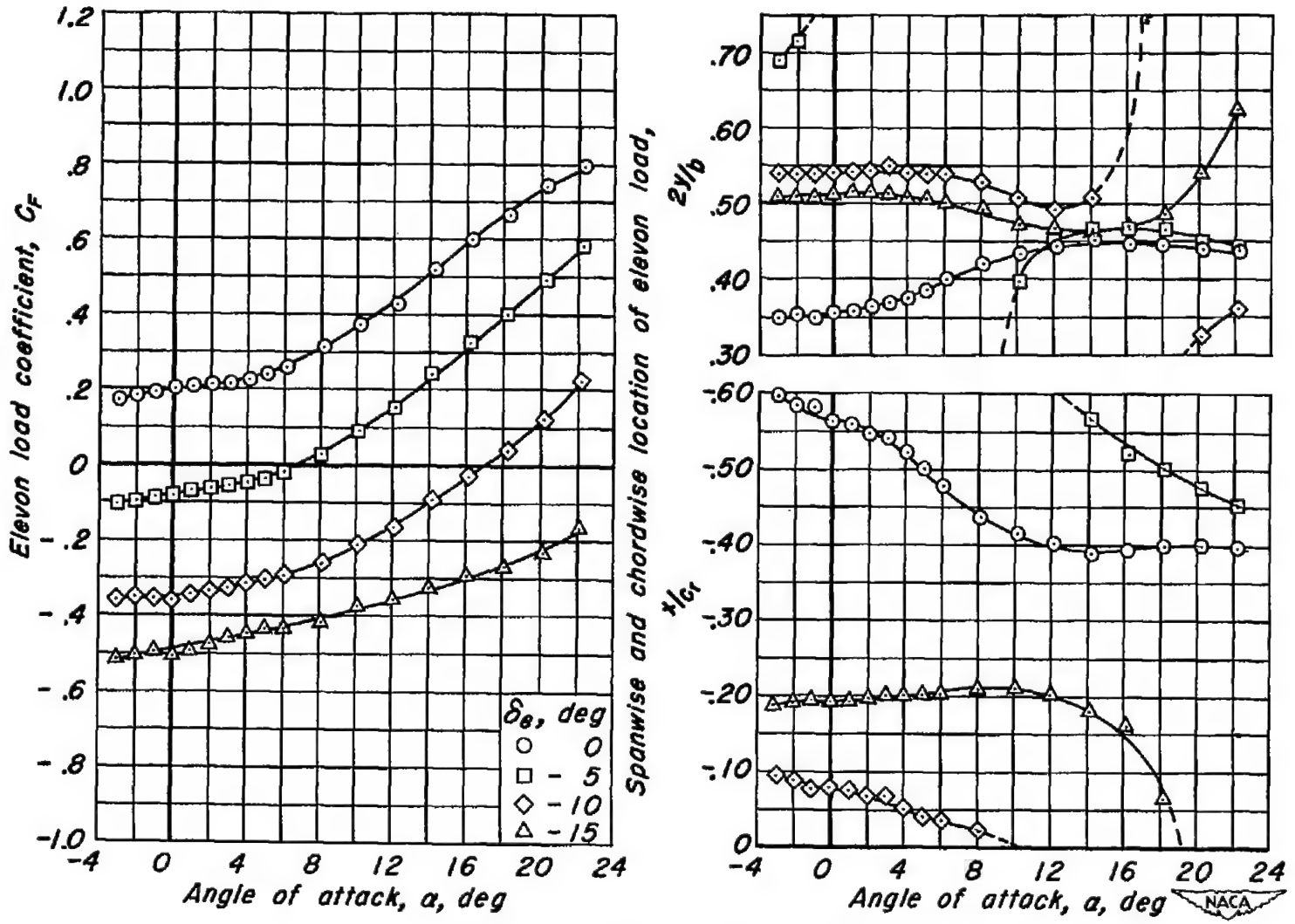

(c) C_F vs α, $2y/b$ vs α, x/c_r vs α

Figure 29.- Concluded.

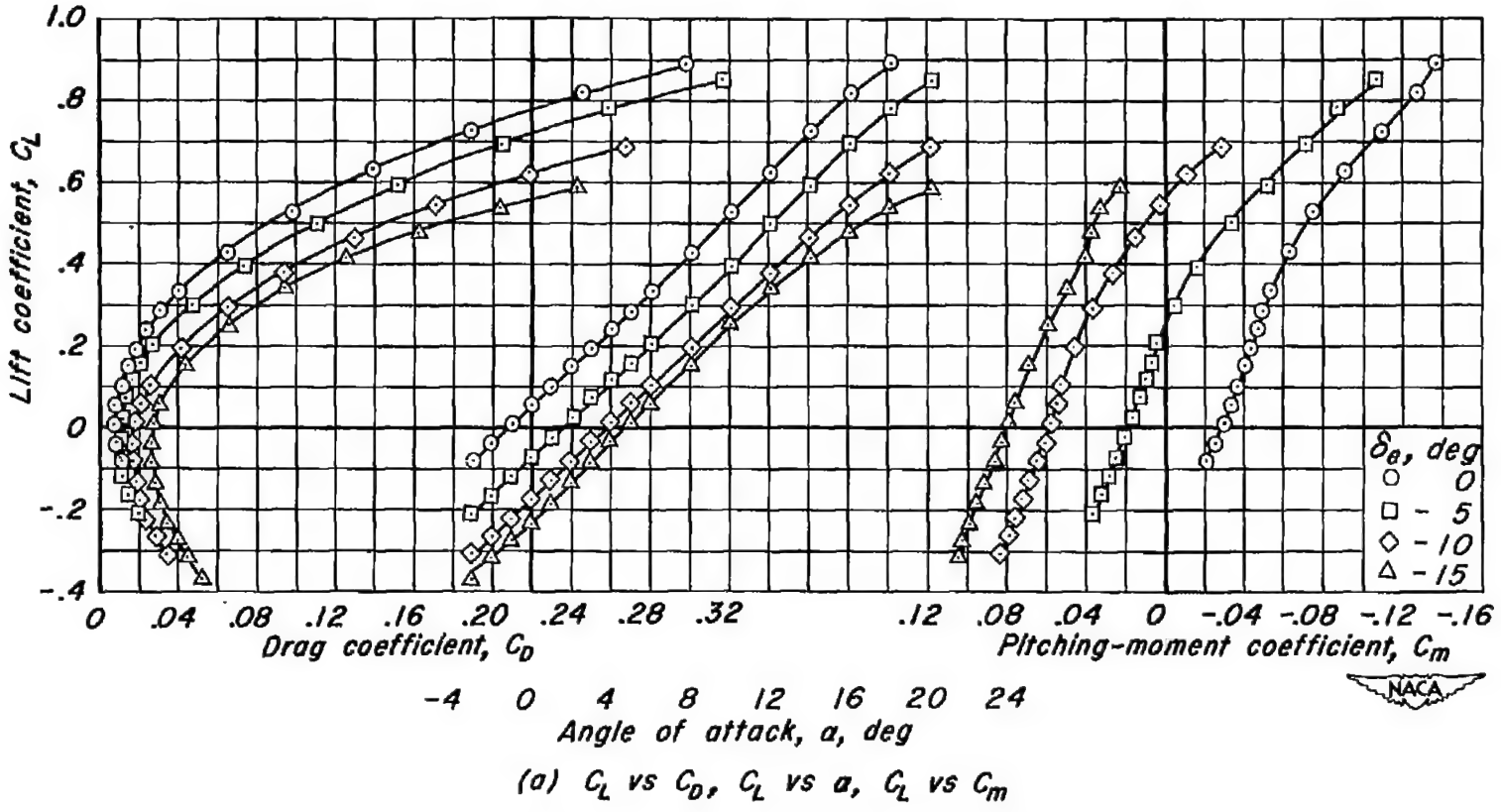

(a) C_L vs C_D, C_L vs α, C_L vs C_m

Figure 30.- The effect of elevon deflection on the aerodynamic characteristics at a Mach number of 0.85. R, 3.0 million; δ_t, 15°.

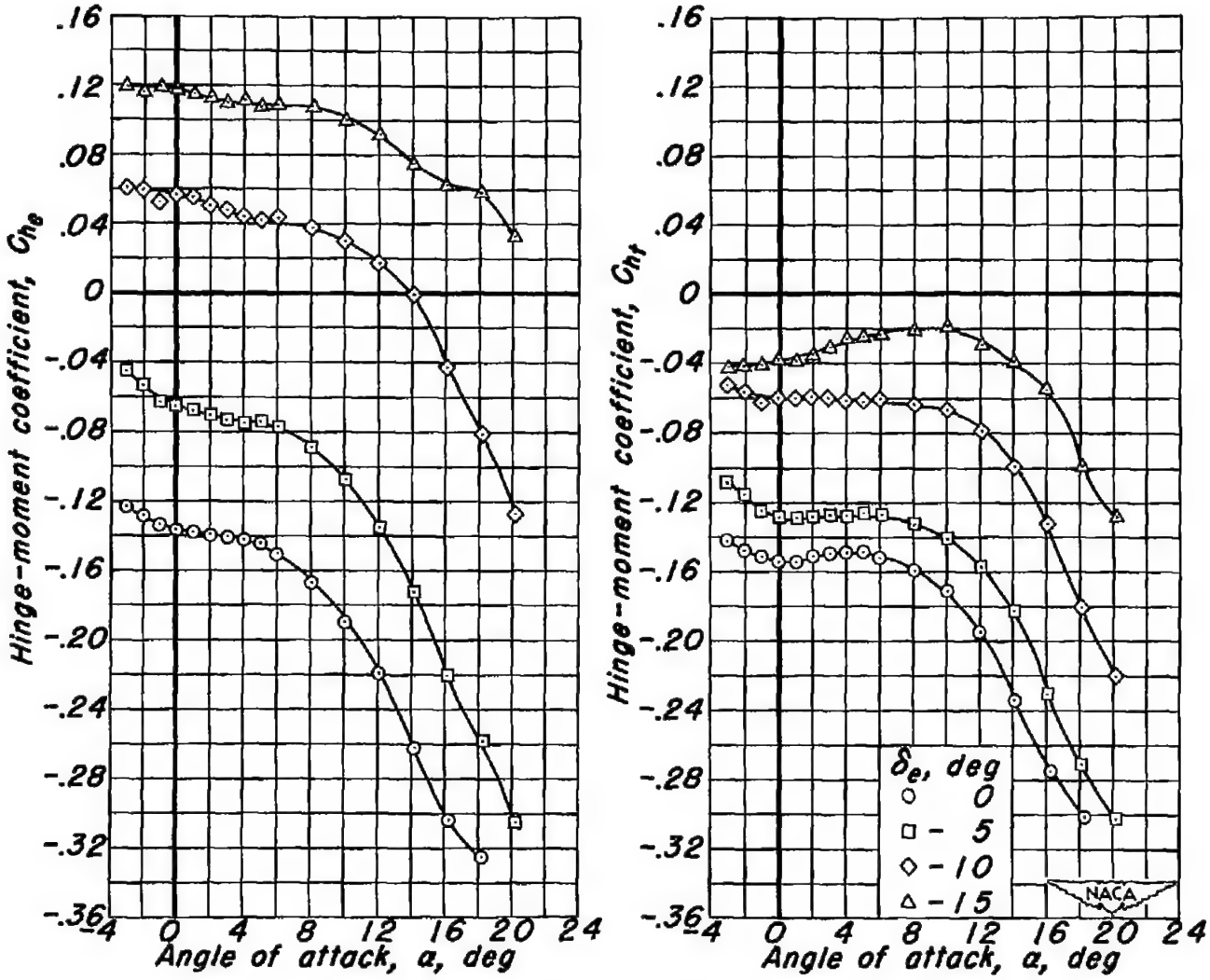

(b) C_{h_e} vs α, C_{h_f} vs α

Figure 30.- Continued.

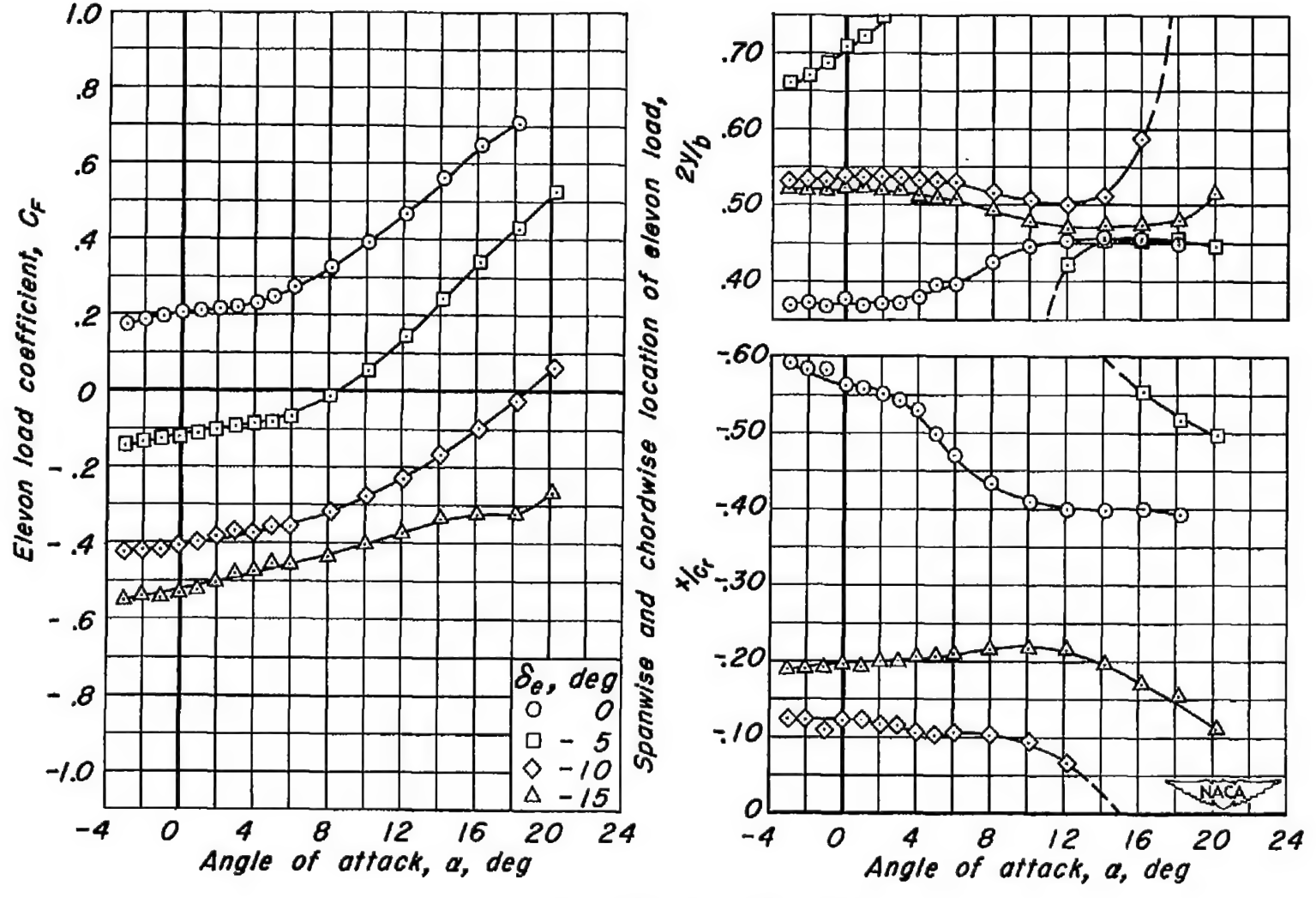

(c) C_F vs α, $2y/b$ vs α, x/c_r vs α

Figure 30.- Concluded.

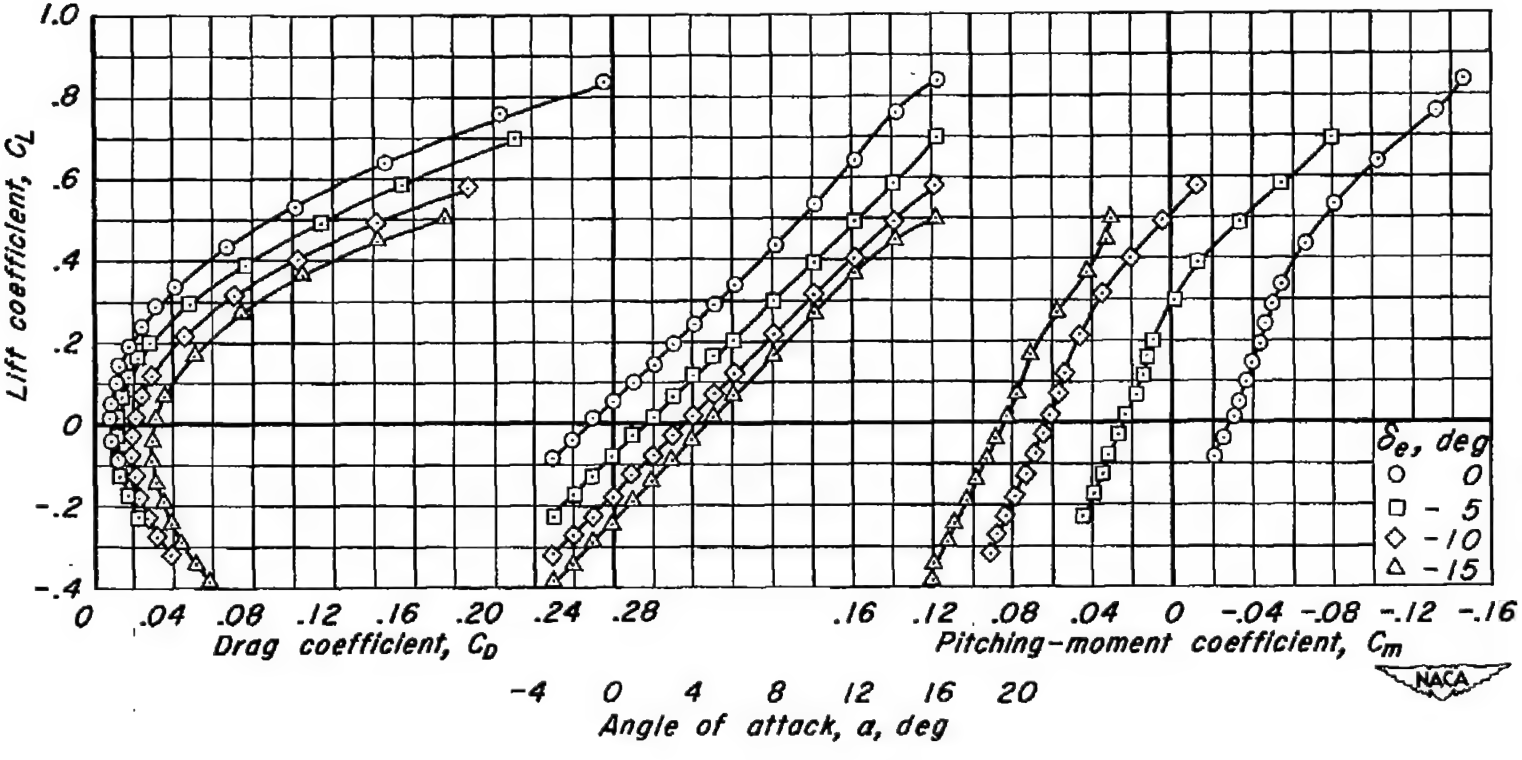

(a) C_L vs C_D, C_L vs α, C_L vs C_m

Figure 31.- The effect of elevon deflection on the aerodynamic characteristics at a Mach number of 0.90. R, 3.0 million; δ_t, 15°.

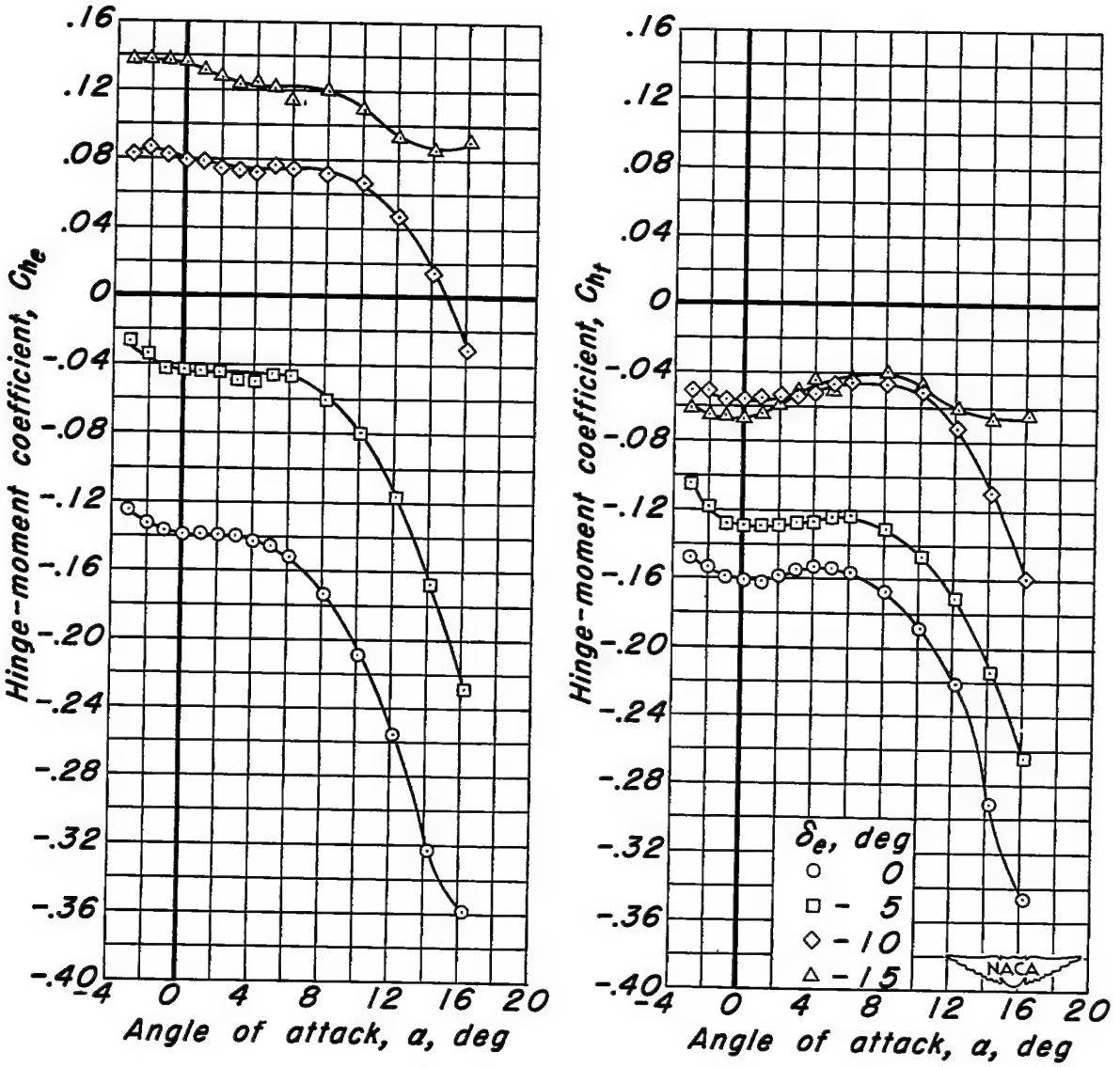

(b) C_{he} vs α, C_{ht} vs α

Figure 31.- Continued.

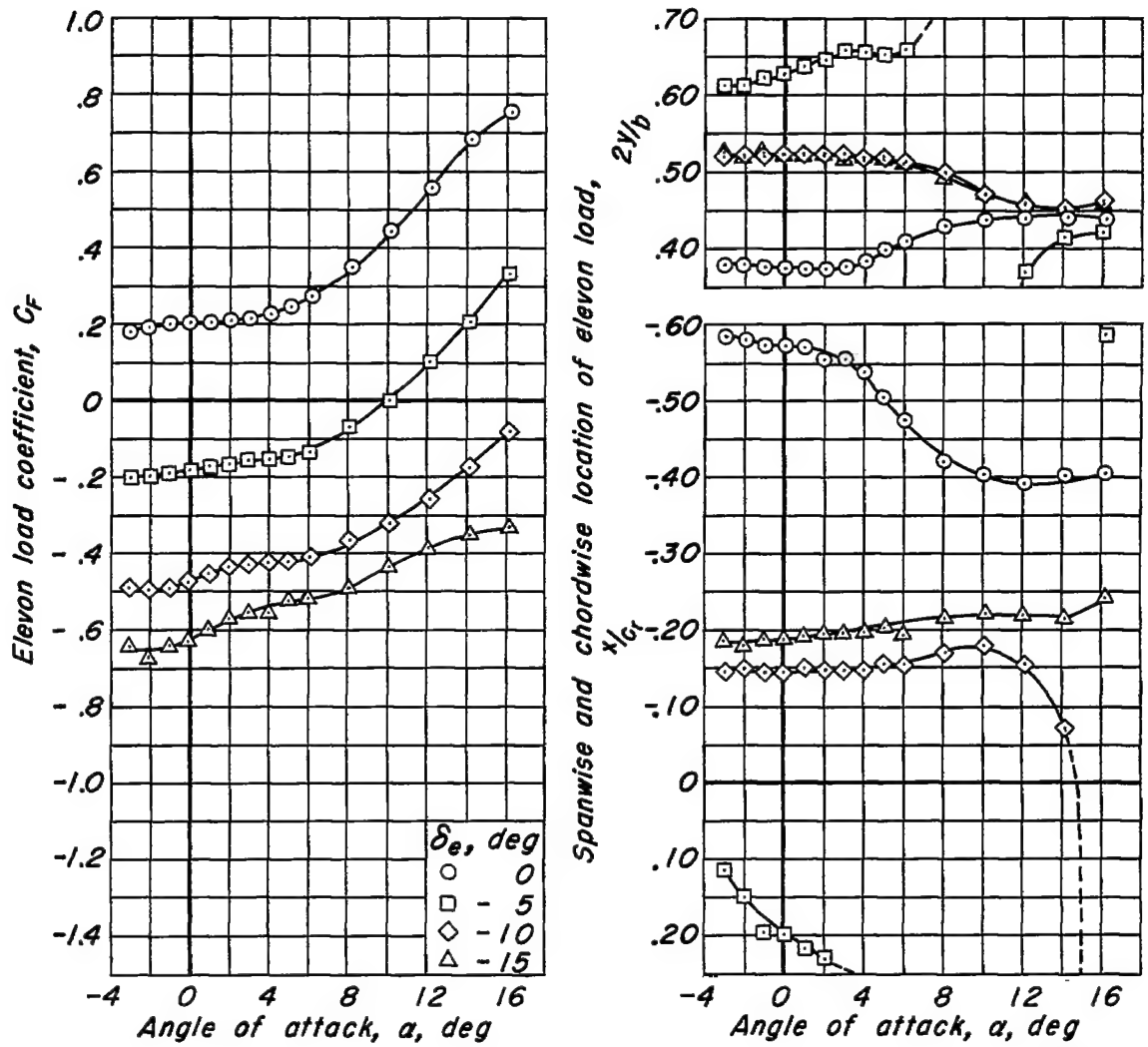

(c) C_F vs α, $2y/b$ vs α, x/c_r vs α

Figure 31.- Concluded.

[redacted]

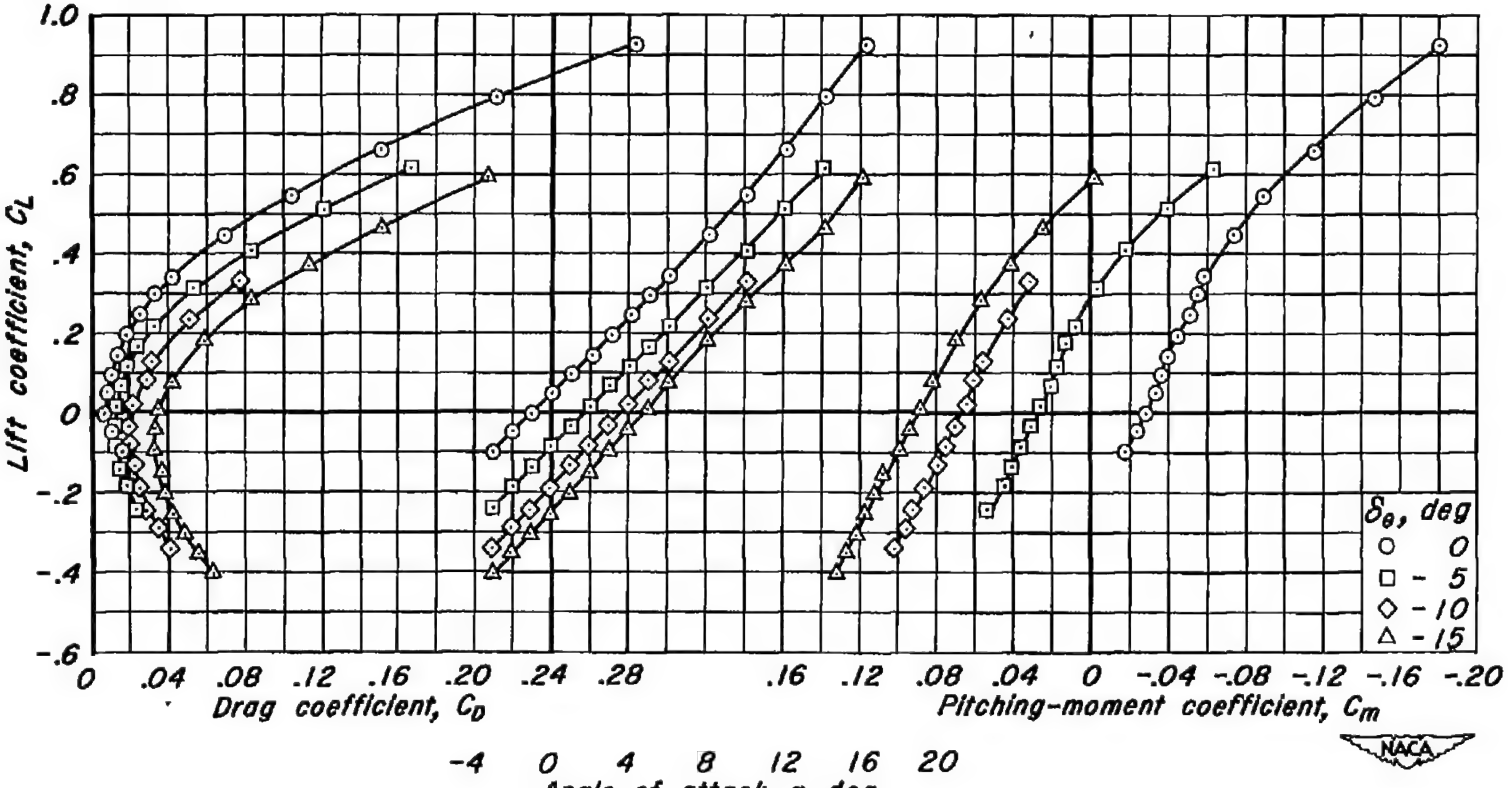

(a) C_L vs C_D, C_L vs α, C_L vs C_m

Figure 32.- The effect of elevon deflection on the aerodynamic characteristics at a Mach number of 0.92 R, 3.0 million; δ_f, 15°.

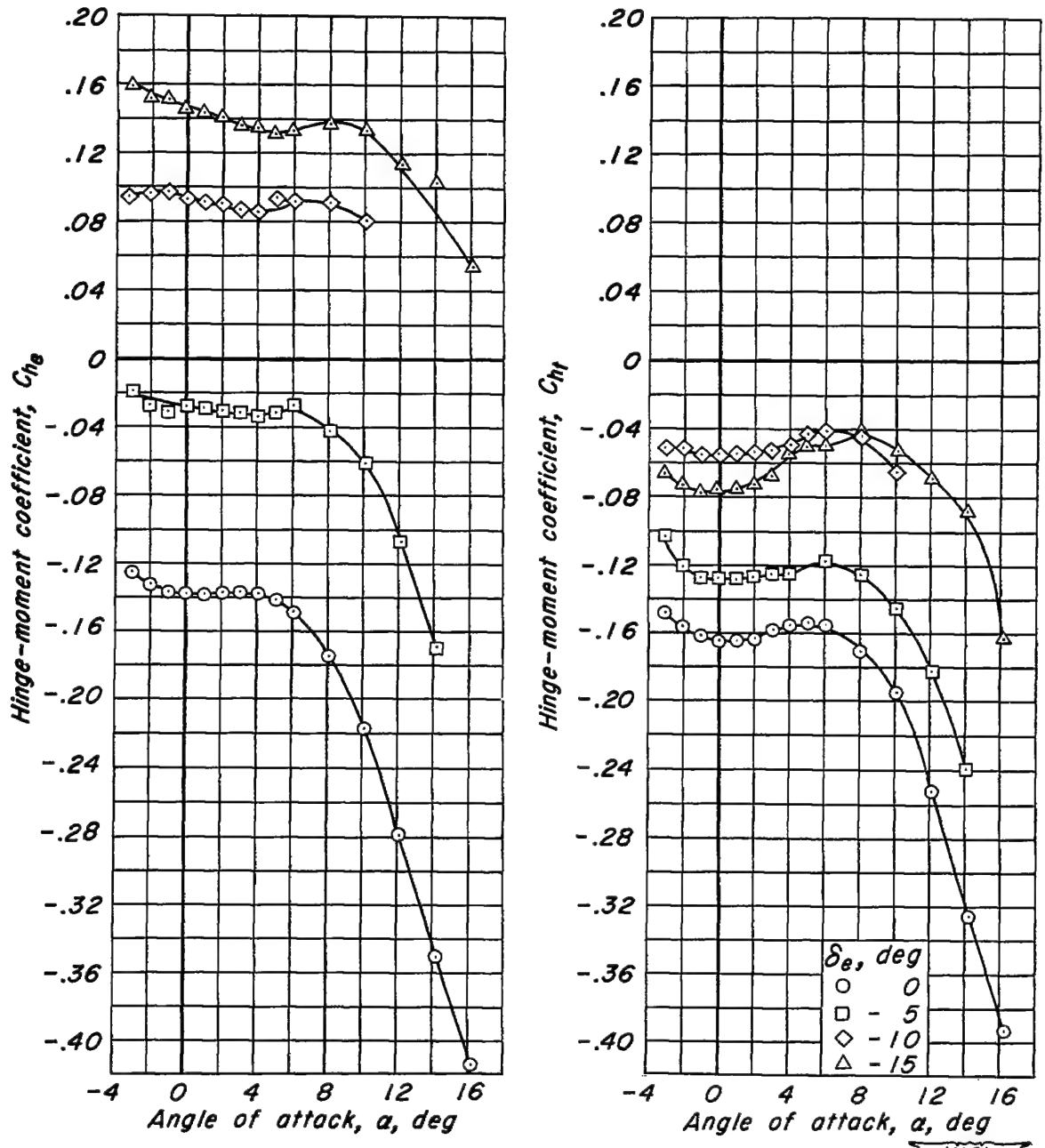

(b) C_{h_e} vs α, C_{h_t} vs α

Figure 32.-Continued.

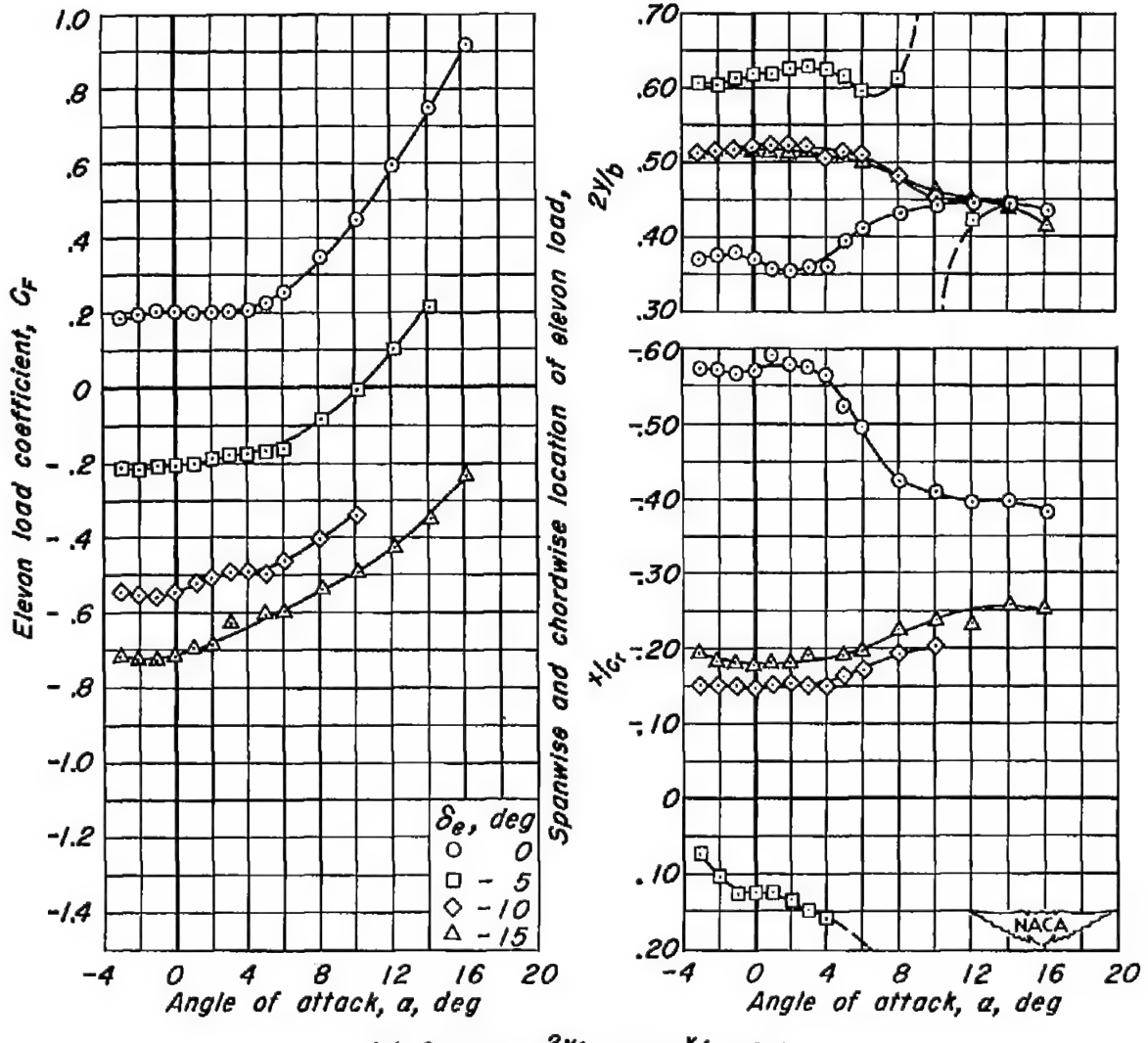

(c) C_F vs α, $2y/b$ vs α, x/c_r vs α

Figure 32.- Concluded.

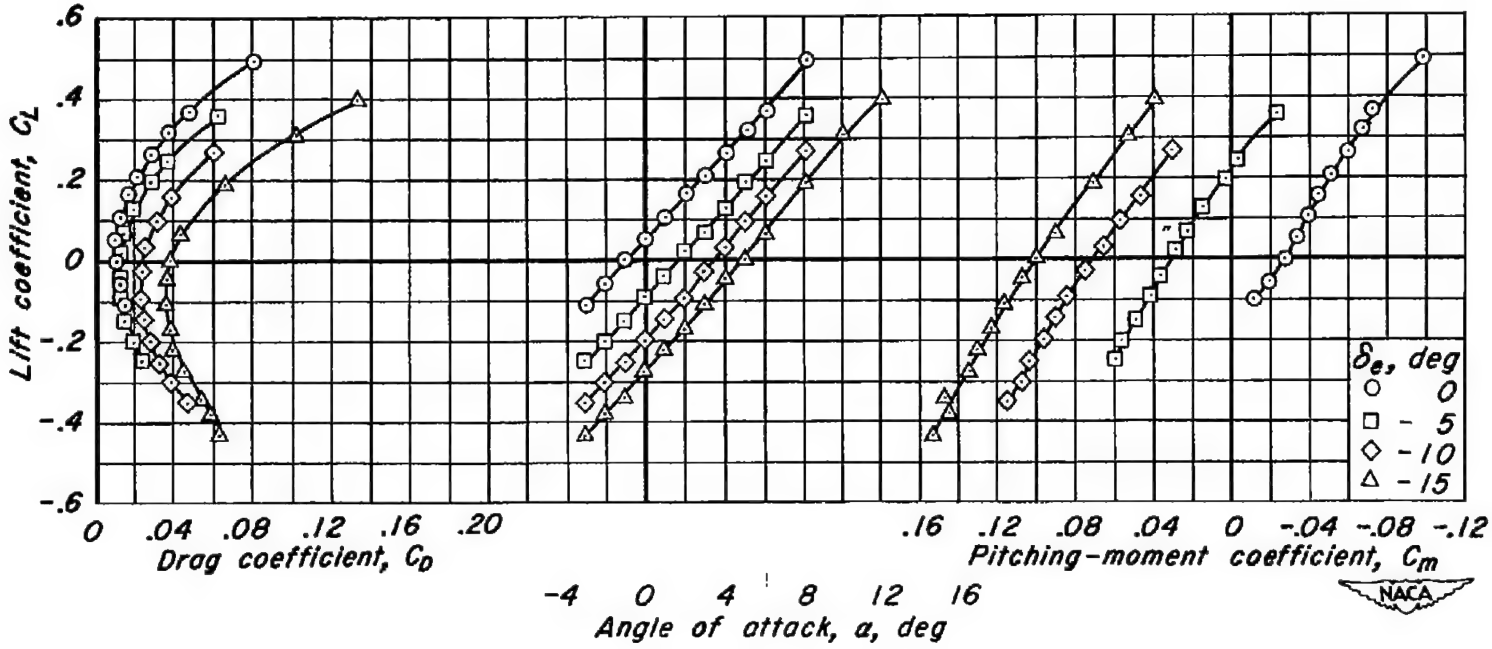

(a) C_L vs C_D, C_L vs α, C_L vs C_m

Figure 33.- The effect of elevon deflection on the aerodynamic characteristics at a Mach number of 0.95 R, 3.0 million; δ_t, 15°.

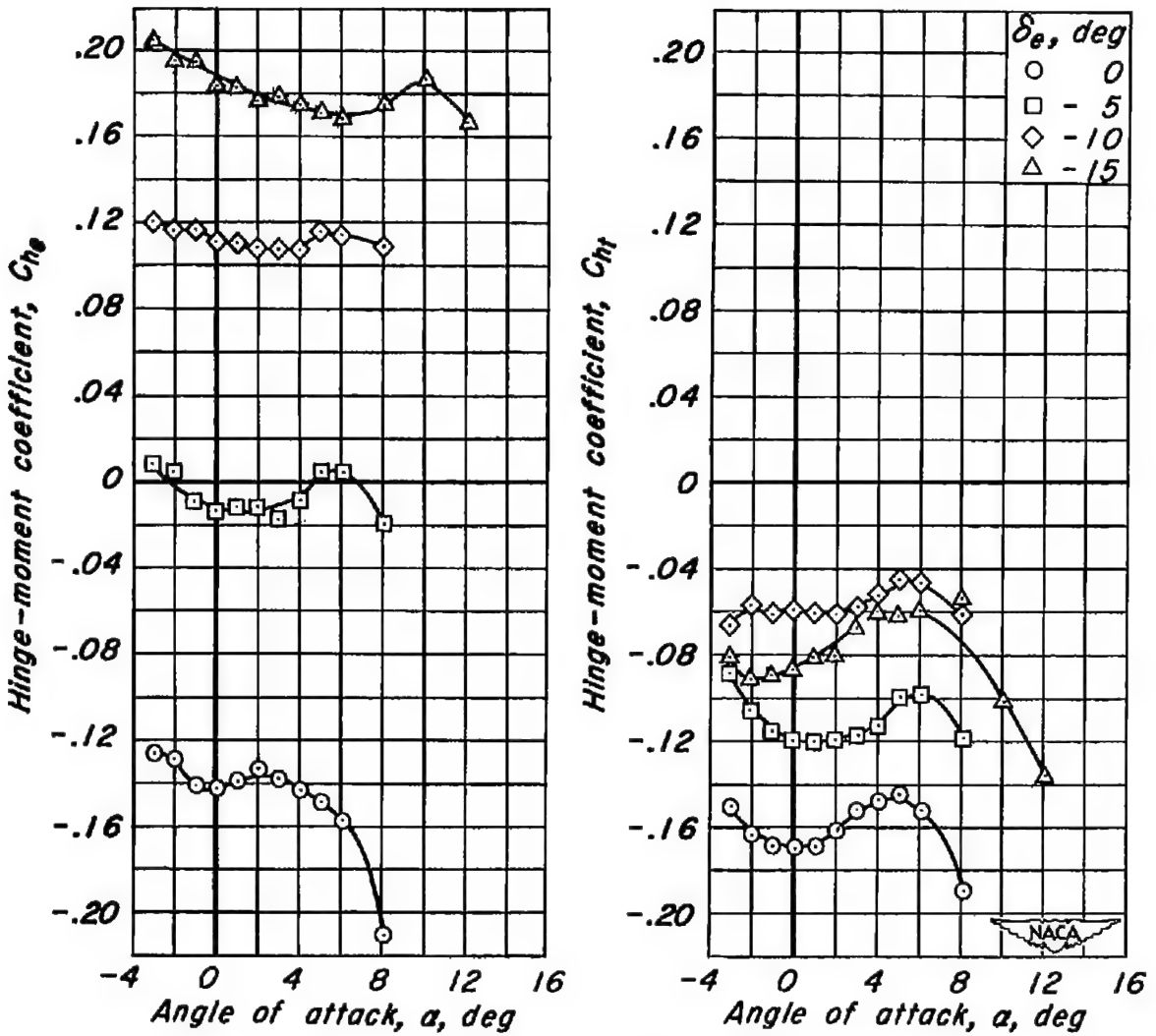

(b) C_{h_e} vs α, C_{h_t} vs α

Figure 33.- Continued.

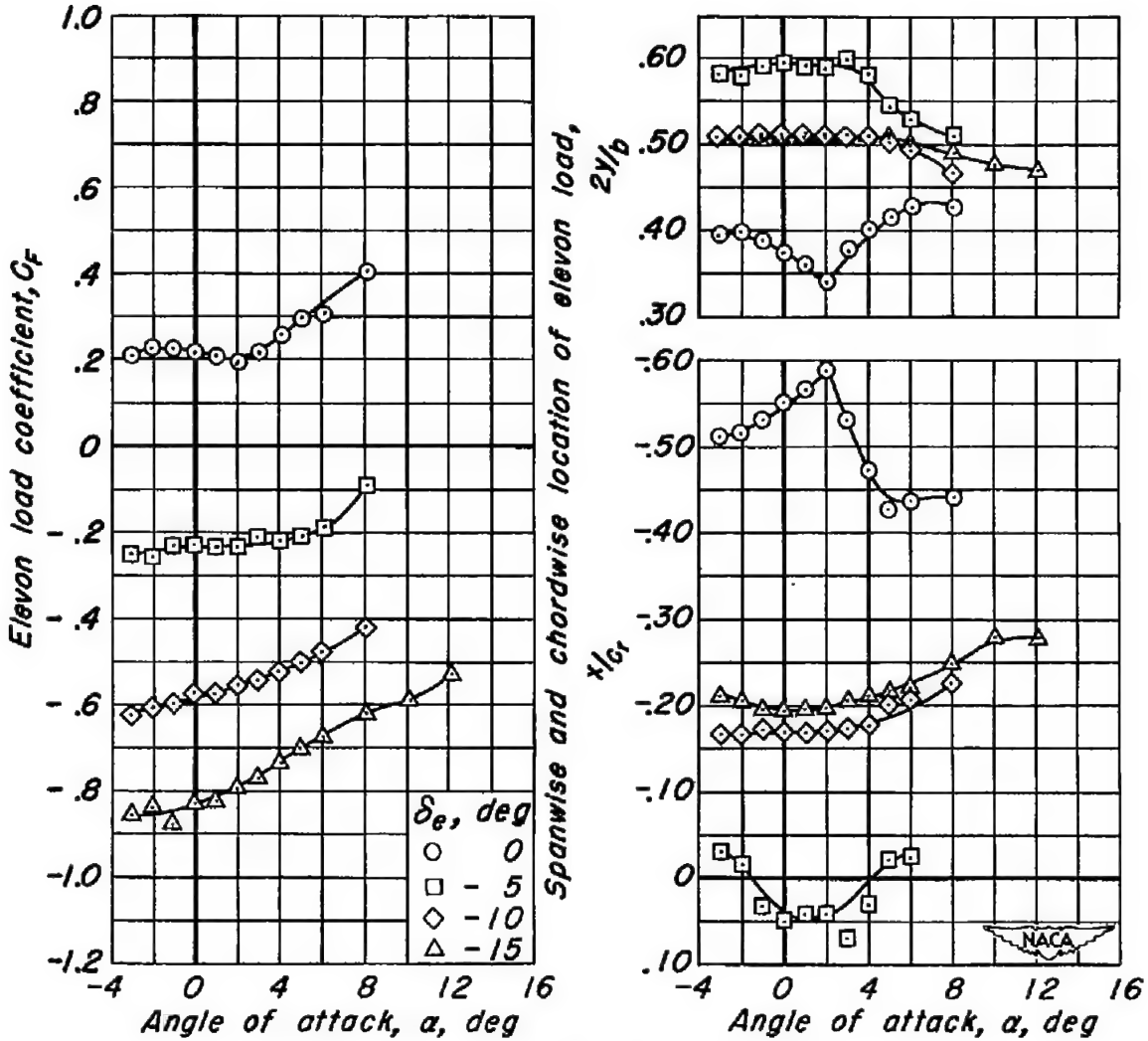

(c) C_F vs α, $2y/b$ vs α, x/c_r vs α

Figure 33.- Concluded.

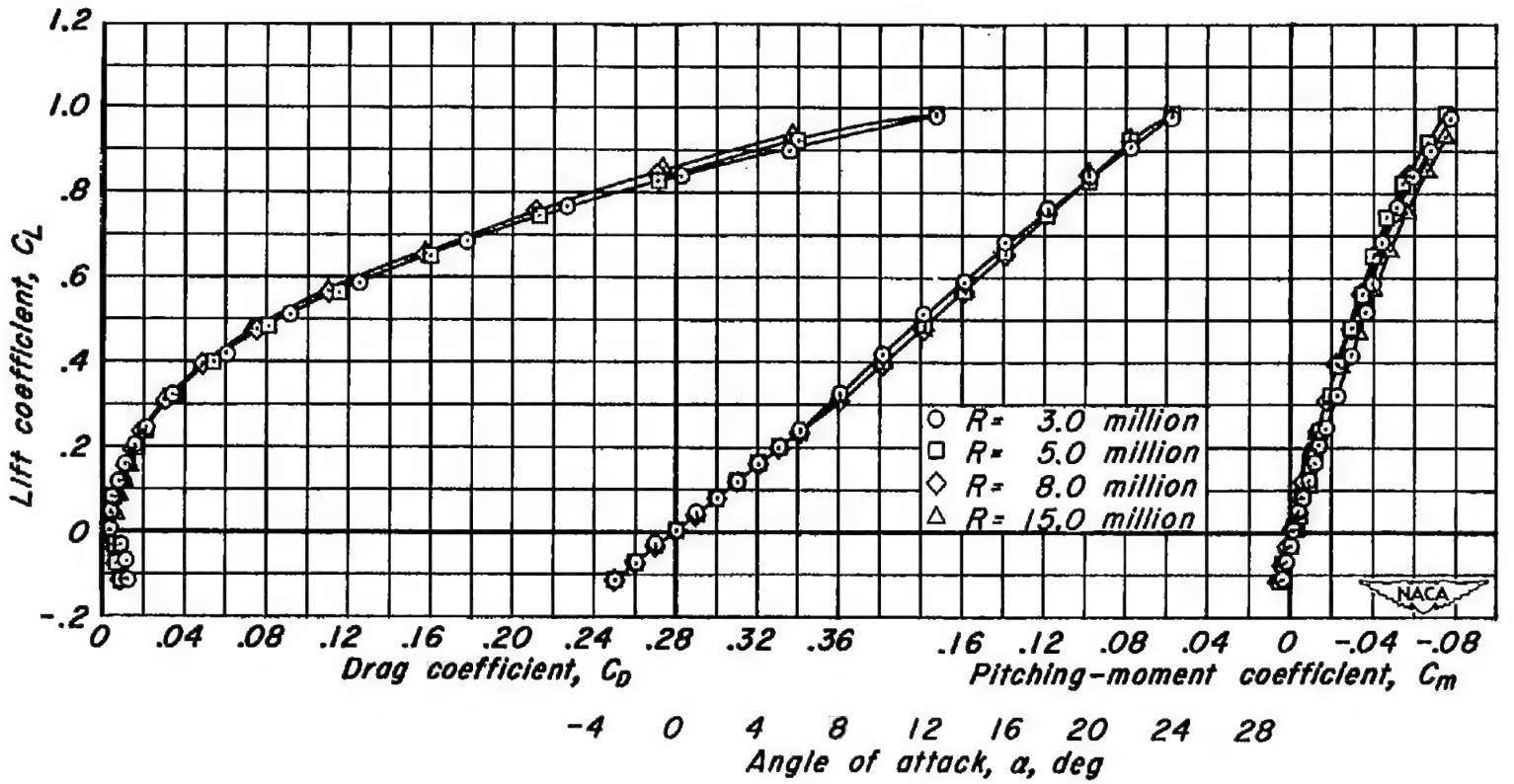

(a) C_L vs C_D, C_L vs α, C_L vs C_m

Figure 34.- The effect of Reynolds number on the aerodynamic characteristics at a Mach number of 0.24. δ_e, 0°; δ_t, 0°.

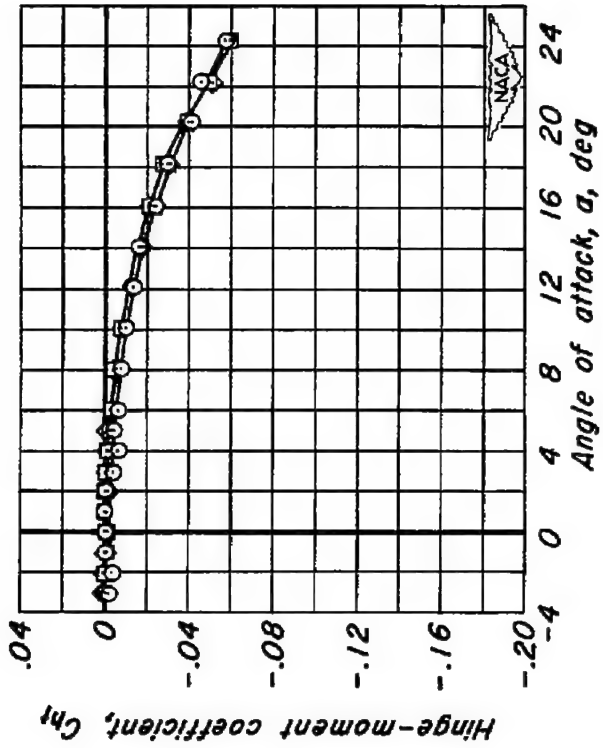

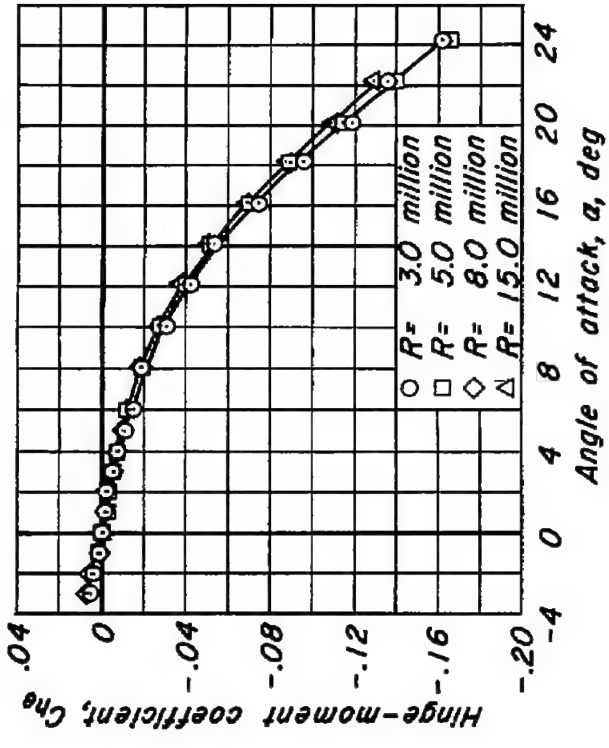

(b) C_{h_e} vs α, C_{h_f} vs α

Figure 34.-Continued.

[redacted]

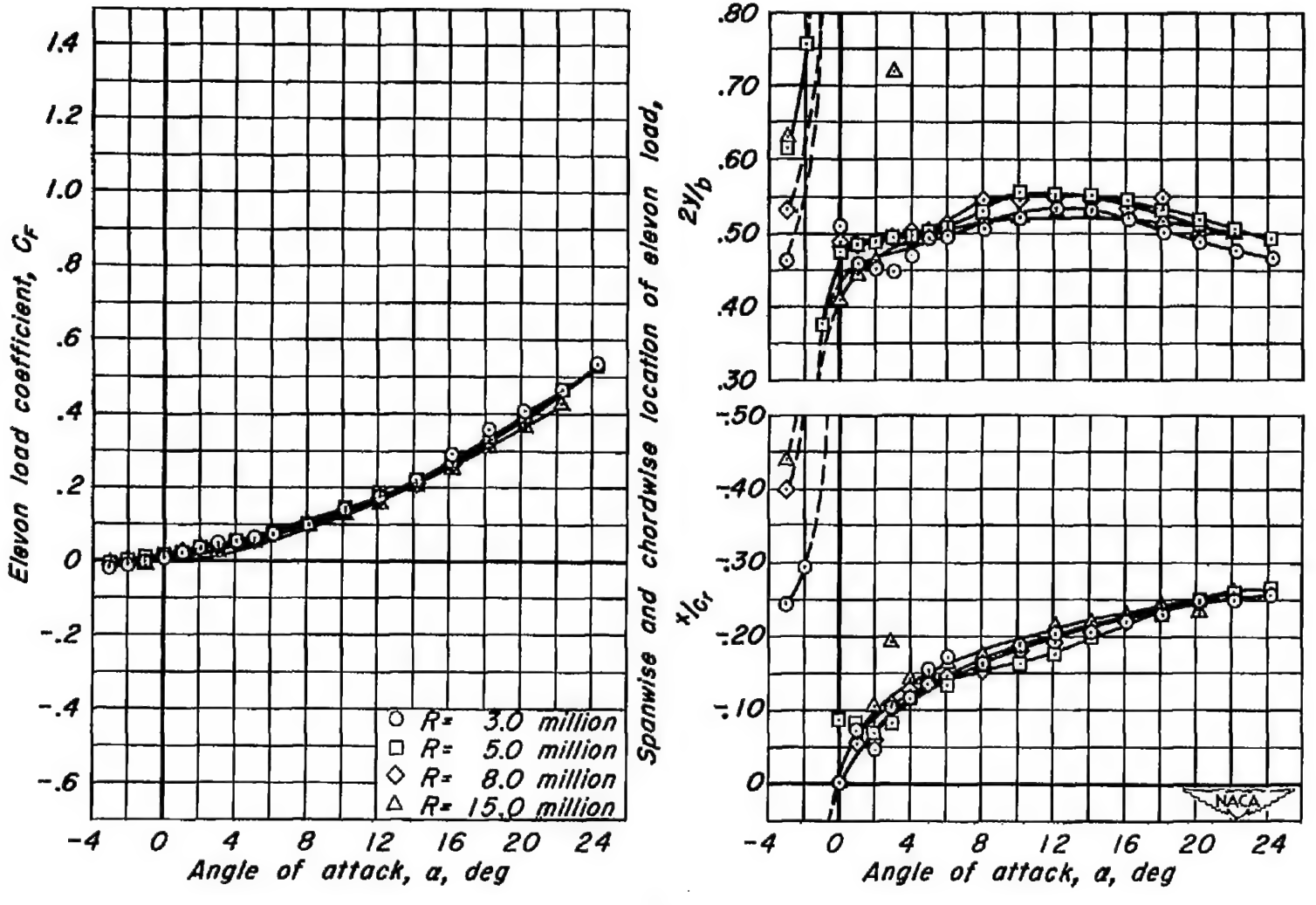

(c) C_F vs α, $^{2y}/_{b}$ vs α, $^{x}/_{c_r}$ vs α

Figure 34.- Concluded.

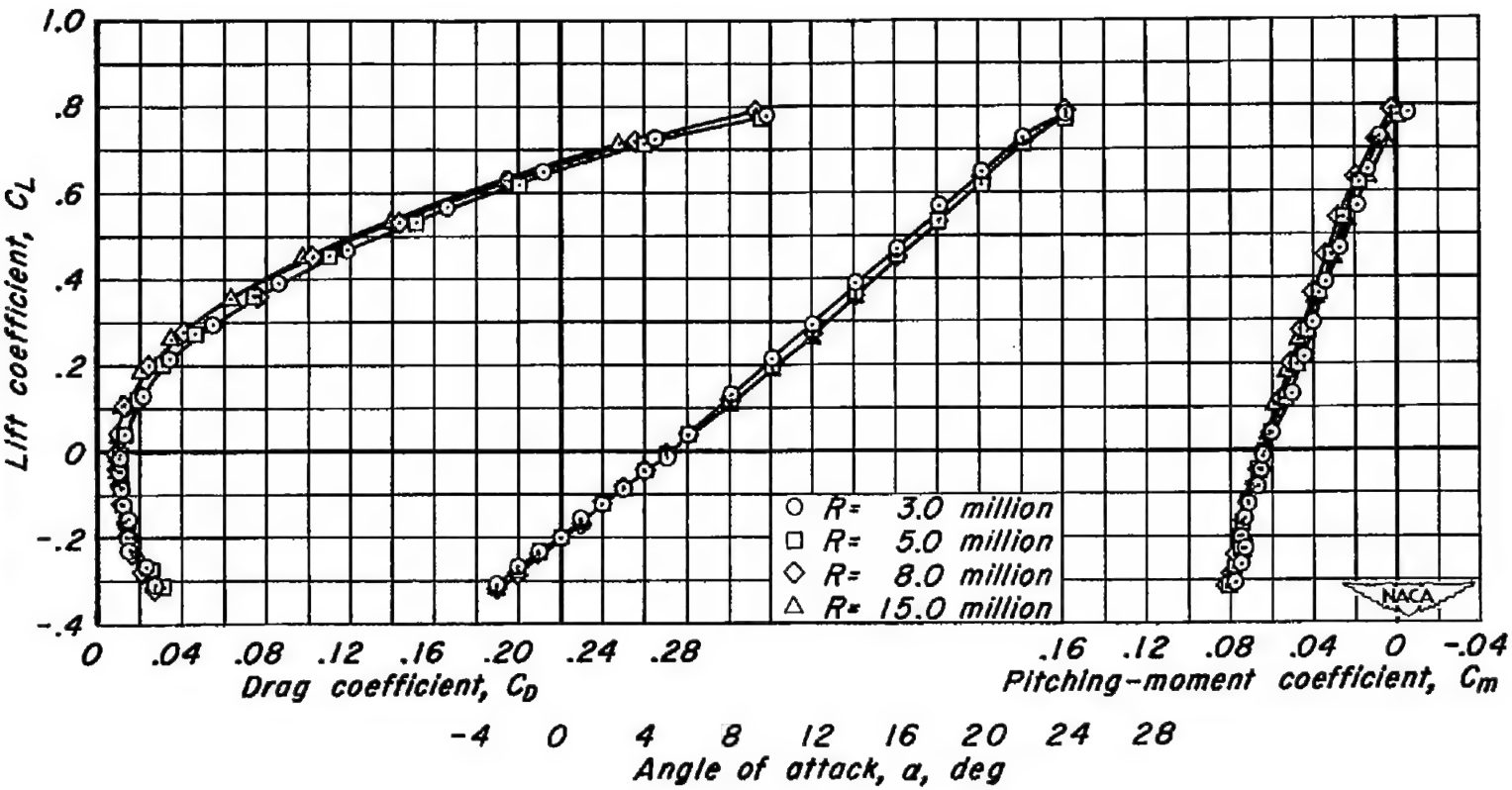

(a) C_L vs C_D, C_L vs α, C_L vs C_m

Figure 35.- The effect of Reynolds number on the aerodynamic characteristics at a Mach number of 0.24. δ_e, -10°; δ_t, 0°.

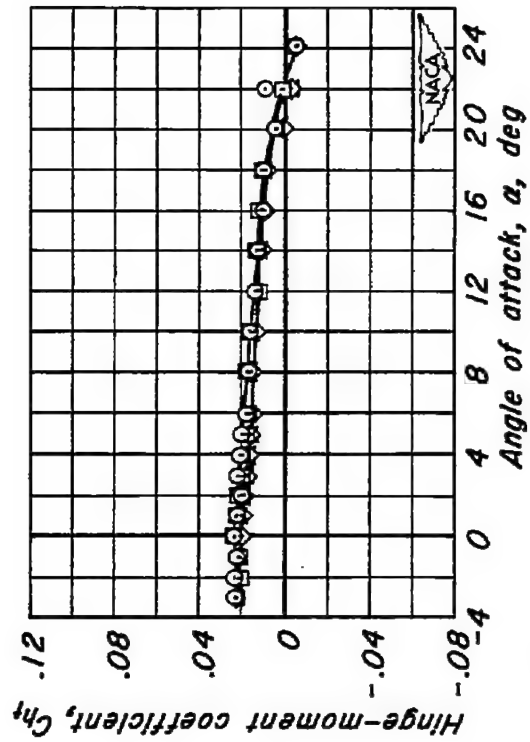

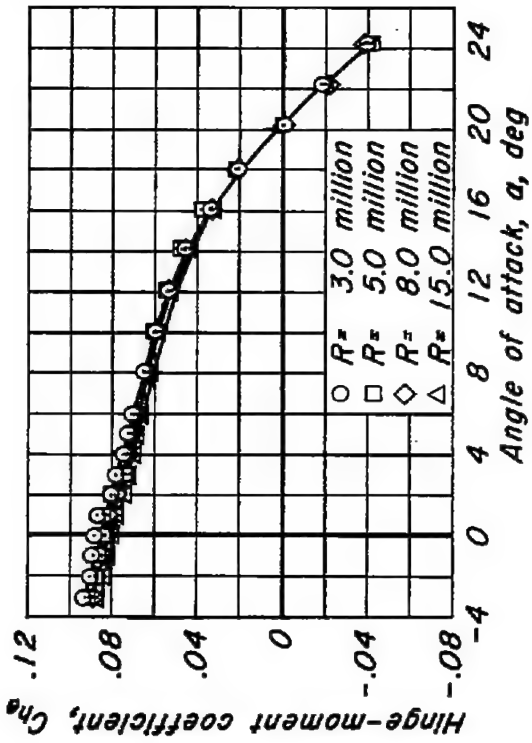

(b) C_{h_e} vs α, C_{h_f} vs α

Figure 35.-Continued.

[redacted]

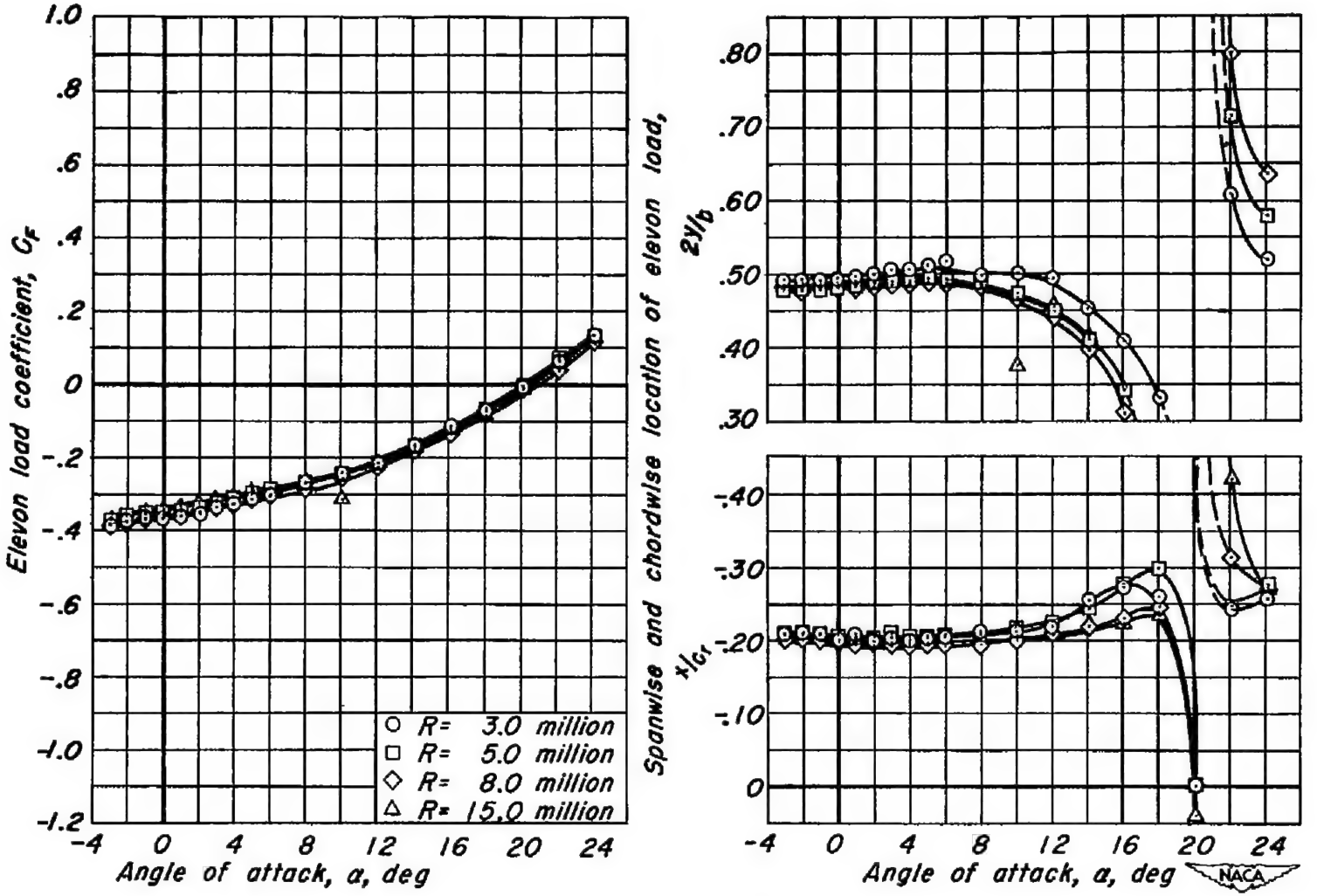

(c) C_F vs α, $2y/b$ vs α, x/c_r vs α

Figure 35.- Concluded.

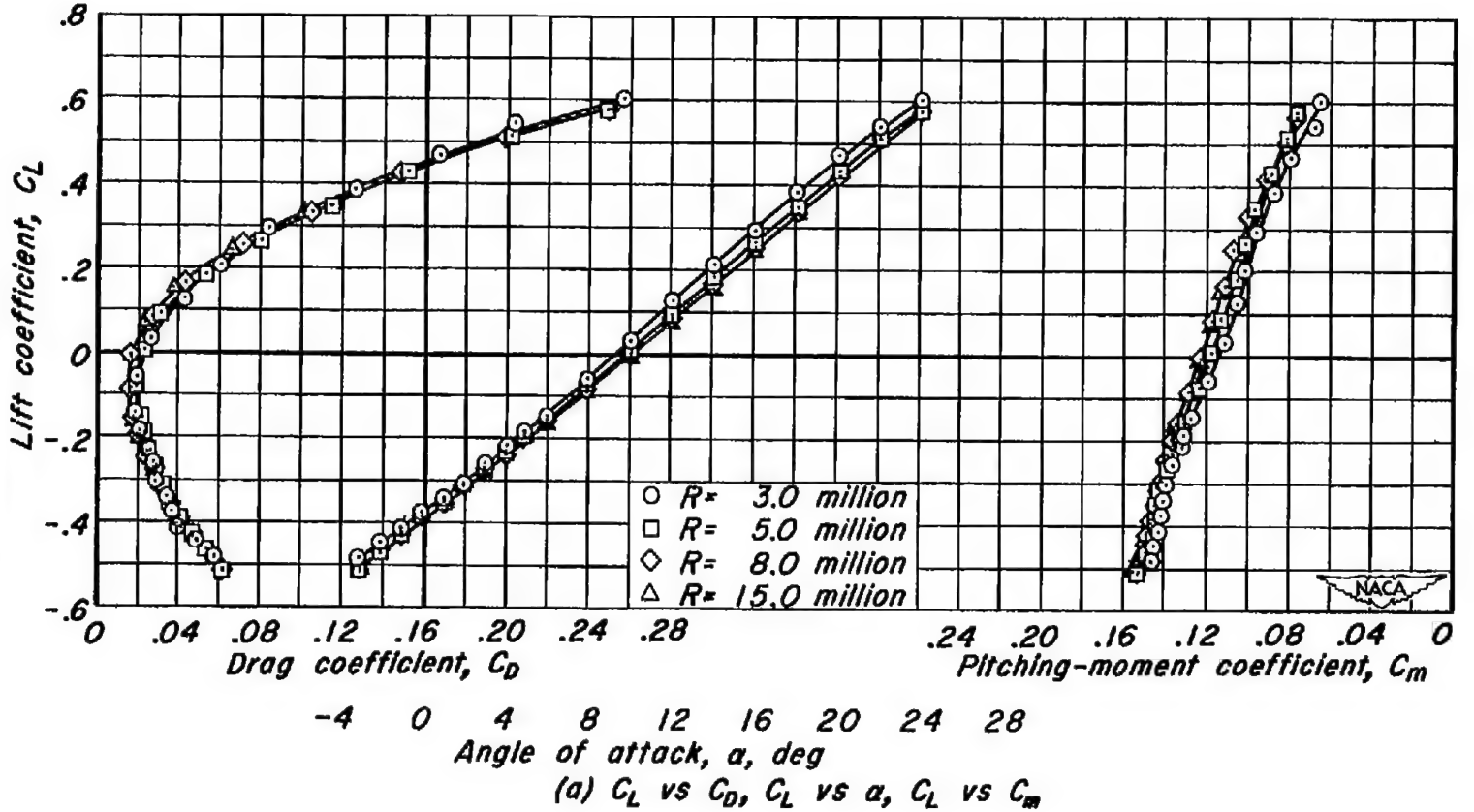

(a) C_L vs C_D, C_L vs α, C_L vs C_m

Figure 36.- The effect of Reynolds number on the aerodynamic characteristics at a Mach number of 0.24. δ_e, -20°; δ_t, 0°.

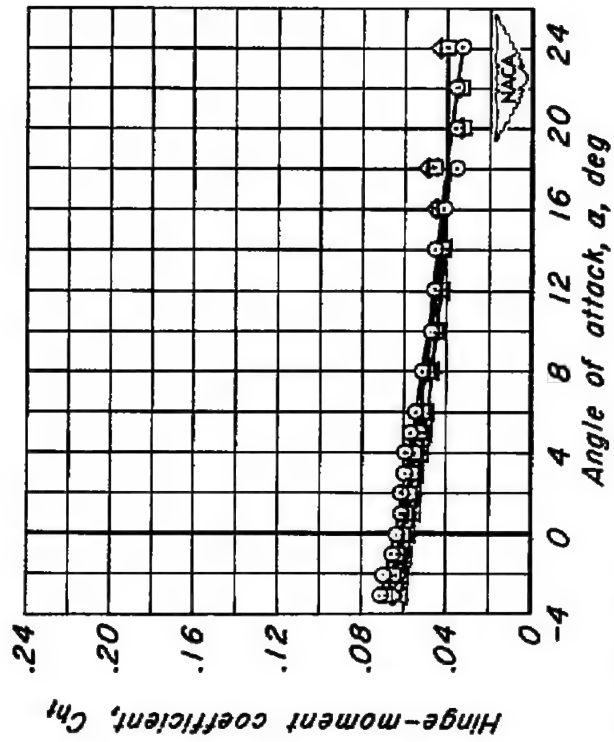

(b) C_{h_e} vs α, C_{h_f} vs α

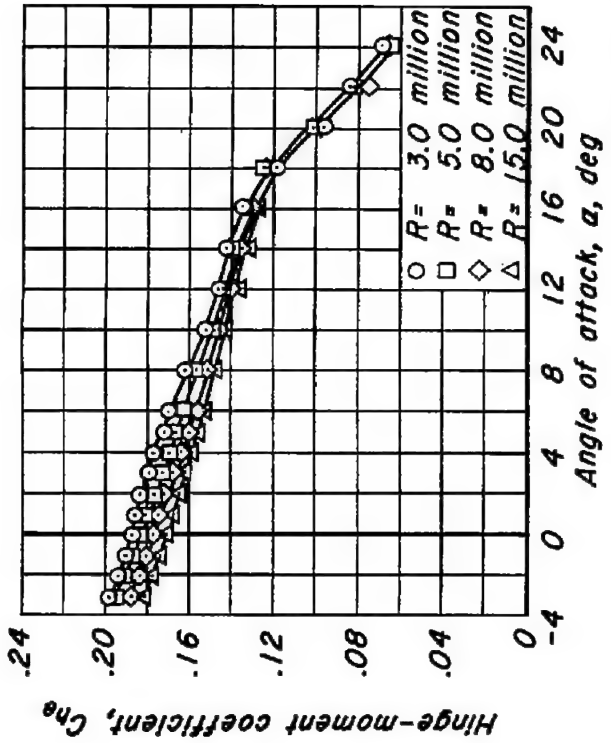

Figure 36.-Continued.

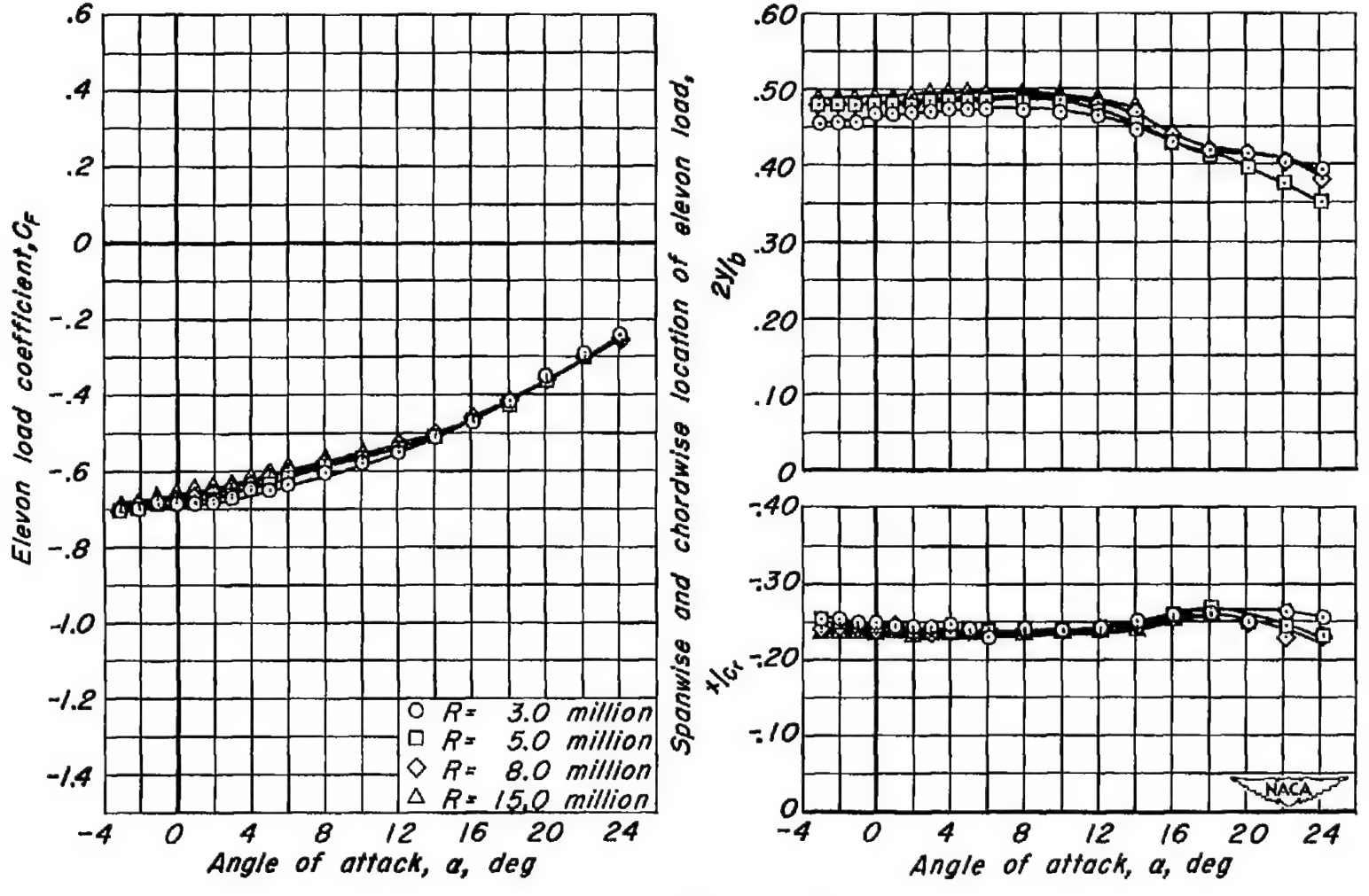

(c) C_F vs α, $2y/b$ vs α, x/c_r vs α

Figure 36.- Concluded.

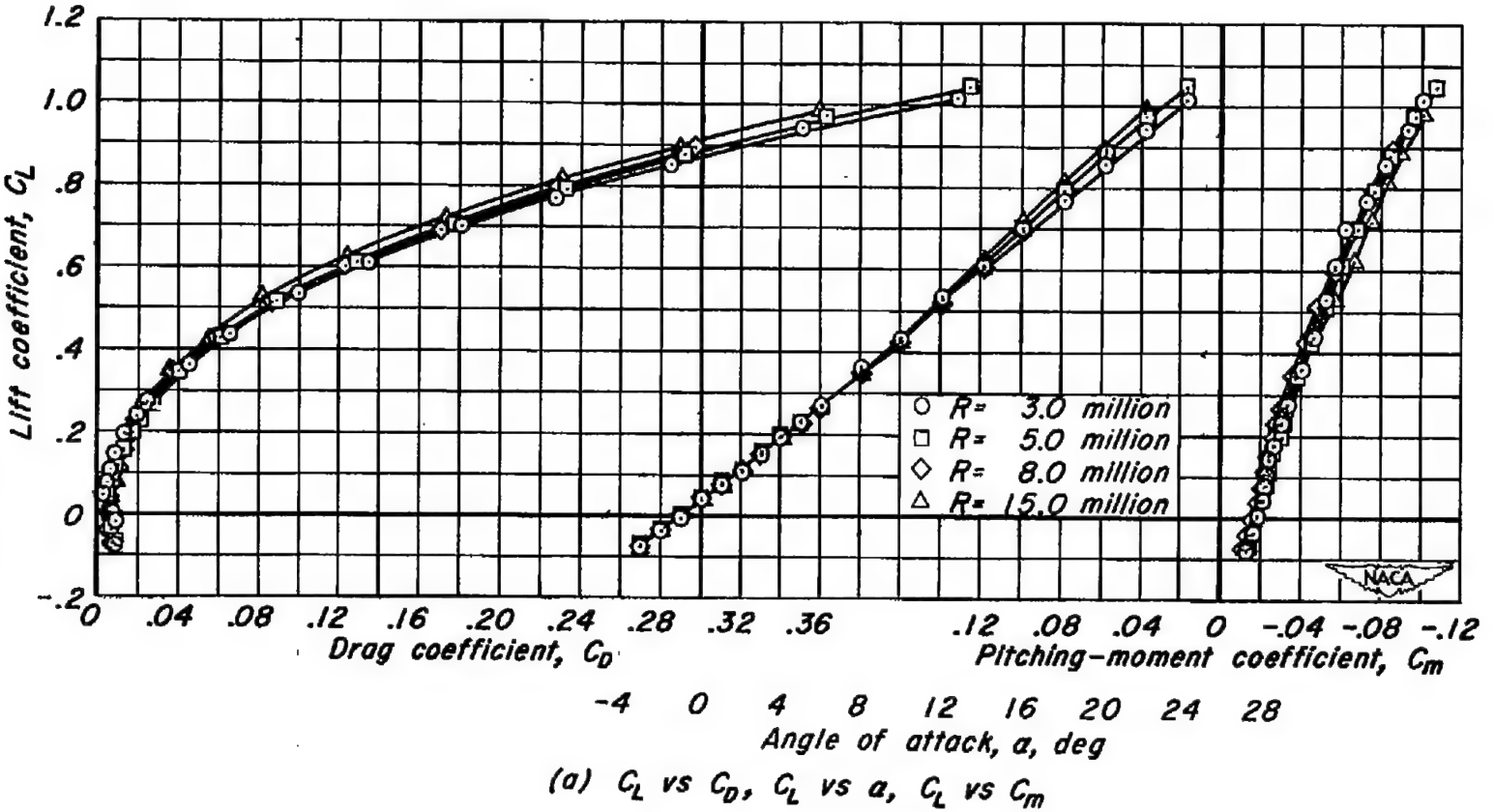

(a) C_L vs C_D, C_L vs α, C_L vs C_m

Figure 37.– The effect of Reynolds number on the aerodynamic characteristics at a Mach number of 0.24. δ_e, 0°; δ_f, 10°.

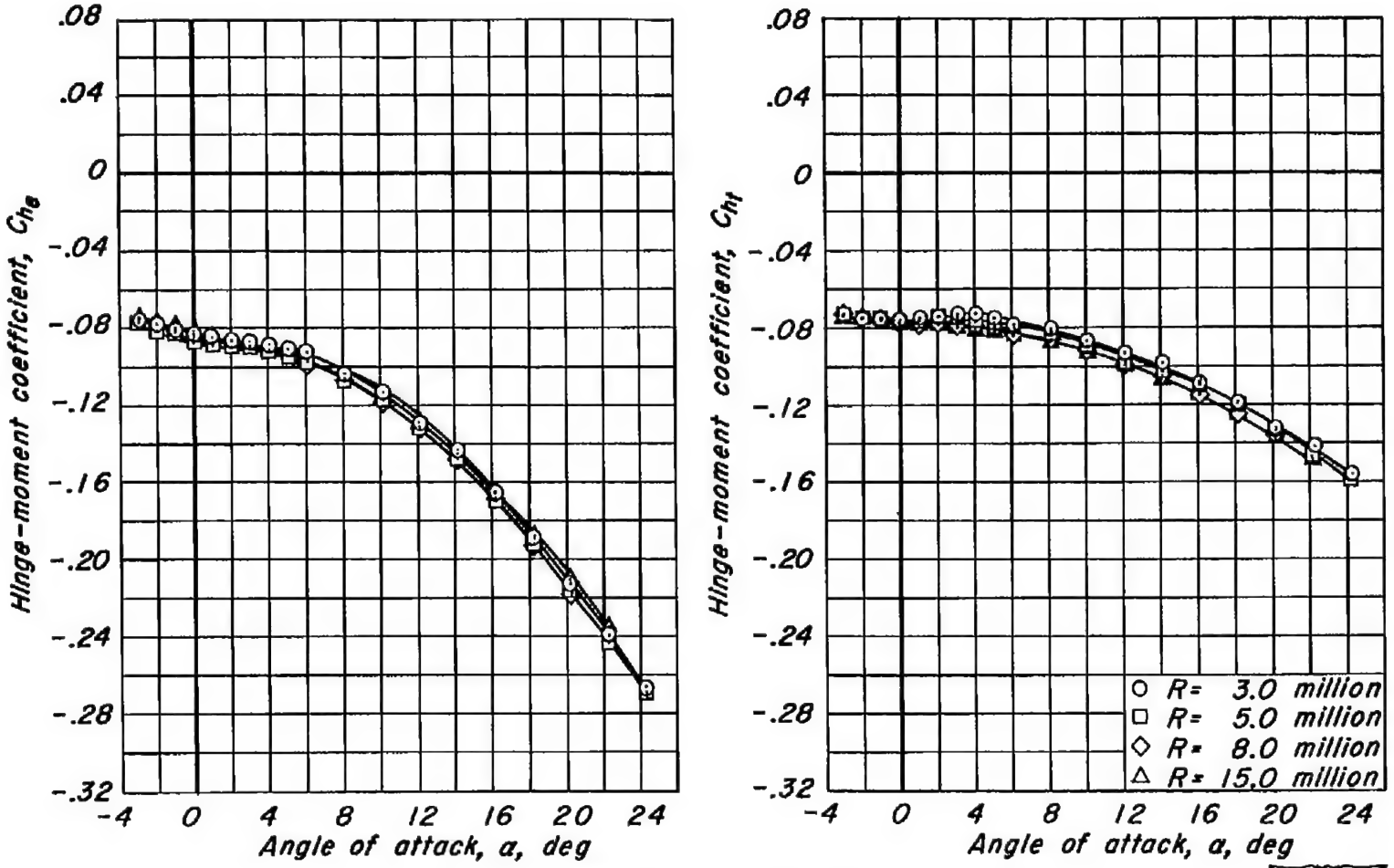

(b) C_{h_e} vs α, C_{h_f} vs α

Figure 37.-Continued.

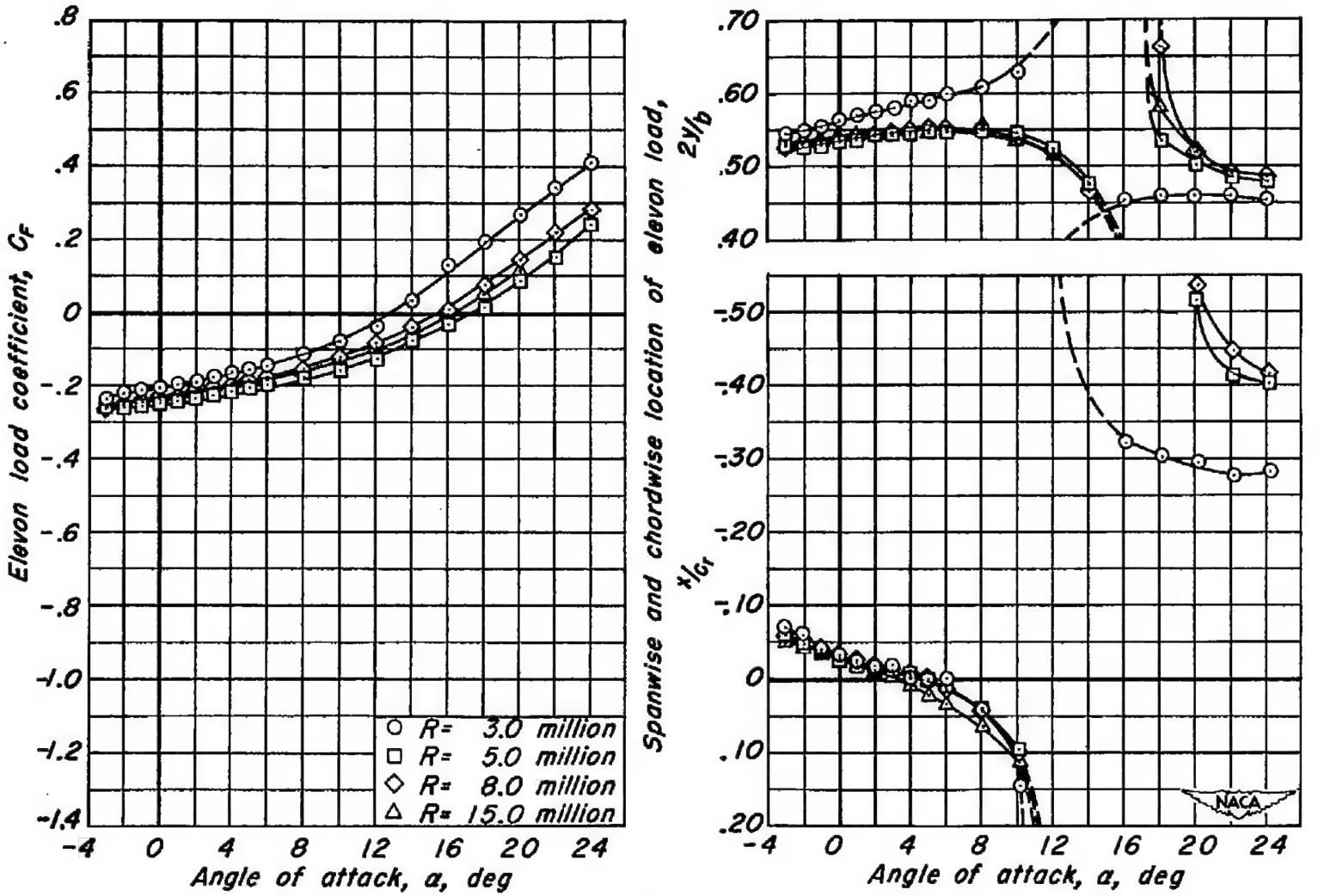

(c) C_F vs α, $2y/b$ vs α, x/c_r vs α

Figure 37.- Concluded.

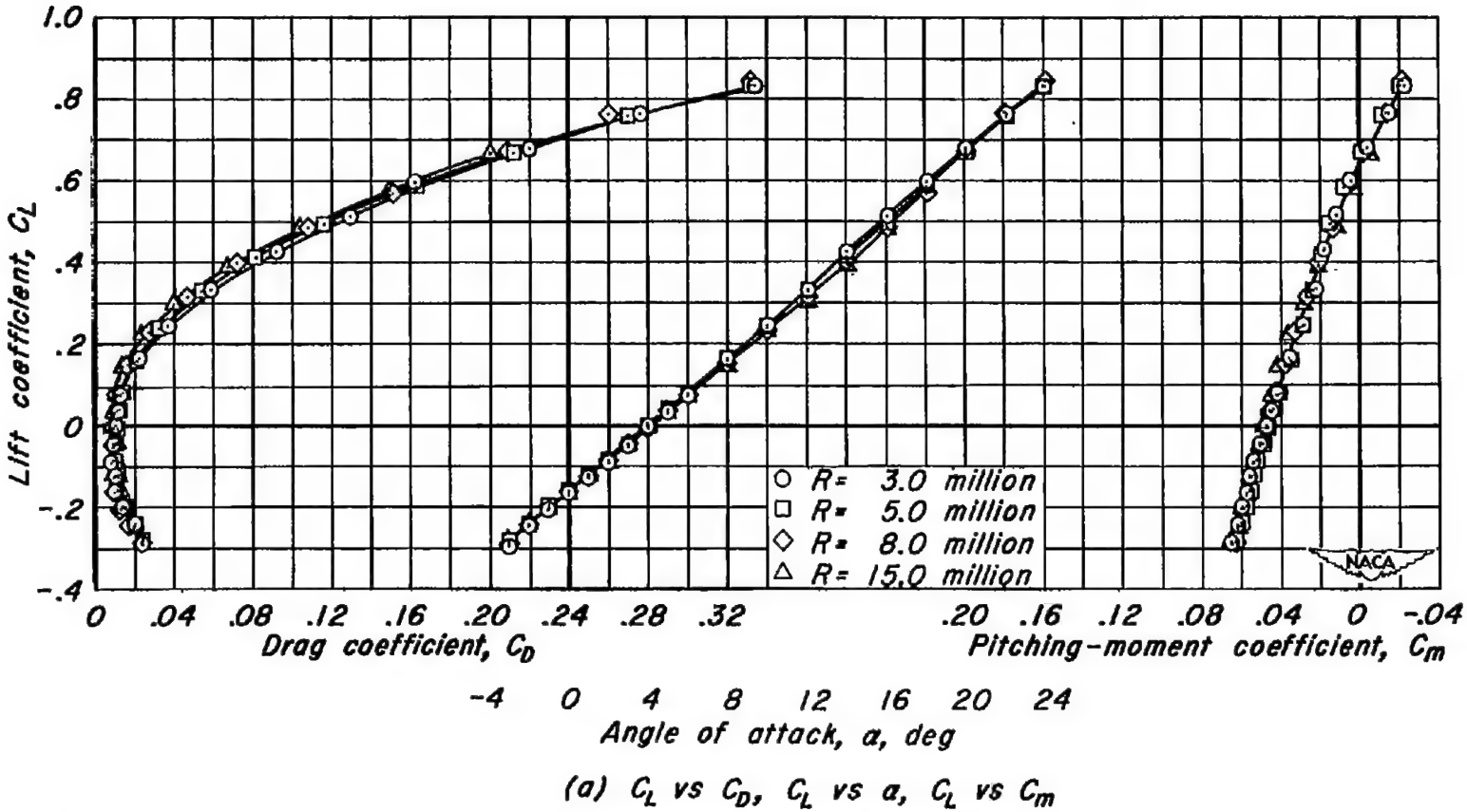

(a) C_L vs C_D, C_L vs α, C_L vs C_m

Figure 38.- The effect of Reynolds number on the aerodynamic characteristics at a Mach number of 0.24. δ_e, -10°; δ_t, 10°.

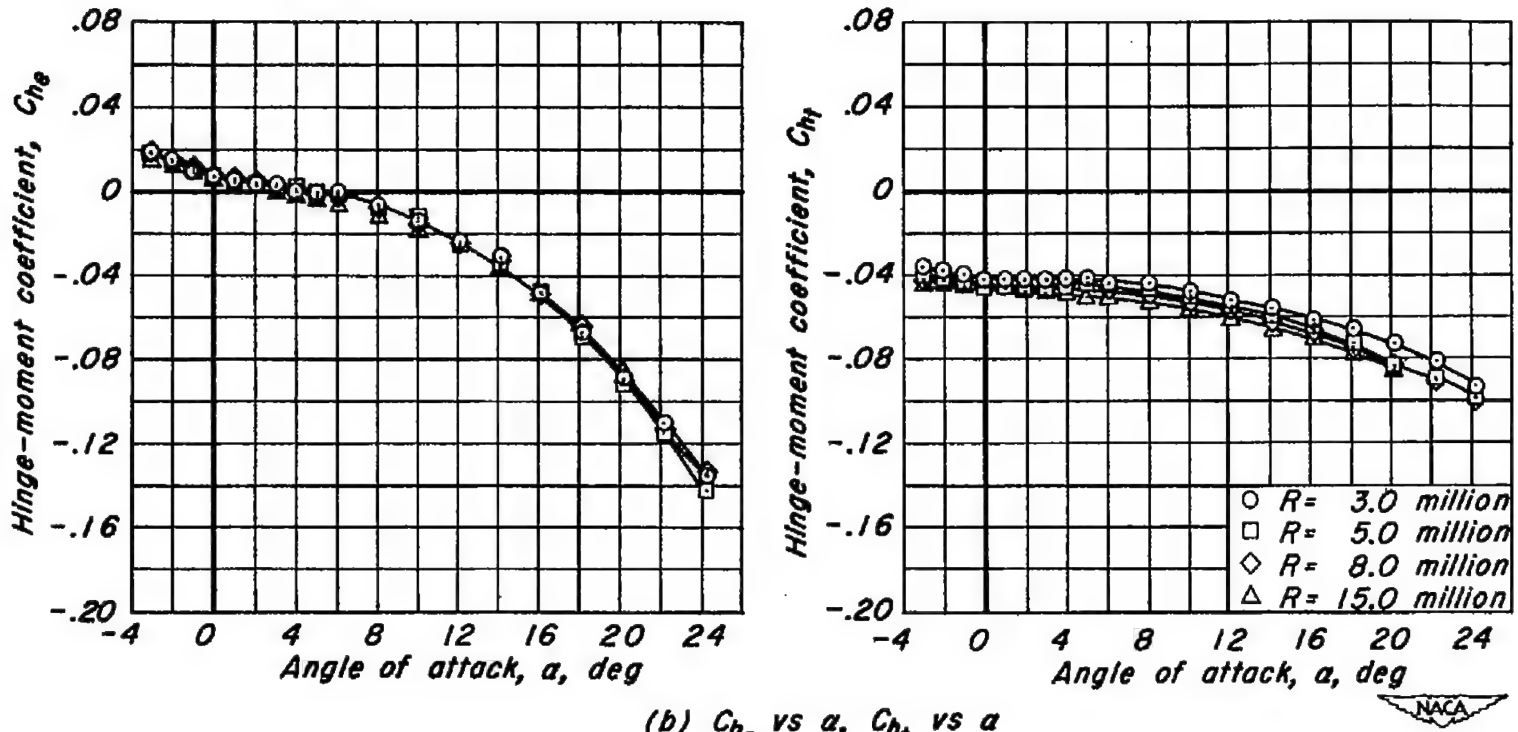

(b) C_{h_e} vs α, C_{h_f} vs α

Figure 38.- Continued.

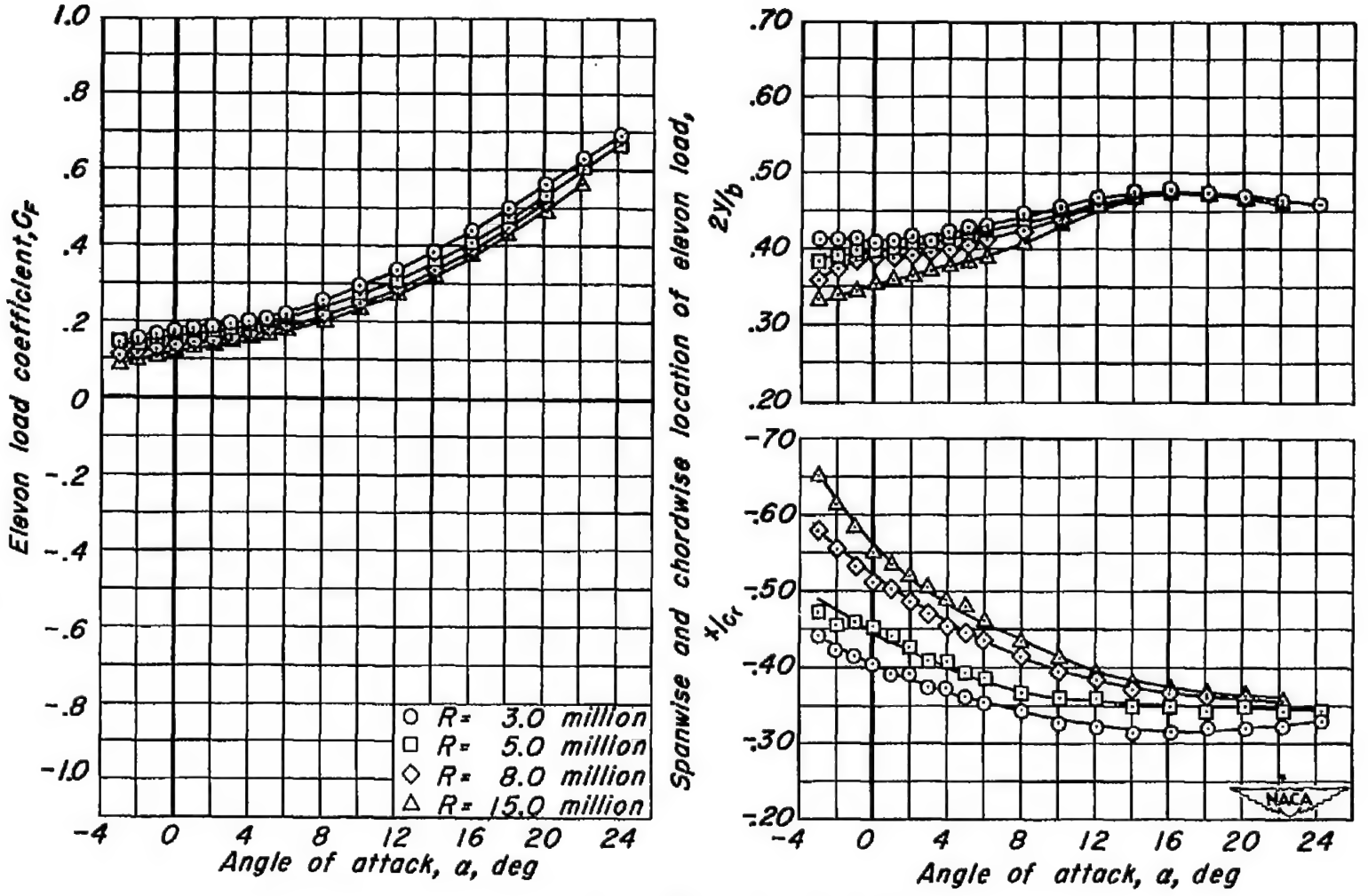

(c) C_F vs α, $2y/b$ vs α, x/c_r vs α

Figure 38.- Concluded.

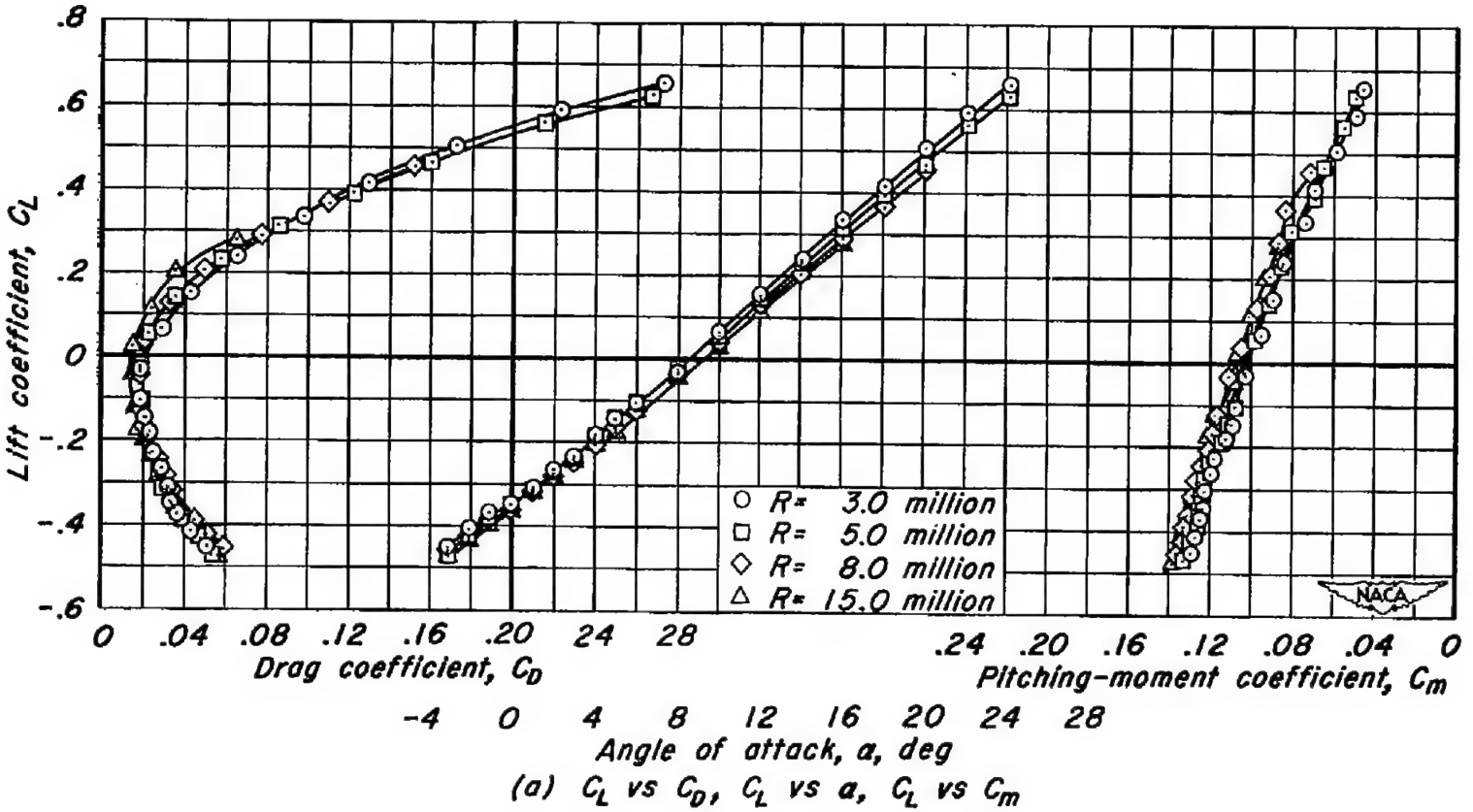

(a) C_L vs C_D, C_L vs α, C_L vs C_m

Figure 39.- The effect of Reynolds number on the aerodynamic characteristics at a Mach number of 0.24. δ_e, -20°; δ_t, 10°.

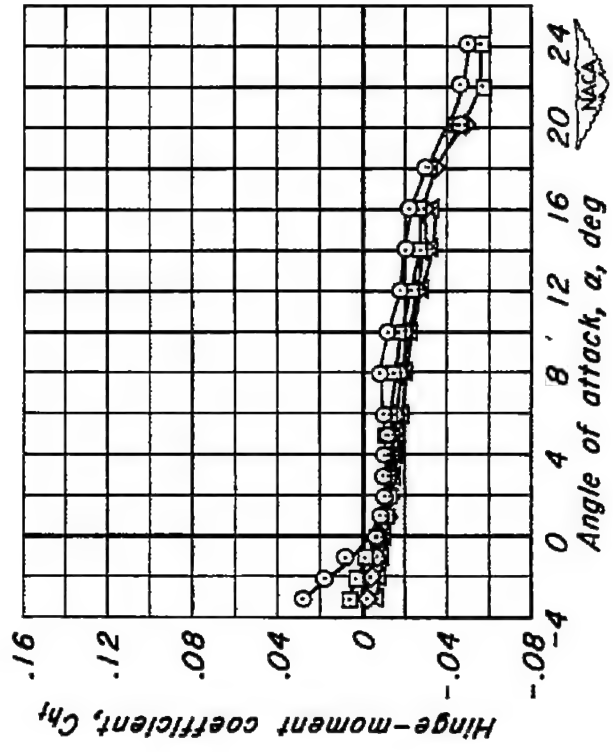

(b) C_{h_e} vs α, C_{h_f} vs α

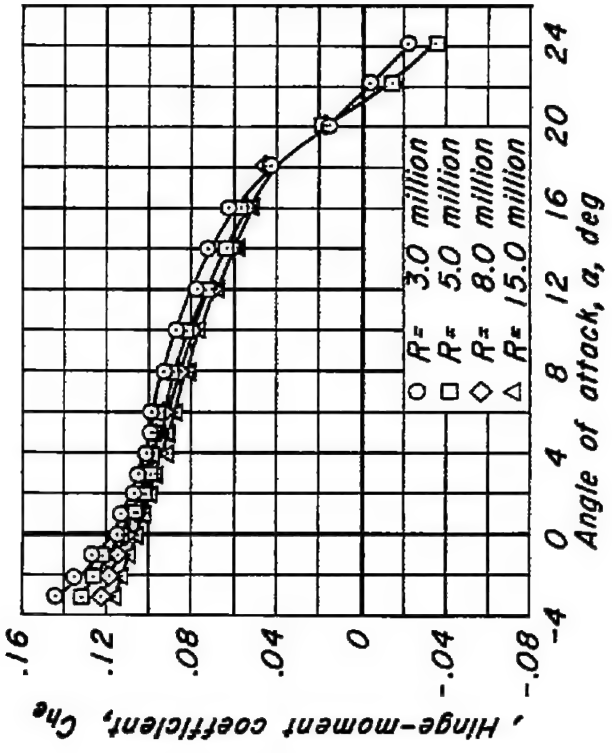

Figure 39.-Continued.

[redacted]

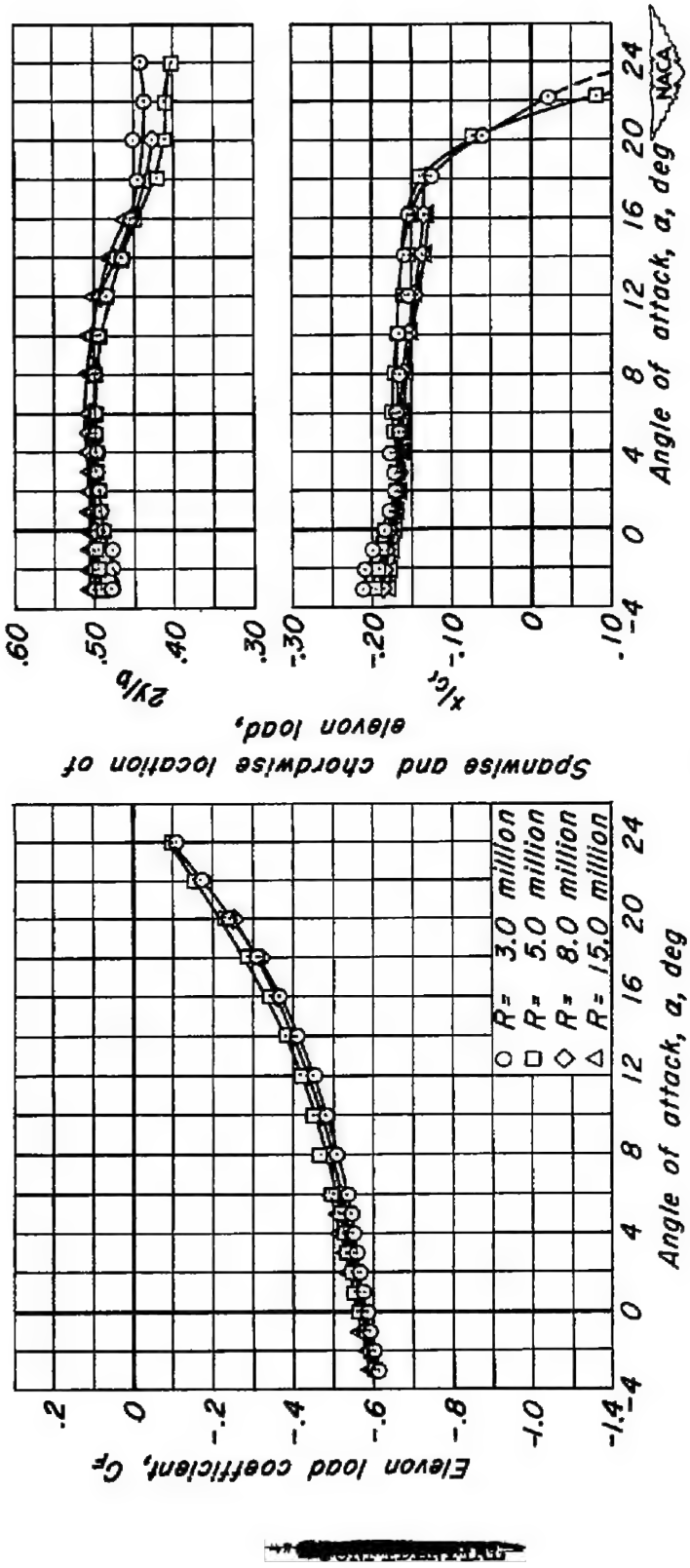

(c) C_F vs α, $2y/b$ vs α, x/c_r vs α

Figure 39.- Concluded.

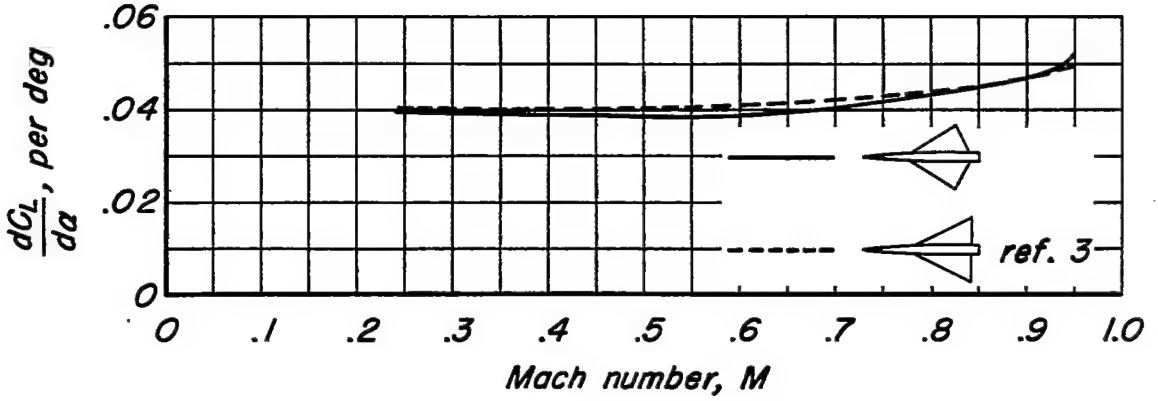

(a) $\frac{dC_L}{d\alpha}$ vs M

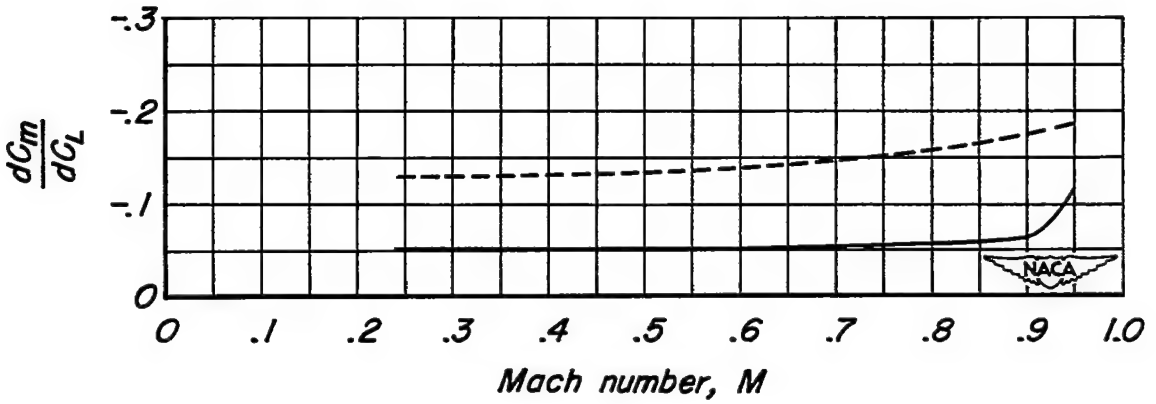

(b) $\frac{dC_m}{dC_L}$ vs M

Figure 40 – The variation with Mach number of the aerodynamic characteristics of two low-aspect-ratio wings. R, 3.0 million; δ_e, 0°; δ_t, 0°.

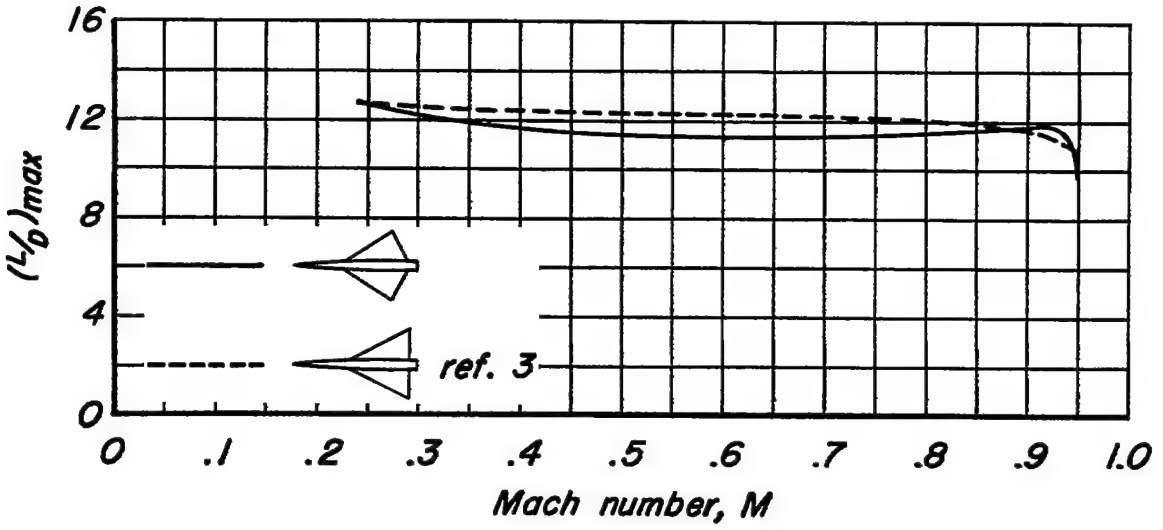

(c) $(L/D)_{max}$ vs M

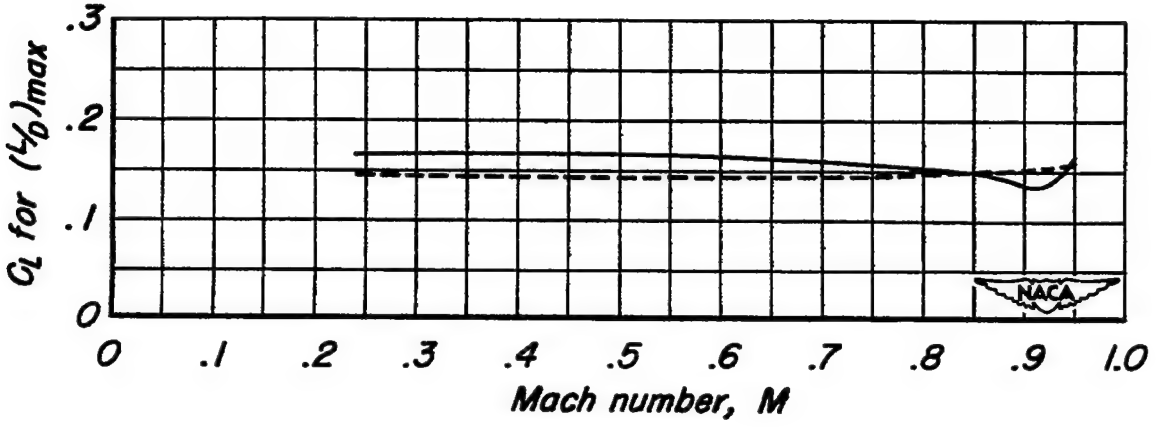

(d) C_L for $(L/D)_{max}$ vs M

Figure 40.- Continued.

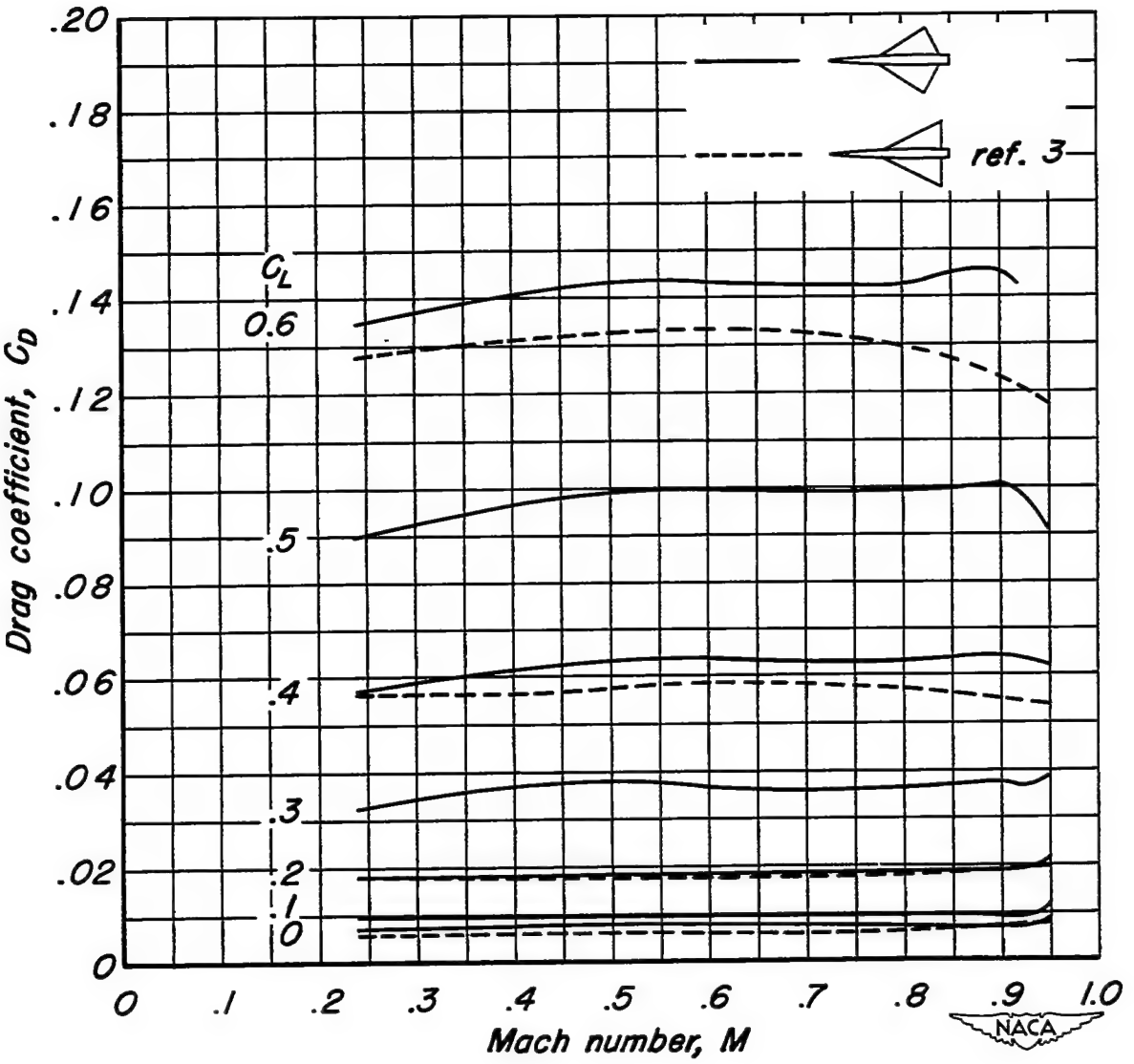

(e) C_D vs M

Figure 40.- Concluded.

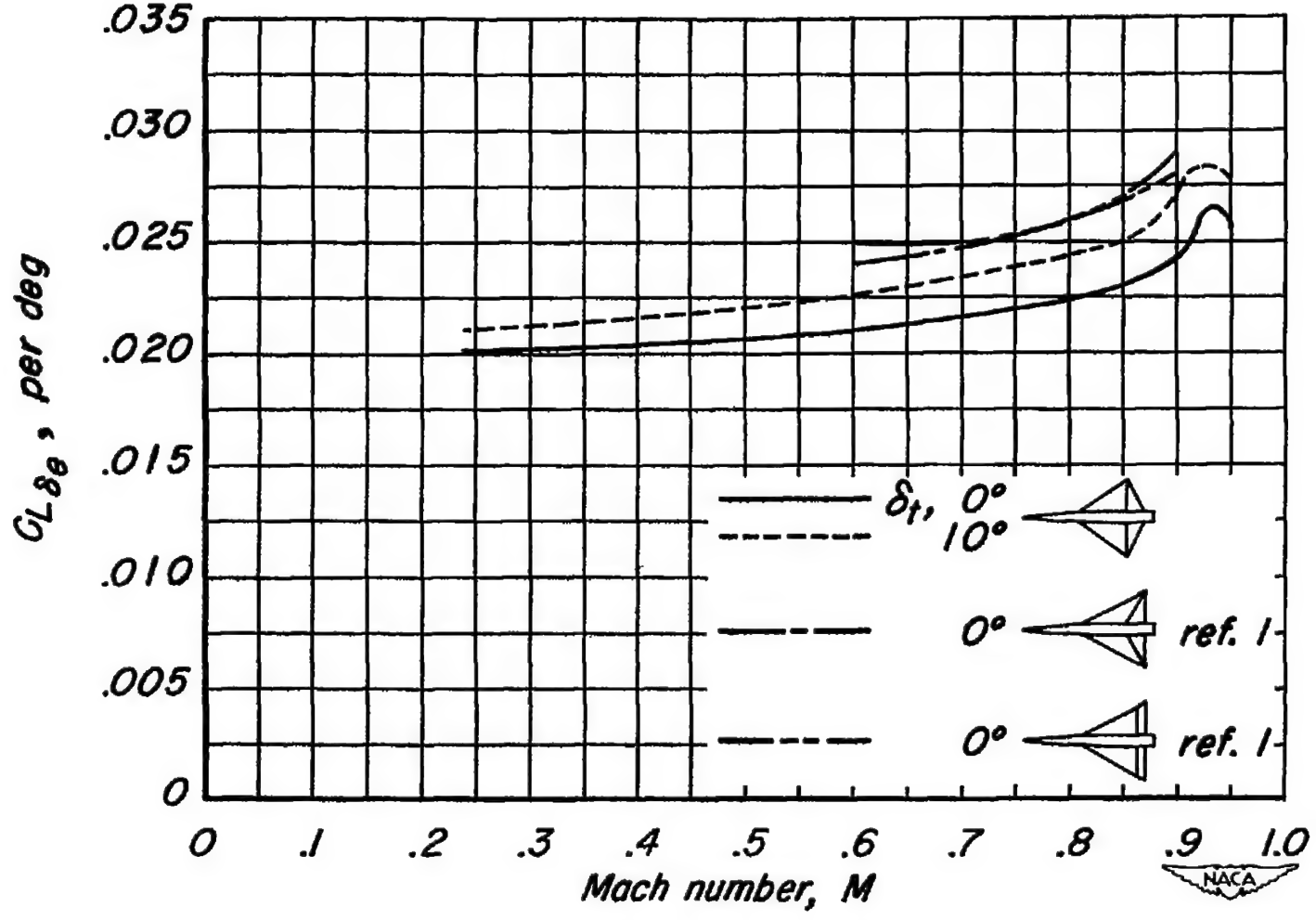

Figure 41.- The variation with Mach number of the lift effectiveness parameter, $C_{L_{\delta e}}$, for various elevon plan forms. R, 3.0 million; α, 0°.

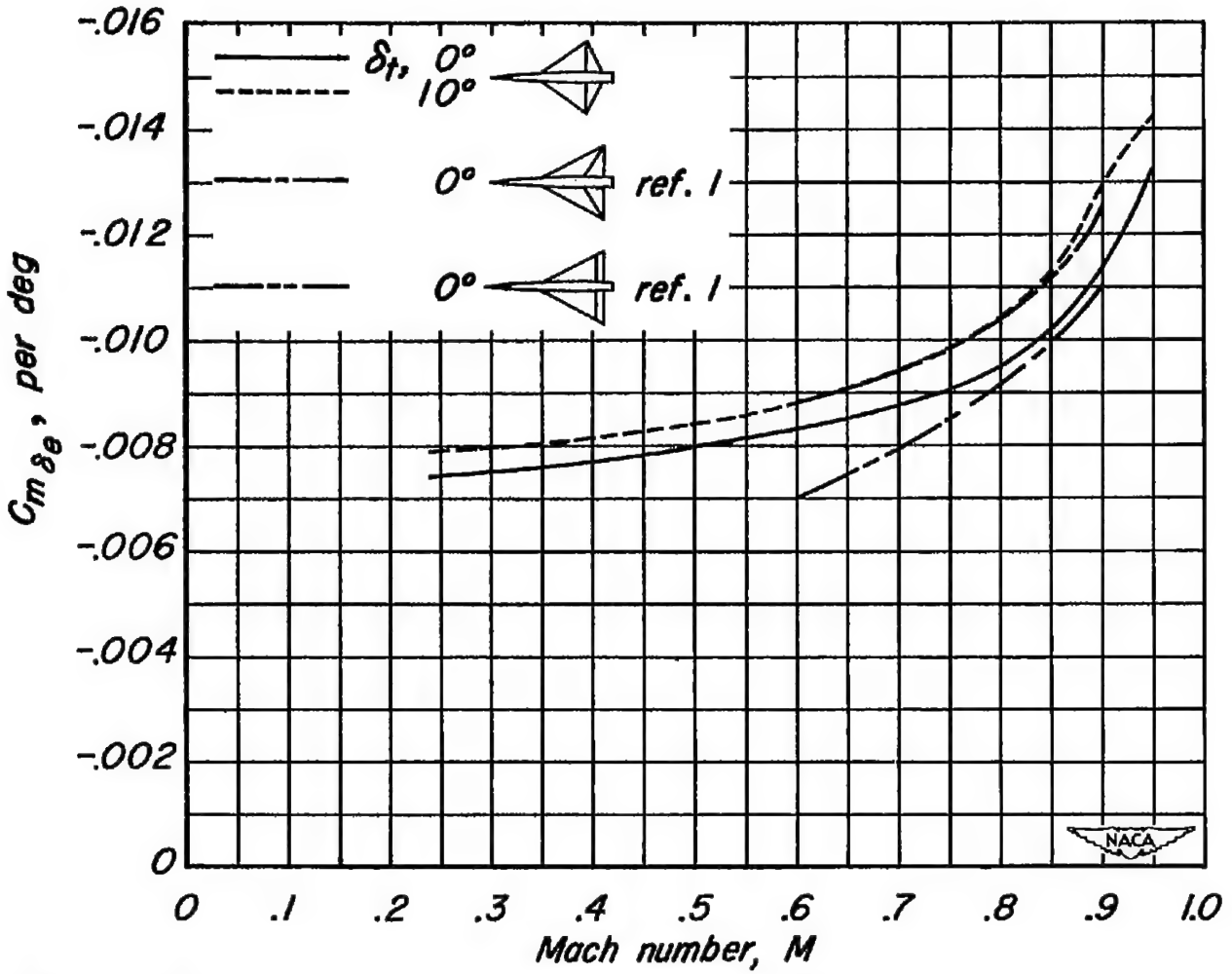

Figure 42.-The variation with Mach number of the pitching-moment effectiveness parameter, $C_{m_{\delta_e}}$, for various elevon plan forms. R, 3.0 million; α, 0°.

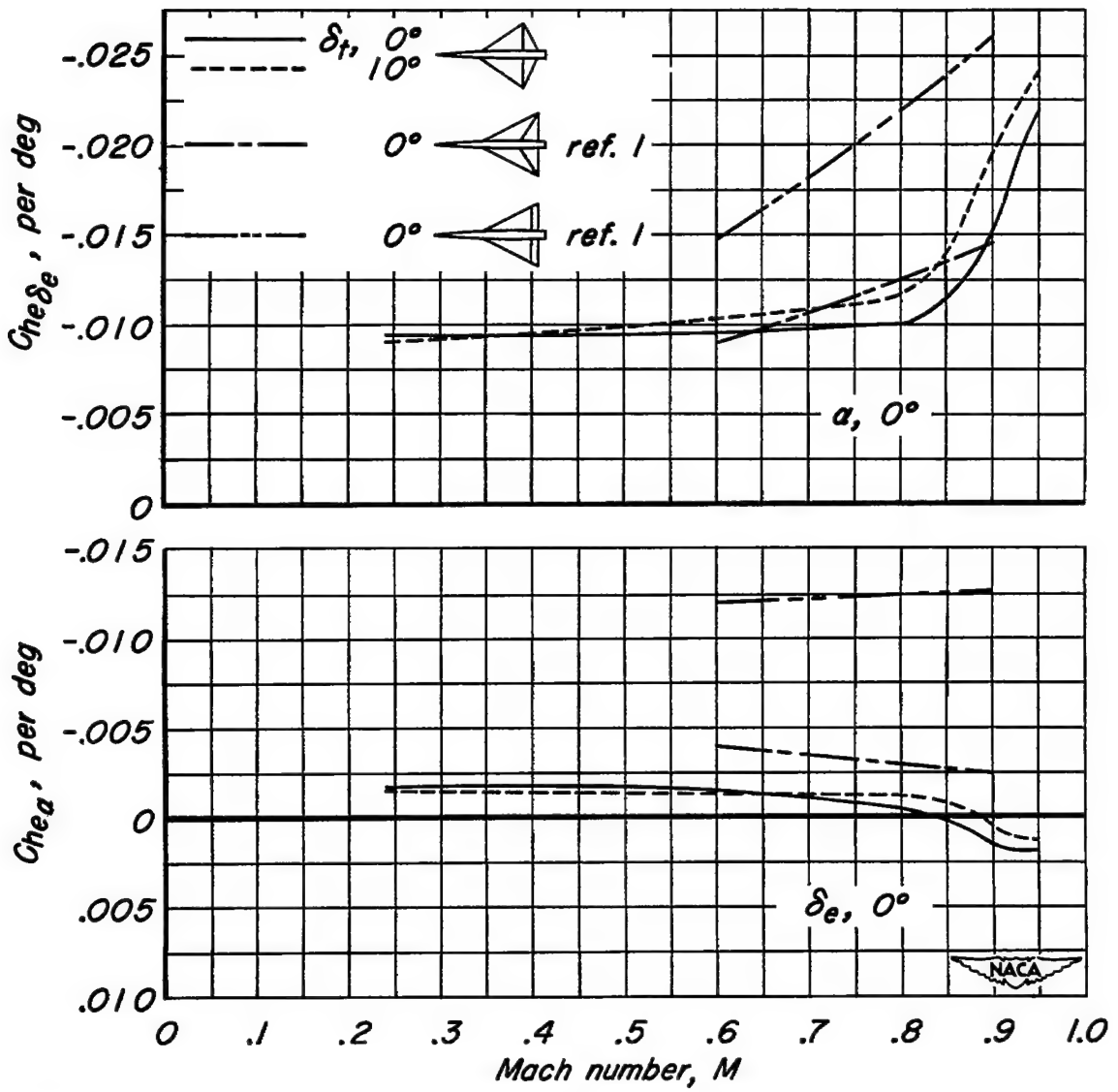

Figure 43.-The variation with Mach number of the elevon-hinge-moment parameters, $C_{he_{\delta_e}}$ and C_{he_α}, for various elevon plan forms. R, 3.0 million.

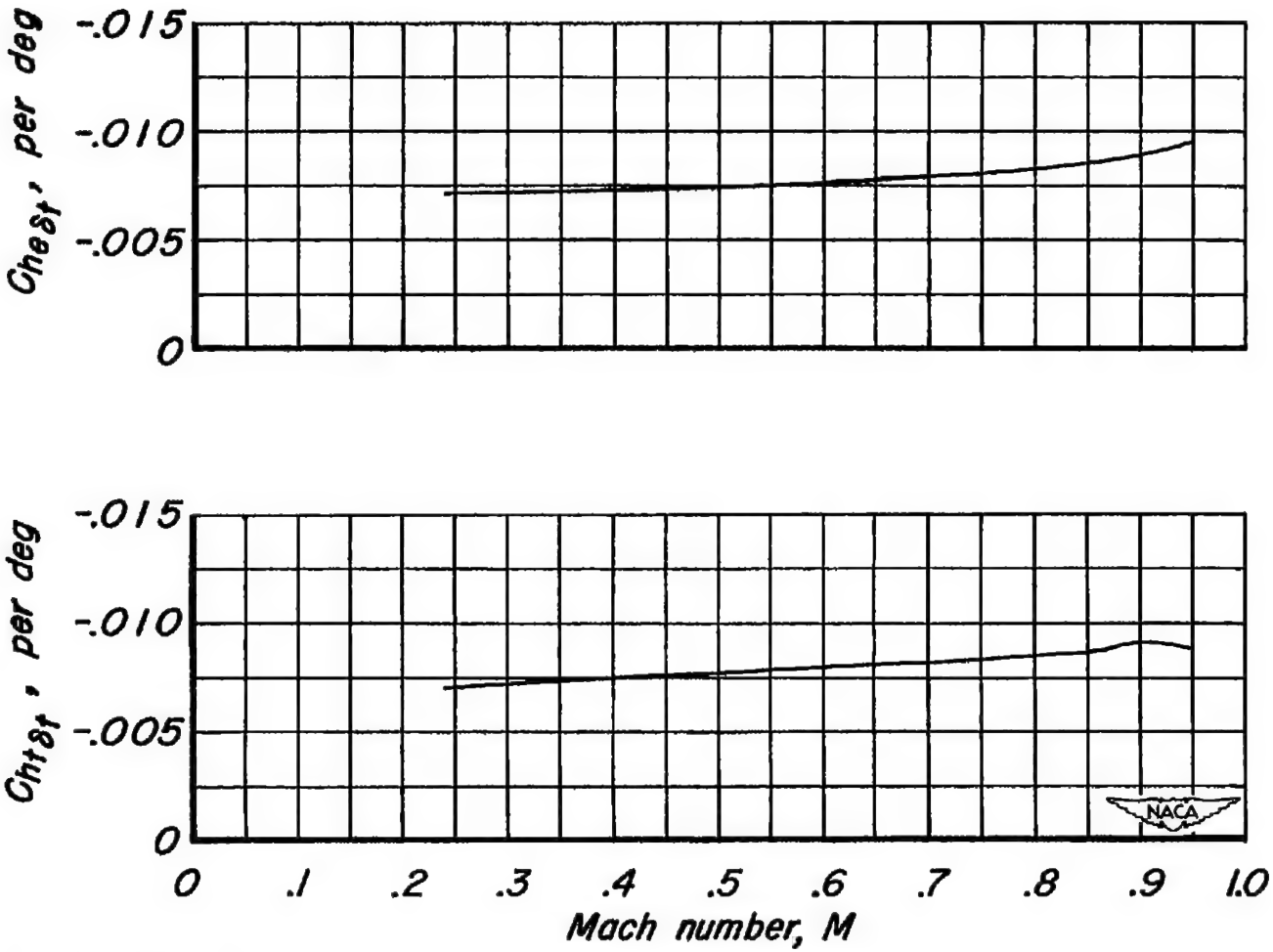

Figure 44.- The variation with Mach number of the elevon- and tab-hinge-moment parameters, $C_{he_{\delta t}}$ and $C_{ht_{\delta t}}$. R, 3.0 million; δ_e, 0°; α, 0°.

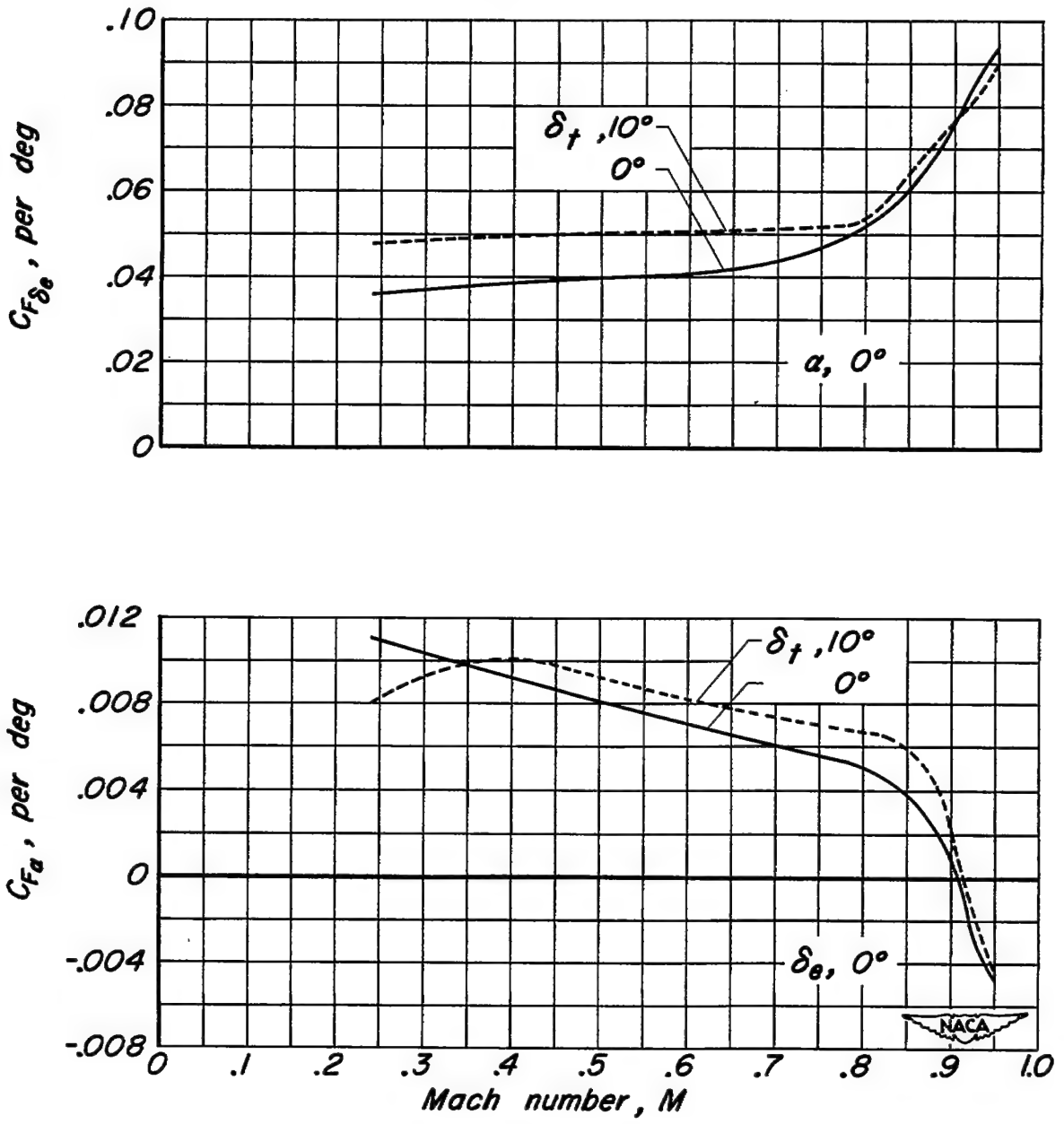

Figure 45.- The effect of Mach number on the elevon load parameters, $C_{F_{\delta_e}}$ and C_{F_a}. R, 3.0 million.

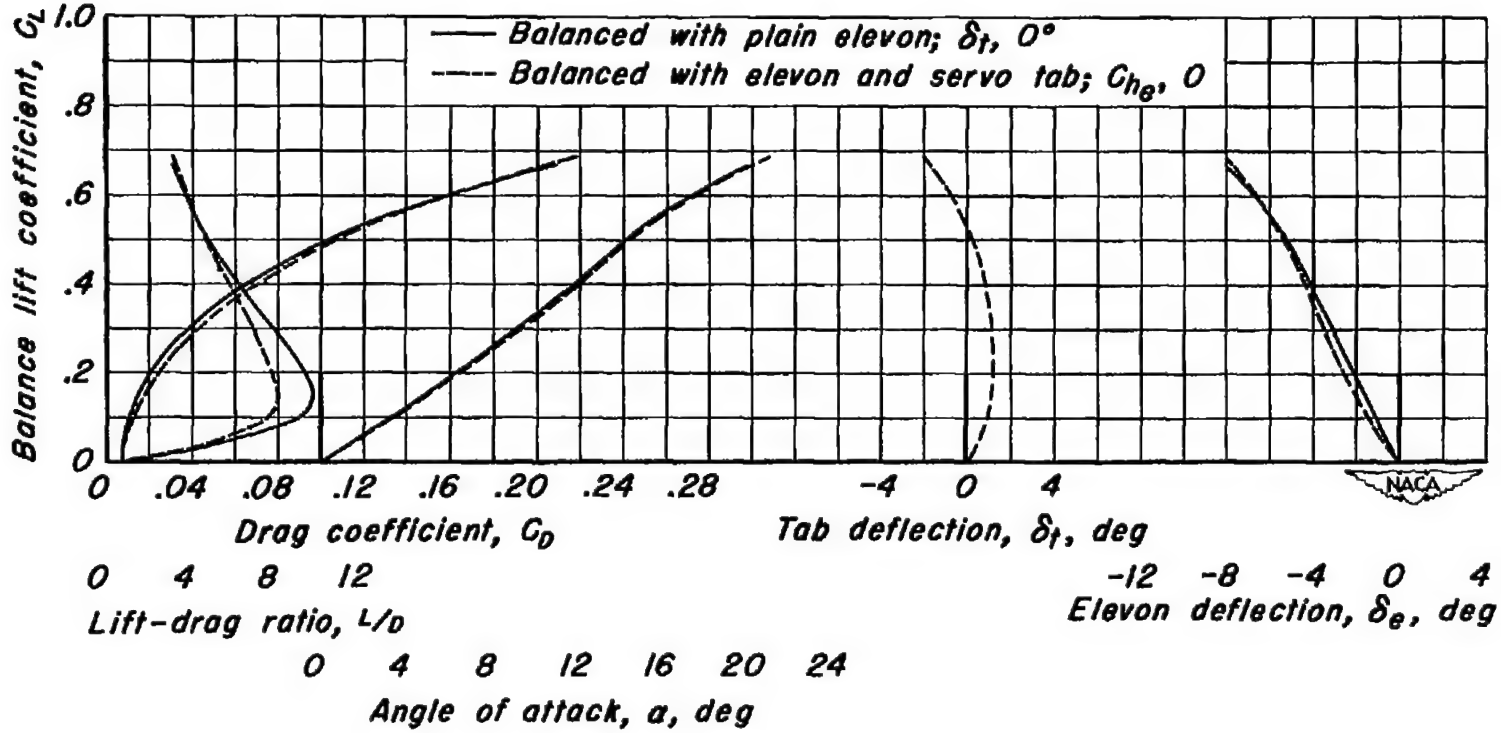

(a) M, 0.24

Figure 46.- The variation with balance lift coefficient of drag coefficient, lift-drag ratio, angle of attack, tab deflection and elevon deflection for a plain elevon control and for an elevon control with a servotab. Center of gravity at 0.25 $\bar{c}$.

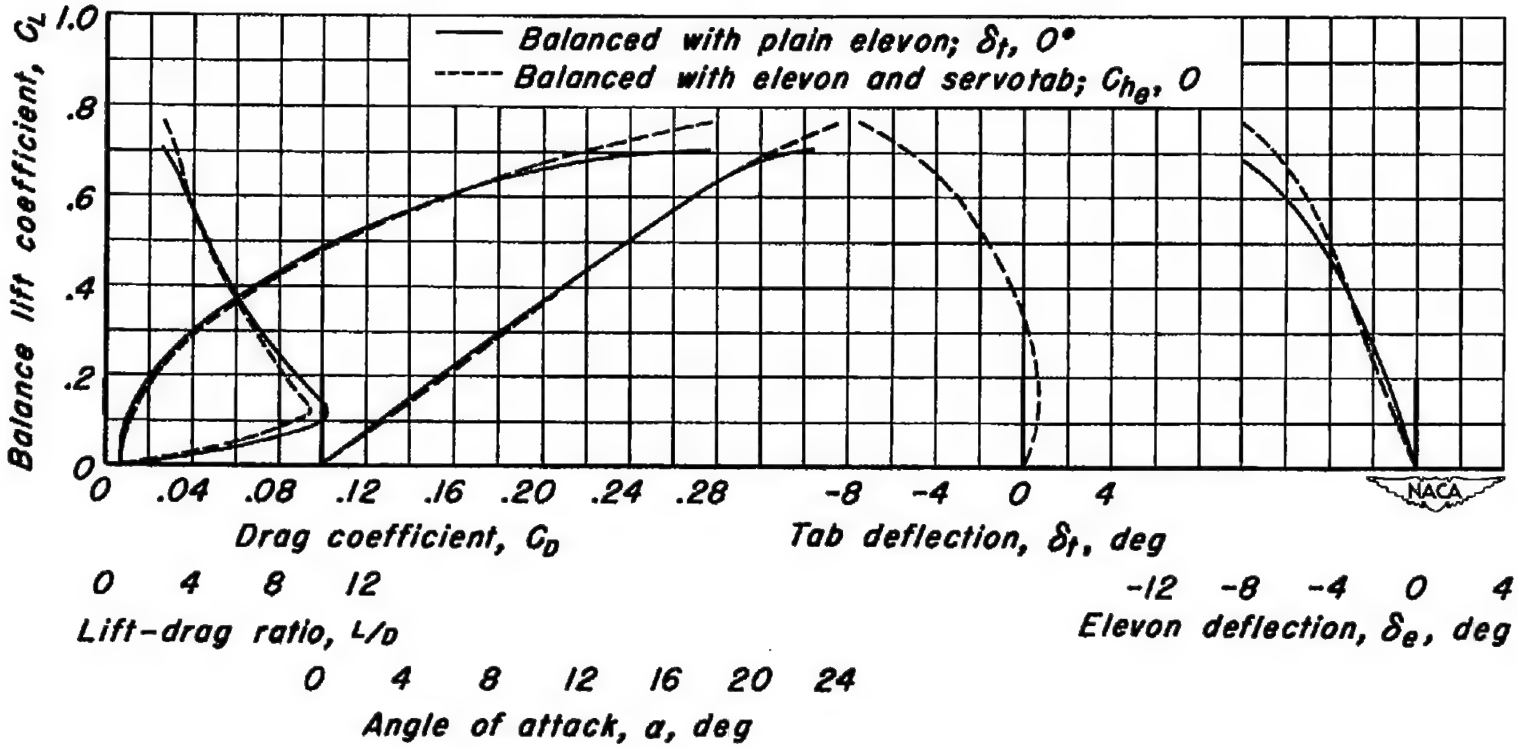

(b) M, 0.60

Figure 46.- Continued.

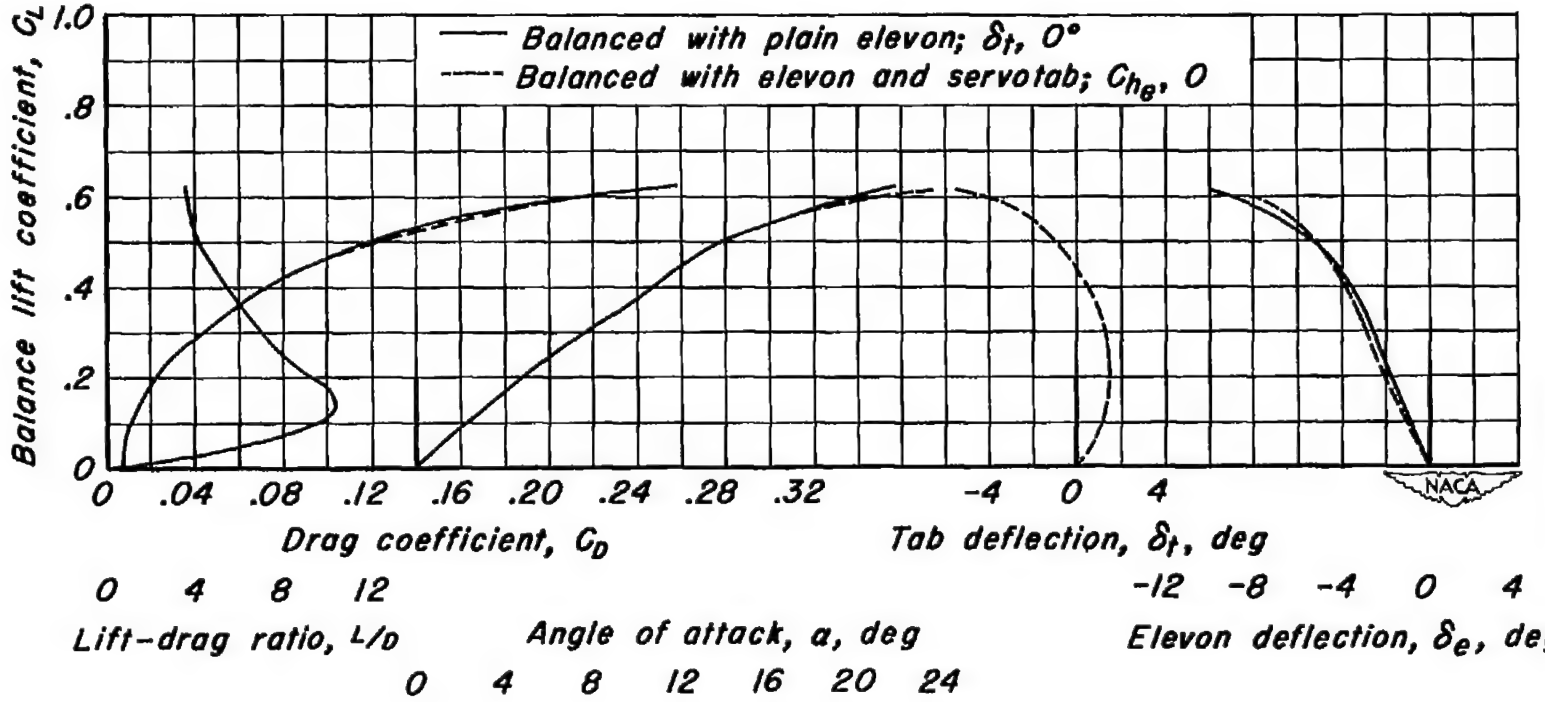

(c) M, 0.80

Figure 46.- Continued.

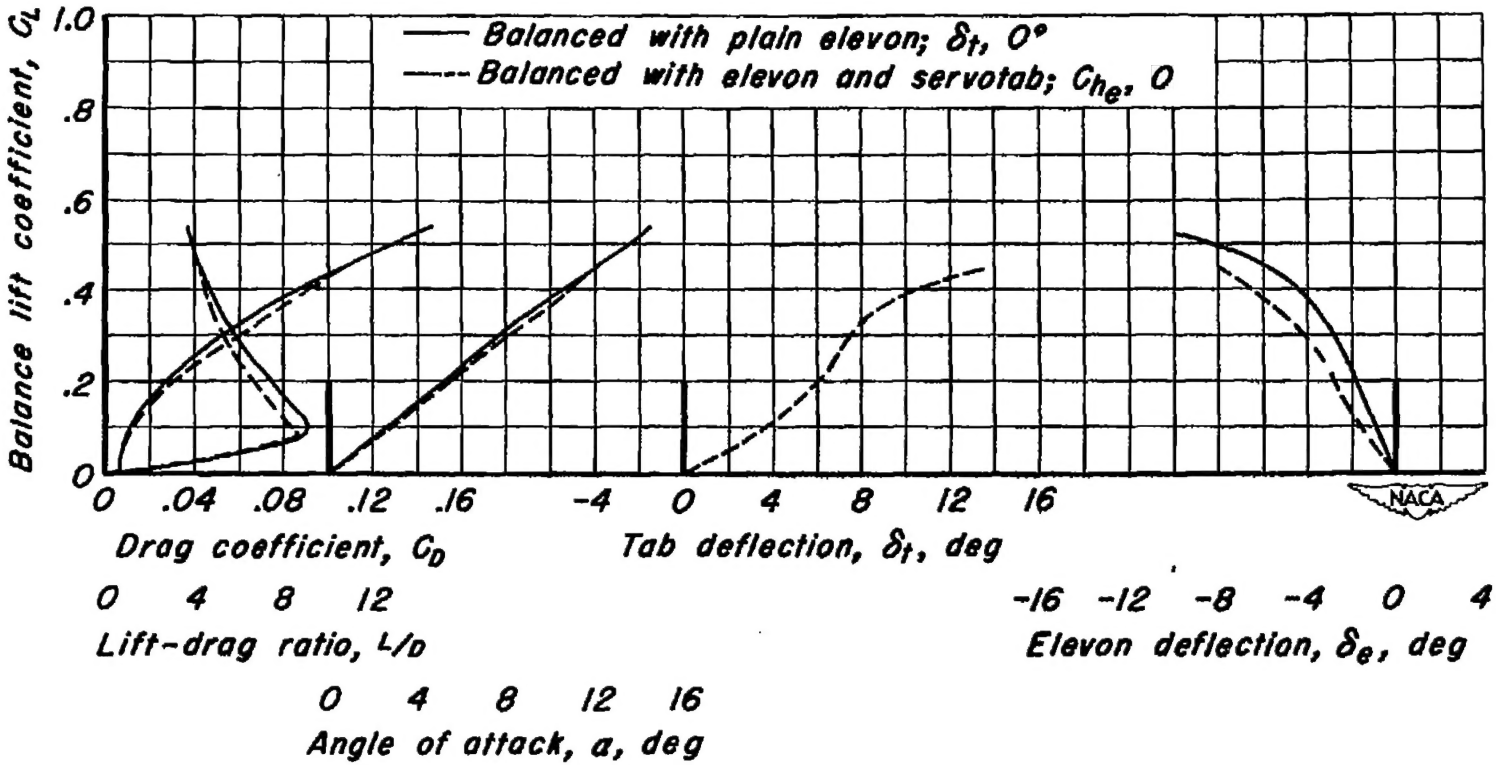

(d) M, 0.92

Figure 46.- Concluded.

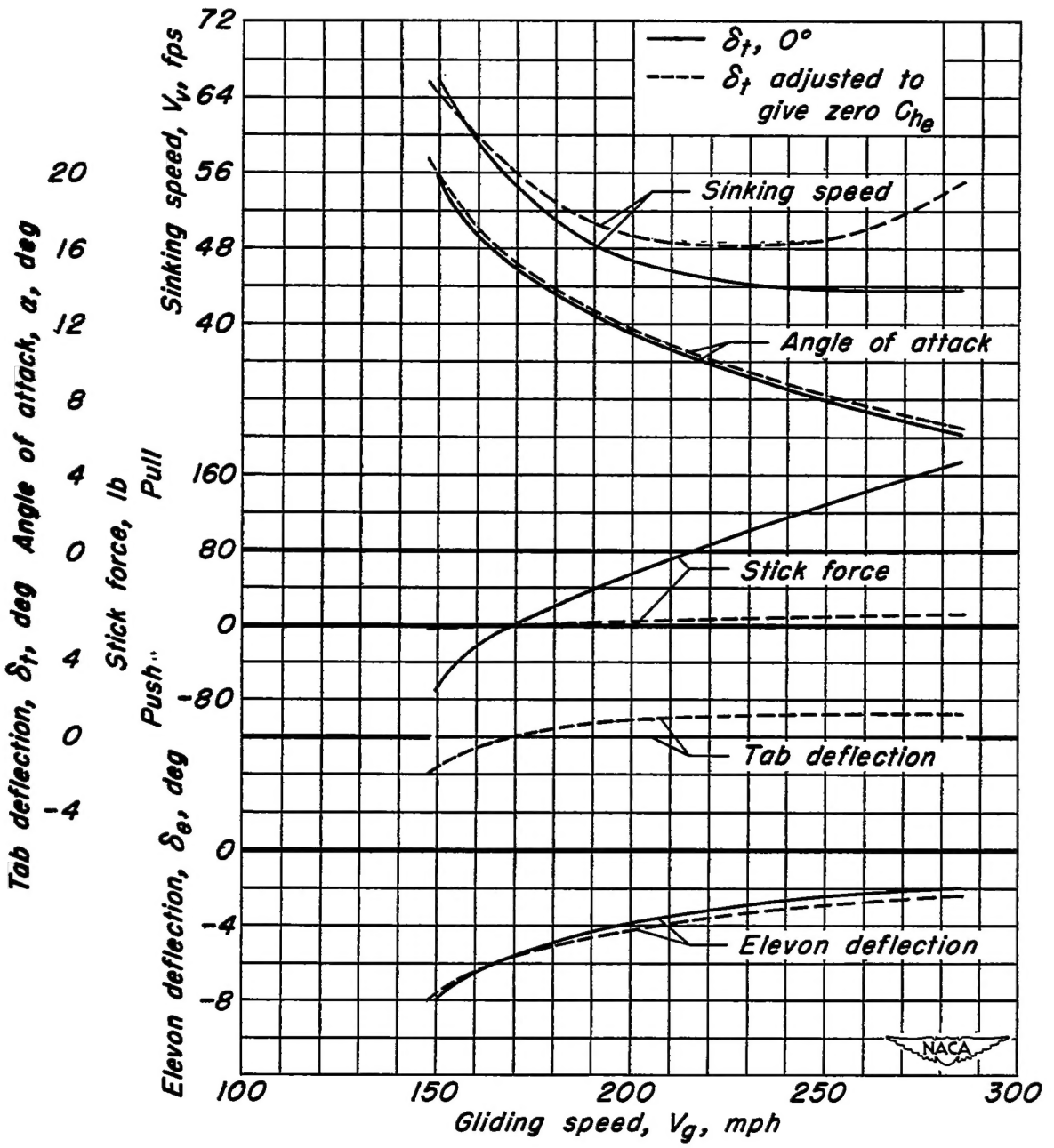

Figure 47.- The gliding characteristics of the assumed airplane with two different longitudinal control systems. Altitude, sea level; wing loading, 40 pounds per square foot; wing area, 450 square feet; center of gravity at 0.25 $\bar{c}$; control gearing, 2.0° per inch of stick travel.

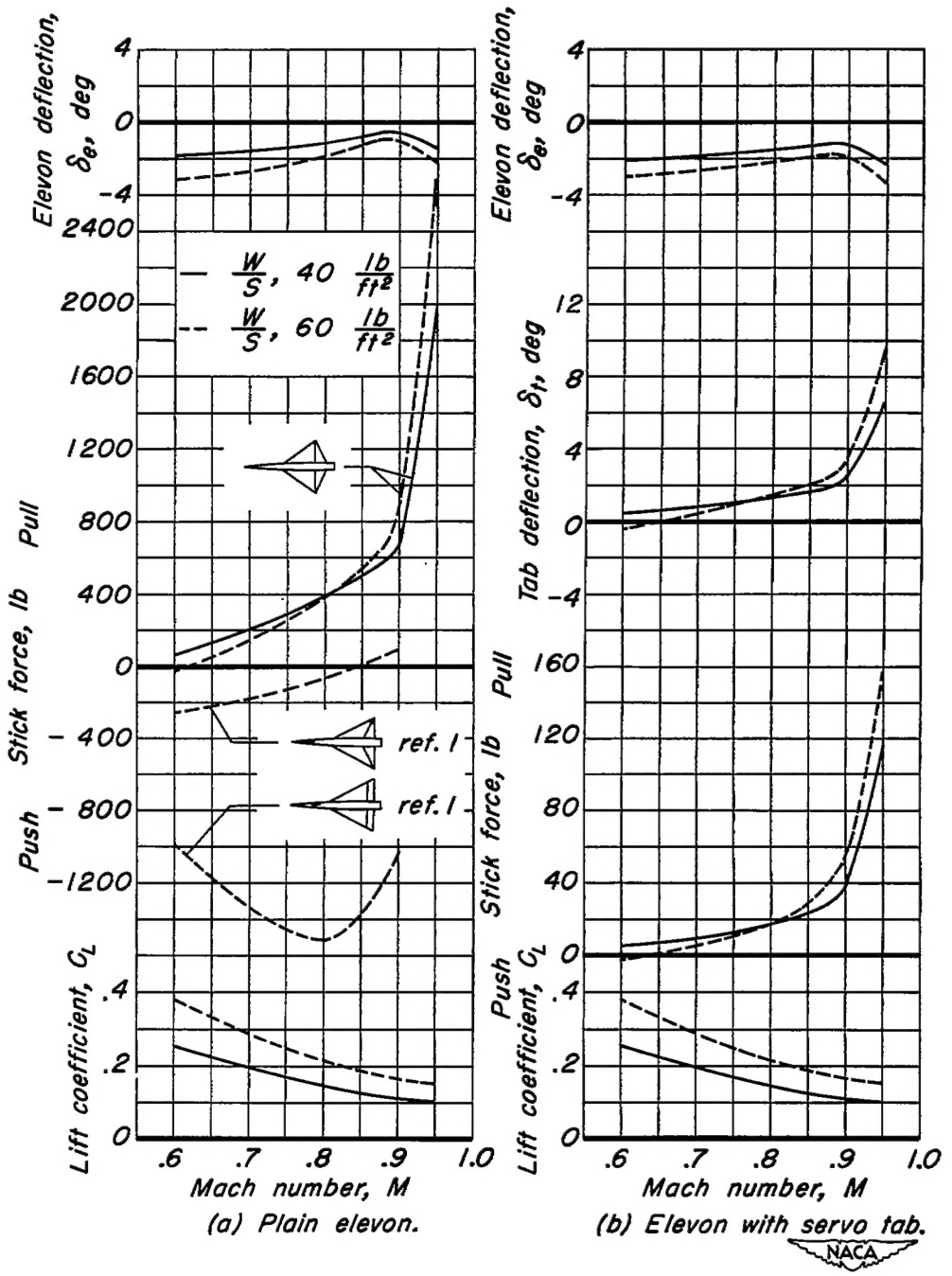

Figure 48.- The effect of wing loading on the level-flight characteristics of the assumed airplane with two different longitudinal control systems. Altitude, 30,000 feet; wing area, 450 square feet; center of gravity at 0.25 $\bar{c}$; control gearing, 2.0° per inch of stick travel.

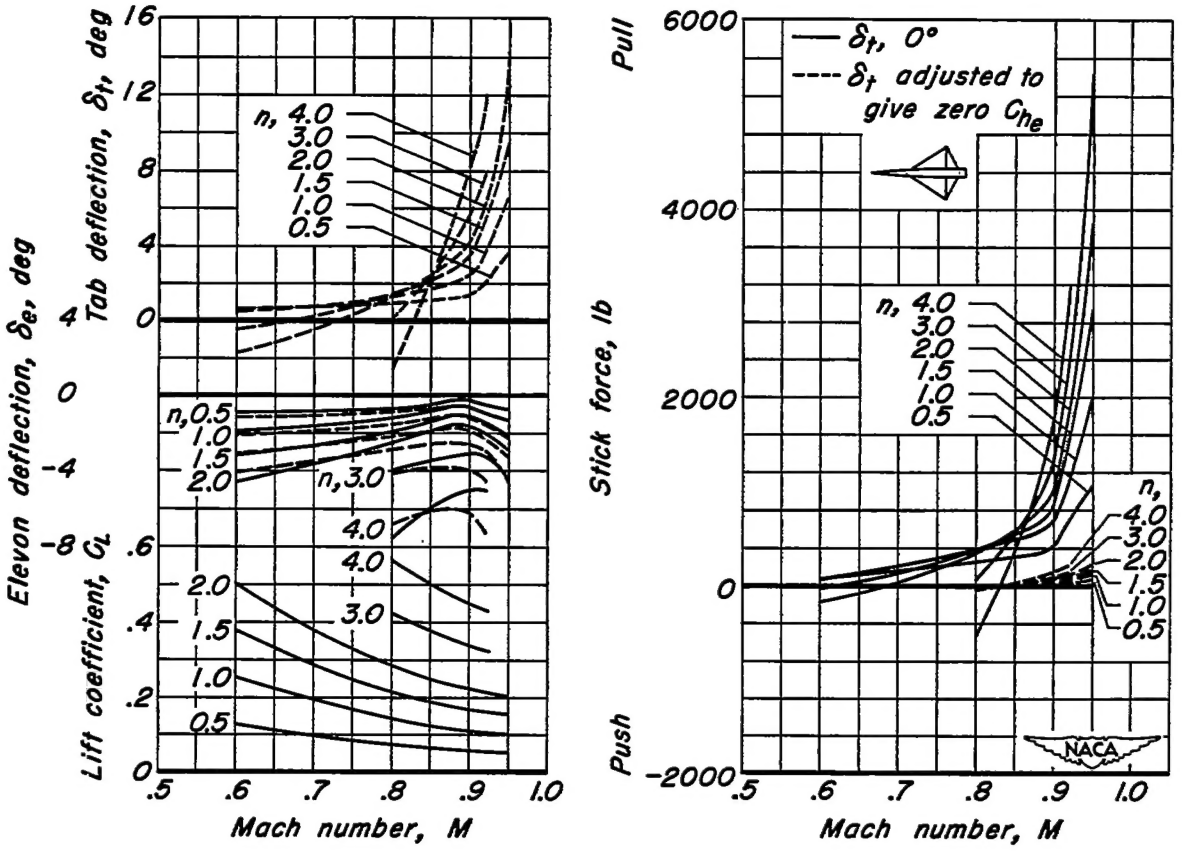

Figure 49.- The effect of Mach number on the level and accelerated flight characteristics of the assumed airplane with two different longitudinal control systems. Altitude, 30,000 feet; wing loading, 40 pounds per square foot; wing area, 450 square feet; center of gravity at 0.25 $\bar{c}$; control gearing, 2.0° per inch of stick travel.

[redacted]